

## THESIS / THÈSE

### DOCTOR OF SCIENCES

**Triptycenes and helicenes as polyaromatic platform for the design of bulky phosphines, boranes and bifunctional catalysts.**

GAMA, Mathieu

*Award date:*  
2022

*Awarding institution:*  
University of Namur

[Link to publication](#)

#### General rights

Copyright and moral rights for the publications made accessible in the public portal are retained by the authors and/or other copyright owners and it is a condition of accessing publications that users recognise and abide by the legal requirements associated with these rights.

- Users may download and print one copy of any publication from the public portal for the purpose of private study or research.
- You may not further distribute the material or use it for any profit-making activity or commercial gain
- You may freely distribute the URL identifying the publication in the public portal ?

#### Take down policy

If you believe that this document breaches copyright please contact us providing details, and we will remove access to the work immediately and investigate your claim.



**UNIVERSITÉ  
DE NAMUR**

**Faculty of Sciences  
Department of Chemistry**

---

**Dissertation submitted for the achievement of the Philosophical  
Degree (Ph. D.) in Sciences**

**Mathieu GAMA**

June 2022

**Triptycenes and helicenes as polyaromatic  
platforms for the design of bulky phosphines,  
boranes and bifunctional catalysts**

---

Thesis directed by:

**Guillaume BERIONNI**

Jury:

**M. Steve LANNERS (University of Namur)**

**M. Johan WOUTERS (University of Namur)**

**M. Gwilherm EVANO (ULB University, Brussels)**

**M. Marc GINGRAS (Aix-Marseille University)**

## Table of contents

<b>Acknowledgments</b> .....	<b>1</b>
<b>Abstract</b> .....	<b>2</b>
<b>Résumé</b> .....	<b>3</b>
<b>List of Abbreviations</b> .....	<b>4</b>
<b>Chapter I: General introduction on frustrated Lewis pairs (FLPs)</b> .....	<b>6</b>
I. Generalities.....	7
II. Hydrogen splitting and metal-free hydrogenation.....	9
1. Discovering metal free H <sub>2</sub> activation.....	9
2. Heterolytic H <sub>2</sub> activation by intramolecular FLPs.....	10
i. Phosphine/Borane FLPs.....	10
ii. Carbene/Borane FLPs .....	13
iii. Nitrogen bases/Borane FLPs .....	14
3. Metal free hydrogenations.....	16
i. Catalytic hydrogenation by P/B FLP systems.....	16
ii. Catalytic hydrogenation by N/B FLP systems.....	21
iii. Asymmetric hydrogenations.....	23
III. Frustrated Lewis pair reactivity with small molecules.....	26
1. Capture of CO <sub>2</sub> , SO <sub>2</sub> and N <sub>2</sub> O.....	26
i. Capture of CO <sub>2</sub> .....	26
ii. Capture of SO <sub>2</sub> .....	26
iii. Capture of N <sub>2</sub> O.....	27
2. CO and CO <sub>2</sub> reductions.....	27
i. CO reductions.....	27
ii. CO <sub>2</sub> reductions.....	28
IV. FLP addition reactions.....	32
1. FLP chemistry with alkenes.....	32
2. FLP chemistry with alkynes.....	34
3. FLP catalyzed hydroaminations of alkynes.....	36
V. Conclusions.....	38
<b>References</b> .....	<b>39</b>
<b>Chapter II: Triptycenes as platform for the design of new types of frustrated Lewis pairs...</b>	<b>43</b>
I. Triptycenes in chemistry.....	44
1. Generalities.....	44
2. Synthesis of triptycene and its derivatives.....	44
i. Triptycene.....	44
ii. Triptycene derivatives.....	47
3. Applications.....	49
i. Supramolecular chemistry.....	49

ii. Anion sensors and receptors.....	50
iii. Organometallic catalysis.....	51
II. Triptycene boronates, boranes, and boron ate-complexes: Toward sterically hindered triarylboranes and trifluoroborates.....	52
1. Objectives.....	52
2. Results and discussions.....	54
3. Conclusion and perspectives.....	60
III. Sterically Hindered Phosphines Derived from Triptycene: Reactivity and Applications in Frustrated Lewis Pairs Chemistry.....	61
1. Ligands descriptors for catalyst design.....	61
i. Electronic descriptors.....	62
ii. Steric descriptors.....	62
2. Objectives.....	64
3. Results and discussions.....	66
i. Synthesis of the triptyceny phosphines.....	66
ii. Complexation of triptyceny phosphines with Rhodium.....	68
iii. Steric and electronic parameters of the triptyceny phosphines.....	69
iv. Evaluation of the Lewis and Brønsted basicities of triptyceny phosphines.....	71
4. Toward frustrated Lewis pair catalysts based on triptycene.....	72
5. Attempted synthesis of intramolecular FLPs.....	75
6. Conclusions.....	76
<b>References.....</b>	<b>78</b>

### **Chapter III: Helicenes as platform for the design of new types of frustrated Lewis pairs.....81**

I. Helicenes in chemistry.....	82
1. Generalities.....	82
2. Helicenes and heterohelicenes synthesis.....	83
i. Helicenes synthesis.....	83
ii. Heterohelicenes synthesis.....	85
a) Photocyclizations.....	85
b) Substitutions.....	86
c) Metal induced synthesis.....	89
d) Other cyclizations.....	91
3. Resolution.....	92
4. Properties.....	93
5. Applications of helicenes.....	95
i. Asymmetric synthesis.....	95
ii. Electro-optical materials.....	97
iii. Helicenes grafted with phosphines.....	98
6. Objectives.....	100
II. Synthesis of new hindered phosphines based on a heterohelicenes scaffold.....	102

III. Conclusion and perspectives.....	110
1. Conclusion.....	110
2. Perspectives.....	111
<b>References.....</b>	<b>113</b>
<b>Chapter IV: General conclusion.....</b>	<b>116</b>
<b>Appendix A: Experimental part.....</b>	<b>119</b>
<b>Appendix B: List of conferences.....</b>	<b>178</b>
<b>Appendix C: List of publications.....</b>	<b>180</b>

## Acknowledgements

Firstly, I would like to express my gratitude to my doctoral supervisor, Prof. Guillaume Berionni, Director of RCO (Réactivité et catalyse organique) unit from the University of Namur, for providing all for my research work and for his exceptional support, patient guidance, motivation and useful critiques of this research work.

This thesis is supported by the FNRS and UNamur. These organisations are sincerely thanked for their fundings.

I would like also to specially thank Prof. Steve Lanners, Prof. Johan Wouters, Prof. Gwilherm Evano and Prof. Marc Gingras to have accepted to revise my doctoral dissertation and to participate in the Thesis Jury.

I thank the Dr. Nikolay Tumanov and PC<sup>2</sup> platform UNamur for providing XRD facility and their priceless help.

I would like to particularly thank my co-workers from RCO labs, Dr. Aurélien Chardon, Dr. Thu Hong DOAN, Damien Mahaut, Arnaud Osi, Nicolas Niessen, Lucie Pedussaut and all the master students that were part of it, especially Xavier Antognini Silva and Thomas Bernard. Without you guys, the days in the lab would not have been the same! Thank you for your kindness, your help and the fun we had during those four years.

J'aimerais maintenant remercier ma famille et mes amis en France ou ailleurs pour leur support de tous les jours. Et tout particulièrement ma mère qui, telle une bouteille d'oxygène, est toujours sur mon dos mais indispensable à ma survie et mon père qui a su me soutenir dans les moments où je n'étais pas bien. Je n'en serais pas là sans vous.

Enfin, j'aimerais te remercier toi Deborah. Ton amour et ton soutien indéfectible m'ont donné la force de toujours continuer et de croire en moi. Tu es la preuve que même si le paradis n'existait pas, les anges, eux, sont bien réels. Je t'aime.

## Abstract

Ambiphilic compounds possessing two antagonistic chemical functions, such as a Lewis acidic and a Lewis basic site, are increasingly used as bifunctional catalysts, chemosensors and ligands. Lewis acids and bases are usually incompatible chemical species since they combine to form a Lewis adduct, which annihilates their respective acidic and basic properties.

According to the concept of Lewis acid and base introduced in 1923 by Gilbert N. Lewis: "The basic substance furnishes a pair of electrons for a chemical bond, the acid substance accepts such a pair". By sharing the electron pair, a Lewis adduct containing a covalent bond between the acid and the base is formed, bearing in mind that this process can be reversible depending on the acidity and basicity strength of both species.

Numerous strategies can be employed to control this association process, notably by modulating the steric and electronic properties of the substituents attached to the acidic and basic atoms. Indeed, with large substituents, the steric hindrance prevents the antagonistic functions to react and quench each other's because of steric repulsions, and result in a so called "Frustrated Lewis Pairs" (or FLPs).

It is thus possible to design new catalysts containing a Lewis acid and a Lewis base and which coexist simultaneously in solution without any covalent interactions between these two reactive sites and without dimerization of the catalysts.

With this in mind, our main goal was to synthesize and investigate the reactivity of new bifunctional phosphine-borane compounds featuring two types of linker never used previously: triptycene and helicene scaffolds.

The first chapter of this dissertation is a detailed presentation of frustrated Lewis pairs and their applications and reactivities towards small molecules. In a second chapter, the synthesis of new hindered boranes and phosphines based on the triptycene scaffold and their reactivity as frustrated Lewis pairs are presented. Finally, in the third chapter, the synthesis and study of bulky phosphines based on hetero[5]helicene scaffolds are discussed.

## Résumé

Les composés ambiphiles possédant deux fonctions chimiques antagonistes, comme un acide de Lewis et une base de Lewis, sont de plus en plus utilisés comme catalyseurs bifonctionnels, chimiocepteurs et ligands. Les acides et les bases de Lewis sont généralement des espèces chimiques incompatibles car ils se combinent pour former un adduit de Lewis, qui annihile leurs propriétés acides et basiques respectives.

Selon le concept d'acide et de base de Lewis introduit en 1923 par Gilbert N. Lewis : « Une base est une substance qui fournit une paire d'électrons pour une liaison chimique, un acide est une substance qui accepte une telle paire ». En partageant la paire d'électrons, un adduit de Lewis contenant une liaison covalente entre l'acide et la base est formé, sachant que ce processus peut être réversible en fonction de la force de l'acidité et de la basicité des deux espèces.

De nombreuses stratégies peuvent être employées pour contrôler ce processus d'association, notamment en modulant les propriétés stériques et électroniques des substituants des atomes acides et basiques. En effet, avec des substituants encombrants, les répulsions stériques empêchent les fonctions antagonistes de réagir entre elles, et aboutit à ce que l'on appelle des "paires de Lewis frustrées" (ou FLP).

Il est ainsi possible de concevoir de nouveaux catalyseurs contenant un acide et une base de Lewis coexistant simultanément en solution sans aucune interaction covalente entre ces deux sites réactifs et sans dimérisation des catalyseurs.

Dans cet esprit, notre objectif principal était de synthétiser et d'étudier la réactivité de nouveaux composés bifonctionnels phosphines-boranes comportant deux types de liens espaceurs jamais utilisés auparavant : les triptycènes et les hélicènes.

Le premier chapitre de cette thèse est une présentation détaillée des paires de Lewis frustrées, de leurs applications et réactivités vis-à-vis de petites molécules. Dans un deuxième chapitre, la synthèse de nouveaux triptycene-boranes et phosphines encombrés ainsi que leur réactivité en tant que paires de Lewis frustrées sont présentées. Enfin, dans un troisième chapitre, la synthèse et l'étude de phosphines encombrées basées sur des squelettes d'hétéro[5]hélicènes sont exposées.



## List of abbreviations

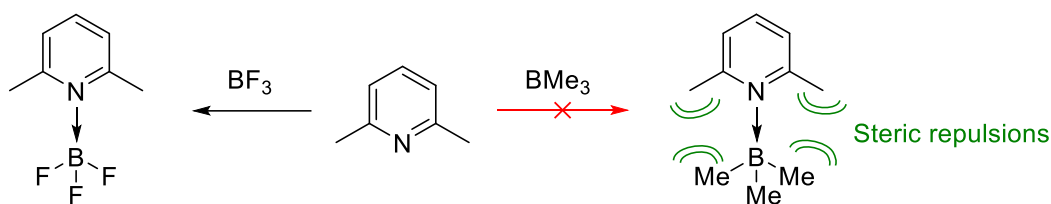
Ac: acetyl  
acac: acetylacetone  
Ar: aryl  
BSA: bis(trimethylsilyl)acetamide  
Bu: butyl  
cat: cathecol  
Cat.: catalyst  
CEP: calculated electronic parameter  
cod: cyclooctadiene  
Cp: cyclopentadienyl  
CPL: circular polarized luminescence  
Cy: cyclohexyl  
DABCO: 1,4-diazabicyclo[2.2.2]octane  
dba: dibenzylideneacetone  
DCM: dichloromethane  
DDQ: 2,3-dichloro-5,6-dicyano-1,4-benzoquinone  
DFT: density functional theory  
DMF: dimethylformamide  
DMSO: dimethylsulfoxide  
ee: enantiomeric excess  
equiv.: equivalent  
Et: ethyl  
EtOAc: ethyl acetate  
FLPs: frustrated Lewis pairs  
FT-IR: Fourier transform infrared spectroscopy  
GC: gas chromatography  
HPLC: high-performance liquid chromatography  
*i*-Pr: isopropyl  
IR: infrared  
max.: maximum  
MCA: methyl cation affinity  
Me: methyl  
Mes: mesityl  
M.p.: melting point  
MW: microwave  
neo : neopentyl glycol  
NHCs: N-heterocyclic carbenes  
NMR: nuclear magnetic resonance  
Oct: octyl  
o.n.: overnight  
ORTEP: Oak Ridge Thermal-Ellipsoid Plot Program

PA: proton affinity  
PES: potential energy surface  
Ph: phenyl  
pin: pinacol  
PL: photoluminescence  
PMP: pentamethylpiperidine  
ppm: parts per million  
rac: racemic  
r.t.: room temperature  
SEP: semiempirical electronic parameter  
T: temperature  
TAPA: ( $\alpha$ -(2,4,5,7-tetranitro-9-fluorenylideneaminoxy)-propionic acid  
TEP: Tolman electronic parameter  
Tf: trifluoromethane sulfonyl  
THF: tetrahydrofuran  
TIPS: triisopropylsilyl  
TLC: thin-layer chromatography  
TMEDA: Tetramethylethylenediamine  
TMP: trimethylpropane  
TOF: turn over frequency  
tol: tolyl  
TON: turn over number  
UV-vis: Ultraviolet–visible  
VAZO: 1,10 -azobis(cyclohexanecarbonitrile)  
vol.: volumic  
 $\%V_{bur}$ : buried volume

**Chapter I:**  
**General introduction on frustrated Lewis pairs (FLPs)**

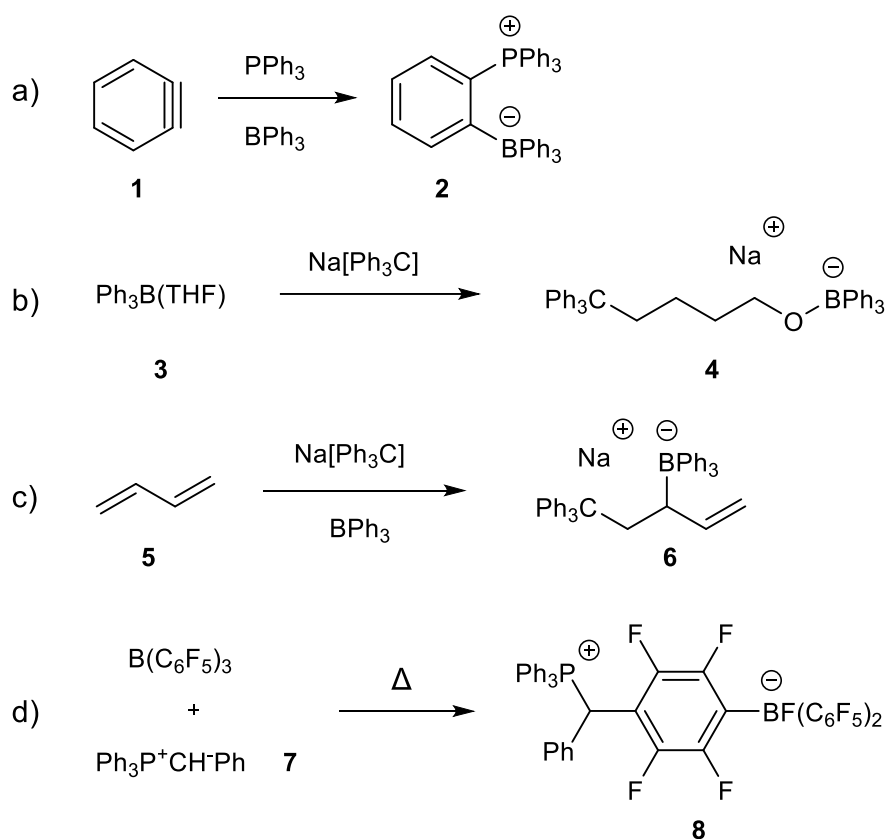
## I. Generalities

According to the Lewis theory, a Lewis base shares an electron pair with a Lewis acid to form a covalent Lewis adduct<sup>[1]</sup>. Once this adduct is formed, the intrinsic acidic and basic properties of both species are lost. However, in 1942, Brown *et al.* discovered while studying interactions between pyridines and boranes that lutidine makes a Lewis adduct with  $\text{BF}_3$  but not with bulkier and less Lewis acidic  $\text{BMe}_3$  (Scheme 1).<sup>[2]</sup> A simple observation of molecular models allowed to attribute this phenomenon to steric repulsions between the methyl substituents of the Lewis base and of the Lewis acid.



**Scheme 1:** Lutidine reactivity toward Lewis acids.

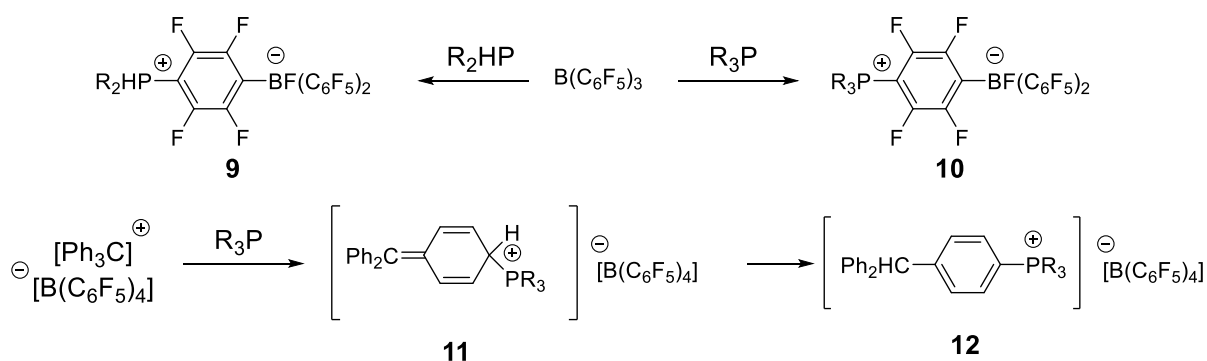
Subsequently other researchers reported that such steric hindrance between Lewis bases and acids can lead to unexpected chemical reactions. For example, Wittig and Benz<sup>[3]</sup> discovered that combining  $\text{PPh}_3$  and  $\text{BPh}_3$  in the presence of benzyne results in the formation of the *o*-phenylene-linked zwitterionic phosphonium-borate  $(\text{C}_6\text{H}_4)(\text{PPh}_3)(\text{BPh}_3)$  **2** (Scheme 2a) while no evidence of the Lewis acid-base adduct was found. Previously, Wittig<sup>[4]</sup> also reported that the corresponding reaction of trityl anion with  $(\text{THF})\text{BPh}_3$  achieve the THF ring-opening and formation of the salt  $\text{Na}[\text{Ph}_3\text{C}(\text{CH}_2)_4\text{OBPh}_3]$  **4** (Scheme 2b). In related work, Tochtermann<sup>[5]</sup> reported that the trityl anion and  $\text{BPh}_3$  perform an addition to butadiene affording  $\text{Na}[\text{Ph}_3\text{CCH}_2(\text{BPh}_3)\text{CHCH}_2]$  **6** (Scheme 2c) although the anion was expected to initiate anionic polymerization of butadiene or to form a Lewis acid-base adduct with  $\text{BPh}_3$ . This unusual reactivity led Tochtermann to call this combination of Lewis acid and base an “antagonistic pair”. Furthermore, the reactions of bulky amines with a trityl cation did not promote the formation of an adduct, instead resulting in hydride abstraction from a carbon alpha to nitrogen by the trityl cation yielding an iminium cation.<sup>[6]</sup> Other examples of the non-conventional behavior of Lewis acids and bases have been later reported. For example, Erker and co-workers<sup>[7]</sup> reported that combining  $\text{B}(\text{C}_6\text{F}_5)_3$ <sup>[8]</sup> and the ylide  $\text{Ph}_3\text{P}^+\text{CH}^-\text{Ph}$  afforded the Lewis acid-base adduct at room temperature. Nonetheless, upon heating the ylide dissociates from boron and effects a nucleophilic attack on the *para*-carbon of the  $\text{C}_6\text{F}_5$  aryl ring while fluoride transfer to boron occurs to afford the zwitterionic salt  $\text{Ph}_3\text{PCH}(\text{Ph})(\text{C}_6\text{F}_4)\text{B}(\text{F})(\text{C}_6\text{F}_5)_2$  **8** (Scheme 2d).



**Scheme 2:** Non-conventional reactions of Lewis acids and bases.

In addition, Stephan<sup>[9,10]</sup> reported the reactivity of bulky tertiary phosphines with  $B(C_6F_5)_3$ . The steric hindrance prevents the formation of a P–B dative bond but these reactions yielded a series of zwitterions,  $R_3P(C_6F_4)B(F)(C_6F_5)_2$  **10** ( $R = tBu, iPr, Cy$ ) (Scheme 3). Indeed, one of the fluoro-arene rings attacked the para-carbon and the concurrent migration of fluoride to boron occurred. It is also possible to prepare related zwitterionic species from phosphine-borane adducts upon heating<sup>[11,12]</sup>. In this way, secondary and tertiary phosphine-borane adducts rearrange to afford the air and moisture stable zwitterions  $[R_3P(C_6F_4)BF(C_6F_5)_2]$  **10** ( $R = Ph, Et, Cy, nBu, p-CF_3C_6H_4, o-(MeO)C_6H_4$ ) and  $[R_2PH(C_6F_4)BF(C_6F_5)_2]$  **9** ( $R = Mes, tBu, Cp, Cy$ ).<sup>[11,12]</sup>

While sterically unencumbered phosphines such as  $PMe_3$  form a Lewis acid-base phosphonium salt  $[Ph_3CPMe_3]X$  when combined with trityl cation, the formation of this salt is not observed with bulky tertiary phosphines. Instead, the intermediate  $[R_3P(C_6H_5)C(C_6H_5)_2]^+$  **11** is generated by the attack of the phosphine at a para-carbon of a phenyl substituent. Then a hydride migration occurs to the formerly cationic carbon, yielding the phosphonium cations of the form  $[R_3P(C_6H_4)CH(C_6H_5)_2]^+$  **12** (Scheme 3)<sup>[13]</sup>.

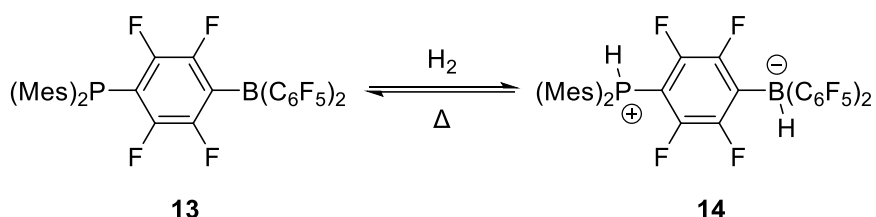


**Scheme 3:** Synthesis of compounds 9-12

## II. Hydrogen splitting and metal-free hydrogenation

### 1. Discovering metal-free $H_2$ activation

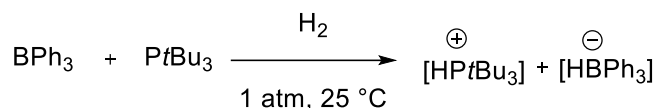
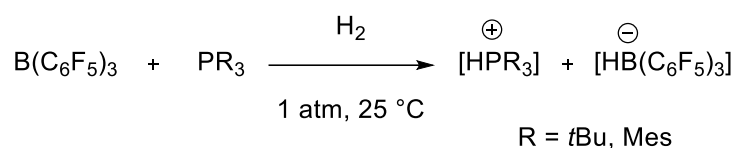
A major development in cooperative Lewis acid/base chemistry was achieved only recently when Stephan *et al.* reported in 2006 the first reversible heterolytic cleavage of dihydrogen using a combination of hindered Lewis acid (arylboration) and base (arylphosphine) (Scheme 4).<sup>[14]</sup>



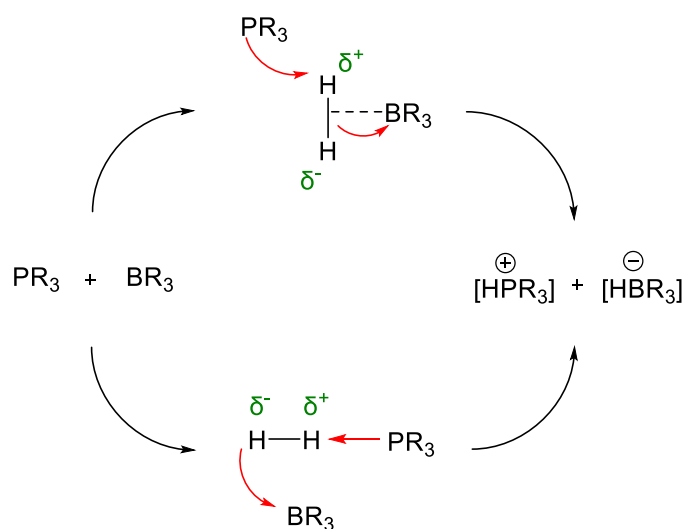
**Scheme 4:** Reversible dihydrogen splitting and release with Stephan's intramolecular FLP.

Afterwards, Stephan reported that other combinations of bulky phosphines with  $B(C_6F_5)_3$  and  $BPh_3$  were also able to cleave dihydrogen to obtain the respective phosphonium/hydridoborate salts<sup>[15]</sup> and proposed two mechanisms for this activation (Scheme 5 and 6) while Erker reported an ethylene bridged Lewis acid/base system which is also highly active for dihydrogen activation.<sup>[16]</sup> In 2008, Stephan defined frustrated Lewis pairs (FLPs) as the association of sterically hindered Lewis acids and bases that cannot form a covalent Lewis adduct because of steric repulsions.<sup>[17]</sup> These systems, possessing at the same time Lewis basic and acidic properties, allow the synergistic reaction of both reactive sites on a substrate in order to activate and functionalize it. This process is strongly influenced by the orientation and the distance between the Lewis acid and the Lewis base. Using intramolecular FLPs was shown to improve the activation of small molecules, in part by minimizing the reactions activation entropies. In this way, FLP systems can perform reactions that are usually carried out by transition metal surfaces or complexes.<sup>[18]</sup> The range of Lewis acidity or basicity needed for the dihydrogen activation has also been investigated. Indeed, reaction of *t*-Bu<sub>3</sub>P and BPh<sub>3</sub> with H<sub>2</sub> gave the corresponding

phosphonium/hydridoborate salt in only 33% yield while the analogous combination of  $(C_6H_2Me_3)_3P$  and  $BPh_3$ ,  $(C_6F_5)_3P$  and  $B(C_6F_5)_3$ , or  $tBu_3P$  and  $B(C_6H_2Me_3)_3$  did not react in presence of dihydrogen.



**Scheme 5:** Heterolytic cleavage of  $H_2$  by phosphines and boranes.



**Scheme 6:** Proposed mechanisms for the heterolytic cleavage of  $H_2$  by phosphines and boranes.

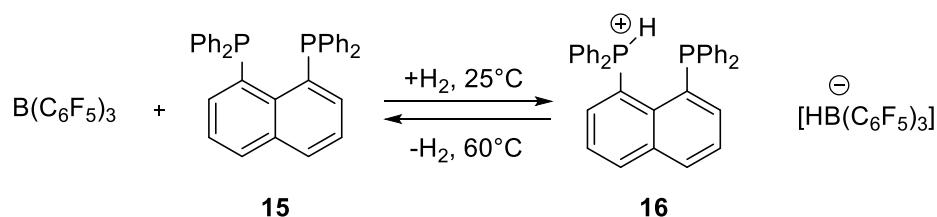
## 2. Heterolytic $H_2$ activation by intermolecular FLPs

The use of FLPs for the activation of dihydrogen has prompted the development of metal-free hydrogenation catalysts. Several investigations probing the substrate scope and the impact of catalyst modification have been reported. Moreover, applications in asymmetric hydrogenations have also advanced the field.

### i. Phosphine/Borane FLPs

After Stephan's initial reports, Erker<sup>[19]</sup> developed an intermolecular FLP composed of 1,8-bis(diphenylphosphino)-naphthalene **15** and  $B(C_6F_5)_3$ . This diposphine contains sterically demanding phosphines which, combined with  $B(C_6F_5)_3$ , generates a FLP that can react with dihydrogen to give the phosphonium hydridoborate salt  $[C_{10}H_6(PPh_2)_2H][HB(C_6F_5)_3]$  **16** (Scheme 7).<sup>[19]</sup>  $^{31}P$  NMR analysis of **16** has shown a rapid proton exchange between the two

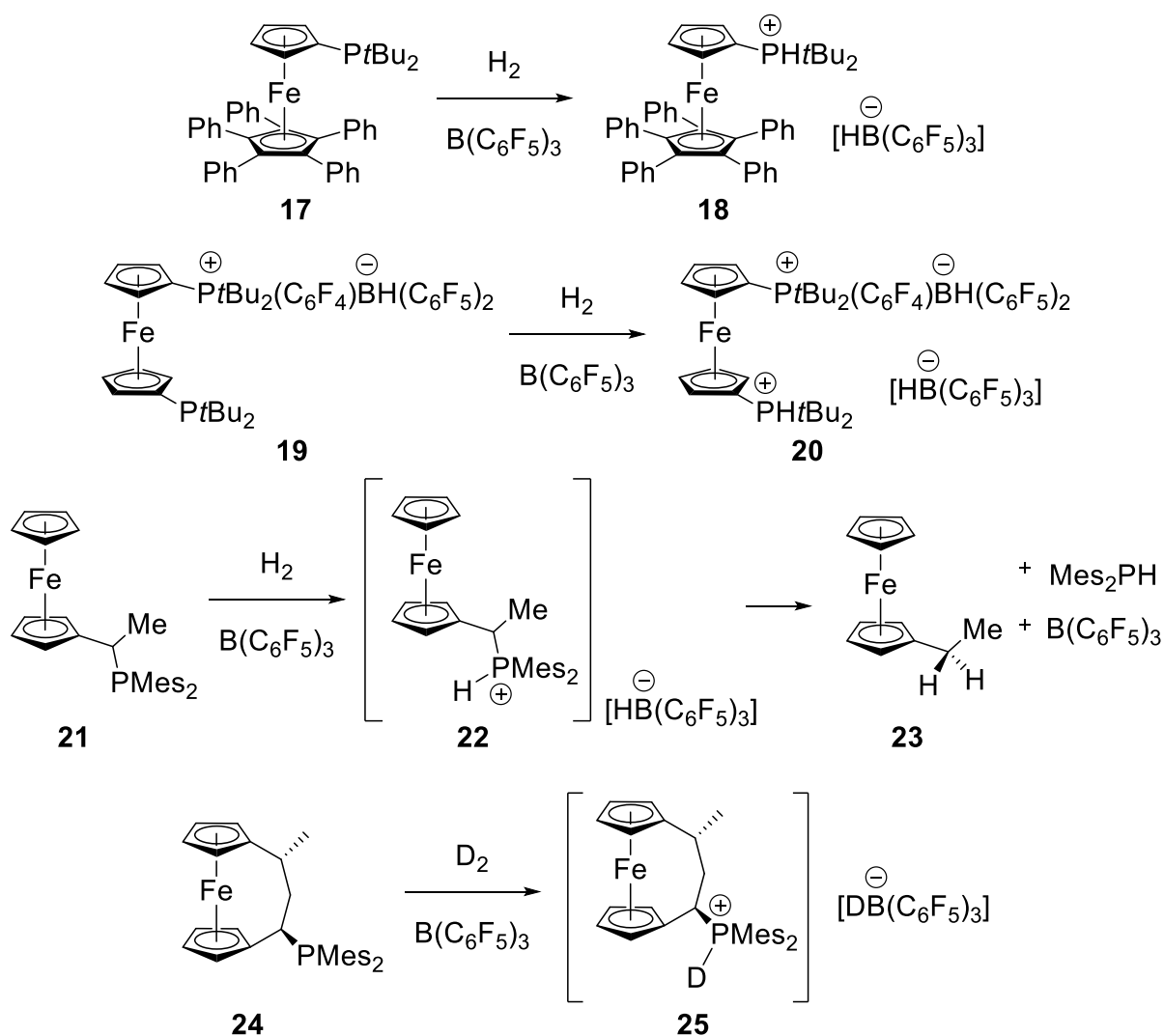
phosphines which slows upon cooling to low temperature. This salt regenerates H<sub>2</sub> when heated to 60°C.<sup>[19]</sup>



**Scheme 7:** Reversible H<sub>2</sub> binding by **15**

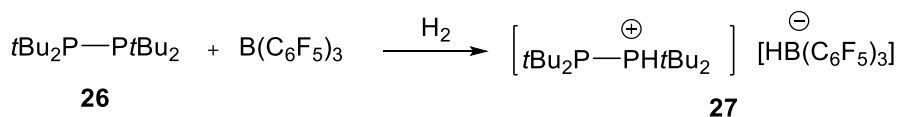
To evaluate the impact of phosphine substituents, the reactions of ferrocenyl phosphines in FLP chemistry was also studied.<sup>[20]</sup> For this purpose, Stephan *et al.* showed that mono and bis-ferrocenylphosphines derivatives ( $\eta^5\text{-C}_5\text{H}_4\text{PtBu}_2$ )Fe(C<sub>5</sub>Ph<sub>5</sub>) **17** and ( $\eta^5\text{-C}_5\text{H}_4\text{PtBu}_2(\text{C}_6\text{F}_4)\text{BH}(\text{C}_6\text{F}_5)_2$ )Fe( $\eta^5\text{-C}_5\text{H}_4\text{PtBu}_2$ ) **19** react with dihydrogen when combined to B(C<sub>6</sub>F<sub>5</sub>)<sub>3</sub> to give the respective phosphonium borate salts **18** and **20** (Scheme 8). In the same fashion, Erker showed that ferrocene-phosphine derivative CpFe(C<sub>5</sub>H<sub>4</sub>CHMePMes<sub>2</sub>) **21** react with B(C<sub>6</sub>F<sub>5</sub>)<sub>3</sub> and H<sub>2</sub> to generate the corresponding phosphonium borate **22**. However, it further reacted by eliminating the borane adduct (Mes<sub>2</sub>PH)B(C<sub>6</sub>F<sub>5</sub>)<sub>3</sub> and transferring the hydride to the ferrocenyl species yielding CpFe(C<sub>5</sub>H<sub>4</sub>CH<sub>2</sub>Me) **23** (Scheme 8).<sup>[21,22]</sup> The related [3]ferrocenophane system **24**<sup>[22]</sup> reacts analogously with B(C<sub>6</sub>F<sub>5</sub>)<sub>3</sub> and D<sub>2</sub> to afford the organometallic phosphonium/hydridoborate salt **25** (Scheme 8).





**Scheme 8:** Phosphino-ferrocenes in FLP activation of dihydrogen

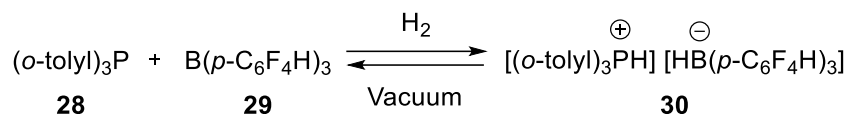
Interestingly, the diphosphine  $t\text{Bu}_4\text{P}_2$  in combination with  $\text{B}(\text{C}_6\text{F}_5)_3$  have also been reported to activate dihydrogen generating the salt  $[\text{tBu}_2\text{P}(\text{PHtBu}_2)]^+[\text{HB}(\text{C}_6\text{F}_5)_3]^-$  **27** (Scheme 9).<sup>[23]</sup>



**Scheme 9:** Reaction of the diphosphine  $t\text{Bu}_4\text{P}_2$  with  $\text{B}(\text{C}_6\text{F}_5)_3$  and  $\text{H}_2$ .

In 2009, Stephan<sup>[24,25]</sup> reported one of the first modification of the Lewis acid partner using  $\text{B}(\text{p-C}_6\text{F}_4\text{H})_3$  **29**. This borane has the benefit over  $\text{B}(\text{C}_6\text{F}_5)_3$  to not be prone to para-attack by Lewis bases which allows the use of a wider range of phosphines in the design of FLPs. Combining **29** with  $\text{PR}_3$  ( $\text{R} = t\text{Bu}, \text{Cy}, o\text{-tolyl}$ ) under an atmosphere of  $\text{H}_2$  at  $25^\circ\text{C}$  generates the phosphonium hydridoborate  $[\text{R}_3\text{PH}][\text{HB}(\text{p-C}_6\text{F}_4\text{H})_3]$  (Scheme 10). The salt  $[(o\text{-tolyl})_3\text{PH}][\text{HB}(\text{p-C}_6\text{F}_4\text{H})_3]$  **30** was found to slowly release  $\text{H}_2$  when exposed to vacuum at  $25^\circ\text{C}$ .<sup>[24,25]</sup> Indeed, the FLP was restored in 85% yield after 9 days in these conditions and the regeneration is complete in 12h at  $80^\circ\text{C}$  (Scheme 10). On the contrary, related FLP systems

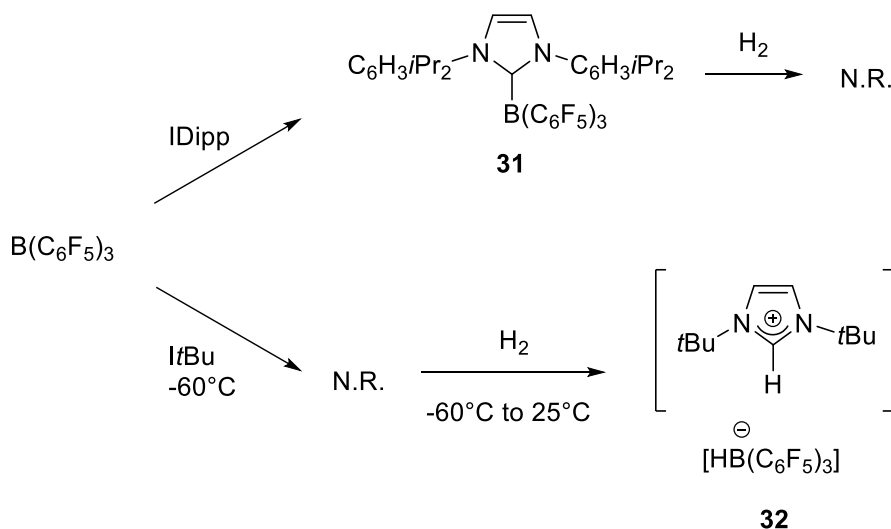
using  $B(C_6F_5)_3$  exhibit resistance to lose  $H_2$ . This property is attributed to the higher Lewis acidity of  $B(C_6F_5)_3$  compared to  $B(p-C_6F_4H)_3$ .



**Scheme 10:** Reactions of  $B(C_6F_4H)_3$  with phosphine and  $H_2$ .

ii. Carbene/Borane FLPs

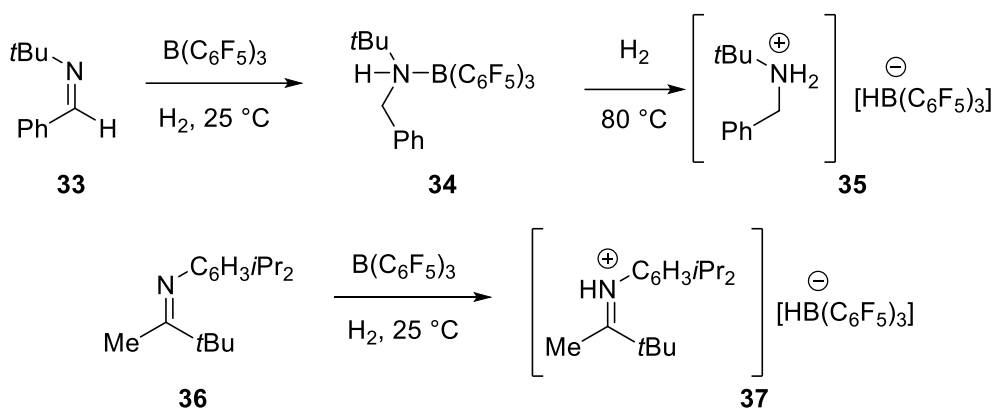
Bertrand *et al.*<sup>[26]</sup> showed that the activation of  $H_2$  can be performed using alkylamino-carbenes such as  $iPr_2NCtBu$  to afford the corresponding amine  $iPr_2NCH_2tBu$  because of the strong Lewis basicity and acidity localized at the carbene carbon. Interestingly, such behavior has not been observed while using N-heterocyclic carbenes (NHCs). Nonetheless, Stephan<sup>[27,28]</sup> and Tamm<sup>[29]</sup> described combinations of sterically demanding NHCs with  $B(C_6F_5)_3$  able to perform the FLP activation of dihydrogen. Indeed, while  $B(C_6F_5)_3$  forms a strong adduct **31** with the NHC IDipp, it does not occur with the NHC  $ItBu$  at low temperature thus generating a FLP system which can heterolytically cleave  $H_2$  to give the related imidazolium hydridoborate,  $[ItBuH][HB(C_6F_5)_3]$  **32** (Scheme 11).



**Scheme 11:** Reactivity of  $B(C_6F_5)_3$  with the NHCs IDipp and  $ItBu$  with  $H_2$ , N.R. = no reaction.

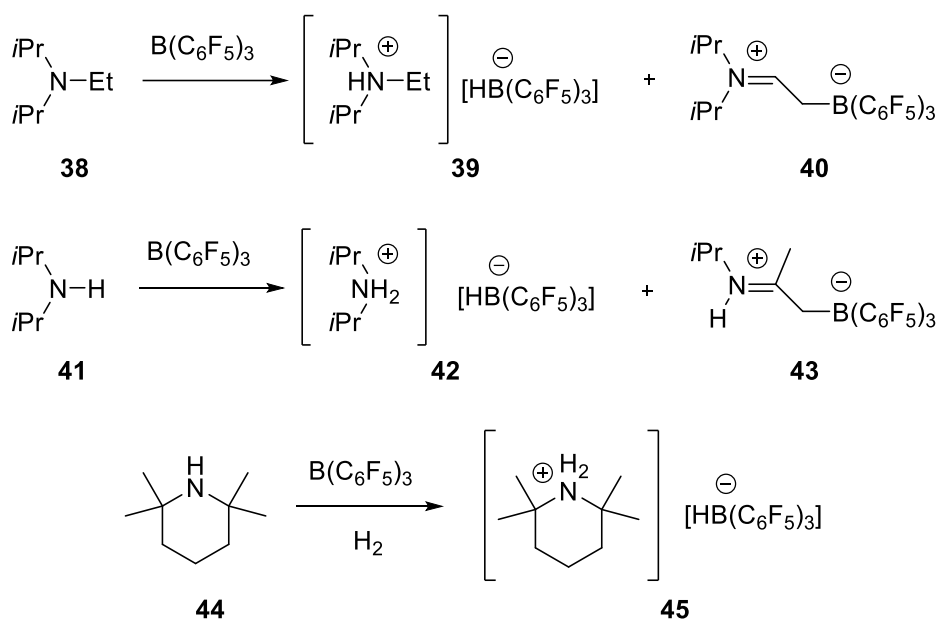
iii. Nitrogen bases/Borane FLPs

In 2008, Stephan showed that the imine  $t\text{BuN}=\text{CHPh}$  **33** reacts stoichiometrically with  $\text{B}(\text{C}_6\text{F}_5)_3$  and  $\text{H}_2$  to give the amine-borane adduct  $t\text{Bu}(\text{PhCH}_2)\text{NH}(\text{B}(\text{C}_6\text{F}_5)_3)$  **34** (Scheme 12).<sup>[30]</sup> The reaction is assumed to occur via an FLP heterolytic cleavage of  $\text{H}_2$  to afford an iminium hydridoborate followed by an hydride transfer to the iminium carbon yielding the amine-borane adduct. Further heating to  $80^\circ\text{C}$  for 1h under  $\text{H}_2$  (4-5 atm) leads to the thermal dissociation of the adduct and an additional heterolytic cleavage of dihydrogen to give  $[\text{tBuNH}_2(\text{CH}_2\text{Ph})][\text{HB}(\text{C}_6\text{F}_5)_3]$  **35** (Scheme 12). The corresponding reaction of the highly sterically hindered imine  $(\text{C}_6\text{H}_3\text{iPr}_2)\text{N}=\text{CMe}(t\text{Bu})$  **36** with  $\text{B}(\text{C}_6\text{F}_5)_3$  under  $\text{H}_2$  corroborate this hypothesis. Indeed, in this case, the steric hindrance prevents hydride transfer to the iminium carbon<sup>[30]</sup> and the dihydrogen activation gives the iminium salt  $[(\text{C}_6\text{H}_3\text{iPr}_2)\text{N}(\text{H})=\text{CMe}(t\text{Bu})][\text{HB}(\text{C}_6\text{F}_5)_3]$  **37** (Scheme 12).



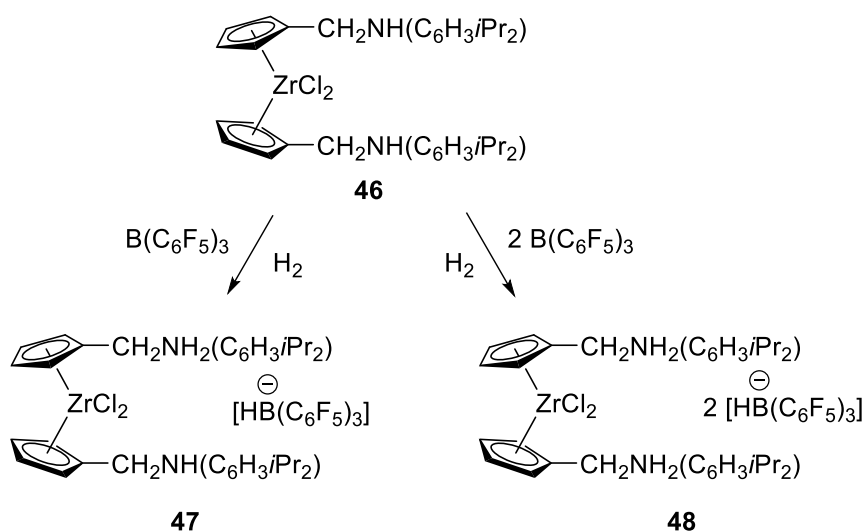
**Scheme 12:** Reactions of imines with  $\text{B}(\text{C}_6\text{F}_5)_3$  and  $\text{H}_2$ .

Furthermore, Rieger, Repo and co-workers<sup>[31]</sup> showed that the amine  $i\text{Pr}_2\text{NEt}$  reacts with  $\text{B}(\text{C}_6\text{F}_5)_3$  to give a 50:50 mixtures of the salts  $[i\text{Pr}_2\text{NHEt}][\text{HB}(\text{C}_6\text{F}_5)_3]$  **39** and  $i\text{Pr}_2\text{N}=\text{CHCH}_2\text{B}(\text{C}_6\text{F}_5)_3$  **40** while the corresponding reaction of  $i\text{Pr}_2\text{NH}$  gave  $[i\text{Pr}_2\text{NH}_2][\text{HB}(\text{C}_6\text{F}_5)_3]$  **42** and  $i\text{PrNH}=\text{C}(\text{CH}_3)(\text{CH}_2)\text{B}(\text{C}_6\text{F}_5)_3$  **43** (Scheme 13). Compounds **39** and **42** are generated by effective addition of dihydrogen whereas compounds **40** and **43** come from the dehydrogenation of the amine. However, reactions of  $i\text{Pr}_2\text{NH}$  or TMP with  $\text{B}(\text{C}_6\text{F}_5)_3$  and  $\text{H}_2$  generates the salts  $[i\text{Pr}_2\text{NH}_2][\text{HB}(\text{C}_6\text{F}_5)_3]$  **42** and  $[\text{TMPH}][\text{HB}(\text{C}_6\text{F}_5)_3]$  **45**, respectively (Scheme 13). The corresponding mixtures with  $\text{BPh}_3$  resulted in no reaction, inferring the Lewis acidity is a key factor although Rieger *et al.* suggested that  $\text{CF}-\text{HN}$  interactions between the amine and borane were necessary for activation of  $\text{H}_2$ .<sup>[31]</sup>

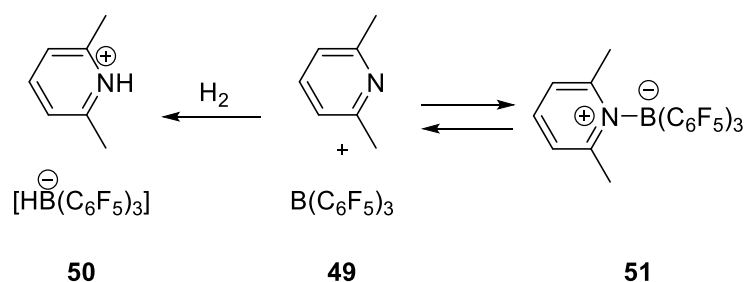


**Scheme 13:** Reactions of amines with  $\text{B}(\text{C}_6\text{F}_5)_3$  and  $\text{H}_2$ .

In the same fashion as the metallocene-phosphine derivatives described earlier, Erker *et al.* reported that the metallocene-amine derivative **46** in the presence of  $\text{B}(\text{C}_6\text{F}_5)_3$  react with  $\text{H}_2$  (2 bar, 25 °C) to give the salts **47** and **48** (Scheme 14).<sup>[32]</sup> It has been showed that pyridines form Lewis acid-base adduct with  $\text{B}(\text{C}_6\text{F}_5)_3$ ,<sup>[33,34]</sup> although the early report of Brown<sup>[2]</sup> revealed that steric hindrance prevent the formation of the Lewis adduct between  $\text{BMe}_3$  and 2,6-lutidine. Based on this statement, Stephan and co-workers studied the reaction between 2,6-lutidine and  $\text{B}(\text{C}_6\text{F}_5)_3$ . They showed that the free Lewis acid and base are in equilibrium with the corresponding Lewis adduct (2,6- $\text{Me}_2\text{C}_5\text{H}_3\text{N})\text{B}(\text{C}_6\text{F}_5)_3$  **51** (Scheme 15).<sup>[35,36]</sup>  $^{19}\text{F}$  NMR analysis demonstrated that the formation of the Lewis adduct is favored by low temperatures. The variable temperature data evaluate the  $\Delta\text{H}$  and the  $\Delta\text{S}$  for this equilibrium to be  $-42 \text{ kJ}\cdot\text{mol}^{-1}$  and  $-131 \text{ J}\cdot\text{mol}^{-1}\cdot\text{K}^{-1}$ , respectively. The reaction of this mixture with  $\text{H}_2$  (1 atm, 2 h) yielding the pyridinium salt  $[\text{2,6-Me}_2\text{C}_5\text{H}_3\text{NH}][\text{HB}(\text{C}_6\text{F}_5)_3]$  **50** proves that the free Lewis acid and base are accessible (Scheme 15).<sup>[35,36]</sup> This report evidence that classical Lewis acid-base adduct and the corresponding FLP are closely related and are not two completely exclusive reaction pathways, thus raising questions about potential unexplored reactivity of known Lewis acid-base adduct.



**Scheme 14:** Amino-borane reactions with H<sub>2</sub>.

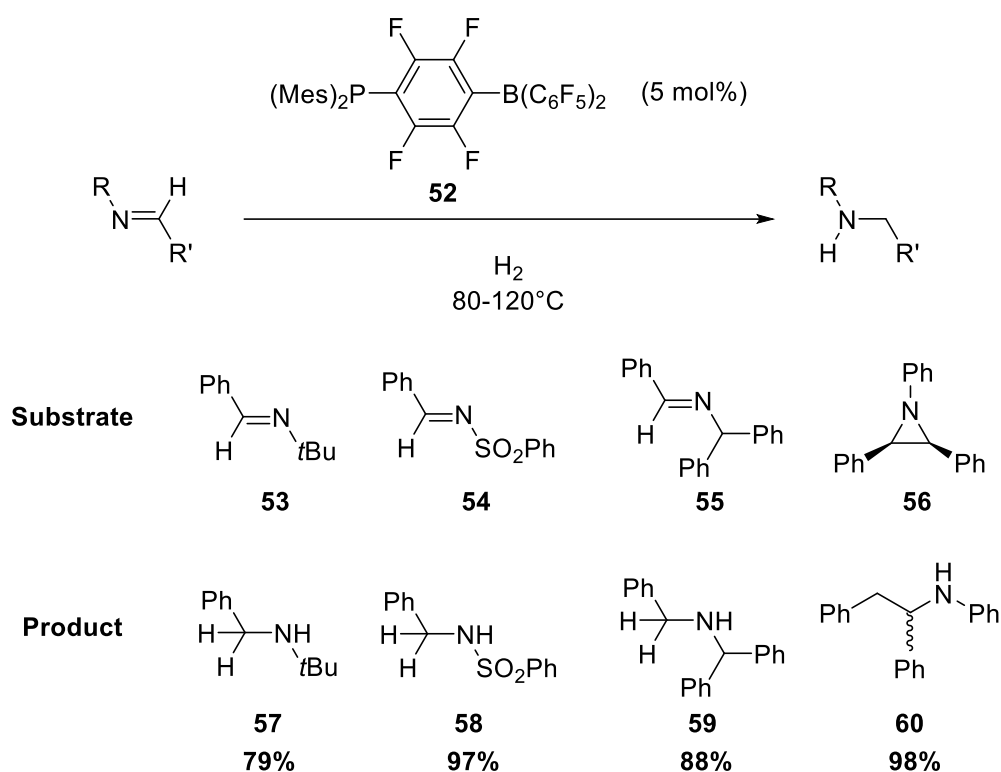


**Scheme 15:** Classical and FLP behavior of lutidine/B(C<sub>6</sub>F<sub>5</sub>)<sub>3</sub>.

### 3. Metal-free hydrogenation

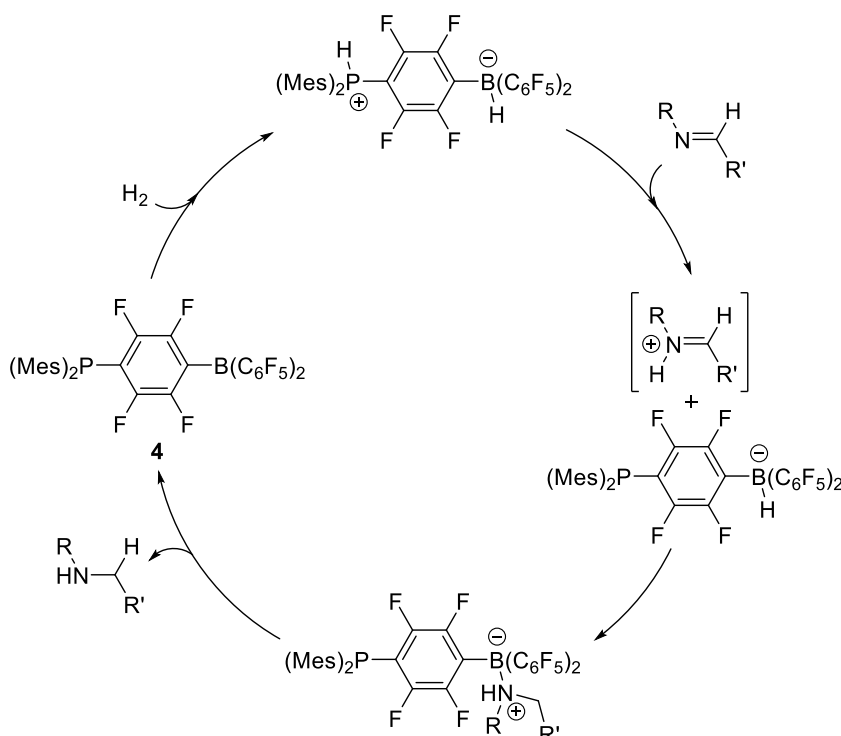
#### i. Catalytic hydrogenation by P/B FLP systems

The ability of many FLP systems to heterolytically cleave dihydrogen led to the development of various metal-free catalysts to perform hydrogenation reactions on a large panel of unsaturated substrates. However, to perform the hydrogenation in a catalytic fashion the proton and hydride transfer must occur with the regeneration of the frustrated Lewis pair. In this way the FLP would be available to cleave another molecule of dihydrogen and reduce another substrate molecule. With this in mind, a catalytic hydrogenation of aldimines was developed using catalyst **52** (Scheme 16). The hydrogenation of the imines and aziridine **53** to **56** was performed in high yields by heating a solution of the substrate and catalyst between 80 and 120°C under 1 to 5 atm of H<sub>2</sub> (Scheme 16).<sup>[37]</sup>



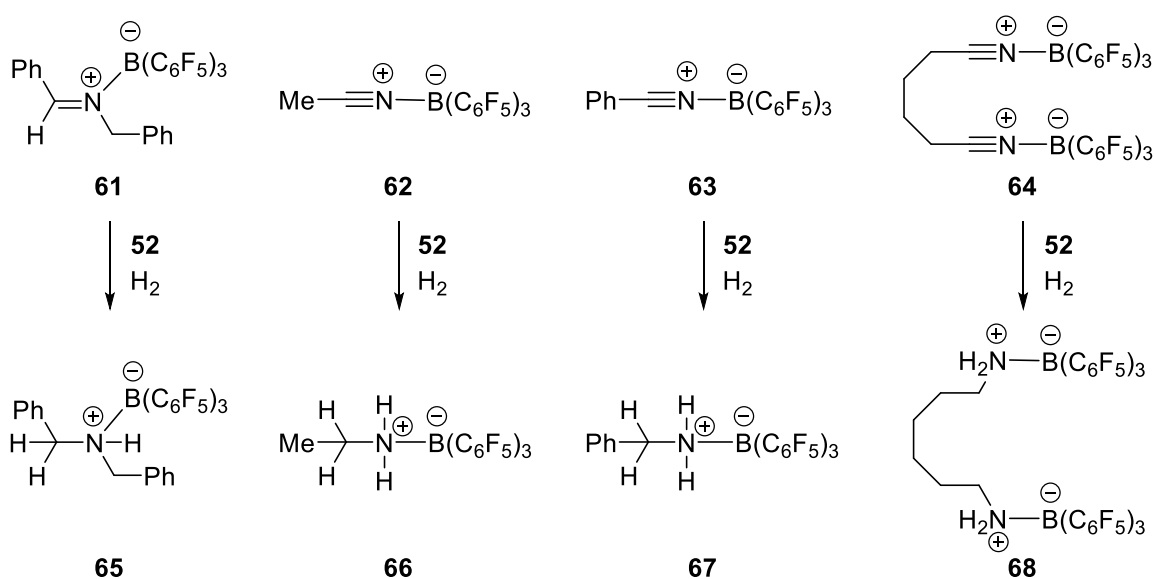
**Scheme 16:** Metal-free catalytic hydrogenation of imines and an aziridines.

The relative rates of imine reductions provided information on the mechanism of catalytic reduction. Indeed, the electron-rich imine **53** is reduced in one hour under 1 atm  $\text{H}_2$  pressure at  $80^\circ\text{C}$  while considerably longer times of reaction (10 to 16h) and higher temperature ( $120^\circ\text{C}$ ) are needed for the reduction of the electron poor imine **54**. As no adducts between these bulky imines (or the corresponding amines) and  $\text{B}(\text{C}_6\text{F}_5)_3$  are formed, it implies that the basicity of the N center determines the rate of reduction rather than the steric hindrance of the imine substituents. The reduction is thus initiated by proton transfer from the P atom to the N rather than by borohydride attack of the imine carbon center. Moreover, no reaction occurred when a 1:1 stoichiometric mixture of the phosphonium borate  $[\text{Cy}_3\text{P}(\text{C}_6\text{F}_4)]^+[\text{BH}(\text{C}_6\text{F}_5)_2]^-$  and imine **53** were heated to  $120^\circ\text{C}$  for 24h which confirms this hypothesis. The complete mechanism is shown in Scheme 17 and consists of a protonation of the imine followed by borohydride attack of the iminium salt intermediate.



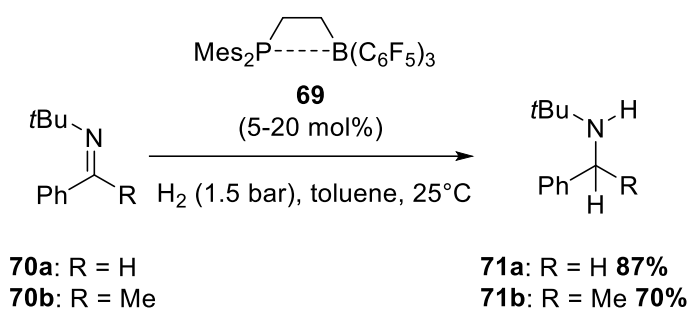
**Scheme 17:** Proposed mechanism for catalytic reduction of bulky imines via catalyst **52**.

However, the major drawback of this method was that less sterically hindered imines tend to form strong adducts with the borane moieties of the catalyst inhibiting the activation of  $\text{H}_2$ . To address this issue, Stephan *et al.* developed a procedure using imines or nitriles protected by  $\text{B}(\text{C}_6\text{F}_5)_3$ . Indeed, as  $\text{B}(\text{C}_6\text{F}_5)_3$  is a stronger Lewis acid than the borane from the catalyst, substrates do not form an adduct with the catalyst and the activation of  $\text{H}_2$  is then possible. Hence compounds **61-64** were reduced in the corresponding  $\text{B}(\text{C}_6\text{F}_5)_3$  protected amines **65-68** in reasonable yields via the phosphonium-borate catalyst **52** (Scheme 18).

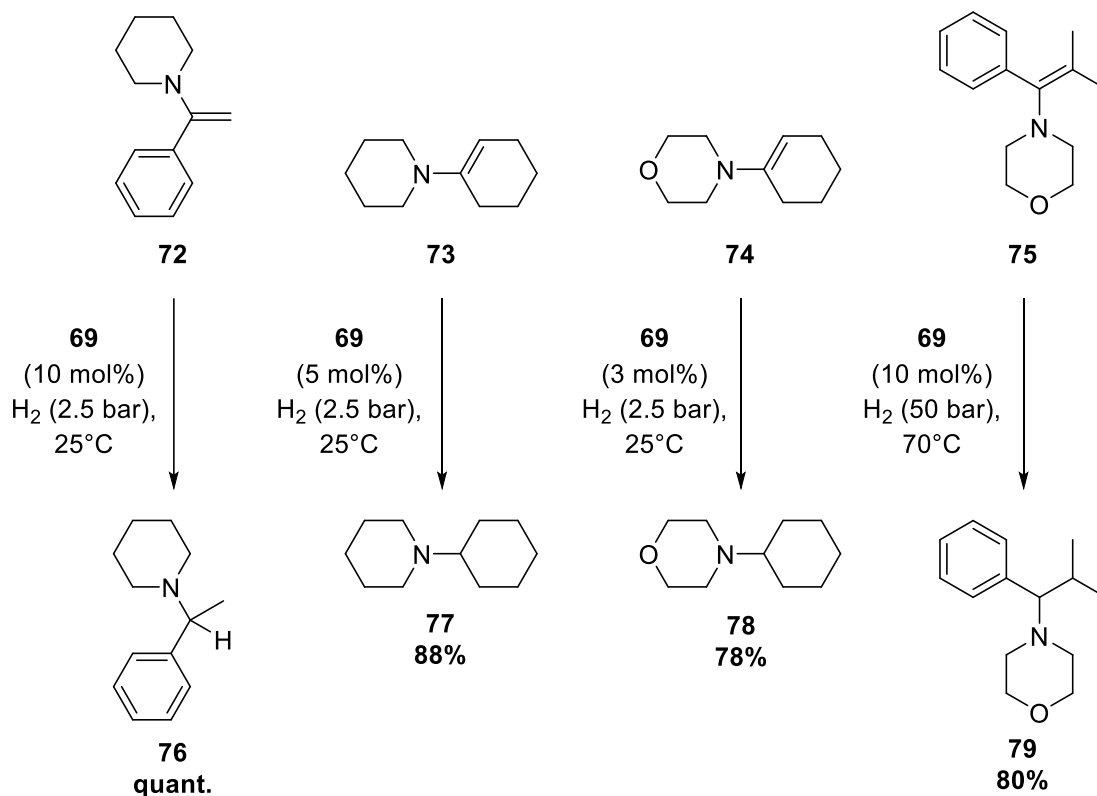


**Scheme 18:** Hydrogenation of protected imines and nitriles via FLP catalyst.

Based on these results, Erker *et al.* developed an even more active catalyst for the metal-free hydrogenation of imines which operates efficiently in mild conditions. Indeed, substituted ethylene-linked phosphine-borane **69** (20 mol%) catalyzes the hydrogenation of the aldimine **70a** with H<sub>2</sub> (2.5 bar) at room temperature in (87% yield of isolated product; Scheme 19). However only 5 mol% of catalyst are needed for the reduction of ketimine **70b** under mild conditions. Besides, the group of Erker reported that FLP catalyst **69** is also able to perform the hydrogenation of several enamines **72-74** to their corresponding tertiary amines **76-78** under very mild conditions. Nevertheless, hydrogenation of very bulky enamines such as **75** requires harsher conditions (Scheme 20).<sup>[38]</sup>



**Scheme 19:** Catalytic hydrogenation of imines under mild conditions using **69**.



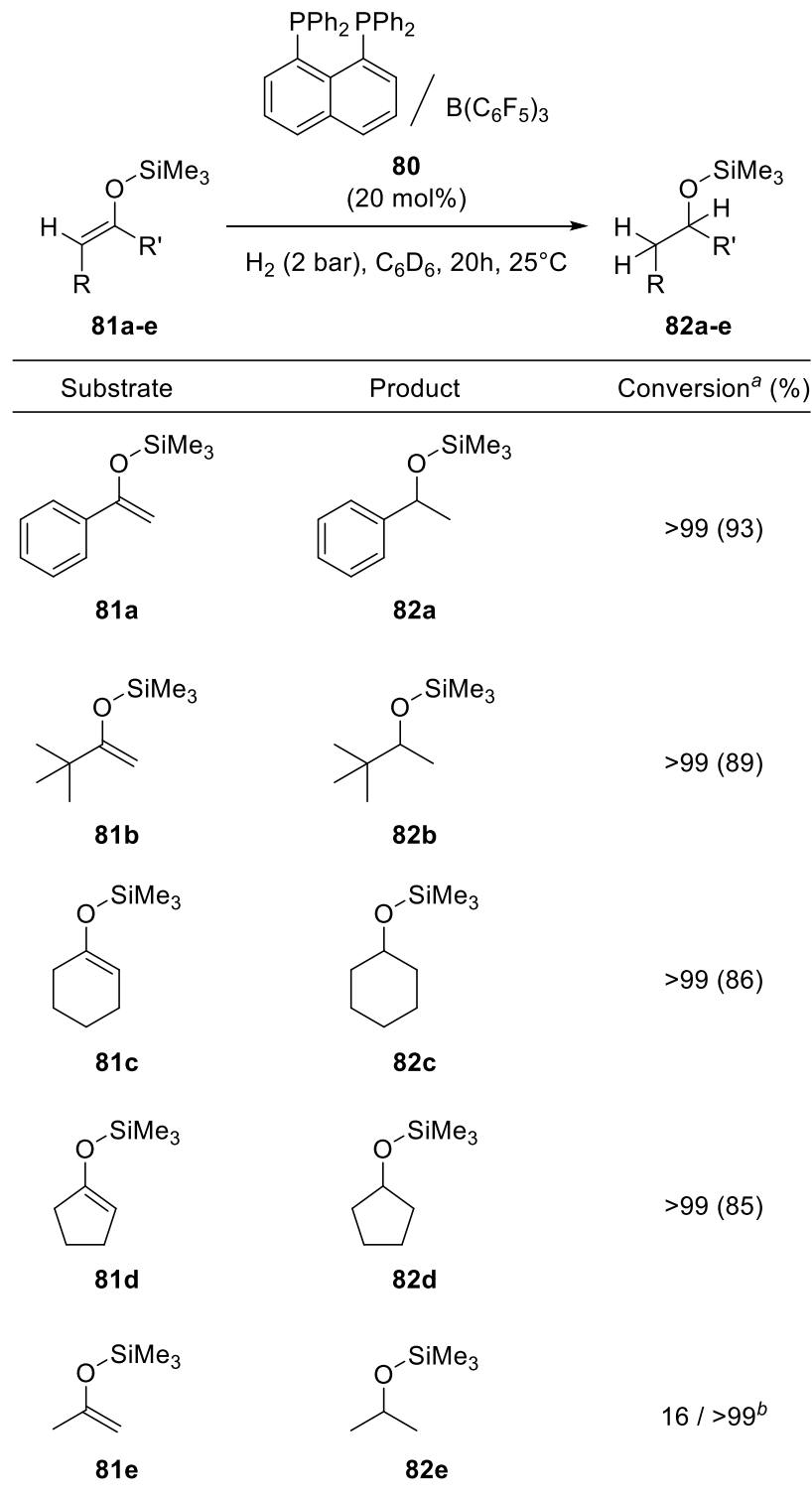
**Scheme 20:** Hydrogenation of enamines using metal-free FLP catalyst **69**.

Furthermore, Erker reported for the first time a metal-free intermolecular FLP system **80** that is able to catalyze the hydrogenation of silyl enoethers at room temperature with low pressure of H<sub>2</sub>.<sup>[19]</sup> For the substrates **81a-d** quantitative hydrogenation was achieved with a 20 mol% loading of catalyst system **80** under mild conditions (2 bar of H<sub>2</sub>, 25°C, 20h).



However, for the least sterically hindered silyl enoether **81e**, these conditions only afford close to stoichiometric conversion. Forcing the conditions at 60 bar of H<sub>2</sub> allowed to achieve complete conversion at room temperature though (Table 1).

**Table 1:** Hydrogenation of silyl enol ethers **81a-e** catalyzed by the FLP catalyst **80**.

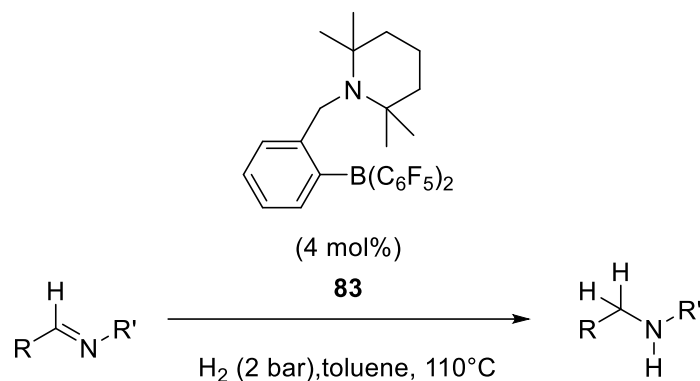


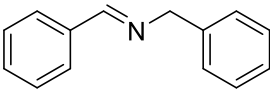
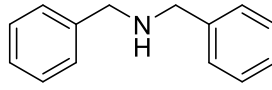
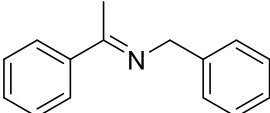
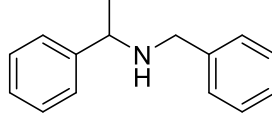
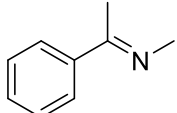
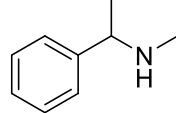
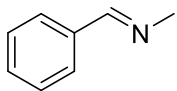
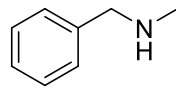
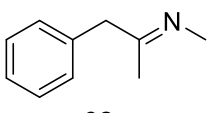
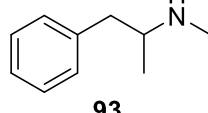
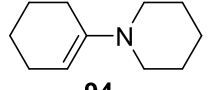
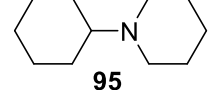
<sup>a</sup> Conversion was determined by <sup>1</sup>H NMR analysis and isolated yield are given in parentheses.

<sup>b</sup> 20 mol% of **80** in C<sub>6</sub>D<sub>6</sub> under 60 bar of H<sub>2</sub> at 25°C for 3h.

*ii. Catalytic hydrogenation by N/B FLP systems*

As their phosphorus analogs, trivalent nitrogen compounds are also Lewis bases. It is thus possible to conceive amine-borane frustrated Lewis pair systems. Indeed, the groups of Repo and Rieger developed an amine-borane catalyst **83** able to achieve the hydrogenation of imines and enamines (Table 2). They first investigated the reduction of the imine substrate PhCH<sub>2</sub>N=CPh(H) **84**. While previous metal-free catalysts have shown only stoichiometric reductions of this substrate,<sup>[30, 37, 39]</sup> performing the hydrogenation using catalyst **83** (4 mol%) in toluene at reflux for 24h under 2 bar of H<sub>2</sub> allowed a 51% conversion of imine to amine. Finally, increasing the catalyst loading to 8 mol% allowed to get nearly quantitative conversion in 12h (Table 2, entry 1). Performing the reaction again on bulky imines gave selective hydrogenation of the substrates in nearly quantitative yields (Table 2, entries 2-3). However mechanistic studies showed that not sterically hindered imines would inhibit the activation of dihydrogen by amine-borane adduct formation and thus lead to poor conversions (Table 2, entries 4-5). Furthermore, the cyclohexanone piperidine enamine was hydrogenated to N-cyclohexylpiperidine in good yield (Table 2, entry 6).

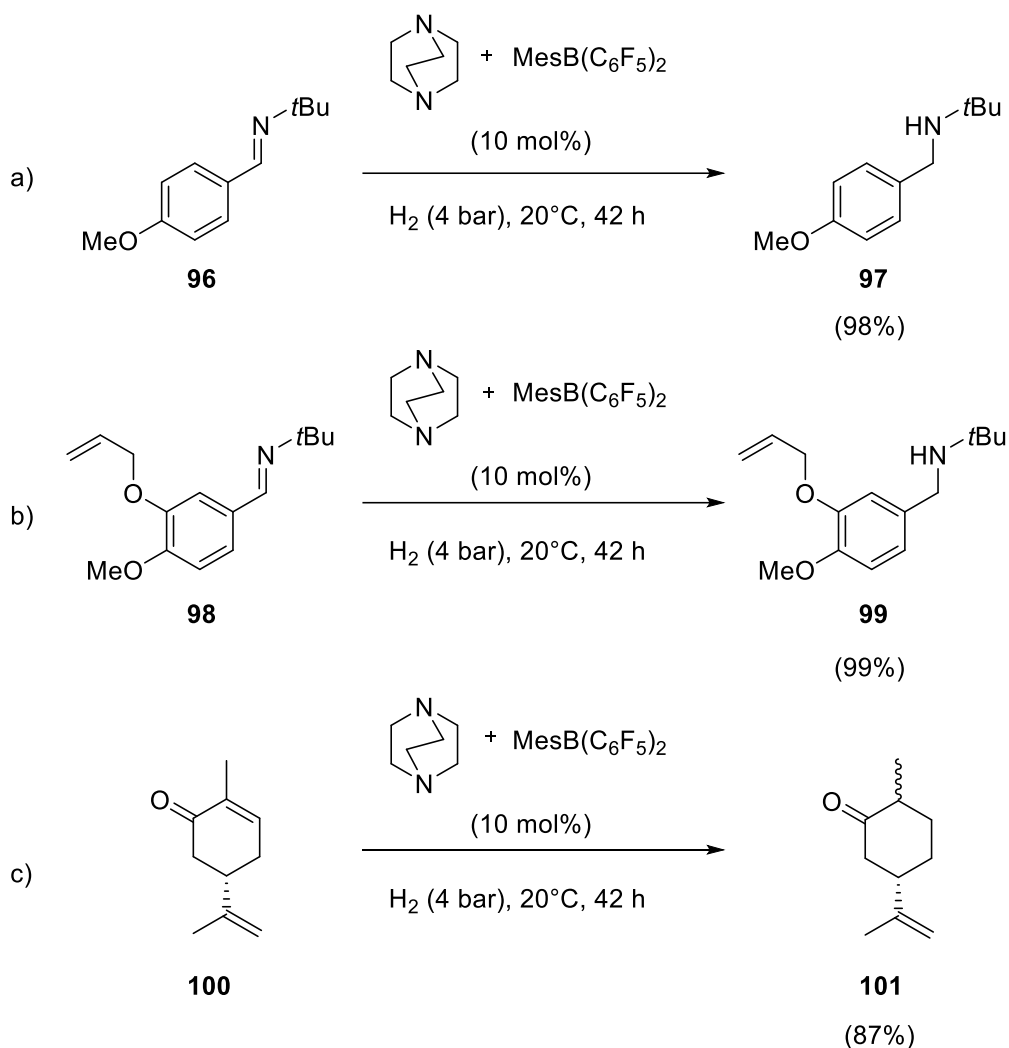
**Table 2:** Hydrogenation of imines via B/N FLP catalyst.

Entry	Substrate	Time (h)	Product	Yield (%) <sup>a</sup>
1	 <b>84</b>	12	 <b>85</b>	99 <sup>b</sup>
2	 <b>86</b>	6	 <b>87</b>	99
3	 <b>88</b>	12	 <b>89</b>	99
4	 <b>90</b>	24	 <b>91</b>	4
5	 <b>92</b>	24	 <b>93</b>	4
6	 <b>94</b>	12	 <b>95</b>	85

<sup>a</sup> Determined by <sup>1</sup>H NMR spectroscopy. <sup>b</sup> Catalyst **83** loading of 8 mol%

Soós and his coworkers reported that the electronically moderated boron Lewis acid (C<sub>6</sub>H<sub>2</sub>Me<sub>3</sub>)B(C<sub>6</sub>F<sub>5</sub>)<sub>2</sub> is able to perform catalytic hydrogenation of imines in the presence of bulky tertiary amines, such as DABCO, under mild reaction conditions (Scheme 21a).<sup>[40]</sup> The major benefit of this sterically fine-tuned frustrated Lewis pair system was displayed on the hydrogenation of multifunctional substrates (**98-100**). Indeed, in the case of the allyloxy derivative **98** reduction, two undesired reactivities were evaded: neither the cleavage of the allyl group nor the FLP addition to the double bond occurred (Scheme 21b). Furthermore,

this FLP system performed the selective reduction of the activated olefin of the carvone **100** to afford dihydrocarvone **101** in good yield without olefin migration or terminal olefin saturation (Scheme 21c).

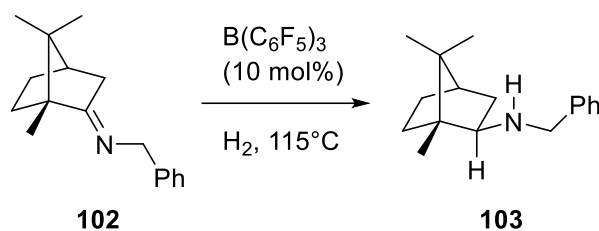


**Scheme 21:** Hydrogenation of selected substrates to evaluate functional group tolerance and chemoselectivity

### iii. Asymmetric hydrogenation

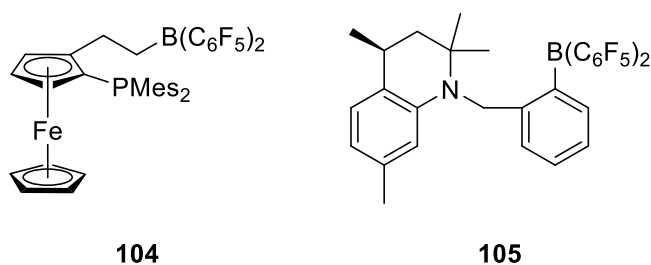
Although asymmetric hydrogenation with transition-metal complexes has been of substantial synthetic importance,<sup>[41,42]</sup> asymmetric catalysis via FLP systems is still in its early days. However, such developments could find useful applications in fields where noble metal contaminations are prohibitive such as pharmaceutical synthesis. Diastereoselective reactions have first been reported by Stephan *et al.*<sup>[43]</sup> Several chiral imines were hydrogenated using  $\text{B(C}_6\text{F}_5)_3$  as bulky Lewis acid partner. Poor diastereoselectivities were obtained when chiral moieties were carried by the nitrogen while imines with chiral auxiliaries on the carbon of the C=N unit led to very high asymmetric inductions (Scheme

22). This observation highlights the importance of sterical demand of the chiral moiety on selectivities.



**Scheme 22:** Diastereoselective hydrogenation

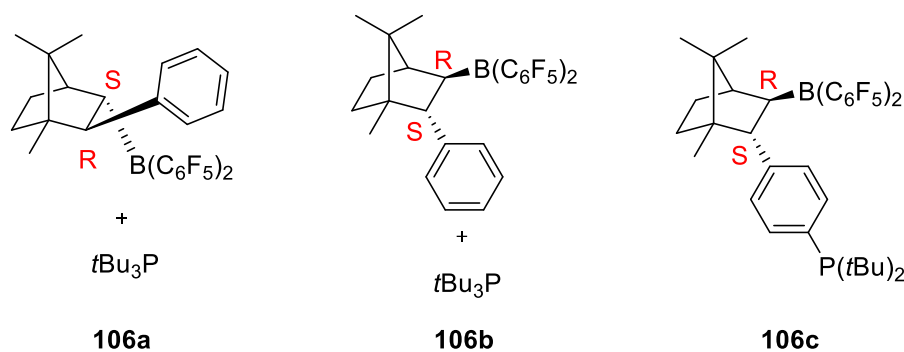
Erker *et al.* have developed the synthesis of the enantiomerically highly enriched chiral ferrocene derivative **104** bearing a sterically demanding borane/phosphine pair on one Cp ring (Scheme 11). They briefly tested this FLP catalyst in the already reported hydrogenation of selected imines and enamines examples. In most cases, the substrates were hydrogenated using 5 to 20 mol% of the catalyst but only rather moderate *ee* values were obtained (max. 26%).<sup>[44]</sup> Repo *et al.*<sup>[45]</sup> reported similar catalytic hydrogenations of imines and a 2-substituted quinoline using the intramolecular N/B FLP catalyst **105** (Scheme 23) achieving up to 37% *ee*.



**Scheme 23:** Chiral FLPs **104** and **105**.

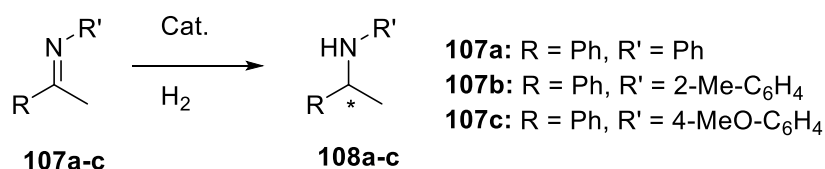
Afterwards, the group of Klankermayer brought a major contribution to this area with the development of chiral frustrated Lewis pair catalysts based on the camphor scaffolds **106a-b** (Scheme 24).<sup>[46]</sup> Indeed, they showed that a 1:1 mixture of **106a** and **106b** in 5 mol% was able to achieve the hydrogenation of N-(1-phenylethylidene)aniline **107a** in the secondary amine **108a** in quantitative yield with an enantioselectivity of 20% *ee* (S enantiomer; Table 3, entry 1). Using diastereomerically pure catalysts **106a** and **106b** gave even better results: full conversion into the S product in 48% *ee* with **106a** (Table 3, entry 2) while **106b** led to the full conversion into R product in 79% *ee* (Table 3, entry 3). This observation could be explain by the fact that dihydrogen splitting is faster with the FLP **106a** than with **106b** thus making the FLP **106a** more active in the catalytic hydrogenation. Moreover, a large panel of imine derivatives were tested to assess the scope of the reaction. The studies emphasized that increasing the bulkiness of the substrate induces low yields (Table 3, entry 4) while adding an electron donating group, such as -OMe, to one of the phenyl rings enhances conversion and selectivity (Table 3, entry 5). Besides, the derived catalyst **106c** was synthesized in several steps from camphor and was tested in the

enantioselective hydrogenation of a series of bulky prochiral imines. The respective secondary amines were consistently obtained with approximately 70% *ee*.<sup>[47]</sup>



**Scheme 24:** Chiral FLP catalysts developed by Klankermayer *et al.*

**Table 3:** Enantioselective hydrogenation of imines catalyzed by chiral FLP.



Entry <sup>a</sup>	Substrate	Catalyst	Yield (%) <sup>c</sup>	<i>ee</i> (%) <sup>d</sup>
1	<b>107a</b>	<b>106a/106b</b> = 1:1	>99	20 (S)
2	<b>107a</b>	<b>106a</b>	>99	48 (S)
3	<b>107a</b>	<b>106b</b>	95	79 (R)
4 <sup>b</sup>	<b>107b</b>	<b>106b</b>	37	74 (-)
5	<b>107c</b>	<b>106b</b>	>99	81 (R)

<sup>a</sup> Reaction conditions: Cat. (5 mol%), H<sub>2</sub> (25 bar), T=65°C, 15h

<sup>b</sup> Reaction time: 20h

<sup>c</sup> Determined by <sup>1</sup>H NMR analysis

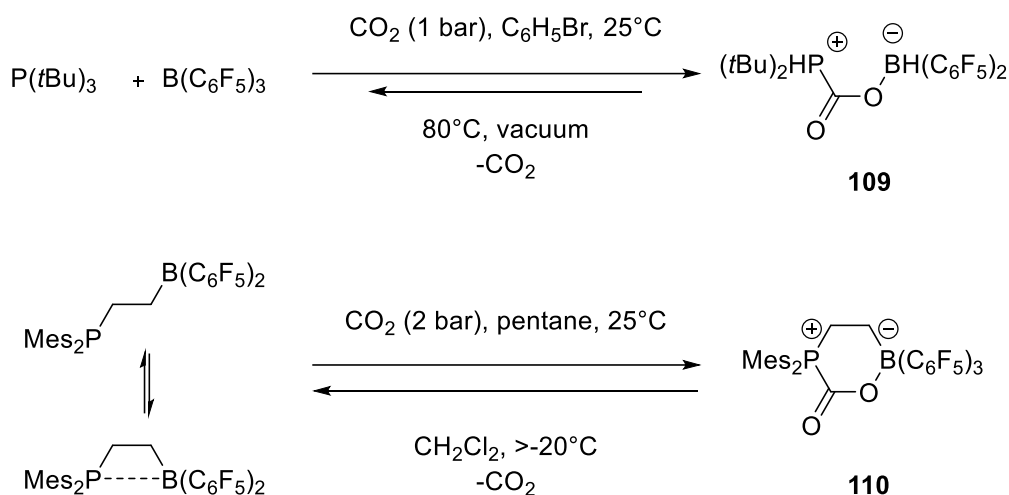
<sup>d</sup> Determined by HPLC or GC methods using a chiral column; absolute configurations assigned by comparison of retention times and optical rotations with literature values

### III. Frustrated Lewis pair reactivity with small molecules

#### 1. Capture of CO<sub>2</sub>, SO<sub>2</sub> and N<sub>2</sub>O

##### i. Capture of CO<sub>2</sub>

Erker and Stephan were the first to report the capture of CO<sub>2</sub> by inter- and intramolecular FLP systems in 2009.<sup>[48]</sup> The resulting adduct *t*Bu<sub>3</sub>PCO<sub>2</sub>B(C<sub>6</sub>F<sub>5</sub>)<sub>3</sub> **109** was shown to liberate about 50% of the CO<sub>2</sub> upon heating at 80°C under vacuum for 5h. On the contrary, the adduct Mes<sub>2</sub>P(CH<sub>2</sub>)<sub>2</sub>B(C<sub>6</sub>F<sub>5</sub>)<sub>2</sub>(CO<sub>2</sub>) **110** rapidly released carbon dioxide in dichloromethane or toluene above -20°C (Scheme 25). These observations were consistent with the calculated reaction energies for the release of CO<sub>2</sub>, 35 kcal.mol<sup>-1</sup> and 18 kcal.mol<sup>-1</sup> respectively.



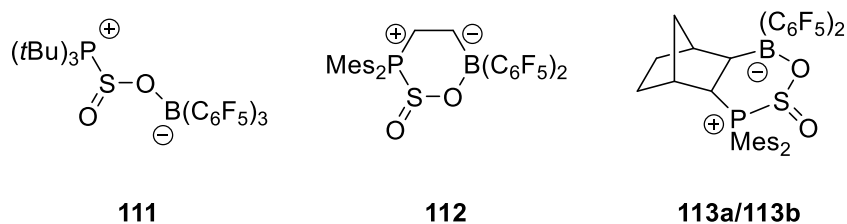
**Scheme 25:** Reversible CO<sub>2</sub> uptake and release by frustrated phosphine-borane Lewis pairs.

Eventually, a large range of intermolecular FLP systems, in which either the borane Lewis acid or the phosphine Lewis base were modified, were synthesized and tested for CO<sub>2</sub> capture.<sup>[49,50]</sup> Besides, the phosphine can be replaced by amines<sup>[51]</sup> or N-heterocyclic carbenes (NHCs).<sup>[52]</sup> In the same fashion, boranes can be traded for aluminium-based Lewis acids.<sup>[53]</sup> Binding of CO<sub>2</sub> by intramolecular FLPs has also been investigated.<sup>[54,55,56,57,58]</sup>

##### ii. Capture of SO<sub>2</sub>

FLPs have been reported to analogously bind to SO<sub>2</sub>. Indeed, Erker *et al.* achieved the formation inter- and intramolecular FLP adducts *t*Bu<sub>3</sub>PSO<sub>2</sub>B(C<sub>6</sub>F<sub>5</sub>)<sub>3</sub> **111** and Mes<sub>2</sub>P(CH<sub>2</sub>)<sub>2</sub>B(C<sub>6</sub>F<sub>5</sub>)<sub>2</sub>(SO<sub>2</sub>) **112** (Scheme 14).<sup>[59]</sup> Although SO<sub>2</sub> connects to FLPs in a similar way than CO<sub>2</sub>, these adducts display a pseudo-pyramidal geometry and thus a stereogenic center at the S atom. Derivatives bearing substituents on the intramolecular FLP are also accessible

and thus the related reaction with the norbornene-linked FLP gave a mixture of diastereomers **113a-b** in a 5:2 ratio (Scheme 26).<sup>[60]</sup>

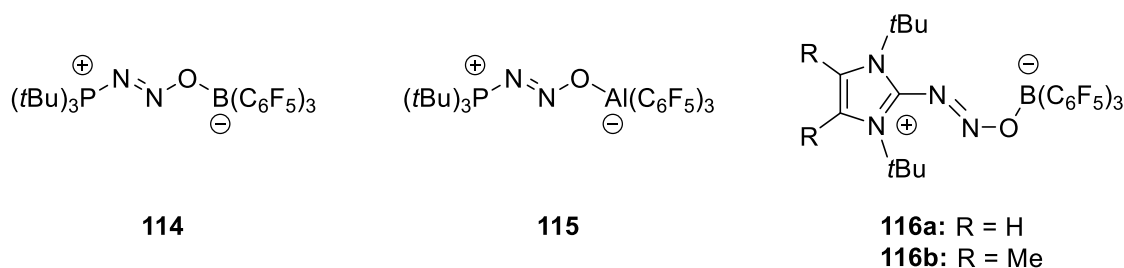


**Scheme 26:** Examples of FLP/SO<sub>2</sub> adducts.

### iii. Capture of N<sub>2</sub>O

Intermolecular FLP systems have also been used to capture N<sub>2</sub>O. The adduct **114** exhibits inequivalent N atoms which indicate a PNNOB linkage (Scheme 27). This observation was confirmed via crystallographic structure analysis.<sup>[61]</sup> The phosphine and OB(C<sub>6</sub>F<sub>5</sub>)<sub>3</sub> fragments are in *trans* in respect to the N=N bond, presumably as a result of steric hindrance. This geometry is consistent with the result that the use of smaller and less basic phosphine leads to easy oxidation of the phosphine and release of N<sub>2</sub>. The adduct **114** is stable but will liberate N<sub>2</sub> upon heating to 135°C for 2 days or on photolysis for 5 min, suggesting that the gas release require the isomerization of the N=N.

While carbenes react with N<sub>2</sub>O in the absence of borane to oxidize the carbene to the corresponding urea derivative,<sup>[62]</sup> their use in a FLP system allows to capture N<sub>2</sub>O intact. Indeed, Severin *et al.* achieved the capture of N<sub>2</sub>O affording the adducts **116a-b**.<sup>[52d]</sup>



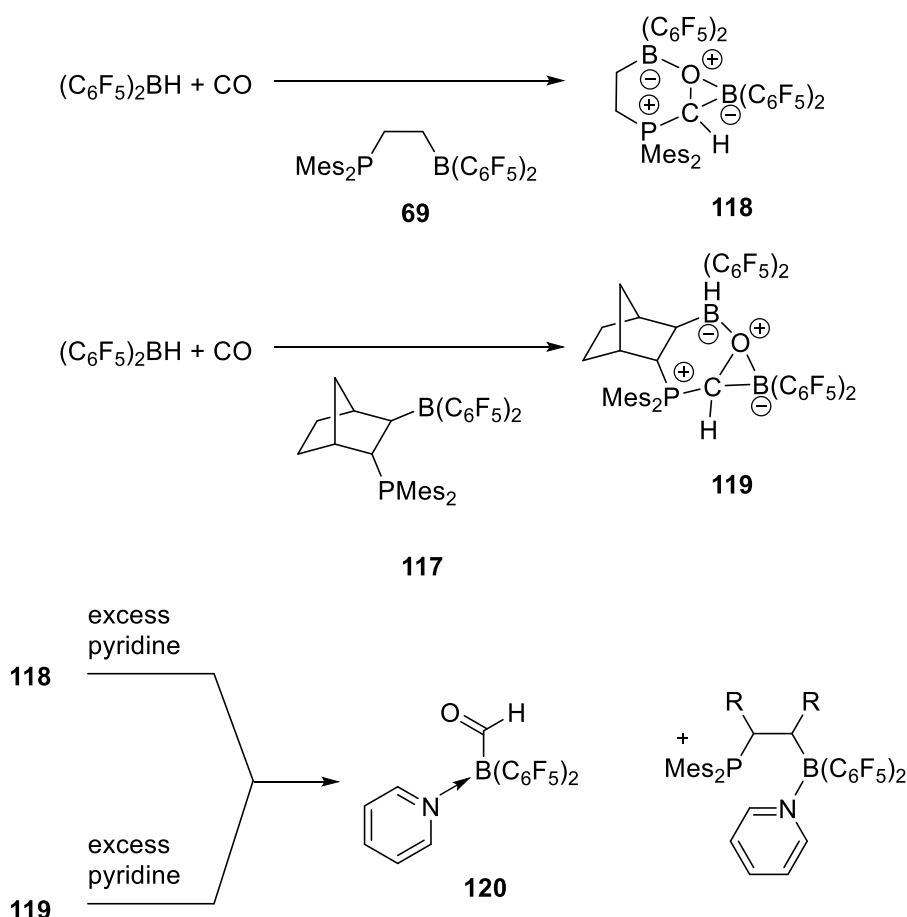
**Scheme 27:** Examples of FLP/N<sub>2</sub>O adducts.

## 2. CO and CO<sub>2</sub> reductions

### i. CO reduction

Boranes R<sub>2</sub>BH react with carbon monoxide to form the respective borane carbonyl R<sub>2</sub>BH(CO). However, these species do not rearrange to give a boron-bound formyl group because of the endothermicity of the reaction. Nevertheless, Erker *et al.*<sup>[63]</sup> reported that coupled to the FLP systems **69** and **117** for example, Piers borane HB(C<sub>6</sub>F<sub>5</sub>)<sub>2</sub> was able to perform the CO-hydroboration generating respectively “η<sup>2</sup>-formylboranes” **118** and **119** (Scheme 28).





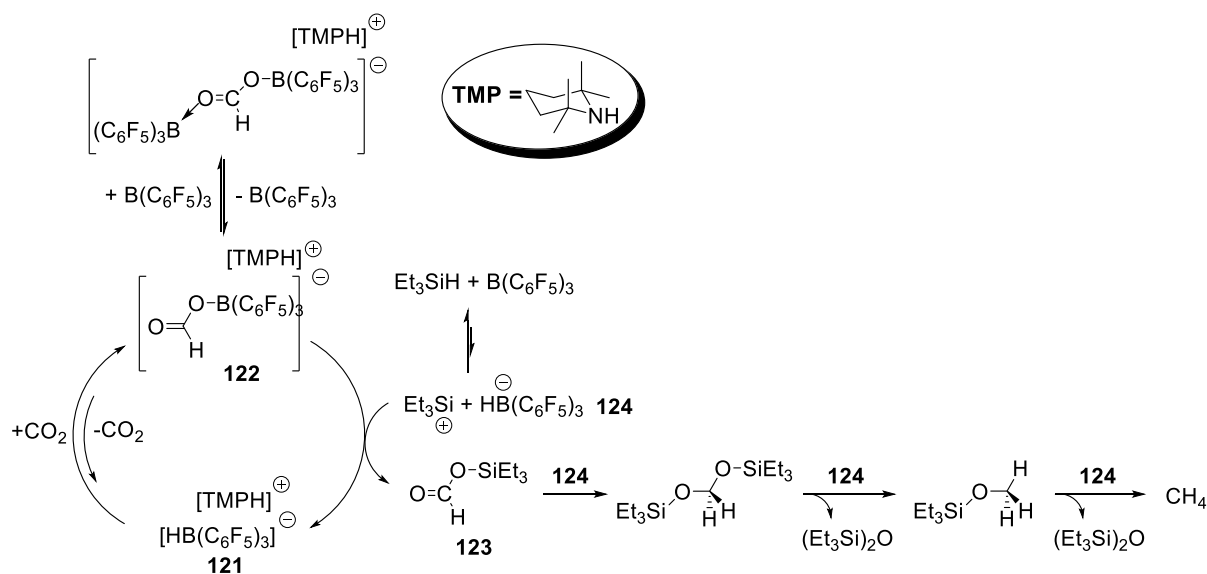
**Scheme 28:** Formation of the “ $\eta^2$ -formylboranes” **118** and **119** followed by pyridine treatment.

The formylborane moiety is then removed from the FLP scaffold after treatment with an excess of pyridine and the stable pyridine adduct **120** was isolated and analyzed by X-ray diffraction.

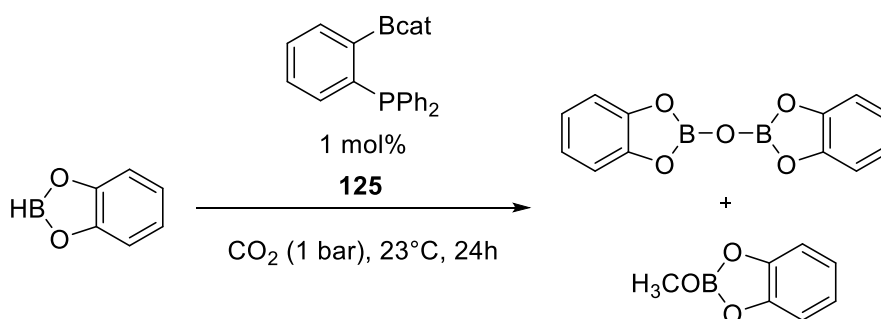
*ii. CO<sub>2</sub> reduction*

In 2009, O’Hare and Ashley<sup>[64]</sup> demonstrated that FLPs can achieve CO<sub>2</sub> reduction. Indeed, using a 1:1 mixture of the FLP tetramethylpiperidine (TMP)/B(C<sub>6</sub>F<sub>5</sub>)<sub>3</sub> under a H<sub>2</sub> atmosphere, CO<sub>2</sub> was quantitatively converted into CH<sub>3</sub>OB(C<sub>6</sub>F<sub>5</sub>)<sub>2</sub> after 6 days at 160°C and indeed methanol was actually isolated in 17-25% yield. Then, Piers<sup>[65]</sup> developed the hydrosilylation of CO<sub>2</sub> via the (TMP)/B(C<sub>6</sub>F<sub>5</sub>)<sub>3</sub> FLP system. Under treatment with H<sub>2</sub>, the FLP was reported to form the ammonium hydridoborate ion pair **121** which reacts with CO<sub>2</sub> (2-4 bar) in the presence of triethylsilane to afford formatoborate **122** via hydride transfer (Scheme 29). Excess of B(C<sub>6</sub>F<sub>5</sub>)<sub>3</sub> and Et<sub>3</sub>SiH then induce rapid hydrosilylation of formatoborane into formatosilane **123** and regenerate [TMPH]<sup>+</sup>[HB(C<sub>6</sub>F<sub>5</sub>)<sub>3</sub>]<sup>-</sup>. Formatosilane **123** is then hydrosilylated by the B(C<sub>6</sub>F<sub>5</sub>)<sub>3</sub>/Et<sub>3</sub>SiH system to methane with (Et<sub>3</sub>Si)<sub>2</sub>O as the byproduct. Besides, subsequent addition of more CO<sub>2</sub>/Et<sub>3</sub>SiH resulted in resumed hydrosilylation

demonstrating that this is a robust, living tandem catalytic system for the deoxygenative reduction of CO<sub>2</sub> to methane.



More recently, Fontaine *et al.*<sup>[66]</sup> achieved the reduction of CO<sub>2</sub> in the presence of HBpin employing 1 mol% of the P/B FLP catalyst **125**. The reaction afforded MeOBpin and O(Bpin)<sub>2</sub> with a turnover frequency (TOF) of 973 h<sup>-1</sup> and turnover numbers (TONs) of 2950 at 70°C (Scheme 30). They noted that no adducts was formed between CO<sub>2</sub> and the catalyst **125**. However, this weak interaction with CO<sub>2</sub> is a key aspect of this system to trigger reaction with boranes. Density functional theory studies revealed that coordination of CO<sub>2</sub> to **125** to generate the intermediate **IM1** is disfavored by 9.9 kcal.mol<sup>-1</sup>. Nevertheless, **IM1** can undergo addition of HBcat to afford **IM2** which is favored by 24.3 kcal.mol<sup>-1</sup> compared to **IM1**. The following addition of HBcat, which allows to form **IM3**, is also favored by 33.3 kcal.mol<sup>-1</sup>. Finally, the third reduction to regenerate the catalyst **125** and MeOBcat is an even more exothermic process (34.0 kcal.mol<sup>-1</sup>) (see Figure 1). This means than once the difficult coordination of CO<sub>2</sub> occurs, the reduction is thermodynamically highly favorable.



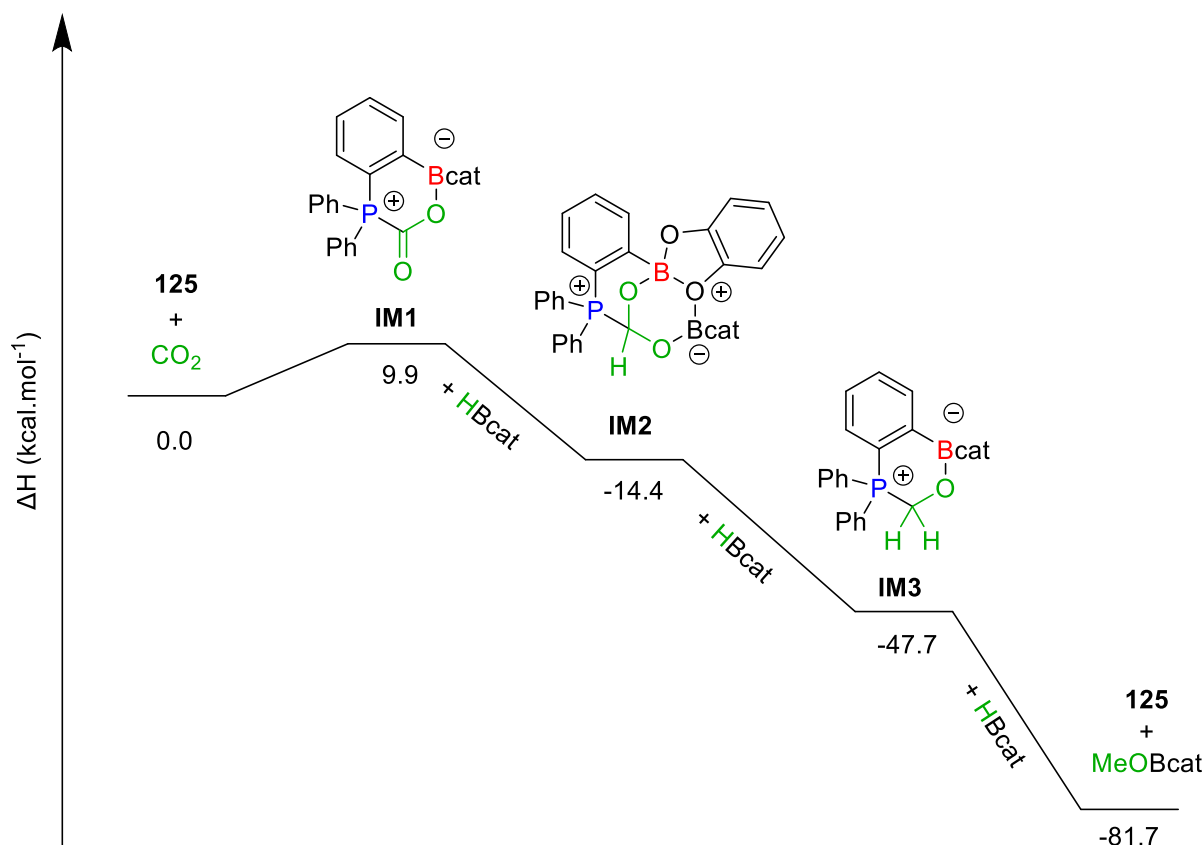
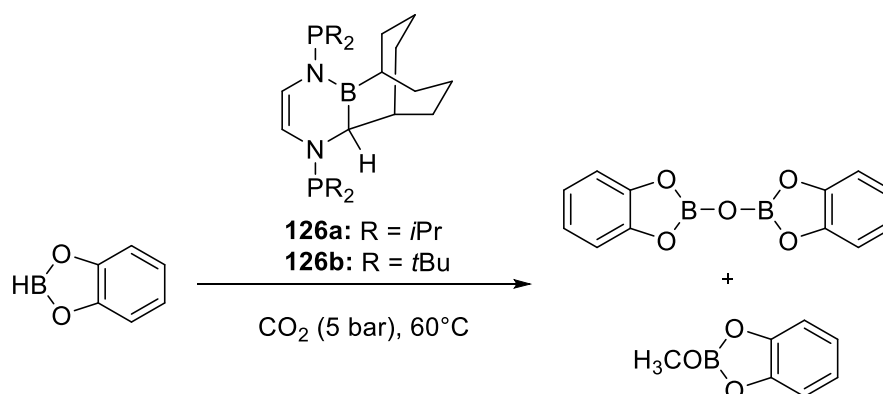


**Figure 1:** Enthalpy profile for the reduction of CO<sub>2</sub> using **125** and catecholborane.

More recently, Wang and Stephan reported the catalytic reduction of CO<sub>2</sub> in presence of boranes (HBpin, HBcat, and BH<sub>3</sub>.SMe<sub>2</sub>) using catalyst **126a-b** (Scheme 31). They also confirmed that a weak Lewis acidity provides lability to the reduced CO<sub>2</sub> fragment and thus facilitates catalytic turn-over.



**Scheme 31:** CO<sub>2</sub> reduction using catalyst **126a-b** and catecholborane.

Last year, Delarmelina *et al.*<sup>[67]</sup> described the first examples of xanthene based intramolecular phosphine-borane FLPs with potential to allow kinetically accessible H<sub>2</sub> cleavage and subsequent CO<sub>2</sub> hydrogenation processes under relatively mild reaction conditions. Indeed, they studied these processes via DFT calculations comparing the activities of xanthene-inspired scaffolds as backbones for intramolecular P/B FLPs, namely

9,9-dimethyl-xanthene **127**, tribenzo[b,d,f]oxepine **128**, naphtho[2,1,8,7-klmn]xanthene **129**, and benzo[kl]xanthene **130** (Figure 2a). These modifications to the parent xanthene scaffold allowed them to study the impact of the distance between the Lewis acid and the Lewis base as well as the rigidity of the backbone on the catalytic activity. Their calculations showed that increasing the P/B distance induces a slight increase in the dihydrogen activation energy but a significant reduction of the energy barrier for the CO<sub>2</sub> hydrogenation step. Moreover, they also demonstrated that a more rigid scaffold would also decrease the free energy barrier for the CO<sub>2</sub> reduction step. These observations have been evidenced thanks to the optimized structure of the stationary points along the potential energy surface (Figure 2b).

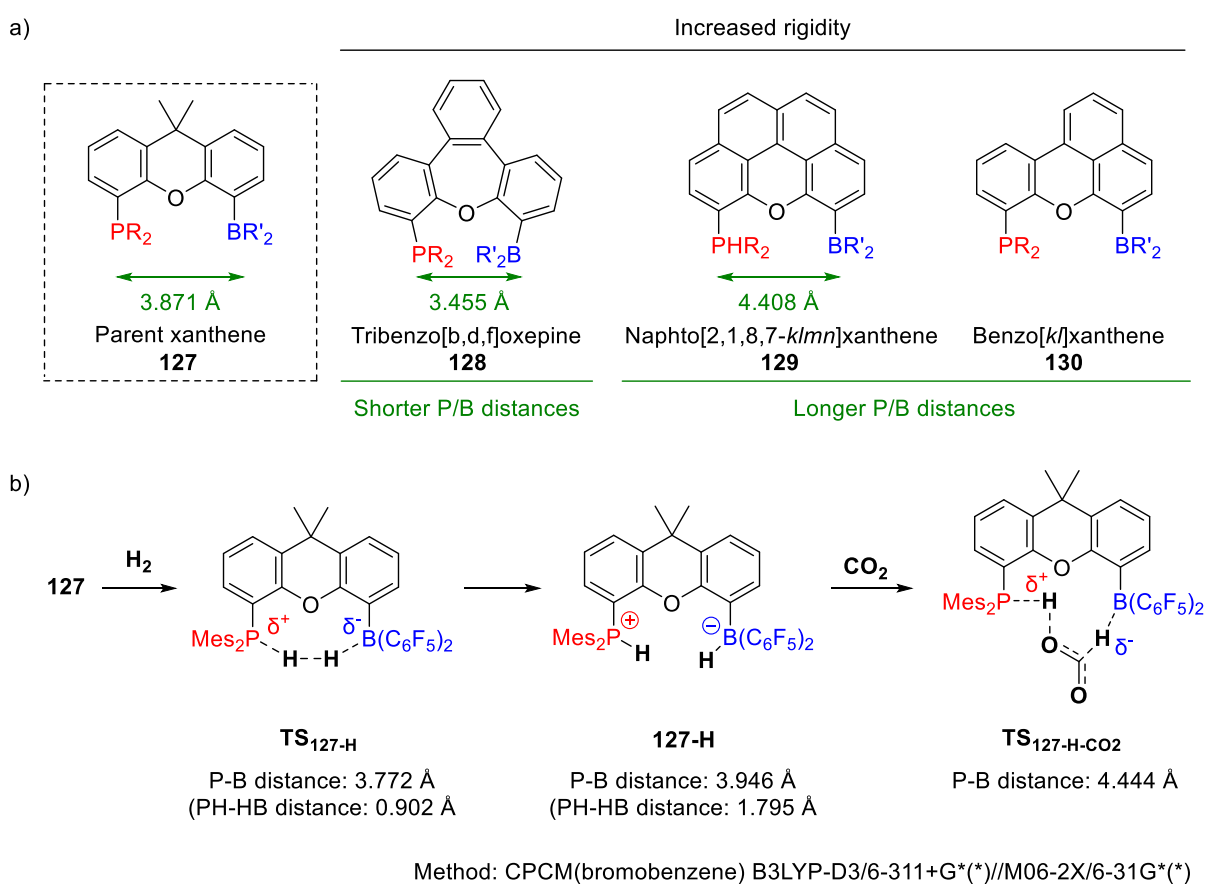


**Figure 2:** a) Proposed modifications of the xanthene-based backbone of P/B FLPs investigated by Delarmelina *et al.*, b) Optimized structures of stationary point along the PES.

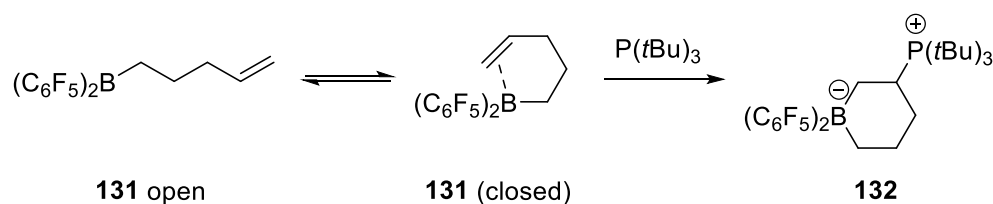
An underexplored polyaromatic scaffold is the helicene motif, which will be the focus of the third chapter of this PhD thesis.

## IV. FLP addition reactions on double and triple bonds

As reported in the literature, FLPs can bind alkenes<sup>[68]</sup> and alkynes<sup>[69]</sup> in stoichiometric additions providing zwitterionic phosphonium borates. This reactivity has been exploited in various new stoichiometric reactions and more recently adapted to catalytic reactions. More reactions have also been investigated such as ring opening reactions to extend the chemistry of FLPs and discover potential new synthetic utilities.

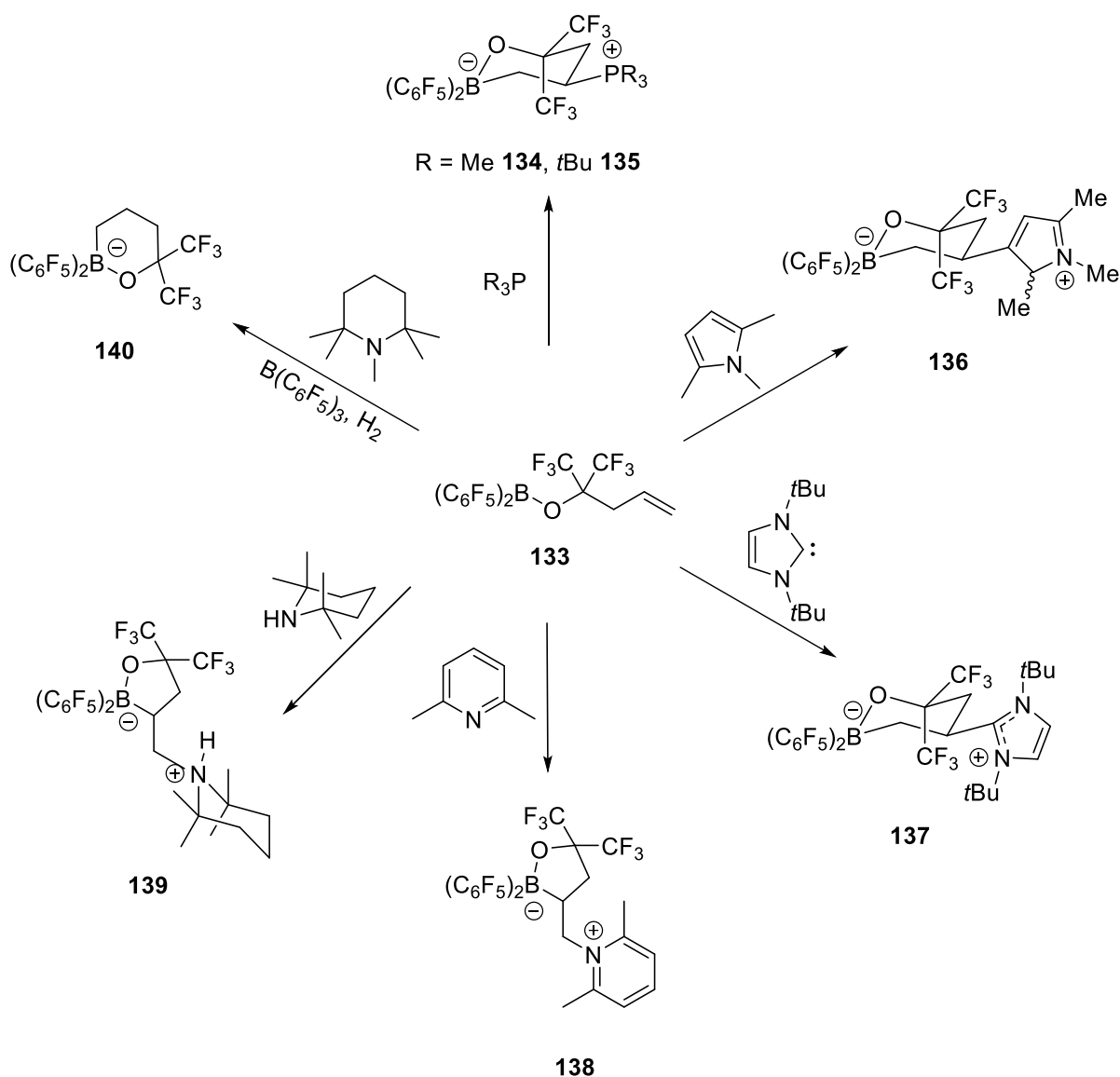
### 1. FLP chemistry with alkenes

If the interaction of FLPs with gases such as dihydrogen or carbon dioxide has been investigated, their interaction with alkenes has also been probed. Indeed, Stephan *et al.*<sup>[70]</sup> found NMR spectroscopic evidence that borane could form an intramolecular van der Waals complex **131** (closed) with the alkene at low temperature which provides the FLP olefin addition product **132** after treatment with a Lewis base (Scheme 32).



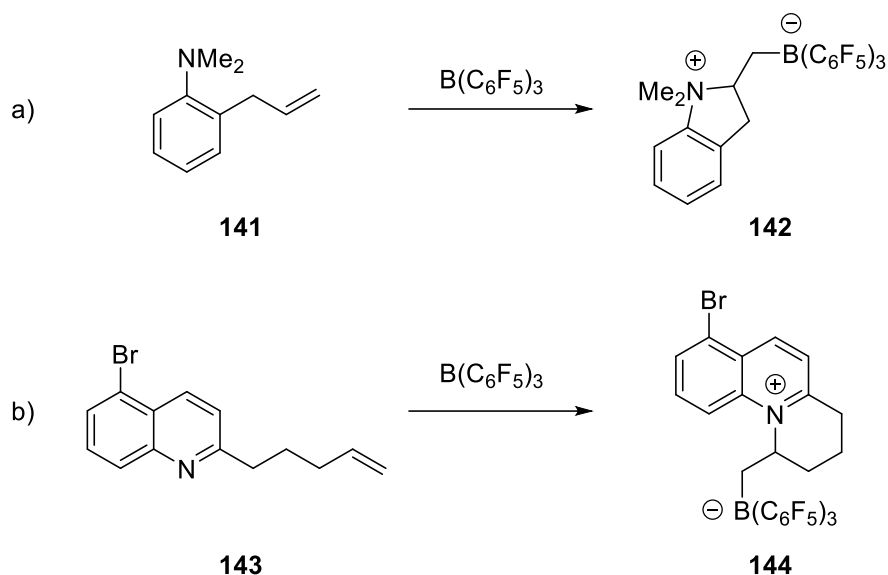
**Scheme 32:** Addition of phosphine on borane/alkene van der Waals complex.

Moreover, this reactivity has also been observed using the van der Waals complex  $B(C_6F_5)_2(OC-(CF_3)_2CH_2CH=CH_2)$  **133**. Indeed Stephan<sup>[71]</sup> studied the addition of various P-, C-, N- and H-nucleophiles on the latter complex (Scheme 33). He discovered that phosphines such as  $PMe_3$  or  $P(tBu)_3$  add to the internal carbon of the olefinic group to give 6-membered ring zwitterions (**134** and **135** respectively). In the same fashion, addition of carbon-based nucleophiles such as 1,2,5-trimethylpyrrole or 1,3-di-tert-butylimidazole-2-ylidene occurred also on the internal carbon of the alkene providing zwitterions **136** and **137**. In contrast, in the case of highly hindered nitrogen-based nucleophiles, such as lutidine or tetramethylpiperidine, the regioselectivity of addition is reversed (zwitterions **138** and **139**). Finally, reaction of pentamethylpiperidine (PMP) with **133** in the presence of a catalytic amount of  $B(C_6F_5)_3$  and  $H_2$  achieves the addition of hydride to the internal carbon of the borane/alkene complex to give the salt **140**.



**Scheme 33:** Reactivity of borane/alkene complexes upon treatment with various nucleophiles.

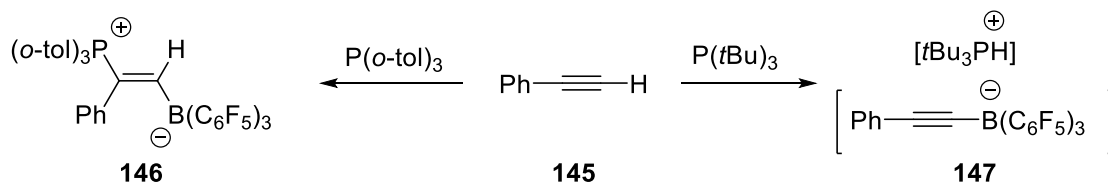
This reactivity has been exploited to achieve cyclization reactions. Indeed, Erker *et al.*<sup>[72]</sup> demonstrated that olefins bearing bulky Lewis base moieties were able to perform cyclizations when treated with  $B(C_6F_5)_3$  to give N-heterocyclic zwitterions (Scheme 34a). More recently, this strategy has been further extended to prepare polycyclic organic derivatives (Scheme 34b).<sup>[73]</sup>



**Scheme 34:** Preparation of N-heterocyclic zwitterions and polycyclic organic derivatives.

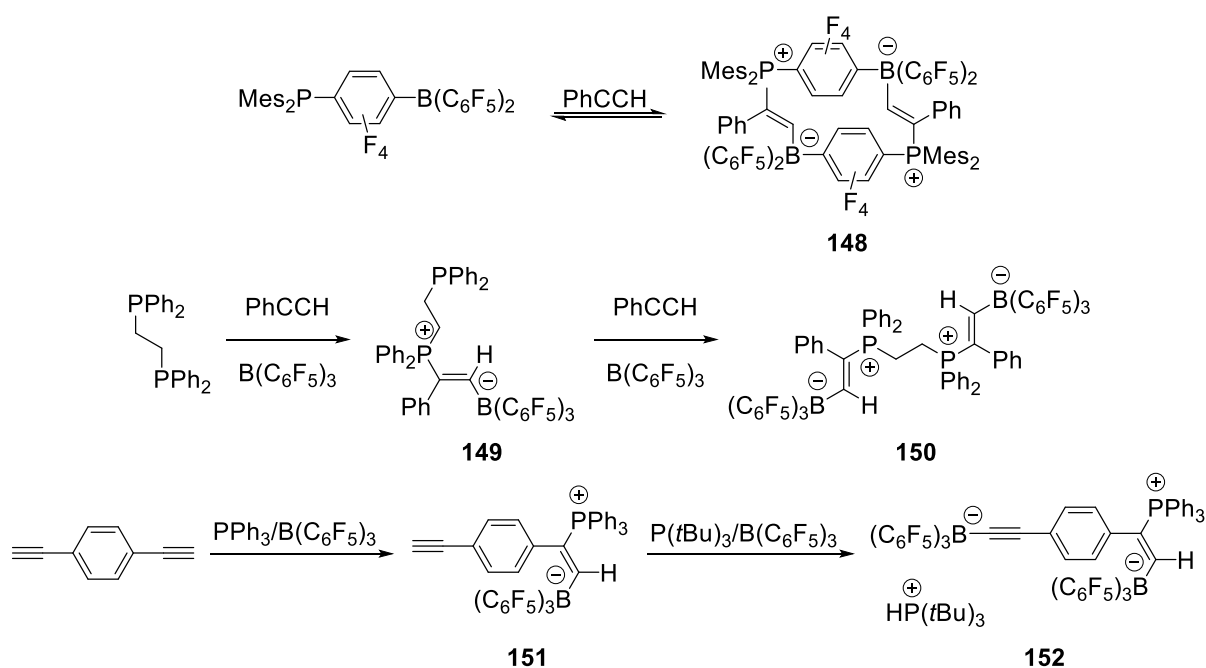
## 2. FLP chemistry with alkynes

FLPs have been reported to react in two possible ways with alkynes depending on the strength of the base. Indeed, in combination with  $B(C_6F_5)_3$ , the strongly basic  $P(tBu)_3$  ( $pK_a=11.4$ ) will achieve deprotonation of the alkyne while the less basic  $P(o-tol)_3$  ( $pK_a=3.1$ ) will perform an addition reaction (Scheme 35).<sup>[74]</sup>



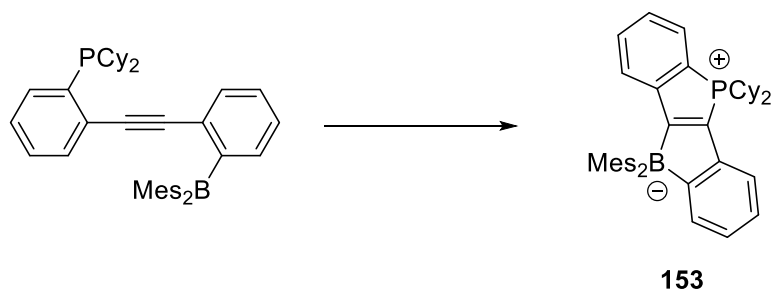
**Scheme 35:** Possible reaction pathway of FLPs with alkynes.

Such addition reactions have been exploited to synthesize the macrocycle **148** from alkyne  $PhCCH$  and  $Mes_2PC_6F_4B(C_6F_5)_2$  (Scheme 36). Alternatively, zwitterions **149** and **150** have been prepared by applying the same strategy on 1,2-bis(diphenylphosphino)ethane,  $PhCCH$  and 2 equivalents of  $B(C_6F_5)_3$ . Besides, addition of  $Ph_3P/B(C_6F_5)_3$  on 1,4-diethynylbenzene gave addition product **151** while subsequent treatment with  $tBu_3P/B(C_6F_5)_3$  afforded the salt/zwitterion **152** which displays both reaction pathways on a single molecule (Scheme 24).<sup>[75]</sup>



**Scheme 36:** Examples reactions of FLPs with alkynes.

A related application of such P/B additions has been described by Yamaguchi and co-workers<sup>[76]</sup> who used the intramolecular addition of phosphines and boranes to synthesize  $\pi$ -conjugated systems including **153** that display interesting photophysical and electrical properties (Scheme 37). The series of molecules described could have potential for linear and non-linear optical materials.

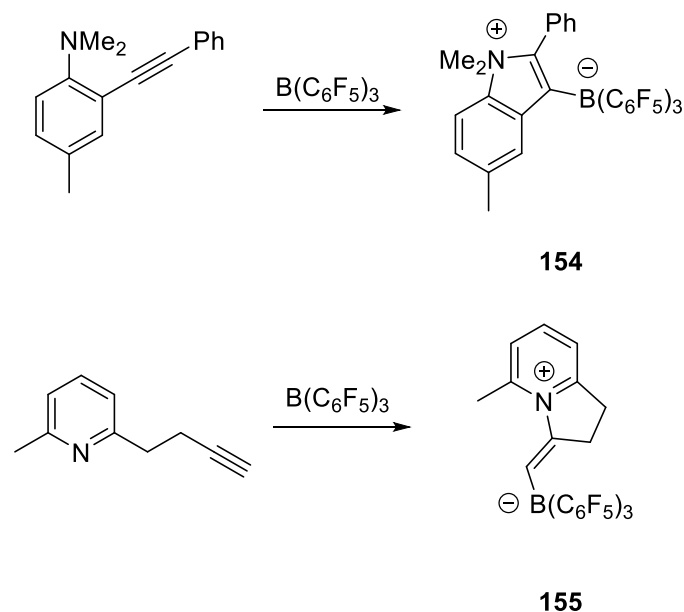


**Scheme 37:** Intramolecular P/B addition route to **153**.

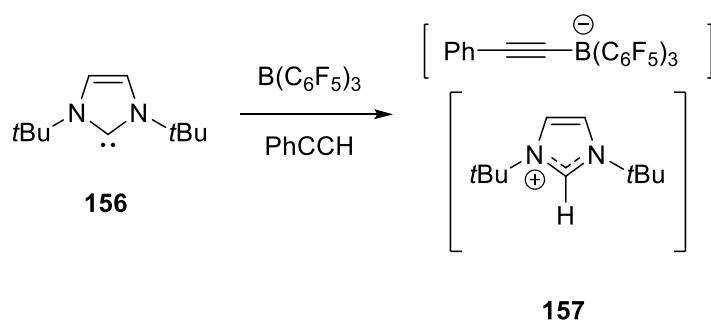
Analogously to pendant olefins, alkyne moieties on aniline or pyridine derivatives have been used to perform intramolecular cyclizations.<sup>[72]</sup> Indeed, the reactions of *o*-(phenylethynyl)-*N,N*-dimethyl toluidine or 2-(but-3-yn-1-yl)-6-methylpyridine with  $B(C_6F_5)_3$  provided the cyclized products **154** and **155** respectively (Scheme 38).

Carbon-based Lewis bases reactions with alkynes and  $B(C_6F_5)_3$  have also been investigated. Indeed, the strongly basic NHC **156** reacts with PhCCH and  $B(C_6F_5)_3$  to yield the deprotonation product **157** (Scheme 39).<sup>[75]</sup>





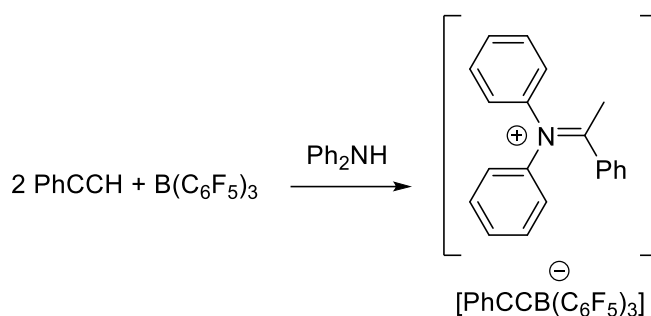
**Scheme 38:** Intramolecular cyclizations with N/B FLPs and alkynes.



**Scheme 39:** Deprotonation of alkyne by carbene/borane FLP.

### 3. FLP catalyzed hydroaminations of alkynes

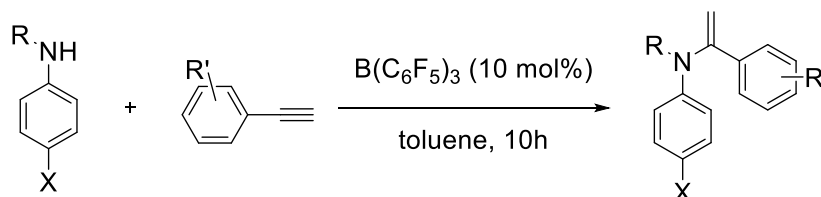
Stephan and coworkers reported that the stoichiometric reaction of  $\text{Ph}_2\text{NH}$ ,  $\text{B}(\text{C}_6\text{F}_5)_3$  and two equivalents of phenylacetylene afforded the salt **158** (Scheme 40). They also developed a catalytic pathway based on this reaction using the amine in the presence of a catalytic amount of borane with slow addition of the alkyne. Thus, a series of arylamines have been used to synthesize the corresponding aryl enamines (**159-172**) (Table 4). Furthermore, this metal-free hydroamination can be followed by the subsequent use of the catalyst in hydrogenation catalysis, allowing the conversion of the enamines to the corresponding amines in a one-pot stepwise manner.<sup>[77]</sup>



158

**Scheme 40:** Stoichiometric hydroaminations affording salt **158**.

**Table 4:** Hydroamination reactions catalyzed by  $\text{B}(\text{C}_6\text{F}_5)_3$ .



Amine	Alkyne	T (°C)	Product	Yield (%)
$\text{Ph}_2\text{NH}$	2-MeOC <sub>6</sub> H <sub>4</sub> CCH	25	$\text{Ph}_2\text{NC}(2\text{-MeOC}_6\text{H}_4)=\text{CH}_2$ <b>159</b>	84
$\text{Ph}_2\text{NH}$	2-MeC <sub>6</sub> H <sub>4</sub> CCH	25	$\text{Ph}_2\text{NC}(2\text{-MeC}_6\text{H}_4)=\text{CH}_2$ <b>160</b>	69
$\text{Ph}_2\text{NH}$	C <sub>10</sub> H <sub>7</sub> CCH	25	$\text{Ph}_2\text{NC}(\text{C}_{10}\text{H}_7)=\text{CH}_2$ <b>161</b>	62
$\text{Ph}_2\text{NH}$	PhCCH	25	$\text{Ph}_2\text{NC}(\text{Ph})=\text{CH}_2$ <b>162</b>	74
$\text{Ph}_2\text{NH}$	2-BrC <sub>6</sub> H <sub>4</sub> CCH	25	$\text{Ph}_2\text{NC}(2\text{-BrC}_6\text{H}_4)=\text{CH}_2$ <b>163</b>	52
$(p\text{-FC}_6\text{H}_4)_2\text{NH}$	2-BrC <sub>6</sub> H <sub>4</sub> CCH	25	$(p\text{-FC}_6\text{H}_4)_2\text{NC}(2\text{-BrC}_6\text{H}_4)=\text{CH}_2$ <b>164</b>	67
$(p\text{-FC}_6\text{H}_4)_2\text{NH}$	2-FC <sub>6</sub> H <sub>4</sub> CCH	25	$(p\text{-FC}_6\text{H}_4)_2\text{NC}(2\text{-FC}_6\text{H}_4)=\text{CH}_2$ <b>165</b>	78
$(p\text{-FC}_6\text{H}_4)_2\text{NH}$	2-SC <sub>4</sub> H <sub>4</sub> CCH	25	$(p\text{-FC}_6\text{H}_4)_2\text{NC}(\text{SC}_4\text{H}_4)=\text{CH}_2$ <b>166</b>	54
<i>i</i> PrPhNH	2-SC <sub>4</sub> H <sub>4</sub> CCH	25	<i>i</i> PrPhNC(2-SC <sub>4</sub> H <sub>4</sub> )=CH <sub>2</sub> <b>167</b>	58
$\text{Ph}_2\text{NH}$	C <sub>14</sub> H <sub>9</sub> CCH	25	$\text{Ph}_2\text{NC}(\text{C}_{14}\text{H}_9)=\text{CH}_2$ <b>168</b>	75
$(p\text{-FC}_6\text{H}_4)_2\text{NH}$	C <sub>14</sub> H <sub>9</sub> CCH	25	$(p\text{-FC}_6\text{H}_4)_2\text{NC}(\text{C}_{14}\text{H}_9)=\text{CH}_2$ <b>169</b>	75
$(p\text{-FC}_6\text{H}_4)_2\text{NH}$	3-FC <sub>6</sub> H <sub>4</sub> CCH	-30	$(p\text{-FC}_6\text{H}_4)_2\text{NC}(3\text{-FC}_6\text{H}_4)=\text{CH}_2$ <b>170</b>	74
$\text{Ph}_2\text{NH}$	3,5-F <sub>2</sub> C <sub>6</sub> H <sub>3</sub> CCH	-30	$\text{Ph}_2\text{NC}(3,5\text{-F}_2\text{C}_6\text{H}_3)=\text{CH}_2$ <b>171</b>	68
$\text{Ph}_2\text{NH}$	3-CF <sub>3</sub> C <sub>6</sub> H <sub>4</sub> CCH	-30	$\text{Ph}_2\text{NC}(3\text{-CF}_3\text{C}_6\text{H}_4)=\text{CH}_2$ <b>172</b>	77

The mechanism of these hydroaminations is thought to proceed via amine-borane addition to the alkyne to give the zwitterionic intermediate. Then the acidic ammonium proton migrates to the carbon atom adjacent to boron center, inducing enamine product formation and  $\text{B}(\text{C}_6\text{F}_5)_3$  release. The borane is then available to participate in further hydroamination catalysis.

## V. Conclusion

Upon review, we saw that the steric hindrance of boranes and phosphines plays a key role in the addition of frustrated Lewis pairs to unsaturated bonds but also in the activation of small molecules. The purpose of this work is thus to extend the scope of phosphine/borane catalysts employing unprecedented substituents and linkers in order to study new types of reactivity in the field of FLP chemistry. The synthesis of new sterically demanding boranes and phosphines will be followed by studies of their steric and electronic properties for the design of bifunctional catalysts. As the main goal is the hydrogenation of CO<sub>2</sub> by FLPs, we will focus our attention on two different linkers with large distance between the Lewis acid and the Lewis bases. Indeed, according to Delarmelina *et al.*,<sup>[67]</sup> a distance of approximately 4.4 Å between the Lewis base and the Lewis acid is ideal for the hydrogenation of CO<sub>2</sub> via a FLP system. Moreover, the rigidity of the scaffold has been proven to have an impact on the catalytic activity of the FLP for this reaction. We will thus first study the effect of using a rigid structure with the triptycene scaffold and finally we will investigate the properties of a flexible structure employing hetero[5]helicenes as linkers between the Lewis acid and Lewis base moieties.

## References:

- [1] G. N. Lewis, *Valence and the structure of atoms and molecules*, **1923**
- [2] H. C. Brown, H. I. Schesinger and S. Z. Cardon, "Studies in Stereochemistry. I. Steric Strains as a Factor in the Relative Stability of Some Coördination Compounds of Boron", *J. Am. Chem. Soc.* **1942**, *64*, 2, 325.
- [3] G. Wittig, E. Benz, *Chem. Ber.* **1959**, *92*, 1999–2013
- [4] G. Wittig, A. Ruckert, *Liebigs. Ann. Chem.* **1950**, *566*, 101.
- [5] W. Tochtermann, *Angew. Chem. Int. Ed. Engl.* **1966**, *5*, 351-371.
- [6] R. Damico, C. D. Broaddus, *J. Org. Chem.* **1966**, *31*, 1607.
- [7] S. Doering, G. Erker, R. Fröhlich, R. O. Meyer, K. Bergander, *Organometallics*, **1998**, *17*, 2183.
- [8] A. G. Massey, A. J. Park, *J. Organomet. Chem.* **1964**, *2*, 245.
- [9] G. C. Welch, L. Cabrera, P. A. Chase, E. Hollink, J. D. Masuda, P. R. Wei, D. W. Stephan, *Dalton Trans.* **2007**, 3407.
- [10] G. C. Welch, R. R. S. Juan, J. D. Masuda, D. W. Stephan, *Science*, **2006**, *314*, 1124.
- [11] G. C. Welch, T. Holtrichter-Roessmann, D. W. Stephan, *Inorg Chem*, **2008**, *47*, 1904.
- [12] G. C. Welch, R. Prieto, M. A. Dureen, A. J. Lough, O. A. Labeodan, T. Holtrichter-Roessmann, D. W. Stephan, *Dalton Trans*, **2009**, 1559.
- [13] L. Cabrera, G. C. Welch, J. D. Masuda, P. R. Wei, D. W. Stephan, *Inorg. Chim. Acta.*, **2006**, *359*, 3066.
- [14] G. C. Welch, R. R. S. Juan, J. D. Masuda, D. W. Stephan, *Science*, **2006**, *314*, 1124–1126.
- [15] G. C. Welch, D. W. Stephan, *J. Am. Chem. Soc.* **2007**, *129*, 1880–1881.
- [16] P. Spies, G. Erker, G. Kehr, K. Bergander, R. Fröhlich, S. Grimme, D. W. Stephan, *Chem. Commun.*, **2007**, 5072–5074
- [17] D. W. Stephan, "'Frustrated Lewis pairs": a concept for new reactivity and catalysis", *Org. Biomol. Chem.* **2008**, *6*, 1535
- [18] a) F. L. Ramp, E. J. DeWitt, L. E. Trapasso, *J. Org. Chem.* **1962**, *27*, 4368–4372; b) E. J. DeWitt, L. E. Trapasso, F. L. Ramp, *J. Am. Chem. Soc.* **1961**, *83*, 4672; c) E. Osthaus, M. W. Haenel, *Coal Science and Technology*, Bd. 11 (Hrsg.: J. A. Moulijn, K. A. Nater, H. A. G. Chermin), Elsevier, Amsterdam, **1987**, S. 765–768; d) M. W. Haenel, J. Narangerel, U. B. Richter, A. Rufinska, *Angew. Chem. Int. Ed.* **2006**, *45*, 1061–1066; *Angew. Chem.* **2006**, *118*, 1077–1082; e) M. Yalpani, R. Koster, M. W. Haenel, *Erdöl Kohle Erdgas Petrochemie* **1990**, *43*, 344–347; f) M. Yalpani, T. Lunow, R. Kçster, *Chem. Ber.* **1989**, *122*, 687-693; g) M. Yalpani, R. Kçster, *Chem. Ber.* **1990**, *123*, 719–724.
- [19] H. Wang, R. Fröhlich, G. Kehr, G. Erker, *Chem. Commun.*, **2008**, 5966–5968.
- [20] A. Ramos, A. J. Lough, D. W. Stephan, *Chem. Commun.* **2009**, 1118.
- [21] P. Liptau, M. Neumann, G. Erker, G. Kehr, R. Fröhlich, S. Grimme, *Organometallics*, **2004**, *23*, 21.
- [22] D. P. Huber, G. Kehr, K. Bergander, R. Fröhlich, G. Erker, S. Tanino, Y. Ohki, K. Tatsumi, *Organometallics*, **2008**, *27*, 5279.
- [23] S. J. Geier, T. M. Gilbert, D. W. Stephan, *J. Am. Chem. Soc.*, **2008**, *130*, 12632.
- [24] M. Ullrich, A. J. Lough, D. W. Stephan, *J. Am. Chem. Soc.*, **2009**, *131*, 52.

- [25] M. Ullrich, A. J. Lough, D. W. Stephan, *Organometallics*, **2010**, *29*, 3647.
- [26] G. D. Frey, V. Lavallo, B. Donnadieu, W. W. Schoeller, G. Bertrand, *Science*, **2007**, *316*, 439.
- [27] P. A. Chase, A. L. Gille, T. M. Gilbert, D. W. Stephan, *Dalton Trans*, **2009**, 7179.
- [28] P. A. Chase, D. W. Stephan, *Angew. Chem. Int. Ed.*, **2008**, *47*, 7433.
- [29] D. Holschumacher, T. Bannenberg, C. G. Hrib, P. G. Jones, M. Tamm, *Angew. Chem. Int. Ed.*, **2008**, *47*, 7428.
- [30] P. A. Chase, T. Jurca, D. W. Stephan, *Chem. Commun.*, **2008**, 1701–1703.
- [31] V. Sumerin, F. Schulz, M. Nieger, M. Leskelä, T. Repo, B. Rieger, *Angew. Chem. Int. Ed.*, **2008**, *47*, 6001.
- [32] K. V. Axenov, G. Kehr, R. Fröhlich, G. Erker, *J. Am. Chem. Soc.*, **2009**, *131*, 3454.
- [33] W. E. Piers, *Adv. Organomet. Chem.*, **2005**, *52*, 1.
- [34] F. Focante, P. Mercandelli, A. Sironi, L. Resconi, *Coord. Chem. Rev.*, **2006**, *250*, 170.
- [35] S. J. Geier, A. L. Gille, T. M. Gilbert, D. W. Stephan, *Inorg. Chem.* **2009**, *48*, 10466.
- [36] S. J. Geier, D. W. Stephan, *J. Am. Chem. Soc.*, **2009**, *131*, 3476.
- [37] P. A. Chase, G. C. Welch, T. Jurca, D. W. Stephan, *Angew. Chem.* **2007**, *119*, 8196–8199; *Angew. Chem. Int. Ed.* **2007**, *46*, 8050 – 8053.
- [38] D. Stephan and G. Erker, “Frustrated Lewis Pairs: Metal-free Hydrogen Activation and More”, *Angewandte Chemie Int. Ed.*, **2010**, *49*, 46–76.
- [39] D. Chen, J. Klankermayer, *Chem. Commun.*, **2008**, 2130–2131.
- [40] G. Erős, K. Nagy, H. Mehdi, I. Pápai, P. Nagy, P. Király, G. Tárkányi, T. Soós, *Chem. Eur. J.*, **2012**, *18*, 574 – 585
- [41] R. Noyori, *Angew. Chem. Int. Ed.*, **2002**, *41*, 2008–2022; *Angew. Chem.*, **2002**, *114*, 2108–2123
- [42] a) T. Ikariya, A. J. Blacker, *Acc. Chem. Res.*, **2007**, *40*, 1300–1308; b) R. Noyori, T. Ohkuma, *Angew. Chem. Int. Ed.*, **2001**, *40*, 40–73; *Angew. Chem.* **2001**, *113*, 40–75; c) D. J. Ager, A. H. M. de Vries, J. G. de Vries, *Chem. Soc. Rev.*, **2012**, *41*, 3340–3380; d) Q.-A. Chen, Z.-S. Ye, Y. Duan, Y.-G. Zhou, *Chem. Soc. Rev.*, **2013**, *42*, 497–511; e) P. Etayo, A. Vidal-Ferran, *Chem. Soc. Rev.* **2013**, *42*, 728 –754; f) R. H. Morris, *Chem. Soc. Rev.*, **2009**, *38*, 2282–2291.
- [43] Z. M. Heiden, D. W. Stephan, *Chem. Commun.*, **2011**, *47*, 5729–5731.
- [44] X. Wang, G. Kehr, C. G. Daniliuc, G. Erker, *J. Am. Chem. Soc.*, **2014**, *136*, 3293–3303.
- [45] V. Sumerin, K. Chernichenko, M. Nieger, M. Leskelä, B. Rieger, T. Repo, *Adv. Synth. Catal.*, **2011**, *353*, 2093–2110.
- [46] D. Chen, Y. Wang, J. Klankermayer, *Angew. Chem. Int. Ed.*, **2010**, *49*, 9475–9478; *Angew. Chem.*, **2010**, *122*, 9665–9668.
- [47] G. Ghattas, D. Chen, F. Pan, J. Klankermayer, *Dalton Trans.*, **2012**, *41*, 9026–9028.
- [48] C. M. Mömming, E. Otten, G. Kehr, R. Fröhlich, S. Grimme, D. W. Stephan, G. Erker, *Angew. Chem. Int. Ed.*, **2009**, *48*, 6643–6646; *Angew. Chem.*, **2009**, *121*, 6770–6773.
- [49] a) I. Peuser, R. C. Neu, X. Zhao, M. Ulrich, B. Schirmer, J. A. Tannert, G. Kehr, R. Fröhlich, S. Grimme, G. Erker, D. W. Stephan, *Chem. Eur. J.*, **2011**, *17*, 9640–9650; b) M. Harhausen, R. Fröhlich, G. Kehr, G. Erker, *Organometallics*, **2012**, *31*, 2801–2809.
- [50] R. C. Neu, G. Ménard, D. W. Stephan, *Dalton Trans.*, **2012**, *41*, 9016–9018.

- [51] T. Voss, T. Mahdi, E. Otten, R. Fröhlich, G. Kehr, D. W. Stephan, G. Erker, *Organometallics*, **2012**, *31*, 2367–2378.
- [52] a) M. Feroci, I. Chiarotto, S. V. Cipriotti, A. Inesi, *Electrochim. Acta*, **2013**, *109*, 95-101; b) J. D. Holbrey, W. M. Reichert, I. Tkatchenko, E. Bouajila, O. Walter, I. Tommasi, R. D. Rogers, *Chem. Commun.*, **2003**, 28-29; c) E. L. Kolychev, T. Bannenberg, M. Freytag, C. G. Daniliuc, P. G. Jones, M. Tamm, *Chem. Eur. J.*, **2012**, *18*, 16938-16946; d) E. Theuergarten, T. Bannenberg, M. D. Walter, D. Holschumacher, M. Freytag, C. G. Daniliuc, P. G. Jones, M. Tamm, *Dalton Trans.*, **2014**, *43*, 1651-1662.
- [53] G. Ménard, T. M. Gilbert, J. A. Hatnean, A. Kraft, I. Krossing, D. W. Stephan, *Organometallics*, **2013**, *32*, 4416-4422.
- [54] M. A. Dureen, D. W. Stephan, *J. Am. Chem. Soc.*, **2010**, *132*, 13559-13568.
- [55] E. Theuergarten, J. Schlosser, D. Schluns, M. Freytag, C. G. Daniliuc, P. G. Jones, M. Tamm, *Dalton Trans.*, **2012**, *41*, 9101-9110.
- [56] C. Appelt, H. Westenberg, F. Bertini, A. W. Ehlers, J. C. Slootweg, K. Lammertsma, W. Uhl, *Angew. Chem. Int. Ed.*, **2011**, *50*, 3925-3928; *Angew. Chem.*, **2011**, *123*, 4011-4014.
- [57] J. Boudreau, M. A. Courtemanche, F. G. Fontaine, *Chem. Commun.*, **2011**, *47*, 11131-11133.
- [58] X. Zhao, D. W. Stephan, *Chem. Commun.*, **2011**, *47*, 1833-1835.
- [59] M. Sajid, A. Klose, B. Birkmann, L. Y. Liang, B. Schirmer, T. Wiegand, H. Eckert, A. J. Lough, R. Fröhlich, C. G. Daniliuc, S. Grimme, D. W. Stephan, G. Kehr, G. Erker, *Chem. Sci.*, **2013**, *4*, 213-219.
- [60] K. Axenov, C. Momming, G. Kehr, R. Fröhlich, G. Erker, *Chem. Eur. J.*, **2010**, *16*, 14069–14073
- [61] E. Otten, R. C. Neu, D. W. Stephan, *J. Am. Chem. Soc.*, **2009**, *131*, 9918-9919.
- [62] a) A. G. Tskhovrebov, E. Solari, M. D. Wodrich, R. Scopelliti, K. Severin, *J. Am. Chem. Soc.*, **2012**, *134*, 1471-1473; b) A. G. Tskhovrebov, B. Vuichoud, E. Solari, R. Scopelliti, K. Severin, *J. Am. Chem. Soc.*, **2013**, *135*, 9486-9492.
- [63] M. Sajid, G. Kehr, C. G. Daniliuc, G. Erker, *Angew. Chem. Int. Ed.*, **2014**, *53*, 1118-1121; *Angew. Chem.*, **2014**, *126*, 1136-1139.
- [64] A. E. Ashley, A. L. Thompson, D. O'Hare, *Angew. Chem. Int. Ed.*, **2009**, *48*, 9839–9843; *Angew. Chem.*, **2009**, *121*, 10023-10027.
- [65] A. Berkefeld, W. E. Piers, M. Parvez, *J. Am. Chem. Soc.*, **2010**, *132*, 10660–10661.
- [66] M. A. Courtemanche, M. A. Legare, L. Maron, F. G. Fontaine, *J. Am. Chem. Soc.*, **2013**, *135*, 9326-9329.
- [67] M. Delarmelina, J. W. de M. Carneiro, C. Richard, A. Catlow, M. Bühl, *Catalysis Communications*, **2022**, *162*, 106385.
- [68] J. S. J. McCahill, G. C. Welch, D. W. Stephan, *Angew. Chem. Int. Ed.*, **2007**, *46*, 4968-4971; *Angew. Chem.*, **2007**, *119*, 5056-5059.
- [69] M. A. Dureen, D. W. Stephan, *J. Am. Chem. Soc.*, **2009**, *131*, 8396-8397.
- [70] X. Zhao, D. W. Stephan, *J. Am. Chem. Soc.*, **2011**, *133*, 12448-12450.
- [71] X. Zhao, D. W. Stephan, *Chem. Sci.*, **2012**, *3*, 2123-2132.
- [72] T. Voss, C. Chen, G. Kehr, E. Nauha, G. Erker, D. W. Stephan, *Chem. Eur. J.*, **2010**, *16*, 3005-3008.

- [73] P. K. Dornan, L. E. Longobardi, D. W. Stephan, *Synlett*, **2014**, 25, 1521-1524.
- [74] M. A. Dureen, D. W. Stephan, *J. Am. Chem. Soc.*, **2009**, 131, 8396-8397.
- [75] M. A. Dureen, C. C. Brown, D. W. Stephan, *Organometallics*, **2010**, 29, 6594-6607.
- [76] A. Fukazawa, H. Yamada, S. Yamaguchi, *Angew. Chem. Int. Ed.*, **2008**, 47, 5582-5585; *Angew. Chem.*, **2008**, 120, 5664-5667.
- [77] T. Mahdi, D. W. Stephan, *Angew. Chem. Int. Ed.*, **2013**, 52, 12418-12421; *Angew. Chem.*, **2013**, 125, 12644-12647.

## **Chapter II:**

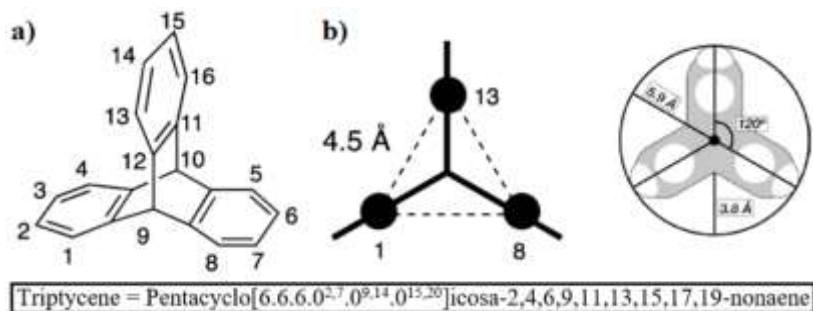
**Triptycenes as platform for the design of new types of frustrated Lewis pairs**



# I. Triptycenes in chemistry

## 1. Generalities

Triptycene belongs to the triptycene family, which is constituted of molecules composed of arenes connected together with a bicyclo[2.2.2]octane framework (Scheme 41). Triptycene is constituted by three aromatic rings forming an angle of 120° between each other linked by a rigid three-pronged scaffold.

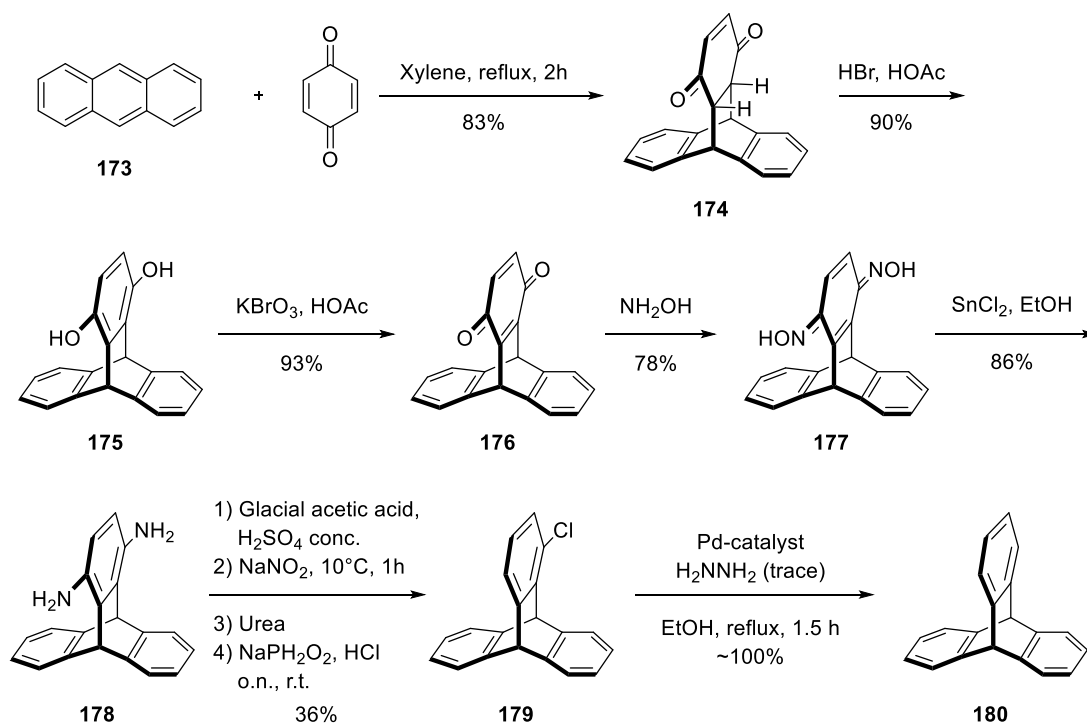


Scheme 41: (a) Structure, nomenclature and (b) geometrical properties of triptycene.

## 2. Synthesis of triptycene and its derivatives

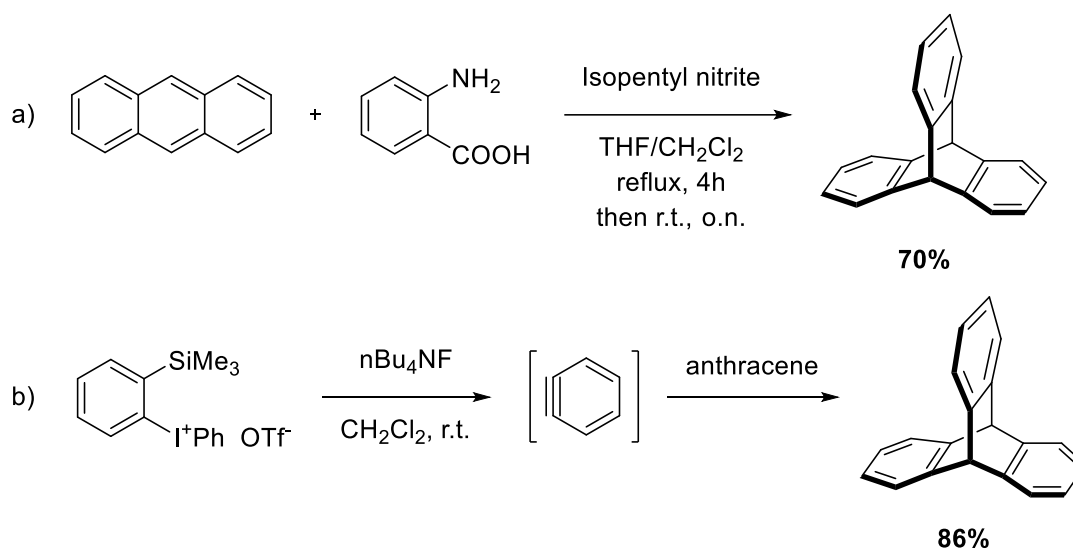
### i. Triptycene

Triptycene was first synthesized in 1942 in a low yield by a multistep synthesis starting from the Diels Alder reaction of anthracene and benzoquinone (Scheme 42).

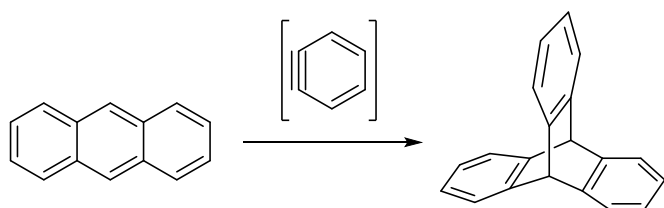


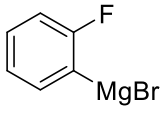
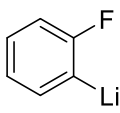
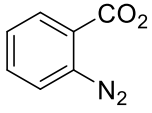
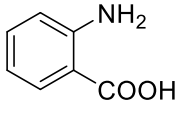
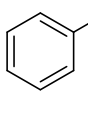
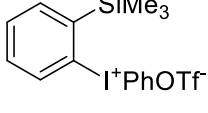
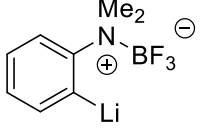
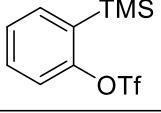
Scheme 42: First reported synthesis of triptycene

Since this report, numerous strategies have been developed to synthesize triptycene and its derivatives. Nowadays, the most convenient and efficient way to synthesize triptycene is to perform a Diels Alder reaction of benzyne on anthracene. Indeed, Friedman and Logullo<sup>[78]</sup> reported a synthesis of triptycene using benzyne generated *in situ*. As shown in Scheme 43a, the diazotation of anthranilic acid using isoamyl nitrite generates benzyne which reacts with anthracene to provide triptycene in 50-60% yield. Moreover, the yield could be improved to 70-80% by using a large excess of benzyne precursors. Besides, in order to generate benzyne under milder conditions, Kitaruma *et al.* employed a new hypervalent iodine precursor which leads to triptycene with a high yield of 86% (Scheme 43b). Numerous others precursors that can also be used to prepared benzyne *in situ* are shown in Table 5.



**Scheme 43:** a) Synthesis of triptycene by using *o*-diazonium benzoate as benzyne precursor  
 b) Synthesis of triptycene with hypervalent iodine benzyne precursor

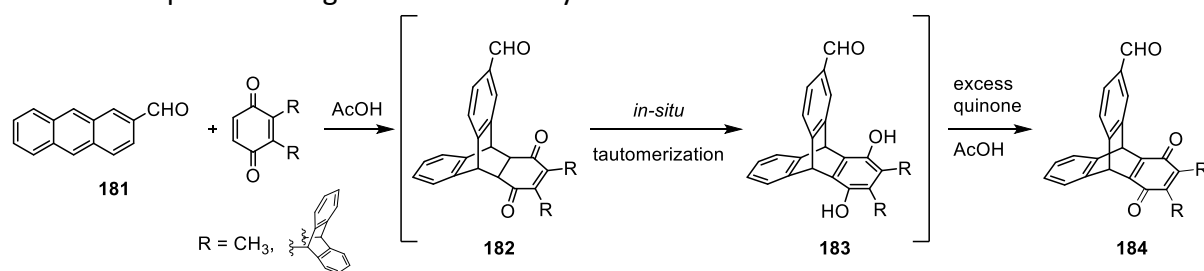
**Table 5** : Preparation of benzyne *in-situ* and cycloaddition with anthracene.

Precursor	Conditions	Yield (%)
	Heat	28
	Room temperature	10
	Heat	30
	Isopentyl nitrite Heat	59
	<i>t</i> -BuOK	21
	Bu <sub>4</sub> NF	86
	Heat	11
	Me <sub>4</sub> NF	96

The triptycene scaffold found numerous applications in chemistry. It has been used for example to design molecular machines,<sup>[79]</sup> molecular balances,<sup>[80]</sup> rigid complexes in catalysis,<sup>[81]</sup> hosts in supramolecular chemistry,<sup>[82]</sup> or as tridimensional platform for materials chemistry or crystal engineering.<sup>[83]</sup> Some key applications related to our research topics are given in the next section.

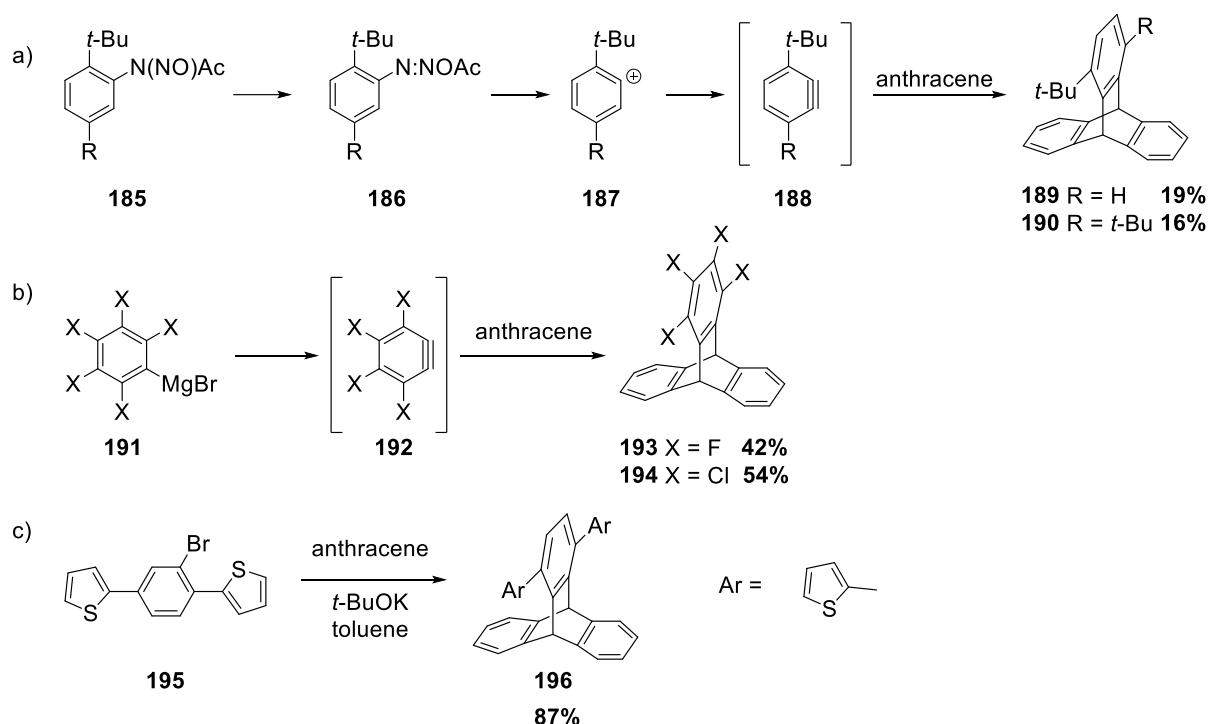
ii. Triptycene derivatives

Wiehe *et al.* developed a general method for the synthesis of triptycene quinones.<sup>[84]</sup> It consists in the [4+2] cycloaddition of an anthracene derivative **181** and a quinone to form a triptycene hydroquinone which is then oxidized by the excess of quinone to afford the corresponding triptycene quinone as shown in Scheme 44. This method tolerates a large variety of functional groups and found numerous applications such as the synthesis of various porphyrin quinones. Furthermore, it allows the obtention of precursors for the synthesis of polytritycene derivatives such as polymers with low dielectric constant, low water absorption and high thermal stability.<sup>[85]</sup>



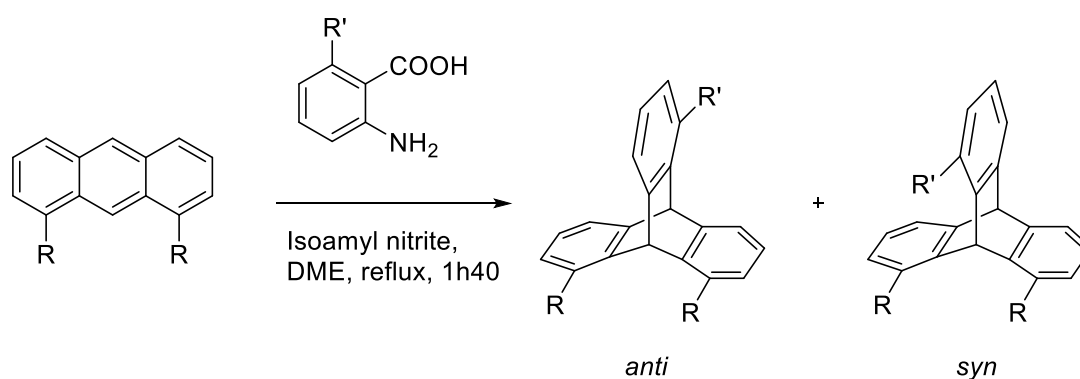
**Scheme 44:** Synthesis of triptycene quinones

While the use of quinones as dienophile is possible for the synthesis of triptycene and its derivatives, arynes are much more common to perform the [4+2] cycloaddition. Indeed, benzyne can be easily prepared *in situ* from various precursors (Table 5) and substituted benzyne can introduce functional groups to triptycenes easily. Consequently, Cadogan and co-workers<sup>[86]</sup> developed the synthesis of mono- and di-*tert*-butyl-substituted triptycenes via the [4+2] cycloaddition of anthracene to the corresponding *tert*-butylsubstituted aryne, which was itself generated from the heterolytic cleavage of *o*-*tert*-butyl-N-nitrosoacetanilide in benzene (Scheme 45a). In 1968, Heaney performed the cycloaddition of tetrafluoro- and tetrachloro-benzyne, generated from the corresponding pentahalo-aryl Grignard reagents, with anthracenes to synthesize tetrahalogenated triptycenes in reasonable yields<sup>[87]</sup> (Scheme 45b). With the development of new methods for the generation of benzyne and arynes, a significant number of triptycenes derivatives have been obtained in satisfactory yields such as the di(thien-2-yl)tritycene which has been synthesized in 87% yield by the group of Anzenbacher<sup>[88]</sup> (Scheme 45c).



**Scheme 45:** a) Synthesis of *tert*-butyl substituted triptycenes  
 b) Synthesis of tetrahalogenated triptycenes  
 c) Synthesis of di(thien-2-yl)triptycene

Using substituted anthracenes instead of substituted arynes can also lead to the obtention of the corresponding substituted triptycenes *via* Diels–Alder reactions. Indeed, the Diels–Alder addition reaction between chlorobenzynes and anthracene gave monochlorotriptycene in 16% yield. Under similar reaction conditions, a yield of up to 30% of the corresponding mono-chlorotriptycene could be obtained via the Diels–Alder addition of benzyne with a chloroanthracene according to Misumi *et al.*<sup>[89]</sup> Rogers and Averill<sup>[90]</sup> subsequently synthesized a series of trisubstituted triptycenes and further investigated the influence of the substituents on the anthracene and benzyne on the *anti* to *syn* isomer ratios of the trisubstituted triptycenes. As shown in Table 6, the nature of the substituents on the benzyne had a significant effect on the observed regioselectivity of the Diels–Alder reaction. When R' = Me, the *syn* isomer was the major adduct. When R' = Cl, the situation was the other way around. The *anti* adduct was the major product with over a 3:1 ratio relative to the *syn* isomer. These results are interpreted as the simple electrostatic matching of the polarized benzyne and anthracene orbitals to determine the major adduct. However, when R' = CO<sub>2</sub>Me, it's the nature of the R substituent on the anthracene that plays the dominant role in dictating the observed regioselectivity of the cycloaddition.



Entry	R	R'	<i>anti</i> (%)	<i>syn</i> (%)	Yield (%)
1	Cl	Me	25	75	74
2	CN	Me	28	72	57
3	CO <sub>2</sub> Me	Me	31	69	58
4	Cl	Cl	77	23	27
5	CO <sub>2</sub> Me	Cl	73	27	20
6	Cl	CO <sub>2</sub> Me	44	56	47
7	CN	CO <sub>2</sub> Me	99	1	38
8	CO <sub>2</sub> Me	CO <sub>2</sub> Me	76	24	62

**Table 6:** Ratios of the *anti/syn* isomers of trisubstituted triptycenes

### 3. Applications

#### i. Supramolecular chemistry

Triptycenes have been extensively used in supramolecular chemistry and more recently for the design of molecular machines. A molecular machine can be defined as a discrete number of molecular components that exhibit mechanical movements in response to an external stimulus.<sup>[91]</sup> For instance, Toyota *et al.*<sup>[92]</sup> reported a series of systems with the bis(9-triptycyl)ethynes **197** (Figure 3) with rotations around C(sp)-C(sp<sup>3</sup>) bonds. These systems display rotation barrier from 11.6 kcal/mol (with R = F) to 17.3 kcal/mol (with R = I). When the halogen substituents were replaced by phenyl or benzyl groups, the rotation barrier would increase up to 15.8-18.8 kcal/mol. These results revealed that rotation barrier would be determined by the size, shape and flexibility of the substituents.

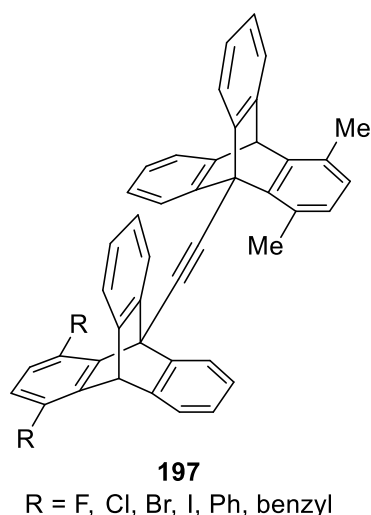
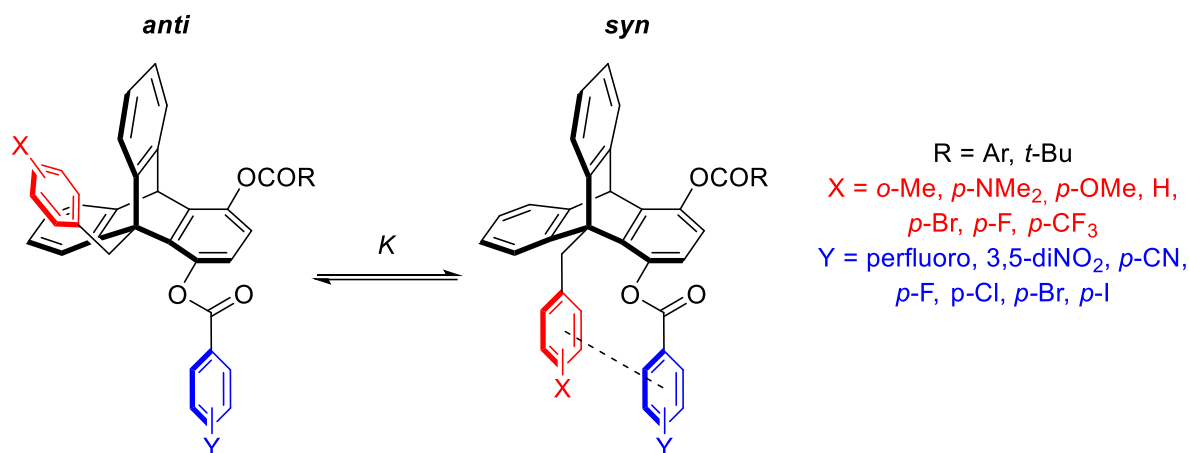


**Figure 3:** Structure of bis(9-triptycyl)ethynes **197**.

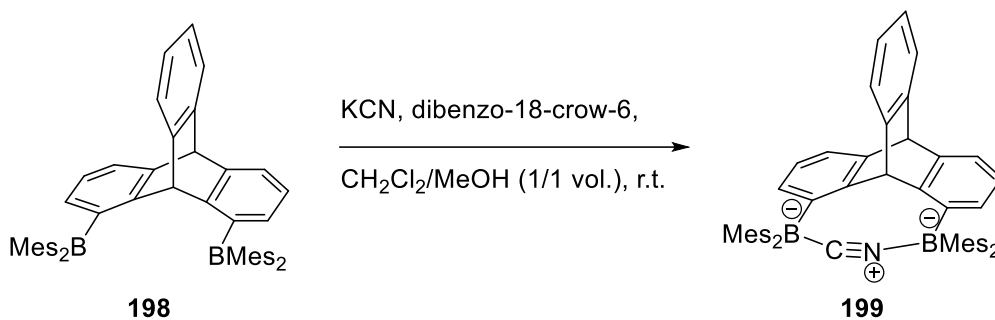
Triptycenes can also be used to build molecular balances. Molecular balances are systems that are able to quantify non-covalent interactions thanks to the determination of the relative stabilities of conformational states. An example of molecular balance with the triptycene scaffold for the quantification of offset aromatic stacking interactions has been established by the group of Gung in 2005<sup>[93]</sup> (Scheme 46).



**Scheme 46:** Molecular balances with a triptycene scaffold for the quantification of offset aromatic stacking.

## ii. Anion sensors and receptors

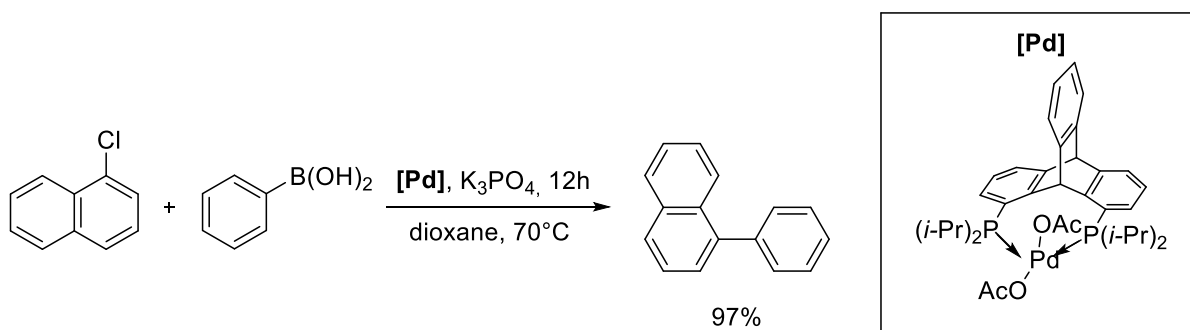
Similarly, in 2018, Gabbai *et al.* used the triptycene scaffold for the development of a “large bite” diborane ideally suited for the selective and quasi irreversible complexation of cyanide<sup>[94]</sup> (Scheme 47). Gabbai indicates in this report that this kind of diborane could find applications as slow releasers of reactive compounds.



**Scheme 47:** Coordination of cyanide to diborane based on triptycene scaffold.

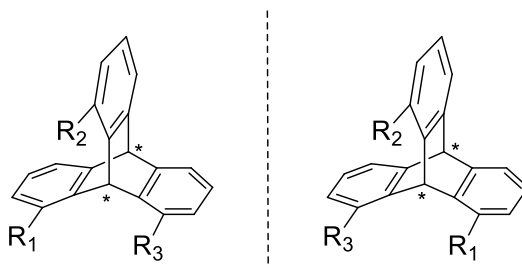
iii. *Organometallic catalysis*

Triptycenes also found numerous applications as rigid bidentate ligands for catalysis. Indeed, the rigidity of a ligand towards the chelation of a metal leads to an enhanced affinity between both species due to kinetic stabilization of the complex. The group of Gelman developed in 2006 an example of this kind of rigid palladium complex which was used as catalyst for C-C bond formation by cross-coupling (Scheme 48)<sup>[95]</sup>.



**Scheme 48:** Synthesis of 1-phenylnaphthalene by C-C bond formation with a palladium complex with triptycene based biphosphine.

One important feature of disubstituted and trisubstituted triptycenes is that if these substituents are different, the triptycene becomes chiral (Scheme 49). Thus, FLP systems based on triptycene scaffold could find applications in asymmetric catalysis.



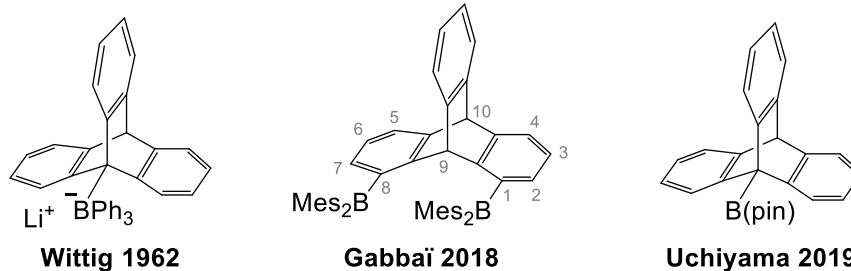
**Scheme 49:** Stereogenic centers of chiral triptycenes.



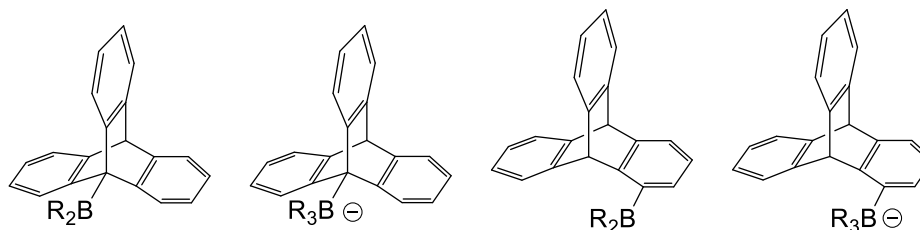
## II. Triptycene boronates, boranes, and boron ate-complexes: Toward sterically hindered triarylboranes and trifluoroborates

To the best of our knowledge, only two examples of 9-substituted boron triptycenes were reported by Wittig<sup>[96]</sup> and Uchiyama,<sup>[97]</sup> while only one triptycene substituted in the positions 1 and 8 has been reported by Gabbai (Scheme 50).<sup>[98]</sup>

a) Known 1 and 9 substituted borylated triptycenes (only three examples so far)



b) This work: seven new examples with R = F, OMe, Ph, Mes, pin, neo

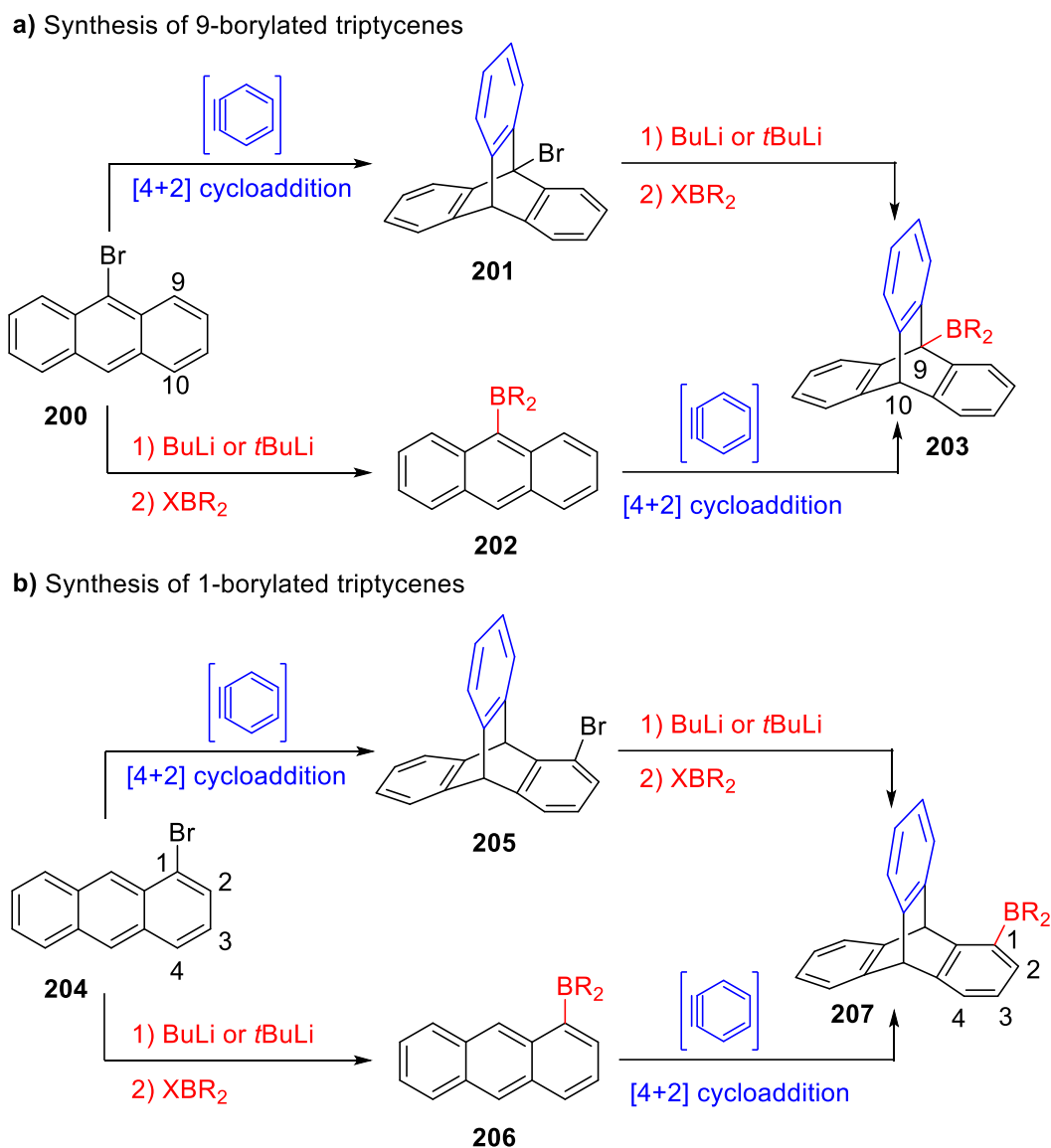


▪ Dual synthetic approach ▪ X-ray structures ▪ Photophysical properties

**Scheme 50:** Triptycene boronates and borates substituted in positions 1 and 9.

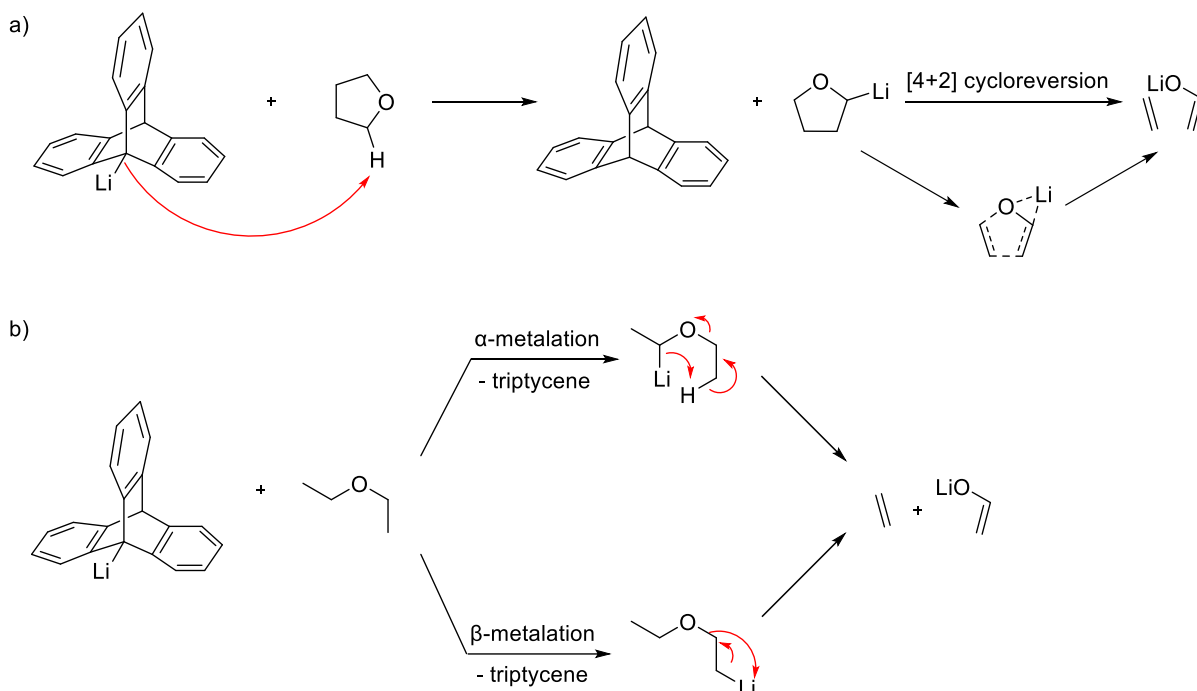
### 1. Objectives

We now report two synthetic approaches towards the 9- and the 1-borylated triptycenes **203** and **207** starting from the bromo-anthracenes **200** or **204**, respectively (Scheme 40). While the first method starts with a [4+2] cycloaddition reaction between the bromoanthracenes **1** or **5** with benzyne (Scheme 51a-Scheme 51b, top), in the second method, a Br/Li exchange and borylation of **200** and **204** is followed by a [4+2] cycloaddition reaction with benzyne (Scheme 51a-Scheme 51b, bottom).

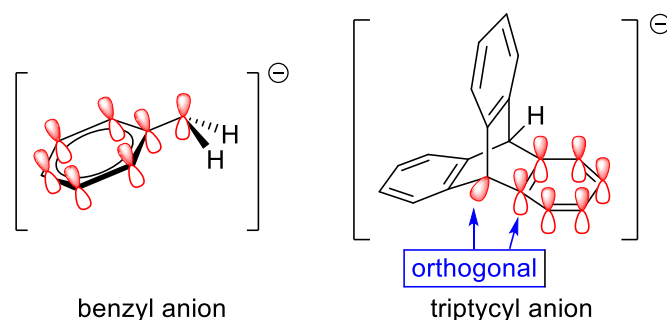


**Scheme 51:** General two-steps approaches to borylated triptycenes **203** and **207** from bromoanthracenes **200** and **204**.

It is particularly challenging to insert a boron atom on the bridgehead carbon on the position 9 of triptycene because the triptycene-9-yl lithium intermediate obtained after bromine/lithium exchange of **201** (Scheme 51a, top path) is extremely reactive<sup>[97]</sup> owing to its high basicity and readily deprotonates reaction solvents or reagents (Scheme 52a and 52b).<sup>[99]</sup> Indeed, the geometry of triptycene scaffold causes the  $\pi$ -orbitals of the aromatic cycles to be orthogonal to the one of the carbon at the bridgehead position. Thus, the negative charge is not delocalized in the structure as it is the case for benzyl anion and the basicity is highly increased (Scheme 53).



**Scheme 52:** a) Deprotonation of THF by 9-triptycyl lithium  
b) Deprotonation of Et<sub>2</sub>O by 9-triptycyl lithium.



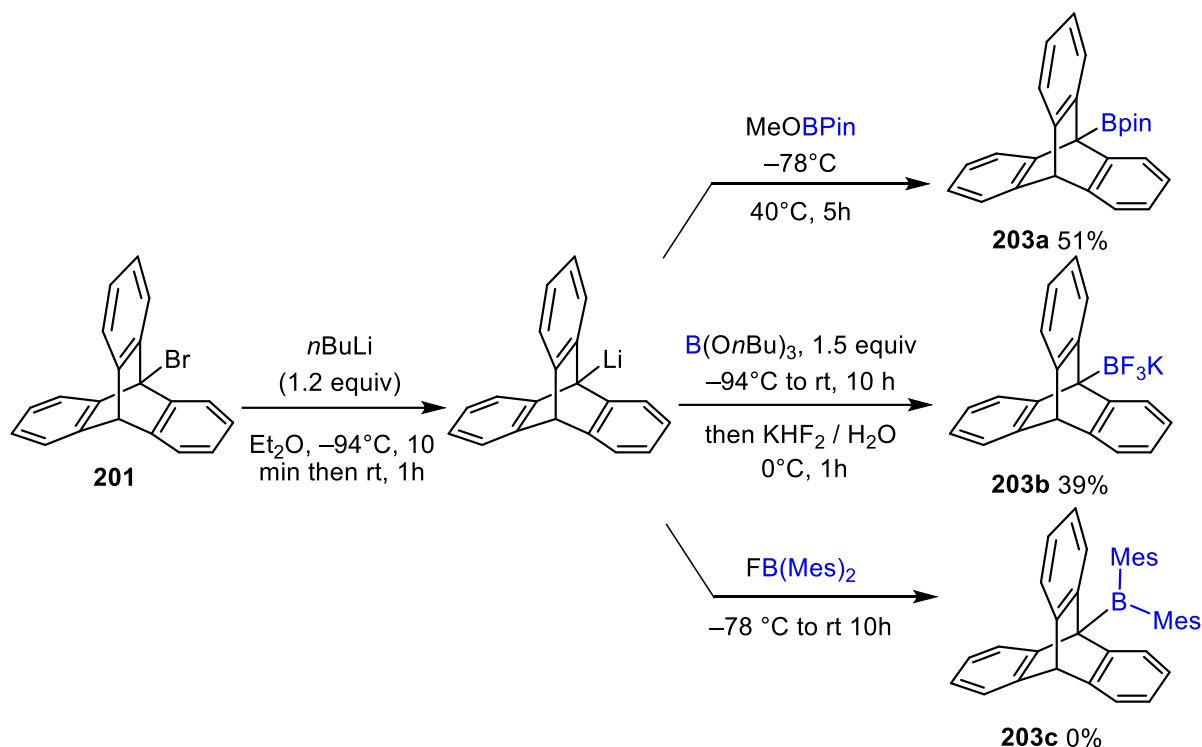
**Scheme 53:** Orientation of  $\pi$ -orbitals for benzyl and triptycylanions.

Thus, our key goal was to develop an alternative synthetic pathway in which we could use a stable anthracene-9-yl lithium species to produce the borylated anthracenes **206** first (Scheme 2a, bottom path), and then convert them into 9-substituted triptycene borates **207** and boronates via optimized [4+2] cycloaddition reactions with benzyne. We structurally characterized a series of obtained triptycene boranes and boronates in the solid-state by X-ray diffraction analysis and investigated the steric and electronic effects of the triptycene scaffold at the central Csp<sup>3</sup> position (C9) or at the side aryl Csp<sup>2</sup> position (C1) on the boron atom structure and physicochemical properties.

## 2. Results and discussions

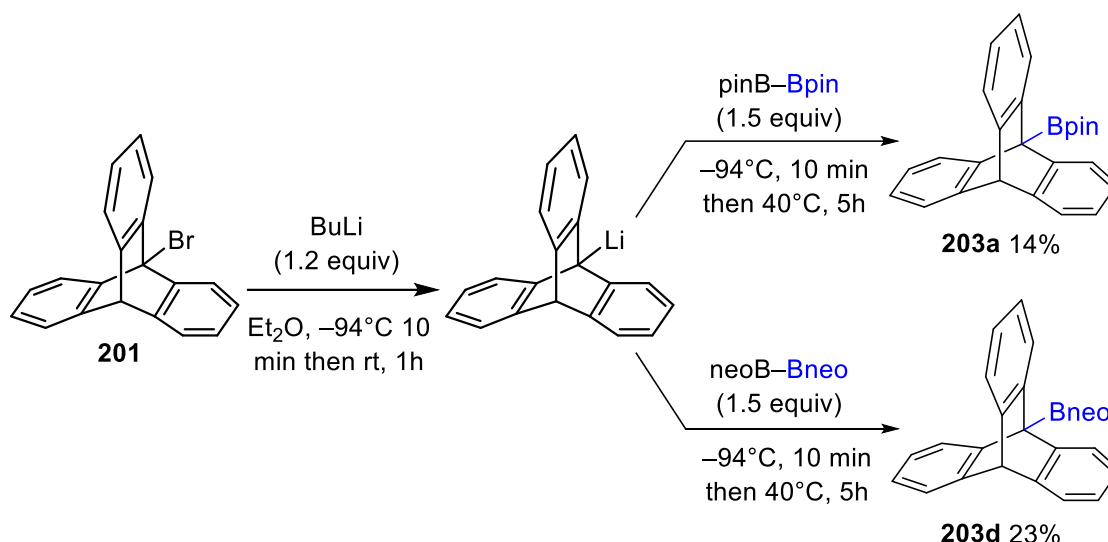
To our surprise, the 9-bromotriptycene **201** (synthesized from 9-bromoanthracene **200** and benzyne)<sup>[100]</sup> neither reacted with Mg powder or turnings even after activation by several methods nor with *i*-PrMgCl or *i*-PrMgCl.LiCl. Thus, the Br/Li exchange on **201** was

performed with BuLi or *t*BuLi in Et<sub>2</sub>O or THF at low temperatures. The reaction time and temperature were crucial for ensuring the stability of the 9-triptycenyllithium intermediate. Quenching with electrophilic borylating reagents provided the 9-borylated triptycenes **203a–b** in moderate yields (Scheme 54). The bulkier boron reagent FB(Mes)<sub>2</sub>, known to react with triptycen-1-yl lithium,<sup>[98]</sup> however did not react with the triptycen-9-yl lithium. We thus could not obtain compound **203c** presumably due to high steric hindrance around the triptycene bridgehead position (Scheme 54, bottom). Because of the limited stability of the triptycen-9-yl lithium reagent, we could not perform this reaction at higher temperatures and our attempts repeatedly led to the undesired formation of triptycene.



**Scheme 54:** Synthesis of the 9-borylated triptycenes **203a-c**.

We then used the bis-boron reagents B<sub>2</sub>Pin<sub>2</sub> and B<sub>2</sub>Neo<sub>2</sub>. The borylated triptycene **203a** was obtained in a lower yield (14%) than with the aforementioned MeOBpin reagent (51%), which shows that the yield of **203a** cannot be further increased. The compound **203d** was isolated only in 23% yield when using B<sub>2</sub>Neo<sub>2</sub> (Scheme 55).



**Scheme 55:** Synthesis of the pinacol and neopentylglycol triptycen-9-yl boronates **203a** and **203d**.

Since the known 9-triptyceny pinacol boronate **203a** has not been previously characterized by  $^{11}\text{B}$  NMR spectroscopy,<sup>[97]</sup> we recorded the  $^{11}\text{B}$  NMR spectra of **203a**, **203b** and **203d**, which showed a characteristic peak at 33.2 ppm, 4.0 and 30.2 ppm, respectively. The X-ray diffraction analysis of the single crystals of **203a** and **203d** revealed that the C-B bonds in both compounds are respectively of 1.588(2) and 1.590(3) Å in length (Figure 4), thus comparable to that in other bulky alkyl-boronates such as in adamantyl pinacol boronate esters (1.582 Å).<sup>[101]</sup>

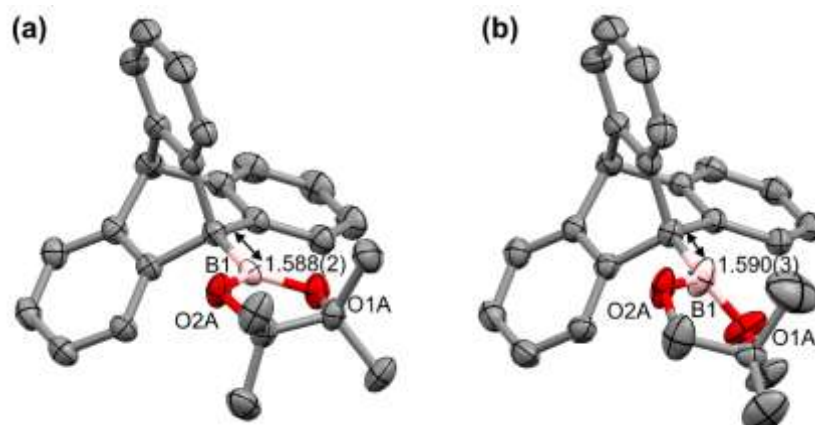
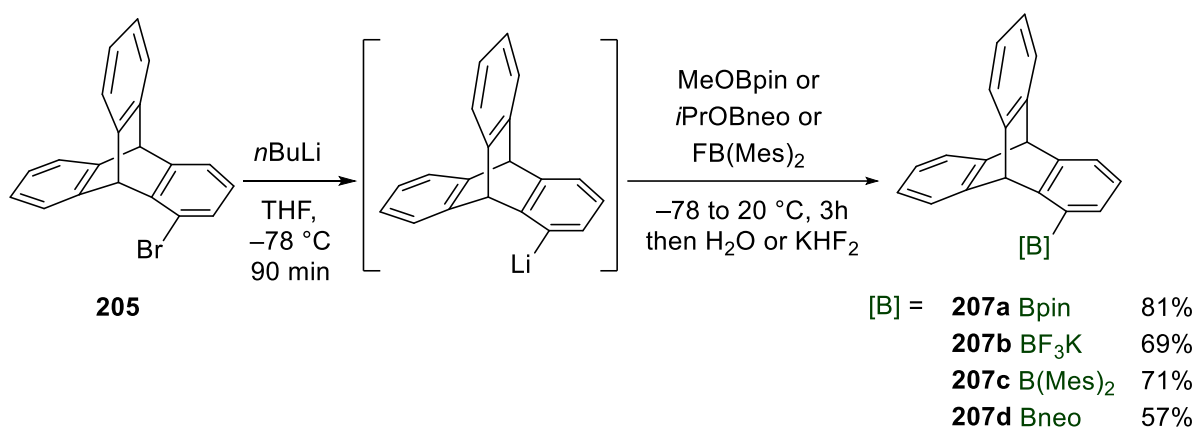


**Figure 4:** Molecular structure of compounds **203a** and **203d**. Here and further, thermal ellipsoids are shown at 50% probability level, hydrogen atoms are omitted for clarity.

We then synthesized 1-bromotriptycene **205** by a cycloaddition between 1-bromoanthracene and benzyne (see the experimental section).<sup>[102]</sup> The Br/Li exchange on **205** with  $n\text{BuLi}$  produced the triptycen-1-yl lithium reagent which was further used in reaction with various electrophilic boron reagents (Scheme 56). The four borylated triptycenes **207a-d** were obtained in good yields after purification by flash-chromatography or crystallization. Their  $^{11}\text{B}$  NMR characteristic signals were at 30.2, 2.9, 75.2 and 26.7 ppm, respectively.



**Scheme 56:** Synthesis of 1-borylated triptycenes **207a-d**.

The solid-state structures of compounds **207a** and **207d** determined by X-ray diffraction crystallography showed that their C-B bond lengths are of 1.560(3) and 1.566(3) Å (Figure 5). These shorter C-B bond lengths compared to **203a** and **203d** can be explained by the overlap between  $\pi$ -orbitals of the aryl ring with the empty p orbital of the boron allowing the extended conjugation of the  $\pi$  system and making the C-B bond gains some double bond character.

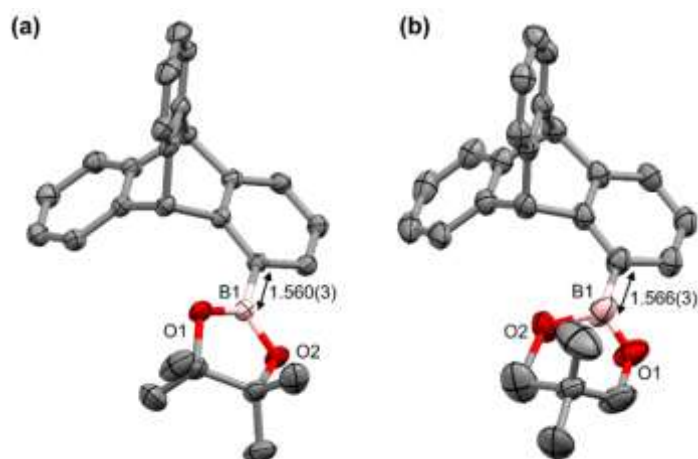


**Figure 5:** Molecular structures in the solid state of: a) compound **207a** and, b) of compound **207d** showing the dimeric like packing. The pinacol boronate ester derivative **207a** crystallized in a non-centrosymmetric space group.

The mesityl-triptycenyborane **207c** has an extremely sterically hindered environment around the boron atom, which might explain a long C1-B1 bond length of 1.567(6) Å (Figure 6), similar to those observed in the analogous 1,9-bis(mesityl)triptycenyborane (C1-B1 = 1.564(4) and C2-B2 = 1.572(4)).<sup>[98]</sup> Since in **207c** the triptycene scaffold is connected at the position 1, this triarylborane has roughly the same size as Mes<sub>2</sub>B(*o*-tolyl)borane, and is thus less bulky than B(Mes)<sub>3</sub>.

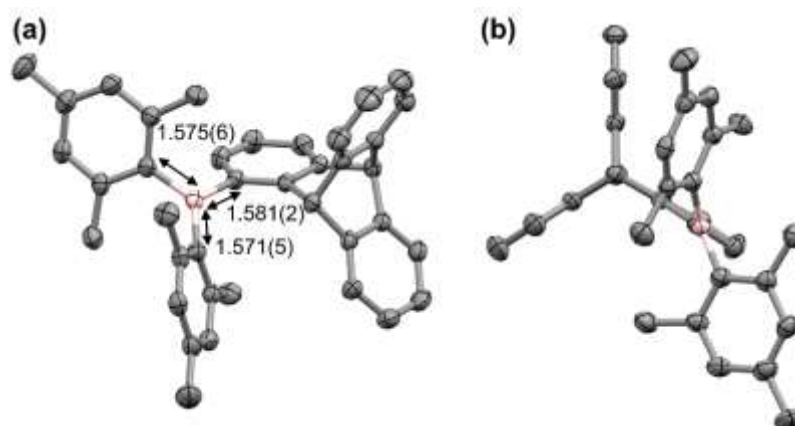


**Figure 6:** Molecular structure of compound **207c** in two orientations, a) showing its C-B bond lengths and b) its pseudo-gauche conformation when viewing along the B-C1 bond.

Now we turn our attention to the second synthetic approach, involving the [4+2] cycloaddition of the borylated anthracenes **202a-b**<sup>[103]</sup> or **206a-b**<sup>[104]</sup> with generated benzyne *in situ* (Schemes 2a and b, bottom). As the structure of **206a** in the solid state has not been previously reported, we characterized it by X-ray diffraction crystallography, and observed that the anthracene moieties crystallized in a severely twisted arrangement with no  $\pi$ -stacking interactions between their aryl rings (Figure 7a). The interplanar twist angle between the planes of the anthracene motif and of the pinacolboronate motif was of 47° (Figure 7b).

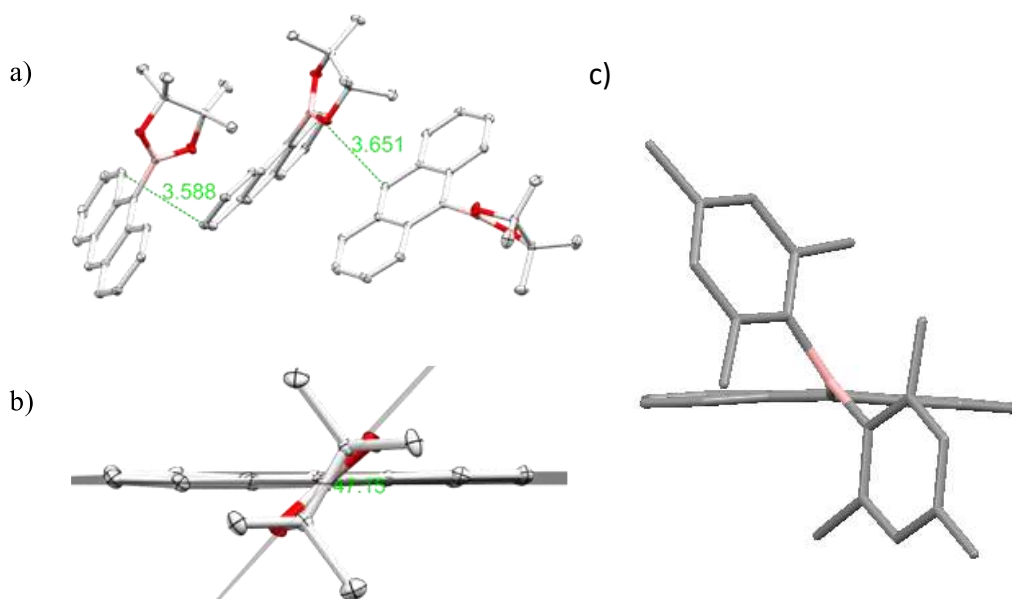
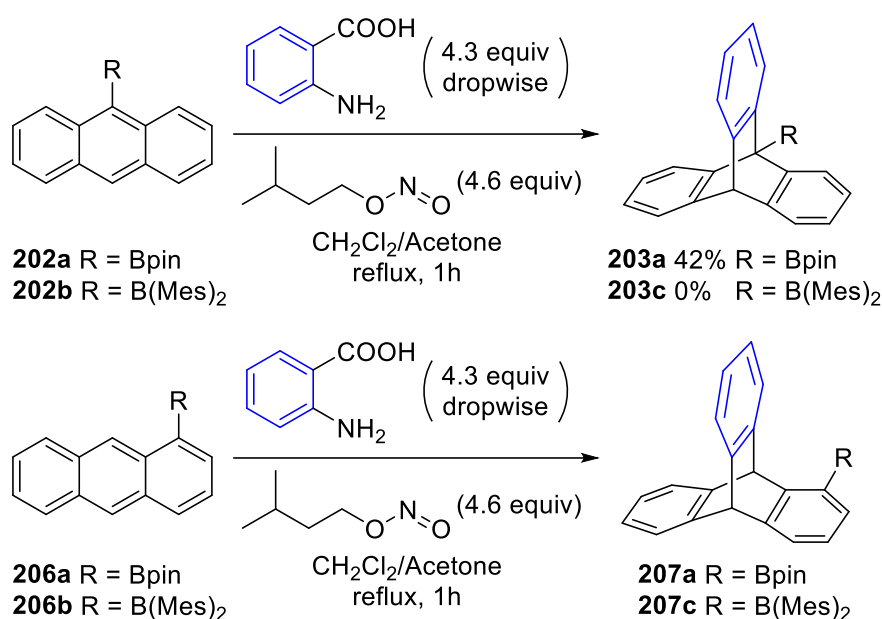


**Figure 7:** Structure of **202a** showing: a) the twisted stacks between anthracene skeletons, b) the dihedral angle between the mean planes of the pinacolboronate and the anthracene and c) the dihedral angle between the mean planes of the mesitylboronate and the anthracene.

A much larger twist is observed in the 9-(BMe<sub>2</sub>) substituted anthracene **202b**.<sup>[105]</sup> The B(Mes)<sub>2</sub> substituent is perpendicular to the anthracene scaffold, due to its much larger size than the Bpin group,<sup>[106]</sup> thus the anthracene central aromatic ring becomes entirely

sterically shielded. While the triptycene-Bpin **203a** was obtained from the first attempt by the cycloaddition reaction of **202a** with benzyne, the di(mesityl)borane triptycene **203c** was not formed by this synthetic approach (Scheme 57). The dimesityl-9-anthrylborane **202b** was recovered nearly quantitatively (>95%) at the end of the cycloaddition reaction illustrating that the B(Mes)<sub>2</sub> substituent is compatible with the reaction conditions and reagents used; however, B(Mes)<sub>2</sub> completely shielded both faces of the anthracene central ring thereby preventing benzyne from approaching. In contrast, the cycloaddition proceeded well with the 1-borylated Bpin and B(Mes)<sub>2</sub> anthracenes **206a-b** resulting in the formation of **207a** and **207c** in good yields (Scheme 57, bottom).



**Scheme 57:** Synthesis of 1 and 9-triptycenyl boron derivatives **203** and **207** by [4+2] cycloaddition reactions. The borylated anthracenes **202a-b** or **207a-b** have been synthesized following the literature procedures.<sup>[103,104]</sup>

To compare the photophysical properties of the B(Mes)<sub>2</sub> triptycene **207c** with that of the known triptycene with two BMe<sub>2</sub> groups at the positions 1 and 8 of the triptycene skeleton,<sup>[98]</sup> we recorded its UV-Vis and photoluminescence spectra in CH<sub>2</sub>Cl<sub>2</sub>. The UV/Vis absorption spectra of **207c** displayed a low-energy absorption band at 325 nm with  $\epsilon$  of 11670 (L.mol<sup>-1</sup>.cm<sup>-1</sup>) and two peaks at 277 and 270 nm with  $\epsilon$  of 5970 and 7000 (L.mol<sup>-1</sup>.cm<sup>-1</sup>), respectively (Figure 8). The emission spectrum showed a peak at 385 nm ( $\lambda_{\text{ex}} = 320$  nm). Thus, **207c** has a slightly red-shifted absorption spectrum (9 nm) and almost a similar emission spectrum compared to the known triptycene derivative with two BMe<sub>2</sub> groups at the positions 1 and 8 of the triptycene skeleton, which has the absorption spectrum at 316 nm and the PL spectrum at 383 nm in CHCl<sub>3</sub>/MeOH (1/1 vol).<sup>[98]</sup>



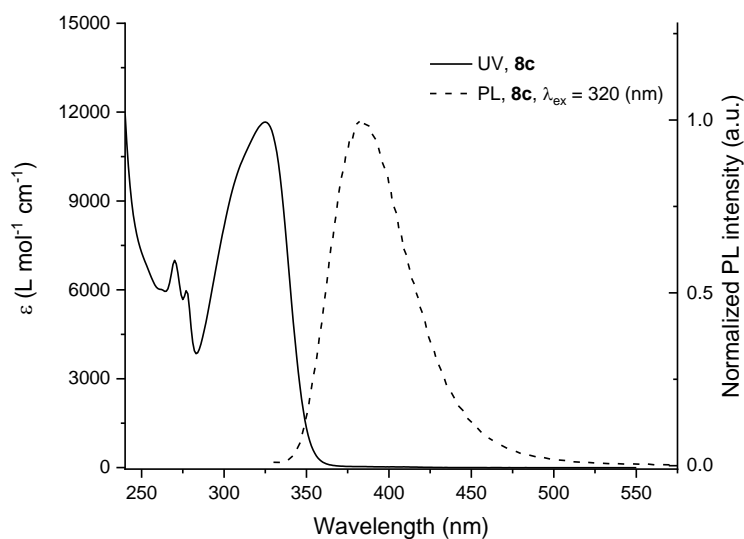


**Figure 8:** UV/Vis (solid line) and photoluminescence (PL) spectra (dashed line) of **207c** in CH<sub>2</sub>Cl<sub>2</sub>.

Finally, the geometry of compound **203c** which we could not obtain synthetically was fully optimized using density functional theory with the M06-2X exchange-correlation (XC) functional and the 6-311G(d) atomic basis set (Figure 9).<sup>[107]</sup> These quantum chemical calculations predicted a very long B–C(sp<sup>3</sup>) bond of 1.63 Å, comparable to the longest B–C(sp<sup>3</sup>) bond (1.655(4) Å) reported so far in the Cambridge Crystallographic Data Center,<sup>[108,109]</sup> which in addition to apparent steric repulsions between a mesityl group with the triptycene backbone aryl ring (Figure 9b), might be a reason of the failed reaction.

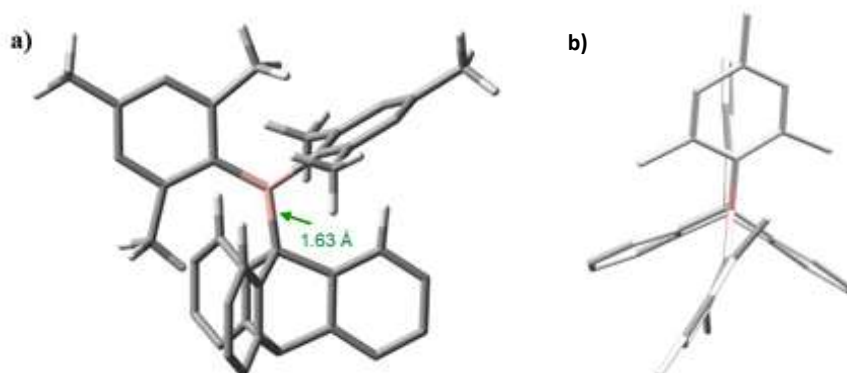
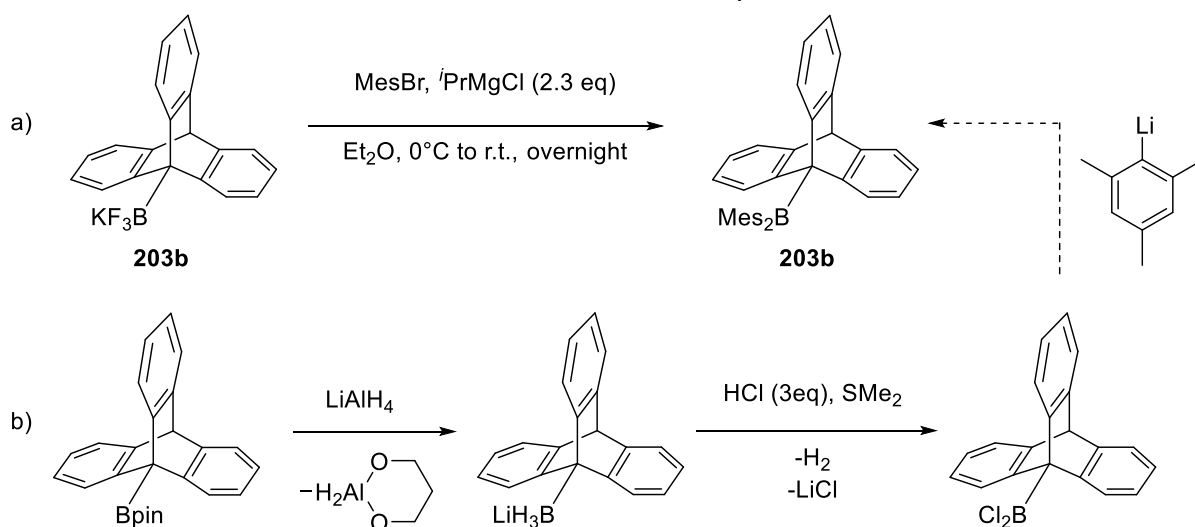


**Figure 9:** a) Computed structure of the (9-triptycenyl)dimesitylborane **203c** obtained from theoretical geometry optimization at the M06-2X level of theory; b) view along the B–C(sp<sup>3</sup>) bond to show the conformation of **203c**.

### 3. Conclusion and perspectives

Although the very crowded borane **203c** could not be obtained, the potassium 9-triptycenyl-trifluoroborate salt **203b** could serve as an alternative starting point. Further

reactions are underway in our laboratories between **203b** with two equivalents of mesityl lithium or mesityl magnesium bromide<sup>[110]</sup> (Scheme 58a). Another possible synthesis of **203c** has been envisioned by employing the pinacol borane **203a** as starting material. Indeed, pinacol borane can be converted to dichloroborane using LiAlH<sub>4</sub> and HCl according to the work of Brown<sup>[111]</sup> (Scheme 58b). This could lead to the formation of bulky boron Lewis acids, more sterically shielded than B(Mes)<sub>3</sub> due to the triptycene scaffold as very large substituent. Such Lewis acids could be used as selective anion detectors or as constituent of molecular machines, and the triptycenes boronates and trifluoroborates could be used as building blocks for the formation of functionalized triptycenes. Furthermore, these bulky Lewis acids could also be studied in the field of frustrated Lewis pairs in combination with bulky Lewis bases to activate small molecules such as H<sub>2</sub>, CO<sub>2</sub> or alkynes.



**Scheme 58:** a) Proposed synthesis of **203c**.  
 b) Proposed synthesis of **203c** precursor.

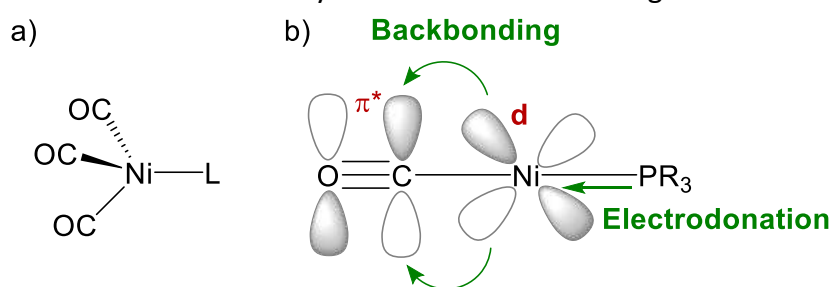
### III. Sterically Hindered Phosphines Derived from Triptycene: Reactivity and Applications in Frustrated Lewis Pairs Chemistry

#### 1. Ligands descriptors for catalyst design

Ligands such as phosphines play a key role in the modification and control of homogeneous catalysts. Indeed, modification of ligands provides a convenient approach to fine-tuning the performance of these catalysts. Thus establishing the relationship between steric or electronic descriptors of ligands properties and measurable consequences of such catalysts is essential to predict the effect of these ligands on catalyst behavior and performances.<sup>[112]</sup>

i. *Electronic descriptors*

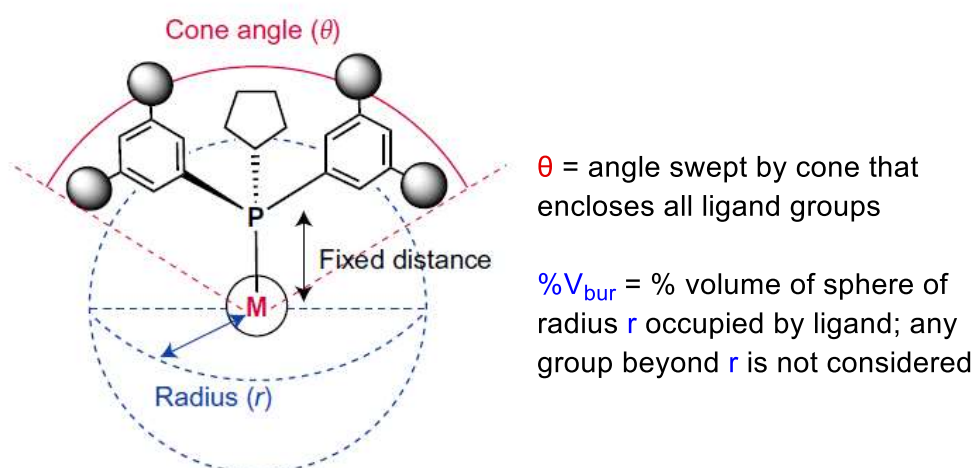
The use of descriptors for P-donor ligands knew a tremendous development since the Tolman's pioneering review.<sup>[113]</sup> He defined the highest CO stretching frequency measured by infrared spectroscopy of  $[\text{Ni}(\text{CO})_3\text{L}]$  complex (Scheme 46) as a parameter to determine the strength of the metal-ligand interaction. Indeed, the better electron donor the ligand is, the higher electron density is on the Ni center. Increasing electron density on the metal leads to better retrodonation to the CO which causes an increase of  $\text{C}\equiv\text{O}$  bond length and thus decreasing its IR stretching frequency. This method was assessed to be free from steric effect because of the cone-like shape of both tertiary phosphine ligand and  $\text{Ni}(\text{CO})_3$  metal fragment (Scheme 59). Besides, it is also possible to calculate this parameter using density functional theory (DFT)<sup>[114]</sup> (CEP = calculated electronic parameter) or with semiempirical calculations employing different complexes such as  $[\text{Rh}(\text{acac})(\text{CO})\text{Cl}]$  (SEP = semiempirical electronic parameter).<sup>[115]</sup> Carbonyl stretching frequencies and related measures of electron donation in a large range of different metal carbonyl complexes tend to highly correlate and have thus been widely used across different ligand classes.



**Scheme 59:** a) Tetrahedral structure of  $\text{Ni}(\text{CO})_3\text{L}$  complexes; b)  $\sigma$ -donation and  $\pi$ -retrodonation.

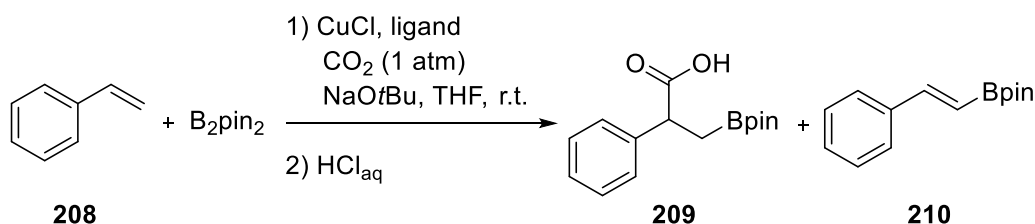
ii. *Steric descriptors*

Since Tolman's milestone review,<sup>[113]</sup> numerous steric descriptors have been proposed. The Tolman cone angle is defined as the apex angle of a cylindrical cone, centered 2.28 Å from the center of P atom, which just touches the Van der Waals radii of the outermost atoms of the model (Scheme 60). It quantifies the steric congestion around the phosphorus atom imposed by its substituents. Tolman cone angles can be derived from structural coordinates, including DFT-optimized structures and Smith and Coville<sup>[116]</sup> reported a process for their calculation. Even if the percent buried volume parameter ( $\%V_{\text{bur}}$ ) was originally developed for NHCs (N-heterocyclic carbenes) which due to the two-dimensional nature of their steric hindrance were not well described by cone angles, it has also been applied to tertiary phosphines. This descriptor can be used with structural coordinates issued either from calculations or from crystallograph. It establishes the percentage of the volume of a metal centered sphere of defined radius that is occupied by the ligands and has been shown to highly correlate with Tolman cone angles (Scheme 60).<sup>[117]</sup>



**Scheme 60:** Tolman cone angle (red) and buried volume (blue).

Notably, it has been employed to assess the steric effects of phosphine and carbene ligands on rate determining  $\text{CO}_2$  insertion for the copper-catalyzed boracarboxylation of styrene<sup>[118]</sup> (Scheme 61). It highlighted the fact that a greater steric hindrance causes a large distortion of the catalyst and  $\text{CO}_2$  in the transition state of  $\text{CO}_2$  insertion and thus its ineffectiveness.



**Scheme 61:** Copper-catalyzed boracarboxylation of styrene.

In 2006, Orpen *et al.*<sup>[119]</sup> developed a series of computational descriptors that are linearly related to energies (such as binding energies, orbital energies or proton affinity). Structural changes induced by complexation can be expressed as a perturbation from ideal geometry of a free ligand. They thus developed a new steric parameter called  $\text{He}_8\text{steric}$  that is defined as the interaction energy between a phosphorus (III) ligand and a ring composed of eight helium atoms. These He atoms are held in regular, fixed positions on a 2.5 Å radius circle. The phosphine structure is then re-optimized with the He ring centroid laying exactly at 2.28 Å above the phosphorus atom, starting from an optimized conformation of the free ligand (see Figure 10). With this model, it has been proven that only the substituents' steric effects contribute to the interaction energy. This parameter is calculated as follows:

$$E_{\text{steric}} = E_{\text{tot}}(\text{system}) - [E_{\text{tot}}(\text{He}_8) + E_{\text{tot}}(\text{L})] \text{ [kcal.mol}^{-1}\text{]}$$

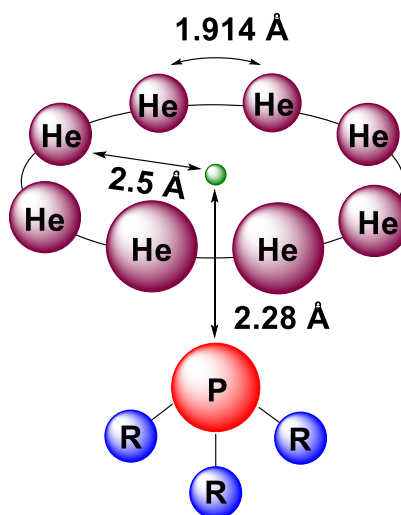


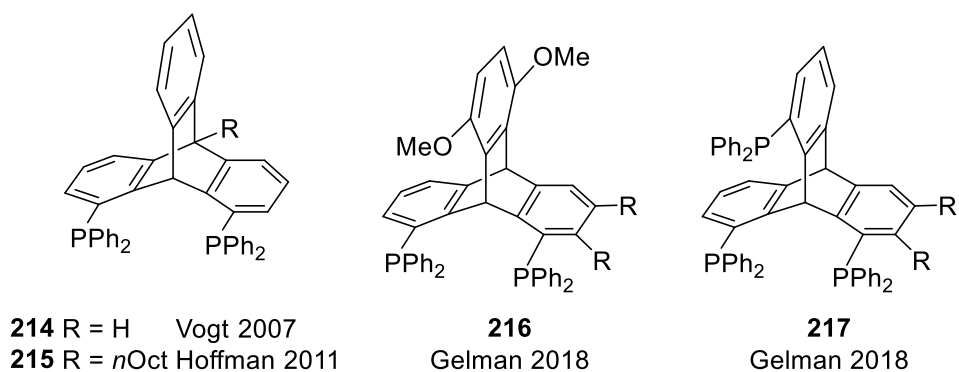
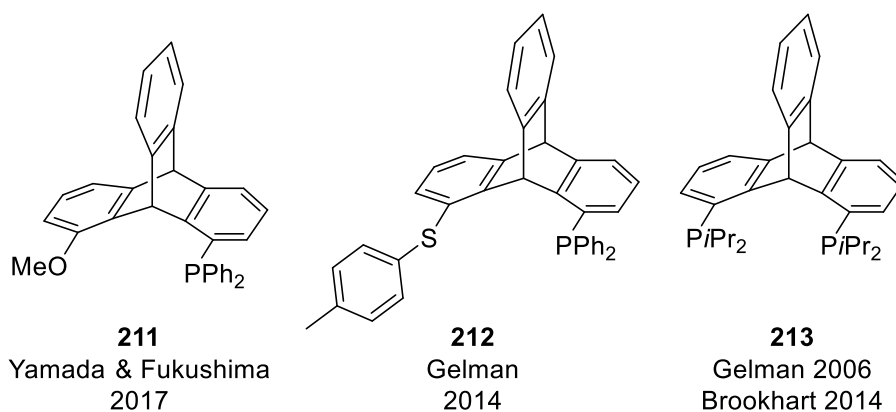
**Figure 10:** He<sub>8</sub>\_steric parameter

The buried volume describes the steric hindrance of the phosphine ligand in the metal's first coordination sphere while the cone angle quantifies it beyond the immediate proximity of the metal. These parameters are thus crucial for ligand design to assess their effectiveness in catalysis.

## 2. Objectives

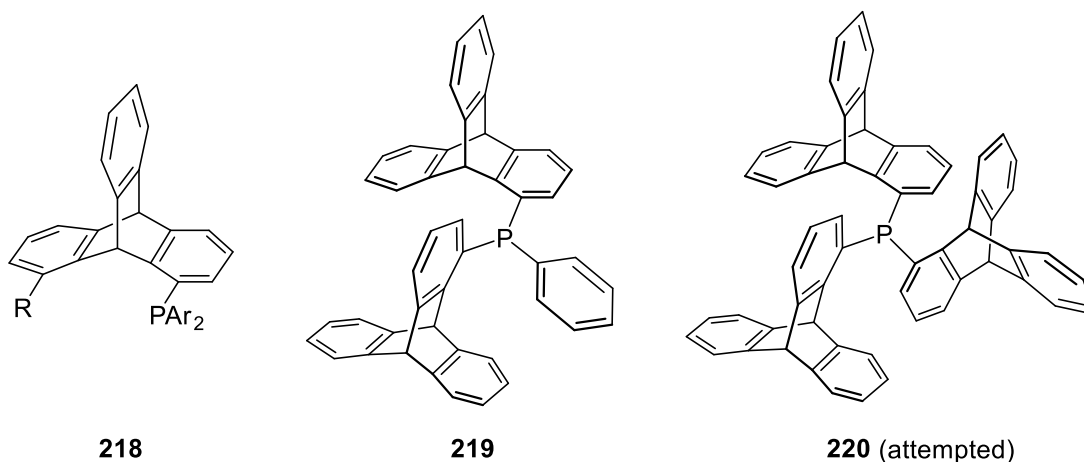
Tertiary phosphines are archetypal trivalent phosphorus compounds, widely used as nucleophilic organocatalysts,<sup>[120]</sup> ligands in transition metal-catalyzed reactions,<sup>[121]</sup> and Lewis bases in frustrated Lewis pair chemistry.<sup>[122]</sup> Electron-rich and sterically hindered phosphines **211-217** derived from triptycene (Scheme 62) have found numerous applications as mono, bi and tridentate ligands in enantioselective Pd-catalyzed hydrosilylation reaction of alkenes,<sup>[123]</sup> transfer hydrogenation of  $\alpha,\beta$ -unsaturated ketones,<sup>[124]</sup> Ir-catalyzed dehydrogenation of ethers,<sup>[125]</sup> transfer dehydrogenation of alkanes,<sup>[126,127]</sup> Ni-catalyzed butenenitrile isomerization,<sup>[128]</sup> hydrocyanation of butadiene,<sup>[129]</sup> and Au(I)-catalyzed cyclization of enynes.<sup>[130]</sup>

The triptycene scaffold, composed of three aromatic rings linked by a bicyclo[2.2.2]octane motif, acts as a particularly large substituent or linker in the triptycenylophosphines **211-217**, resulting in unprecedented types of bulky and unsymmetrical triarylphosphines. The second larger phosphorus substituent in **211-217** is a phenyl group, and, to the best of our knowledge, more sterically hindered phosphines derived from triptycene with larger substituents at the phosphorus atom have not been described so far.



**Scheme 62:** Known mono, bis and tridentate phosphines **211-217** derived from triptycene.<sup>[131,132,133,134,135,136,137]</sup>

Herein we report the synthesis of a series of electron-rich and sterically-hindered phosphines **218-220** featuring large *o*-tolyl and triptycenyl substituents (Scheme 63). Experimental evaluations of their steric hindrance (Tolman cone angle) and  $\sigma$ -donating and  $\pi$ -accepting abilities (Tolman electronic parameter) were first performed by characterizing their Rh complexes by IR spectroscopy and X-ray diffraction analysis. Theoretical computations were performed to determine their steric ( $\text{He}_8$  steric parameter) and their Brønsted and Lewis basicities by calculating their proton and methyl cation affinities.



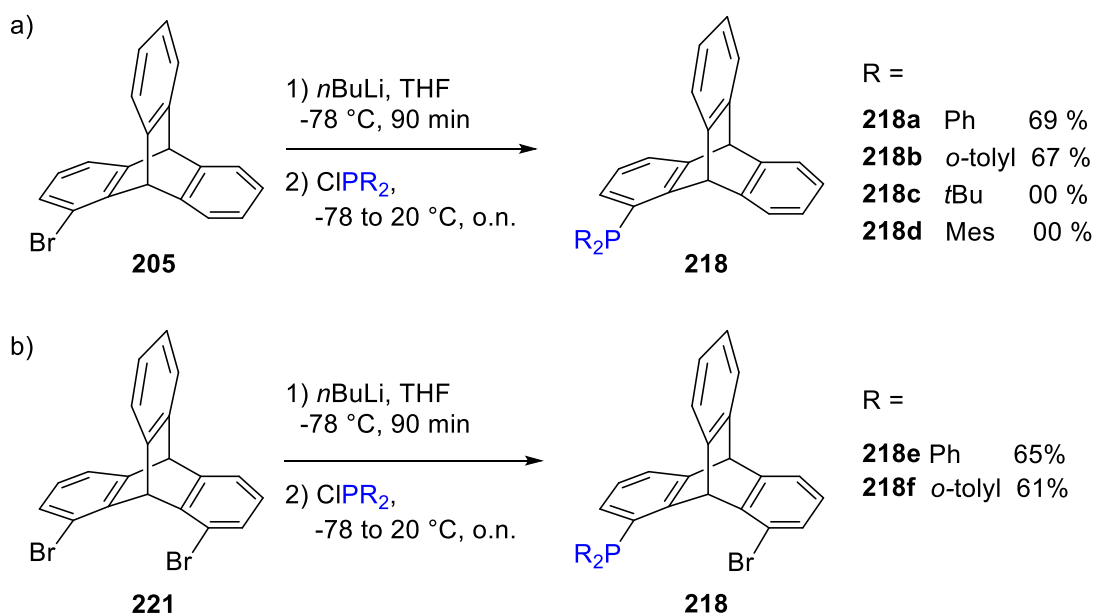
**Scheme 63:** Sterically hindered phosphines **218-220** investigated in this work.

Monitoring of their association with the tris(pentafluorophenyl)boron Lewis acid  $B(C_6F_5)_3$  by NMR spectroscopy showed that the sterically hindered phosphines **218-220** were resulting in unprecedented frustrated Lewis pairs, which were employed for capturing small molecules such as  $H_2$  and alkynes. These investigations provided information on the steric and electronic properties of **218-220** which were used to evaluate accurately for the first time the stereoelectronic quantitative effects of the triptycene scaffold on the phosphine reactivities.

### 3. Results and discussions

#### i. Synthesis of the triptyceny phosphines

The 1-bromo and 1,8-dibromo triptycenes **205-221**, obtained by [4+2] cycloaddition reactions of the corresponding anthracenes with in-situ generated benzyne, were treated with *n*BuLi in THF to perform a bromine/lithium exchange. The triptycen-1-yl-lithium intermediates were reacted with the chlorophosphines  $ClPR_2$  to produce the triptyceny phosphines **218a-b** and **218e-f** in good yields (Scheme 64). The reaction of the triptycen-1-yl-lithium reagents with the bulkiest chlorophosphines  $ClP(tBu)_2$  and  $ClP(Mes)_2$  was however not proceeding even after extended reactions time at higher temperatures and the phosphines **218c-d** were unfortunately not detected.



**Scheme 64:** Synthesis of phosphines **218a-f** from bromo-triptycenes **205-221**.

The triarylphosphines **218a-b-e-f** were recrystallized in chloroform or ethyl acetate, providing crystals suitable for X-ray diffraction analysis. In the solid-state, the P lone pairs pointed toward the central  $Csp^3$ -H bond of triptycene and **218e** formed dimers connected by a short  $C\cdots Br$  contact interaction (Figure 11c).

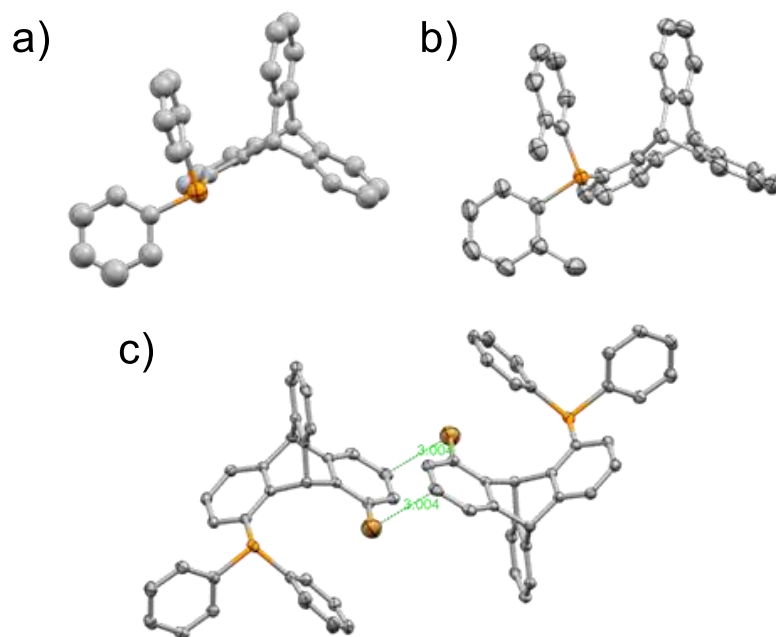
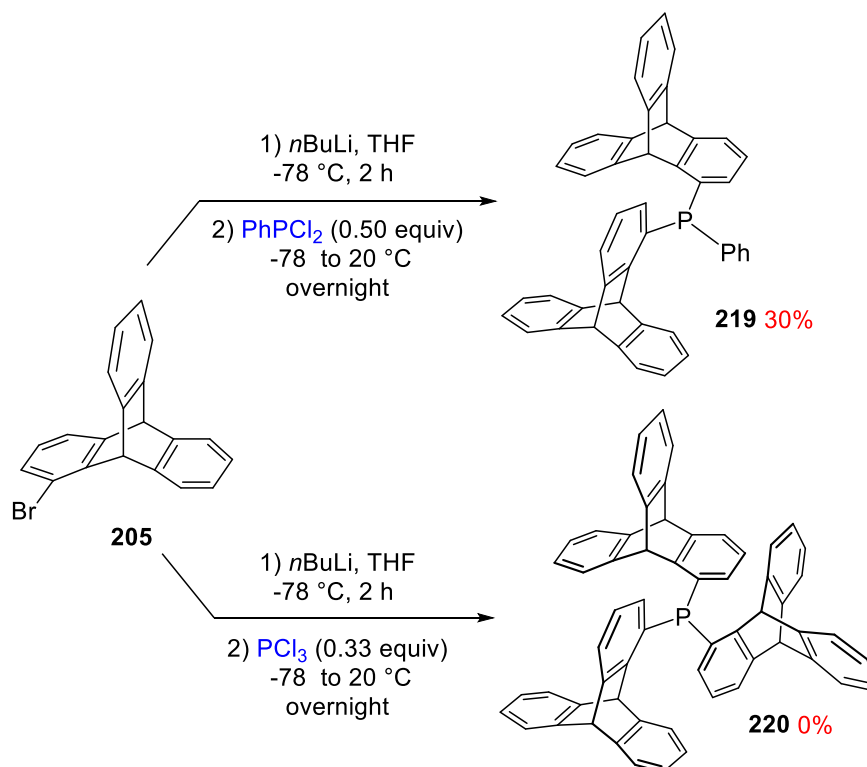


**Figure 11.** Structures of the triptycenylyphosphines a) **218a** and b) **218b** in the solid state (50% probability ellipsoids). c) structure of **218e** showing a Br $\cdots$ C short contact in the solid state.

The reaction of triptycen-1-yl lithium (2 equiv.) with PhPCl<sub>2</sub> provided the bulky bis-triptycenylyphenyl phosphine **219**, whereas reaction of three or more equivalents of triptycen-1-yl lithium with PCl<sub>3</sub> did not form **220** even under forcing conditions (Scheme 65).



**Scheme 65:** Synthesis of bis(triptycenylyphosphines) **219** and attempted synthesis of tris(triptycenylyphosphine) **220**.



Despite all our efforts, the structure of the bis-triptycenyphenyl phosphine **219** couldn't be obtained via X-ray diffraction. However, we managed to recrystallize its oxidized form in chloroform (Figure 12, left). In addition, the structure of **219** and **220** were studied via DFT calculations (Figure 12, centre and right respectively). We can notice that, as for the triarylphosphines **218a-b-e-f**, the P lone pair of **219** pointed toward the central Csp<sup>3</sup>-H bond of triptycenes. Moreover, according to these calculations, the tris-triptyceny phosphine **220** adopts a propeller-like conformation to reduce steric demands.

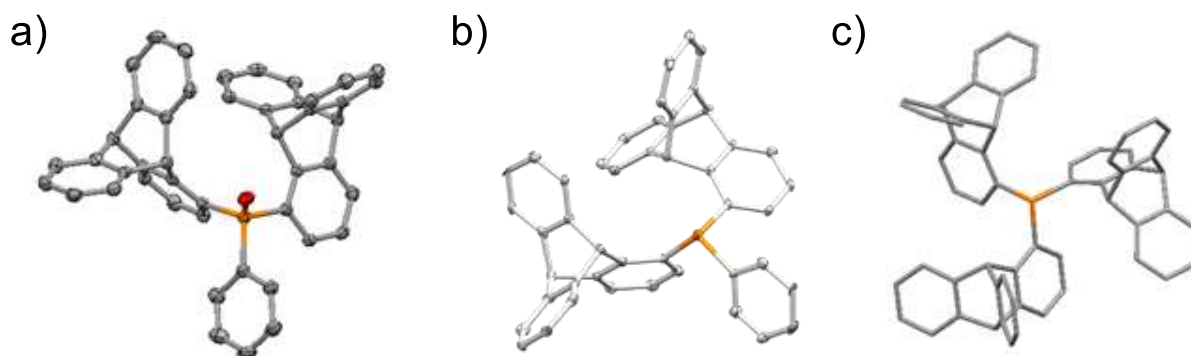


**Figure 12:** Structures of triptyceny-phosphine oxide **219<sub>oxide</sub>** in the solid state (left), calculated structures of triptyceny-phosphines **219** (center) and **220** (right).

ii. *Complexation of triptyceny phosphines with Rhodium*

Since the [Ni(CO)<sub>3</sub>PR<sub>3</sub>] complexes originally used by Tolman are highly toxic, all recent measurements are based on Rh complexes and a linear correlation is used to determine the electronic parameters. Thus, the rhodium complexes Rh(acac)CO(**218**) and Rh(acac)CO(**219**) were prepared and characterized by FT-IR and X-ray diffraction crystallography for determining the  $\sigma$ -donating and  $\pi$ -accepting abilities of two representative triptyceny-phosphines. Surprisingly, **218a** ( $\nu_{\text{CO}} / \text{Rh} = 1958 \text{ cm}^{-1}$ ) was found to be an unusually low stretching frequency, much lower than **218b** ( $\nu_{\text{CO}} / \text{Rh} = 1967 \text{ cm}^{-1}$ ) and similar to that of the strongly donating PCy<sub>3</sub> phosphine<sup>[105]</sup> ( $\nu_{\text{CO}} / \text{Rh} = 1959 \text{ cm}^{-1}$ ). The solid-state structure of the Rh complex Rh(acac)CO(**218a**) showed that both phenyl groups pointed outward from the triptycene core and that the rhodium complex was square planar with a Rh-P bond of 3.00 Å (Figure 13).

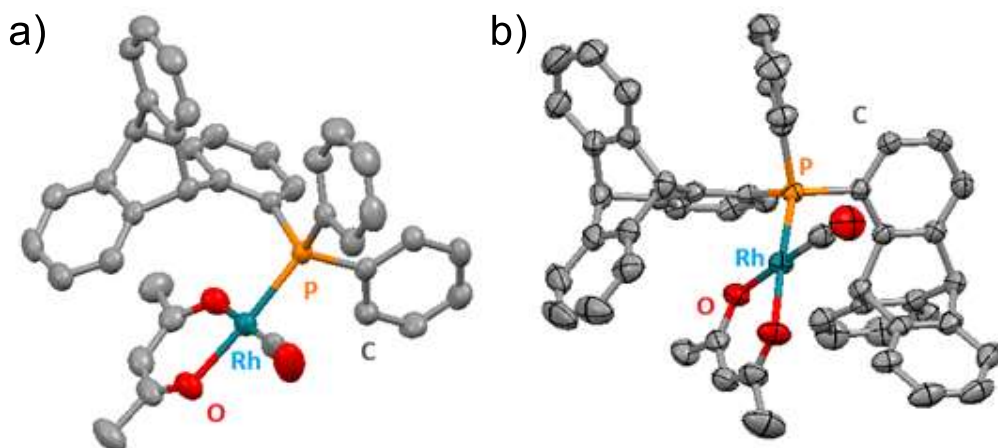


**Figure 13:** Structures of Rh(acac)CO(**218a**) (left) and Rh(acac)CO(**219**) (right) complexes.

iii. *Steric and electronic parameters of the triptycenylyl phosphines*

We next investigated the steric properties of the phosphines **218-220** by determining their crystallographic cone angles from the X-ray structures of their Rh complexes above, and by computing their  $\text{He}_8$ \_steric parameters (Table 1). The  $\text{He}_8$ \_steric parameter of **218a-b** was computed by optimizing the phosphines geometry with their P atoms constrained to lie at 2.28 Å above the centroid, and perpendicular to the plane of a helium ring which is constituted by eight helium atoms with a 2.5 Å radius (representative example for **218b** in Figure 14).

Two conformations were possible, with either the P ortho-tolyl groups avoiding steric repulsion with the triptycene aryl rings, leading to a P lone pair pointing toward the central  $\text{Csp}^3$ -H bond of triptycene (Figure 14a), or the P lone pair oriented toward the exterior or the triptycene scaffold (Figure 14b).

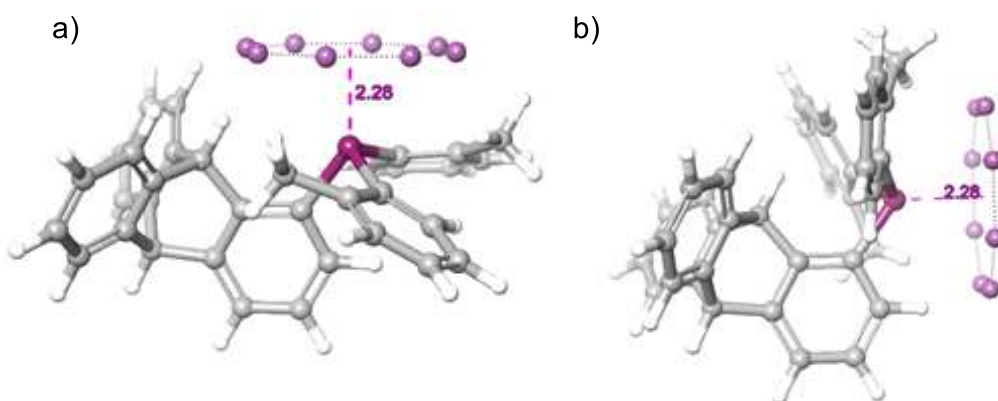


**Figure 14:** Molecular geometry of the two conformations of the Helium-8 rings complexes with the triptycenylyl-phosphine **218b**.

In the same way,  $\text{He}_8$ \_ring parameters have been calculated for triptycenylyl phosphines **219** (Figure 15 left) and **220** (Figure 15 right). Two possible conformations have also been studied for these structures. Indeed, phosphine **220** can adopt a helicoidal conformation or a disordered one laying at a higher relative energy (4.5 kcal/mol). For the

phosphines **219** and **220**, the  $\text{He}_8$ \_ring parameter is significantly lower than **218b** and  $\text{P}(o\text{-tolyl})_3$  (Table 7) which indicate a relatively low steric hindrance. However, these results have to be nuanced as the lone pairs of the phosphines are not pointing toward the centre of the He ring (see Figure 13).

Since the triptycenyphosphines **218a-b** and **218e-f** adopted in the solid state a conformation in which the phosphine P atom lone pair is oriented toward the interior of the triptycene scaffold for minimizing steric interactions of the phosphorus substituents with the triptycene scaffold (Figure 16), we initially supposed that they would be highly hindered phosphines. However, even if the triptycenyldiphenylphosphine **218a** was found to be bigger than  $\text{PPh}_3$ , the triptycenyldi(*o*-tolyl)phosphine **218b** was found to be smaller than  $\text{P}(o\text{-tolyl})_3$ . This observation suggests that the steric demand of triptycene substituent is between a phenyl and a tolyl substituent (Table 7).

Furthermore, the steric parameters of the bis-triptycenyphenyl phosphine **219** are similar to those of  $\text{P}(o\text{-tolyl})_3$  while those of tri(triptyceny)phosphine **220** are found to be smaller. Thus, it seems that we reached a steric hindrance upper limit with two triptyceny substituents.

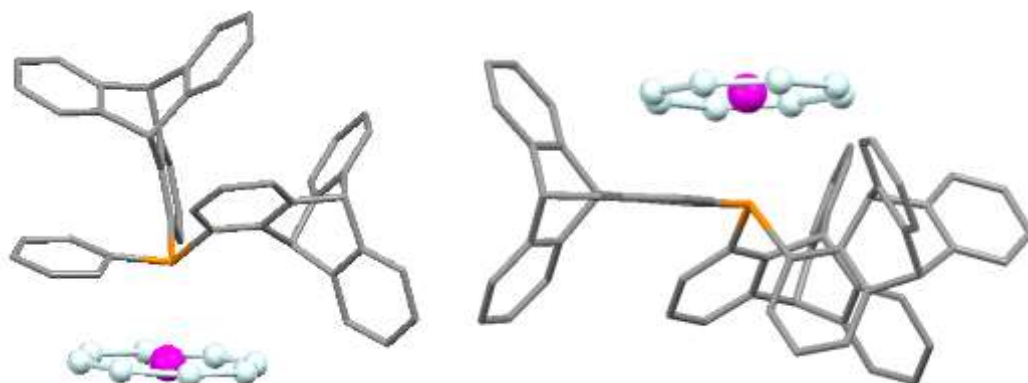


**Figure 15:**  $\text{He}_8$  ring complexes of **219** (left) and **220** (right).

**Table 7.** Experimental  $^{31}\text{P}$  NMR chemical shifts, cone angles and  $\nu_{\text{C}=\text{O}}$  stretching frequencies of  $\text{PPh}_3$ ,  $\text{P}(o\text{-tolyl})_3$ , **218a-b**, **219** and **220** and computed steric descriptors for phosphines derived from triptycene **218a-b**, **219** and **220** calculated with the M06-2X/6-311+G(d,p)//M06-2X/6-31+G(d) method in benzene.

	$\text{PPh}_3$	$\text{P}(o\text{-tolyl})_3$	<b>218a</b>	<b>218b</b>	<b>219</b>	<b>220</b>
$^{31}\text{P}$ NMR (ppm) <sup>a</sup>	-4.7	-29.3	-13.3	-29.0	-22.1	NC
Cone angle (deg)	145 <sup>b</sup>	194 <sup>b</sup>	136	170	203	NC
Buried volume (%)	29.6	46.7	40.8	NC	45.7	41.0 <sup>d</sup>
$\nu_{\text{CO}} / \text{Rh}$ ( $\text{cm}^{-1}$ ) <sup>c</sup>	1978 <sup>b</sup>	1974 <sup>b</sup>	1956	1970	1971	NC
$\text{He}_8$ _steric (kcal/mol) <sup>d</sup>	8.0 <sup>b</sup>	30.1 <sup>b</sup>	15.2 (12.4)	26.3 (21.2)	10.1 <sup>d,e</sup>	17.4 <sup>d,e</sup> (10.8)

<sup>a</sup>  $^{31}\text{P}$  chemical shift for **218e** = -13.9 ppm and **218f** = -30.5 ppm; <sup>b</sup> from ref. 138.; <sup>c</sup>  $\nu_{\text{C}=\text{O}} / \text{Rh}$  for **218e** = 1970  $\text{cm}^{-1}$  and **218f** = 1965  $\text{cm}^{-1}$ ; <sup>d</sup> calculated based on DFT structures; <sup>e</sup> the system had to undergo significant conformational changes in order to accommodate the helium ring.

The surprisingly low  $\text{He}_8$ \_steric parameters found for **219** and **220** can be explained by the fact that the electron pair of the phosphine is not pointing in the direction of the center of the  $\text{He}_8$  ring. Thus, it is necessary to fix the phosphine in a position where its electron pair is directly facing the center of the  $\text{He}_8$  ring to obtain more reliable results.

iv. *Evaluation of the Lewis and Brønsted basicities of triptyceny phosphines*

Interestingly, though the phosphines **218** adopted a conformation where the Ar substituents avoided steric interactions with the peri hydrogens of the triptycene scaffold in their ground-state geometry (Figure 16a), a  $90^\circ$  rotation occurred around the P-C(triptycene) bond upon protonation, resulting in a phosphonium tetrafluoroborate **218** with the two aryl substituents pointing toward the inner part of triptycene and the  $\text{H}^+$  pointing outside of the triptycene scaffold (Figure 16b)

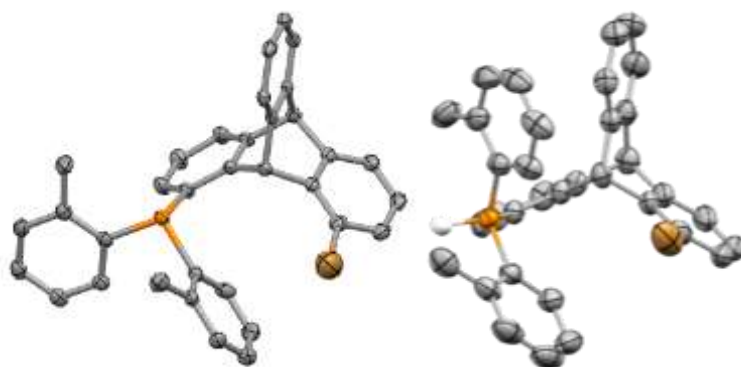


**Figure 16:** ORTEP drawing (50% probability ellipsoids) of, a) the bromo-triptyceny phosphine **218b** and, b) the phosphonium tetrafluoroborate **222** ( $\text{BF}_4^-$  counterion omitted).

The Brønsted and Lewis basicity of **218a-d** were next evaluated by calculating their proton affinities, methyl cation affinities, and  $\text{B}(\text{C}_6\text{F}_5)_3$  affinities (Table 8). Both conformations of the corresponding phosphonium and methyl-phosphonium salts  $[\mathbf{218-X}]^+$  were computed, either with the P-X bond ( $X = \text{H}, \text{Me}$ ) oriented toward the interior, or the exterior part of the triptycene scaffold and the PA and MCA values were found to be equal ( $\pm 1 \text{ kcal mol}^{-1}$ ) at the exception of **218d**.

**Table 8:** Computed energies of complexation of **218a-d**, **219** and **220** with  $\text{H}^+$  (proton affinity PA),  $\text{CH}_3^+$  (methyl cation affinity MCA) and  $\text{B}(\text{C}_6\text{F}_5)_3$  calculated with the M06-2X/6-311+G(d,p)//M06-2X/6-31+G(d) method in benzene.

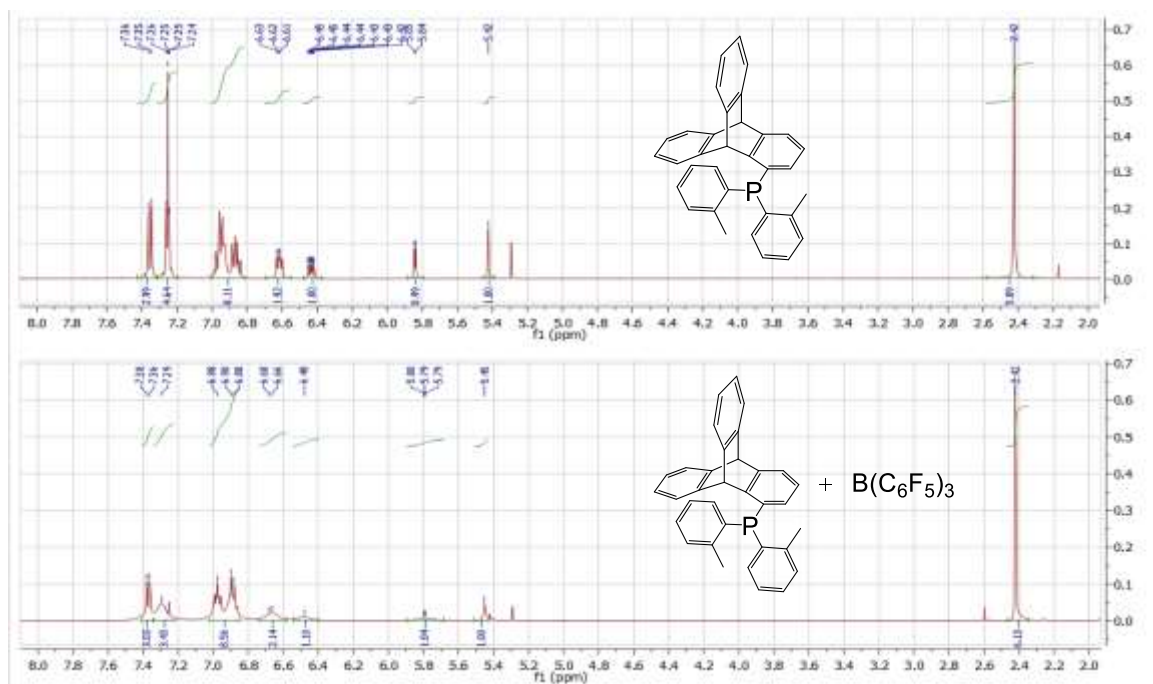
parameters	$\text{PPh}_3$	$\text{P}(\text{otolyl})_3$	<b>218a</b>	<b>218b</b>	<b>218c</b>	<b>218d</b>	<b>219</b>	<b>220</b>
PA / $\text{kcal mol}^{-1}$ <sup>a</sup>	-233	-238	-248	-251	-256	-258	-263	-263
MCA / $\text{kcal mol}^{-1}$ <sup>a</sup>	-136	-147	-114	-113	-120	-116	-121	-121
$\text{B}(\text{C}_6\text{F}_5)_3$ / $\text{kcal mol}^{-1}$	-21.7	-12.7	-16.3	-11.8	-14.2	-7.6	-5.1	NC
P-B bond (Å)	2.246	3.799	2.159	2.139	2.153	4.557	NC	NC

<sup>a</sup> The PA and MCA values (proton affinity and methyl cation affinities) are the average of the values for both conformers, see text above.

The higher proton affinities for compounds **218** to **220** indicate that these phosphines are more basic and electron-rich than  $\text{PPh}_3$  and  $\text{P}(o\text{-tolyl})_3$ . Moreover, the lower methyl cation affinities and  $\text{B}(\text{C}_6\text{F}_5)_3$  affinities for these phosphines suggest that they are more sterically hindered than  $\text{PPh}_3$  and  $\text{P}(o\text{-tolyl})_3$  and thus less likely to bind to methyl cation or tris(pentafluorophenyl)borane. We were thus interested to combine the triptycenyphosphines **218a-b** and **219** with the  $\text{B}(\text{C}_6\text{F}_5)_3$  boron Lewis acid and to evaluate the reactivity of the related frustrated Lewis pairs in the activation of small molecules.

#### 4. Toward frustrated Lewis pair catalysts based on triptycene

In agreement with the small negative calculated  $\Delta H^\circ$  values (Table 8), neither the phosphines **218a** nor **218b** associated with  $\text{B}(\text{C}_6\text{F}_5)_3$  in  $\text{CD}_2\text{Cl}_2$ , since the  $^1\text{H}$ ,  $^{31}\text{P}$  and  $^{11}\text{B}$  chemical shifts remained unchanged after mixing with  $\text{B}(\text{C}_6\text{F}_5)_3$ , suggesting a frustrated Lewis pair like behaviour. Only a slight broadening of the peaks was observed in  $^1\text{H}$  and  $^{31}\text{P}$  NMR spectroscopy at 20 °C, illustrating a highly reversible P-B association (signals of the Lewis adducts were not detected by NMR) (see Figure 17).



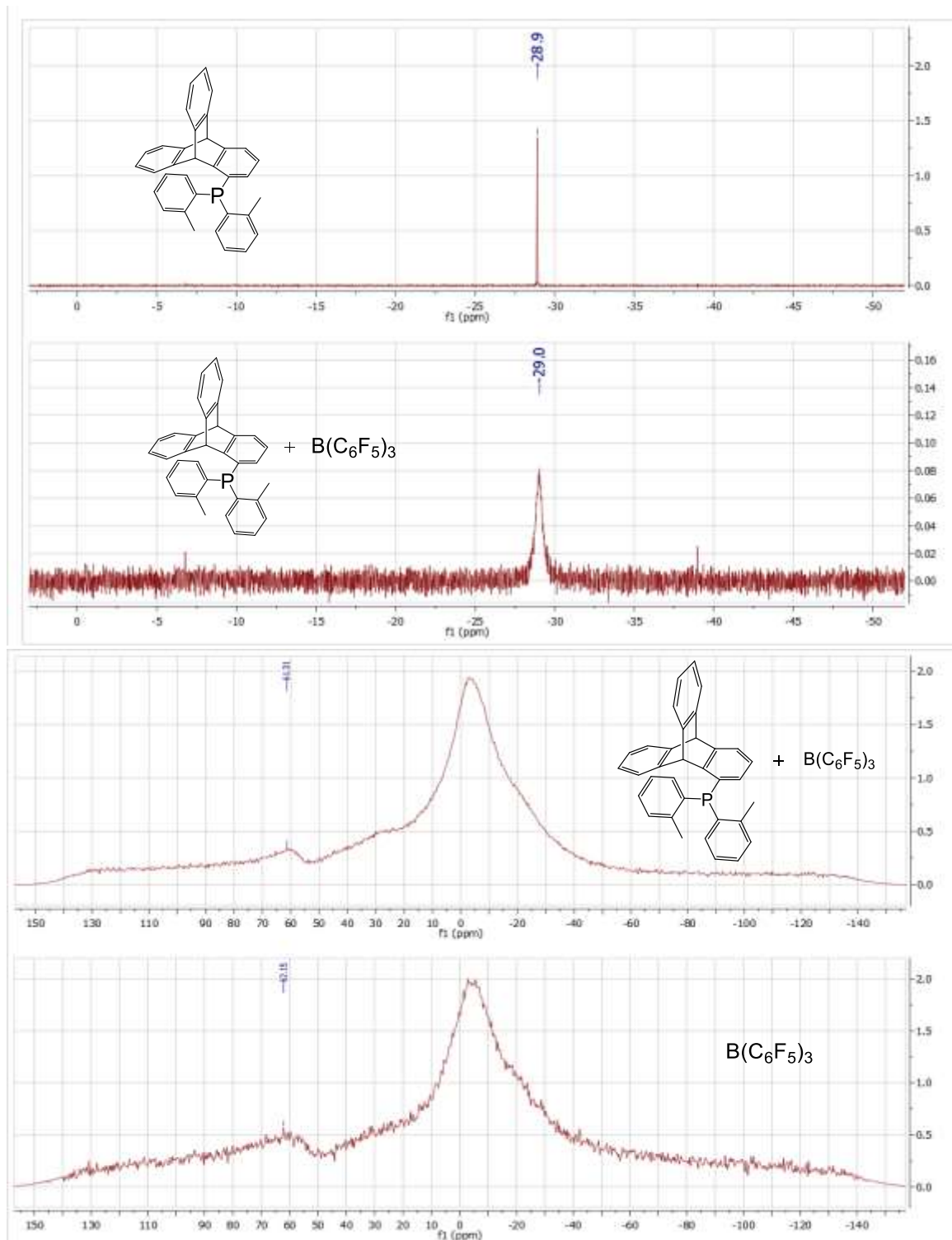
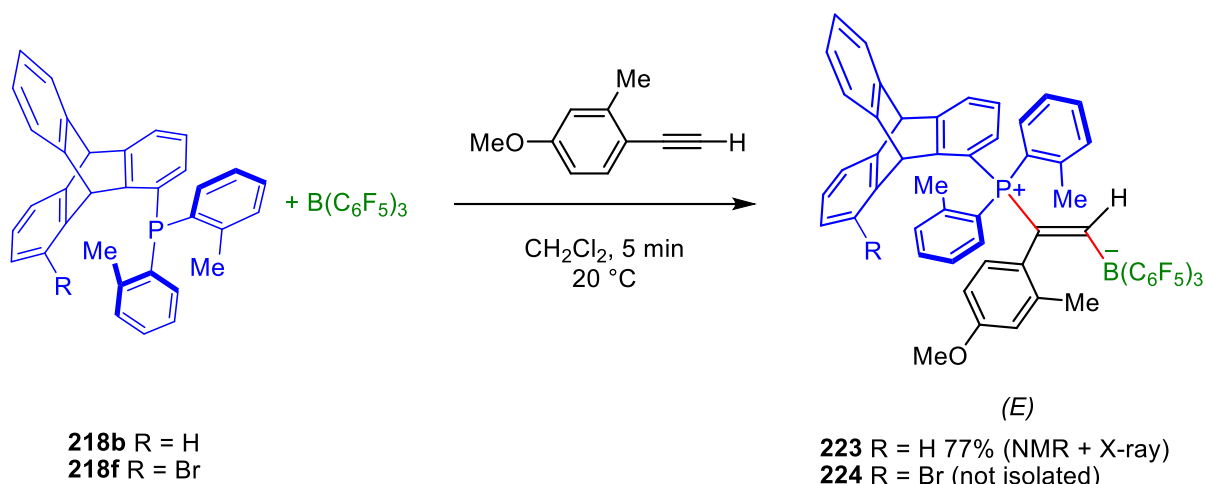


**Figure 17:**  $^1\text{H}$ ,  $^{31}\text{P}$  and  $^{11}\text{B}$  chemical shifts of **218b** upon mixing with  $\text{B}(\text{C}_6\text{F}_5)_3$ .

Addition of a functionalized phenylacetylene to the FLP of **218b**/ $\text{B}(\text{C}_6\text{F}_5)_3$  spontaneously resulted in the precipitation of colourless solid which was isolated in 77% yield after recrystallisation (Scheme 66).



**Scheme 66:** Addition of the FLP derived from **218b** or **218f** and  $B(C_6F_5)_3$  across the triple bond of a terminal alkyne.

The  $^{11}B$  chemical shifts of **223** and **224** were, respectively, of  $-16.1$  and  $-15.9$  ppm and the  $^{31}P$  chemical shifts were of 30.8 ppm and 30.5 ppm, very close to that in a similar alkene with  $P(o\text{-tolyl})_3$  instead of **218b** or **218f** ( $-13.6$  and 31.1 ppm).<sup>[139]</sup> The XRD characterization of **223** unambiguously showed that the FLP performed an addition across the triple bond to give a vinyl-phosphonium triarylborate (Figure 18) rather than an alkyne deprotonation.

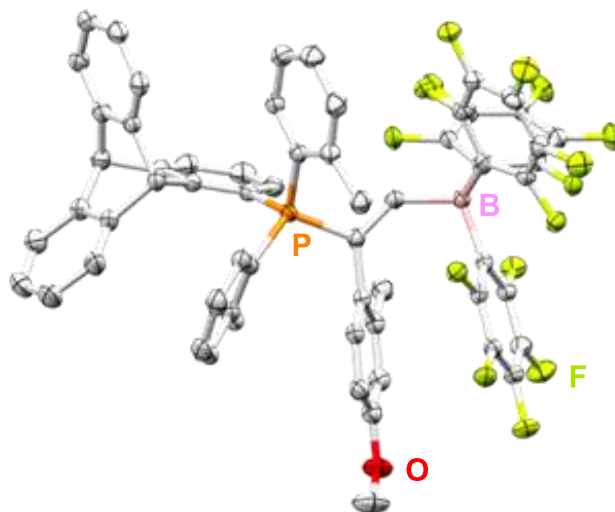
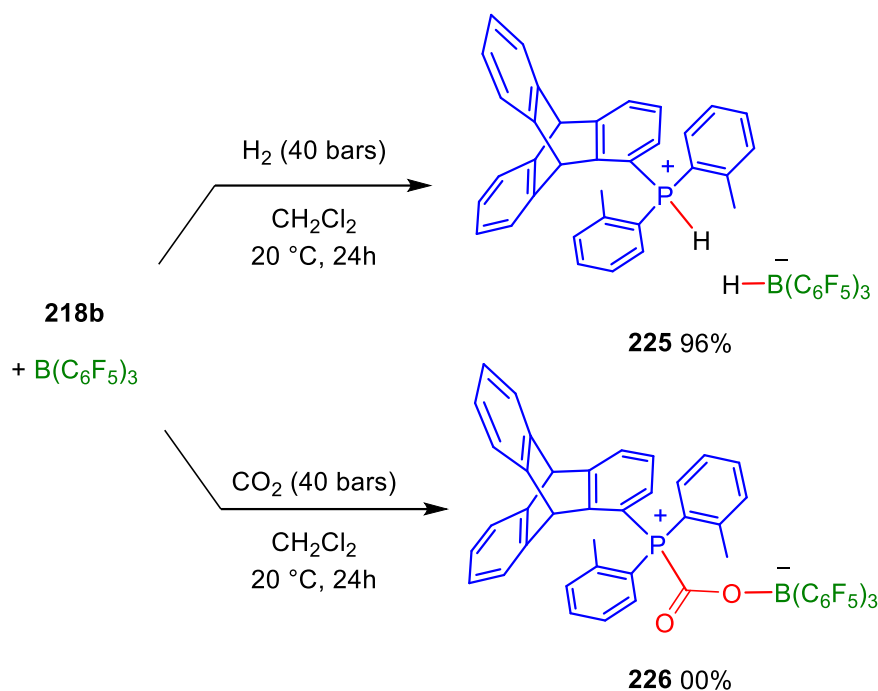


**Figure 18:** ORTEP drawing (50% probability ellipsoids) of the (*E*) vinyl-phosphonium triarylborate **223** ( $CH_2Cl_2$  solvate molecule omitted), P-C = 1.84 Å; C=C = 1.35 Å; B-C = 1.65 Å.

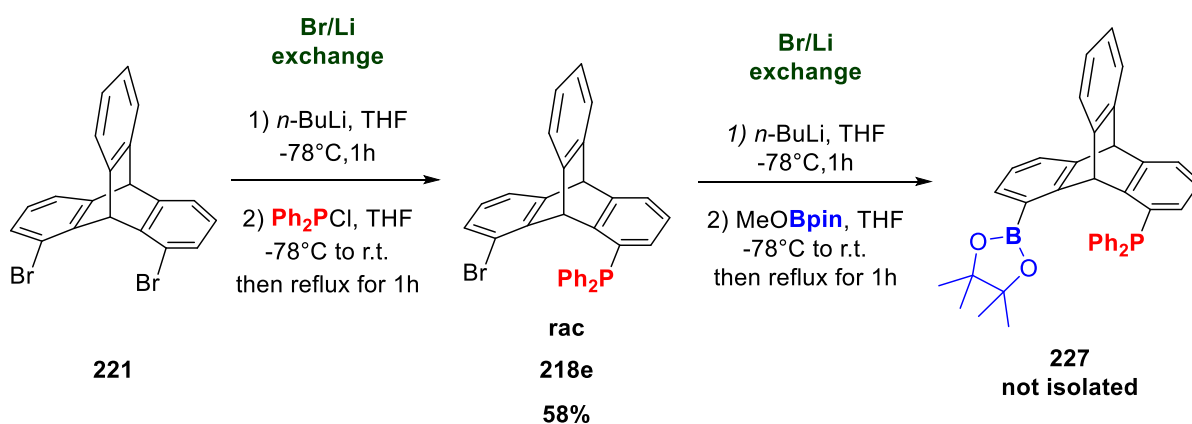
Finally, the heterolytic splitting of  $H_2$  was performed at 25 bars of  $H_2$  in  $CH_2Cl_2$ , providing access to the phosphonium hydridoborate salts **225** in good yield (Scheme 67) with a  $^{11}B$  chemical shift at  $-26.0$  ppm (d,  $^1J_{H-B} = 74$  Hz) and a very broad  $^{31}P$  chemical shift at  $-4.2$  ppm. The  $[R_3P-H^+][H-B(C_6F_5)_3^-]$  salts **225** is an intermediate in FLP catalyzed hydrogenations, showing that **218**/ $B(C_6F_5)_3$  combination can potentially be employed as catalyst for performing transition-metal free hydrogenation reactions. Addition on  $CO_2$  is highly reversible as for most aryl-phosphines. Thus, it is not surprising that we could not detect the  $CO_2$  addition product **226** after characterization of the crude by NMR spectroscopy.



**Scheme 67:** Reactivities of the FLP derived from **218b** and  $\text{B}(\text{C}_6\text{F}_5)_3$  with  $\text{H}_2$  and  $\text{CO}_2$

### 5. Attempted synthesis of intramolecular FLPs

Subsequently, we investigated the synthesis of intramolecular FLP systems starting from 1,8-dibromotriptycene **221**. A first Br/Li exchange was performed using *n*-BuLi in THF. The triptycenylium intermediate was then reacted with the chlorodiphenylphosphine to obtain the brominated phosphine **218e** in 58% yield. After, a second Br/Li exchange was performed using BuLi and the triptycenylium intermediate was treated with MeOBpin to afford the intramolecular FLP **227** in approximately 10% yield (Scheme 68). Unfortunately, the FLP could not be isolated and the yield was determined by  $^1\text{H}$  NMR analysis.



**Scheme 68:** Synthesis of intramolecular FLPs.

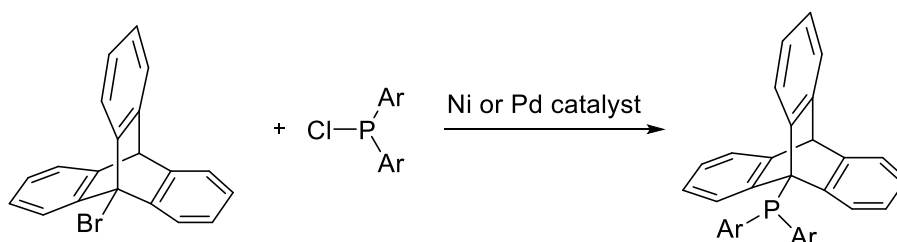


## 6. Conclusion

In conclusion, the study of the steric and electronic parameters of our triptyceny phosphines showed that the steric demand of a triptycene substituent lies between the one of a phenyl and the one of a tolyl substituent. Furthermore, the maximum steric hindrance around the phosphine was reached with two triptycenes as substituents according to the calculations. Moreover, the Lewis basicities of the phosphines **218-221** were used for the rational design of new FLPs in combination with the strong boron Lewis acid  $B(C_6F_5)_3$ . These FLPs readily add to terminal acetylenes, and activated  $H_2$ . These quantitative measurements will be useful for the future design and fine tuning of new FLPs catalysts for hydrogenation reactions and provide an avenue for the rational uses of sterically hindered Lewis bases derived from triptycenes in synthesis.

Besides, these bulky phosphines could be used as ligands for transition metals in the field of organometallic catalysis. Indeed, further studies on their remote steric hindrance should reveal if these phosphines can confer high activity upon Ni catalysts for Suzuki couplings for example. Indeed, remote steric hindrance is a feature specific from ligand with small buried volume and large cone angle. Thus, they are relatively unencumbered in the first coordination sphere of the metal but have large substituents distant from the metal. Thus, given the smaller size of Ni compared to Pd and the shorter Ni-P bond lengths (2.05 versus 2.28 Å), bulky phosphine ligands designed for Pd catalysis would congest a Ni center preventing the coordination of reaction components.<sup>[140]</sup>

The synthesis of bulky alkyl phosphines has also been tried, unfortunately, none could have been synthesized following the synthetic pathway developed in this work. However, the synthesis of such phosphines could be envisioned via coupling reaction between bromoalkyl and arylphosphanes using palladium catalyst. This could lead to the synthesis of even more basic phosphines and of the highly sterically demanding phosphines bearing one or several 9-triptycyl groups (Scheme 69).



**Scheme 69:** Alternative pathway for the synthesis of bulky alkyl 9-triptyceny phosphines.

Moreover, we developed the synthesis of precursors for the preparation of new rigid FLP systems with large distances between the Lewis acid and the Lewis bases. According to Delarmelina *et al.*,<sup>[67]</sup> the presence of a rigid scaffold and large P/B distances leads to an important decrease of the energy barrier for  $CO_2$  hydrogenation and a reduction of the energy

gap between the transition state for H<sub>2</sub> activation and CO<sub>2</sub> hydrogenation. It would thus make these processes feasible under mild experimental conditions.

## References:

- [78] L. Friedman, F. M. Logullo, *J. Am. Chem. Soc.*, **1963**, *85*, 1549.
- [79] a) M. J. McGlinchey, K. Nikitin, *Molecules*, **2020**, *25*, 1950; b) Z. Jia, X. Zhang, H. Li, X. Wang, *Theo. Chem. Acc.* **2020**, *139*, 62; c) K. Okamura, Y. Inagaki, H. Momma, E. Kwon, W. Setaka, *J. Org. Chem.* **2019**, *84*, 14636–14643; d) T. R. Kelly, H. De Silva, R. A. Silva, *Nature*, **1999**, *401*, 150–152; e) C.E. Godinez, G. Zepeda, M.A. Garcia-Garibay, *J. Am. Chem. Soc.* **2002**, *124*, 4701–4707.
- [80] a) B. W. Gung, X. W. Xue, H. J. Reich, *J. Org. Chem.*, **2005**, *70*, 3641–3644; b) I. K. Mati, S. L. Cockroft, *Chem. Soc. Rev.* **2010**, *39*, 4195–4205.
- [81] a) I. Kisev, D. Gelman, *Organometallics*, **2018**, *37*, 526–529; b) O. Grossman, C. Azerraf, D. Gelman, *Organometallics* **2006**, *25*, 375–381.
- [82] a) C.-F. Chen, *Chem. Commun.* **2011**, *47*, 1674–1688; b) J. H. Chong, M. J. MacLachlan, *Chem. Soc. Rev.* **2009**, *38*, 3301–3315.
- [83] a) Y. Jiang, C. F. Chen, *Eur. J. Org. Chem.*, **2011**, *32*, 6377–6403. b) G. Preda, A. Nitti, D. Pasini, *Chemistry Open*, **2020**, *9*, 719–727; c) G. M. Locke, S. S. R. Bernhard, M. O. Senge, *Chem. Eur. J.* **2019**, *25*, 4590–4647.
- [84] A. Wiehe, M. O. Senge, A. Schäfer, M. Speck, S. Tannert, H. Kurreck, B. Röder, *Tetrahedron*, **2001**, *57*, 10089–10110.
- [85] T. M. Long, T. M. Swager, *J. Am. Chem. Soc.*, **2003**, *125*, 14113–14119.
- [86] a) J. I. G. Cadogan, P. G. Hibbert, *Proc. Chem. Soc.*, **1964**, 338; b) J. I. G. Cadogan, J. Cook, M. J. P. Harger, P. G. Hibbert, J. T. J. Sharp, *Chem. Soc. B*, **1971**, 595.
- [87] a) J. P. N. Brewer, I. F. Eckhard, H. Heaney, B. A. J. Marples, *Chem. Soc. C*, **1968**, 664. b) H. Heaney, J. M. J. Jablonski, *Chem. Soc. C*, **1968**, 1895.
- [88] G. V. Zyryanov, M. A. Palacios, P. Anzenbacher, *Org. Lett.*, **2008**, *10*, 3681.
- [89] I. Mori, T. Kadosaka, Y. Sakata, S. Misumi, *Bull. Chem. Soc. Jpn.*, **1971**, *44*, 1649.
- [90] M. E. Rogers, B. A. Averill, *J. Org. Chem.*, **1986**, *51*, 17, 3308–3314.
- [91] X. Jiang, B. Rodriguez-Molina, N. Nazarian, M. A. Garcia-Garibay, *J. Am. Chem. Soc.*, **2014**, *25*, 8871–8874.
- [92] S. Toyota, T. Yamamori, M. Asakura, M. Öki, *Bull. Chem. Soc. Jpn.*, **2000**, *73*, *1*, 205–213. b) S. Toyota, T. Yamamori, T. Makino, M. Öki, *Bull. Chem. Soc. Jpn.*, **2000**, *73*, *11*, 2591–2597. c) S. Toyota, T. Yamamori, T. Makino, *Tetrahedron*, **2001**, *57*, *17*, 3521–3528.
- [93] B. W. Gung, X. Xue, H. J. Reich, *J. Org. Chem.*, **2005**, *9*, 3641–3644.
- [94] C.-H. Chen, F. P. Gabbaï, *Chem. Sci.*, **2018**, *9*, 6210–6218.
- [95] C. Azerraf, S. Cohen, D. Gelman, *Inorg. Chem.*, **2006**, *45*, 7010–7017.
- [96] G. Wittig, W. Tochtermann, *Justus Liebigs Ann. Chem.* **1962**, *660*, 23–33.
- [97] M. Oi, R. Takita, J. Kanazawa, A. Muranaka, C. Wang, M. Uchiyama, *Chem. Sci.* **2019**, *10*, 6107–6112.
- [98] C.-H. Chen, F. P. Gabbaï, *Chem. Sci.* **2018**, *9*, 6210–6218.
- [99] A. Jr. Streitwieser, G. R. Ziegler, *J. Am. Chem. Soc.* **1969**, *91*, 5081–5084.
- [100] Y. Kawada, H. Iwamura, *J. Am. Chem. Soc.* **1983**, *105*, 1449–1459.
- [101] S. K. Bose, K. Fucke, L. Liu, P. G. Steel, T. B. Marder, *Angew. Chem. Int. Ed.* **2014**, *53*, 1799–1803.

- [102] This method was not yet reported for the synthesis of 1-bromotriptycene **5**, which was previously synthesized by other methods, usually from 1,10-dibromotriptycene, see: a) E. A. Margulies, L. E. Shoer, S. W. Eaton, M. R. Wasielewski, *Phys. Chem. Chem. Phys.* **2014**, *16*, 23735–23742.
- [103] For the synthesis of the pinacolboronate-9-anthracene, see: a) S. Tang, W. Li, F. Shen, D. Liu, B. Yang, Y. Ma, *J. Mater. Chem.* **2012**, *22*, 4401. For the synthesis of the dimesityl-9-anthrylborane, see: b) J. F. Blount, P. Finocchiaro, D. Gust, K. Mislow, *J. Am. Chem. Soc.* **1973**, *95*, 7019–7029.
- [104] For the synthesis of the pinacolboronate-1-anthracene, see: a) ; A synthesis of the dimesityl-1-anthrylborane was recently reported from 1,9-dibromoanthracene, however we performed a similar synthesis starting directly from the see 1-bromoanthracene (see the SI): b) R. Teerasarunyanon, L. C. Wilkins, G. Parka, F. P. Gabbaï, *Dalton Trans.* **2019**, *48*, 14777–14782.
- [105] For the X-ray structure of the dimesityl-9-anthrylborane, see: C. Förster, W. Seichter, A. Schwarzer, E. Weber, *Supramolecular Chemistry*, 2010, *22*, 571–581.
- [106] V. Fasano, A. W. McFord, C. P. Butts, B. S. L. Collins, N. Fey, R. W. Alder, V. K. Aggarwal, *Angew. Chem. Int. Ed.* **2020**, *59*, 22403–22407.
- [107] Y. Zhao, D. G. Truhlar, *Theor. Chem. Acc.* **2008**, *120*, 215–241.
- [108] For the longest C-B bond in unstrained trialkyl or aryl boranes, see: R. W. Schurko, I. Hung, S. Schauff, C. L. B. Macdonald, A. H. Cowley, *J. Phys. Chem. A* 2002, *106*, 10096–10107.
- [109] Longer C-B bonds of up to 1.70 Å were reported in strained boron derivatives or in NHCs boronates Lewis adducts, see: a) A. F. Eichhorn, L. Kuehn, T. B. Marder, U. Radius, *Chem. Commun.* **2017**, *53*, 11694–11696; b) S. Fuchs, M. Flock, T. B. Marder, U. Radius, *Angew. Chem. Int. Ed.* **2017**, *56*, 10209–10213.
- [110] Y. Hoshimoto, T. Kinoshita, S. Hazra, M. Ohashi, S. Ogoshi, *J. Am. Chem. Soc.*, **2018**, *23*, 7292-7300.
- [111] H. C. Brown, A. M. Salunkhe, A. B. Argade, *Organometallics*, **1992**, *11*, 3094-3097.
- [112] D. J. Durand, N. Fey, *Chem. Rev.*, **2019**, *11*, 6561-6594.
- [113] C. A. Tolman, Steric effects of phosphorus ligands in organometallic chemistry and homogeneous catalysis., *Chem. Rev.*, **1977**, *77*, 313-348.
- [114] L. Perrin, E. Clot, O. Eisenstein, J. Loch, R. H. Crabtree, Computed ligand electronic parameters, from quantum chemistry and their relation to Tolman parameters, Lever parameters, and Hammett constants., *Inorg. Chem.*, **2001**, *40*, 5806-5811.
- [115] K. D. Cooney, T. R. Cundari, N. W. Hoffman, K. A. Pittard, M. D. Temple, Y. Zhao, A priori assessment of the stereoelectronic profile of phosphines and phosphites. *J. Am. Chem. Soc.*, **2003**, *125*, 4318-4324.
- [116] J. M. Smith, N. J. Coville, *Organometallics*, **2001**, *20*, 1210-1215.
- [117] H. Clavier, S. P. Nolan, *Chem. Commun.*, **2010**, *46*, 841-861.
- [118] X. Lv, Y.-B. Wu, G. Lu, *Catal. Sci. Technol.*, **2017**, *7*, 5049-5054.
- [119] N. Fey, A. C. Tsipis, S. E. Harris, J. N. Harvey, A. G. Orpen, R. A. Mansson, *Chem. Eur. J.*, **2006**, *12*, 291-302.

- [120] a) V. Iaroshenko, (Eds.), *Organophosphorus Chemistry: From Molecules to Applications*, Wiley-VCH, **2019**. b) P. C. Kamer, P. W. Van Leeuwen (Eds.), *Phosphorus(III) Ligands in Homogeneous Catalysis: Design and Synthesis*, Chichester: Wiley, **2012**.
- [121] a) H. Guo, F. Y. Chiao, Z. Sun, Y. Wu, O. Kwon, *Phosphine Organocatalysis.*, *Chem. Rev.* **2018**, *20*, 10049–10293; b) J. L. Methot, W. R. Roush, *Nucleophilic Phosphine Organocatalysis.*, *Adv. Synth. Catal.*, **2004**, *346*, 1035–1050.
- [122] J. Lam, K. M. Szkop, E. Mosaferi, D. W. Stephan, *FLP Catalysis: Main Group Hydrogenations of Organic Unsaturated Substrates.*, *Chem. Soc. Rev.*, **2019**, *48*, 3592–3612.
- [123] F. K-C. Leung, F. Ishiwari, Y. Shoji, T. Nishikawa, R. Takeda, Y. Nagata, M. Suginome, Y. Uozumi, Y. M. A. Yamada, T. Fukushima, *ACS Omega*, **2017**, *2*, 1930–1937.
- [124] I. Kiselets, D. Gelman, *Organometallics*, **2018**, *37*, 526–529.
- [125] T. W. Lyons, D. Bézier, M. Brookhart, *Organometallics*, **2015**, *34*, 4058–4062.
- [126] S. De-Botton, S. Cohen, D. Gelman, *Organometallics*, **2018**, *37*, 1324–1330.
- [127] D. Bézier, M. Brookhart, *ACS Catal.*, **2014**, *10*, 3411–3420.
- [128] M. E. Tauchert, D. C. M. Warth, S. M. Braun, I. Gruber, A. Ziesak, F. Rominger, P. Hofmann, *Organometallics*, **2011**, *10*, 2790–2809.
- [129] L. Bini, C. Müller, J. Wilting, L. Von Chrzanowski, A. L. Spek, D. Vogt, *J. Am. Chem. Soc.*, **2007**, *42*, 12622–12623.
- [130] N. Mézailles, L. Ricard, F. Gagosz, *Org. Lett.*, **2005**, *7*, 4133–4136.
- [131] Leung, K-C., Ishiwari, F., Shoji, Y., Nishikawa, T., Takeda, R., Nagata, Y., Suginome, M., Uozumi, Y., Yamada, Y. M. A., & Fukushima, T. (2017). *ACS Omega*, *2*(5), 1930–1937.
- [132] Cohen, O.; Grossman, O.; Vaccaro, L.; Gelman, D., *J. Organomet. Chem.* 2014, *750*, 13–16.
- [133] C. Azerraf, S. Cohen, D. Gelman, *Inorg. Chem.*, **2006**, *17*, 7010.
- [134] D. Bézier, M. Brookhart, *ACS Catal.* **2014**, *4*, *10*, 3411–3420.
- [135] L. Bini, C. Müller, J. Wilting, L. von Chrzanowski, A. L. Spek, D. Vogt, *J. Am. Chem. Soc.*, **2007**, *129*, *42*, 12622–12623.
- [136] M. E. Tauchert, D. C. M. Warth, S. M. Braun, I. Gruber, A. Ziesak, F. Rominger, P. Hofmann, *Organometallics* **2011**, *30*, *10*, 2790–2809.
- [137] I. Kiselets, D. Gelman, *Organometallics* **2018**, *37*, *4*, 526–529
- [138] L. Hu, D. Mahaut, N. Tumanov, J. Wouters, L. Collard, R. Robiette, G. Berionni, *Dalton Trans.*, **2021**, *50*, 4772–4777.
- [139] M. A. Dureen, C. C. Brown, D. W. Stephan, *Organometallics*, **2010**, *29*, 6594–6607.
- [140] K. Wu, A. G. Doyle, *Nature Chemistry*, **2017**, *9*, 779–784.

## **Chapter III:**

**Helicenes as platform for the design of new types of frustrated Lewis pairs**

# I. Helicenes in chemistry

## 1. Generalities

Helicenes are molecules composed of *ortho*-fused aromatic rings which adopt a chiral helicoidal topology due to intramolecular steric repulsions. This distortion induces electronic interactions between overlying cycles and the intrinsic chirality of helicenes. The torsional strain also results in having different C-C bond lengths in the helicene scaffold. Indeed, in comparison with the bond length of benzene (1.393 Å)<sup>[141]</sup>, the average bond length of the C-C bonds in the inner helix is lengthened to approximately 1.430 Å while the average length of the ones on the outer helix is reduced to about 1.360 Å.<sup>[142,143]</sup> Carbo[n]helicenes are hydrocarbon compounds only composed of successive benzene rings where n stands for the number of aromatic cycles while  $\sigma$ -helicenes contain a partially saturated scaffold. Carbohelicenes can be opposed to heterohelicenes which contain at least one heteroatom in their scaffold. Moreover, the chiral helical shape splits helicenes in two categories: P (plus) for right-handed helicenes and M (minus) for left handed helicenes (Figure 19a). For the nomenclature, carbon atoms are indexed as follows: tertiary carbons are numbered from the internal carbon of terminal cycle and quaternary carbons receive the number of previous tertiary carbon plus a letter (Figure 19b).

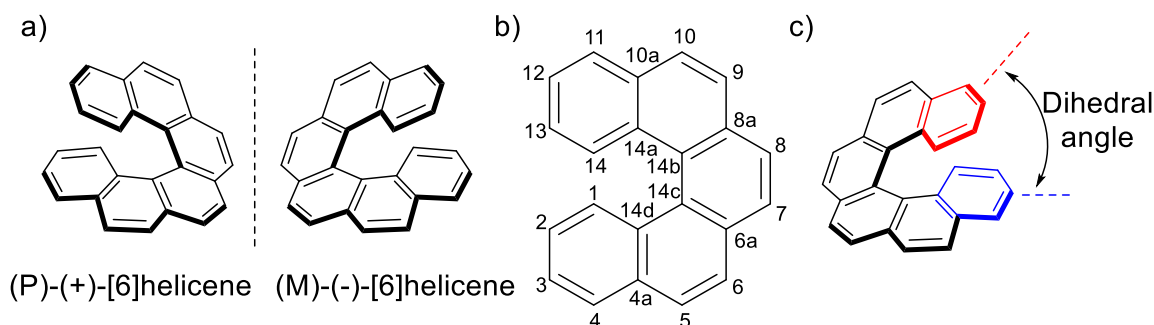


**Figure 19:** a) Chirality of helicenes, b) Atoms numbering according to Newman.  
c) Representation of the dihedral angle between the terminal cycles

The first helicenes have been synthesized in 1903 by Klaus Witte and Jakob Meisenheimer.<sup>[144]</sup> These are aza[5]helicenes with a pyrazine (Figure 20a) or a pyrrole (Figure 20b) ring in the middle of the structure instead of a benzene ring. The first carbo[4]helicene was described few years later in 1912,<sup>[145]</sup> and the first carbo[5]helicene in 1918.<sup>[146]</sup> It's only more than 30 years later in 1955 that carbo[6]helicene and its resolution was reported by Newman *et al.*,<sup>[147]</sup> it was the first example of a non-racemic helicene. Then in 1967, Martin and his co-workers published the synthesis of the carbo[7]helicene introducing for the first time photocyclization as a way to synthesize helicenes.<sup>[148]</sup> This method allowed to generate carbo[8]helicene and carbo[9]helicene in 1968,<sup>[149]</sup> and carbo[13]helicene in 1969,<sup>[150]</sup> and later carbo[11]helicene, carbo[12]helicene and carbo[14]helicene in 1975.<sup>[151]</sup> With 13 rings or more, helicenes have 3 layers which seriously restrain the synthesis. Indeed, it's only in

2015 that the carbo[16]helicene was synthesized by Fujita *et al.* and it is the longest helicene to have ever been reported.<sup>[152]</sup>

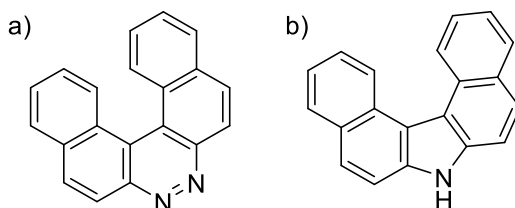


**Figure 20:** The first helicene synthesized in 1903.

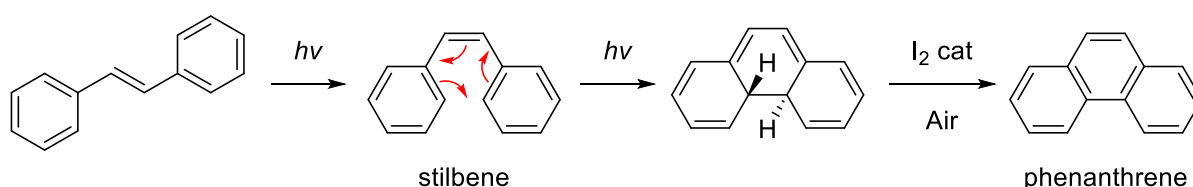
In 1971 and 1974, Wynberg<sup>[153]</sup> and Martin<sup>[154]</sup> respectively published the first reviews on helicenes. Subsequently, many other researchers reviewed helicenes and their derivatives focusing on synthesis, properties or applications.<sup>[155,156]</sup>

## 2. Helicenes and heterohelicenes synthesis

### i. Helicenes synthesis

Before 1967 and the introduction of photocyclization by Martin, synthesizing helicenes was difficult and the development of helicene chemistry was thus limited. For example, carbo[6]helicene was synthesized in 10 steps<sup>[147c]</sup> and there was no general synthetic method for each helicene. Photocyclization as a way to generate *ortho*-fused aromatic rings was reported by Mallory in 1964. Martin then introduced this method for helicenes synthesis diminishing the number of steps needed for the synthesis for the carbo[6]helicene from 10 to 4 for example. This method helped the development of helicene chemistry as it provided a simple and regioselective pathway to large helicenes as Martin could synthesize up to carbo[14]helicenes.<sup>[148,149,150,151]</sup> Fujita *et al.*<sup>[152]</sup> also used this method in 2015 to achieve the synthesis of the carbo[16]helicenes performing six photocyclizations in one-step.

Oxidative photocyclization proceeds in three steps. First, a *cis/trans* alkene isomerization occurs under the irradiation. Then the cyclization takes place on the stilbene derivative yielding a cyclohexadiene ring. Finally, a catalytic amount of I<sub>2</sub> perform an oxidation affording the phenanthrene derivative (Scheme 70).

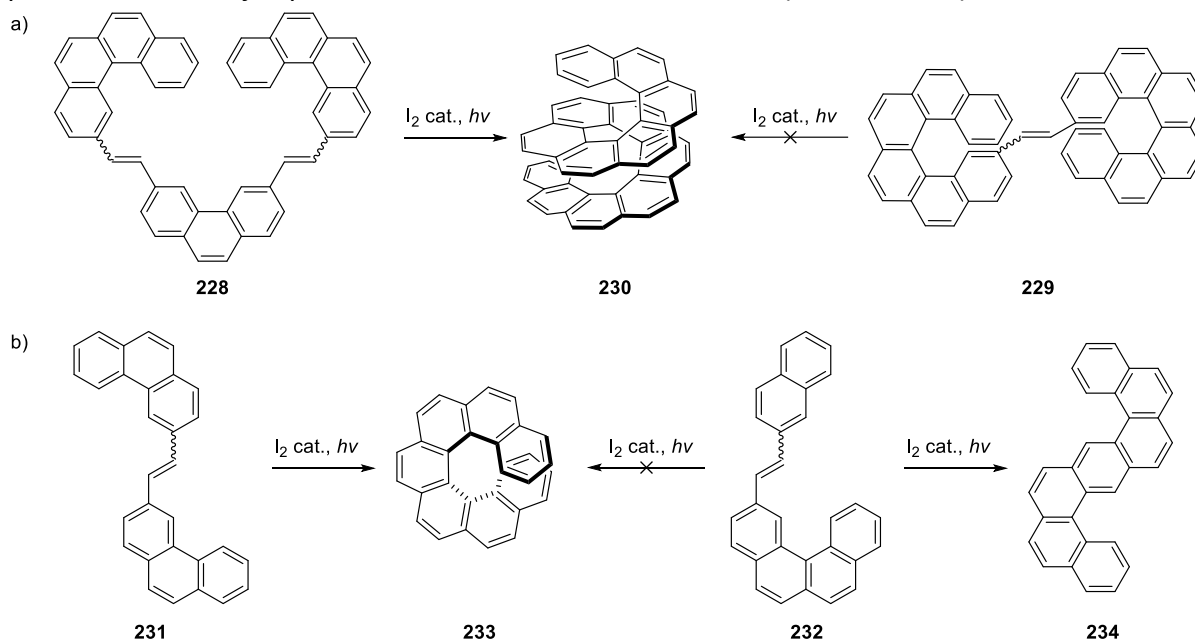


**Scheme 70:** Oxidative photocyclization for the synthesis of phenanthrene derivatives.

To synthesize longer helicenes, the design of the starting stilbene derivative is important. Indeed, the carbo[13]helicene is obtained in 52% yield starting from the

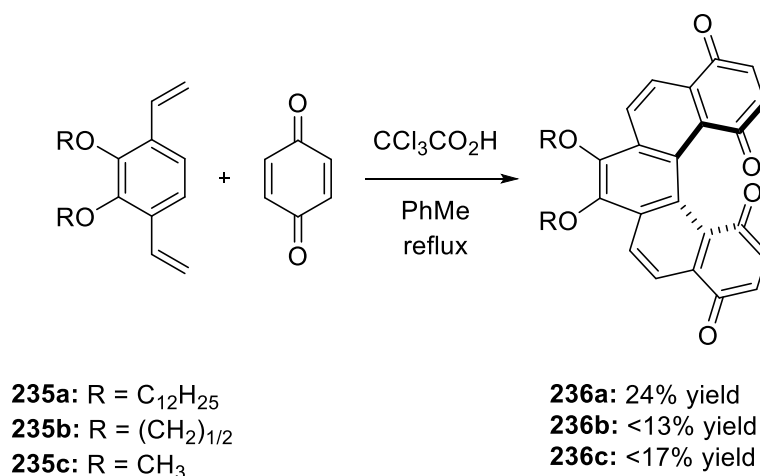


[4]+[3]+[4] precursor performing 2 photocyclizations while starting from the [6]+[6] precursor the reaction does not occur because of steric hindrance<sup>[157]</sup> (Scheme 71a). Moreover, if the synthesis of the carbo[7]helicene can be achieved by performing photocyclization on [3]+[3] precursor, when the starting material is the [4]+[2] precursor the major product is a carbo[4]helicene dimer (Scheme 71b).



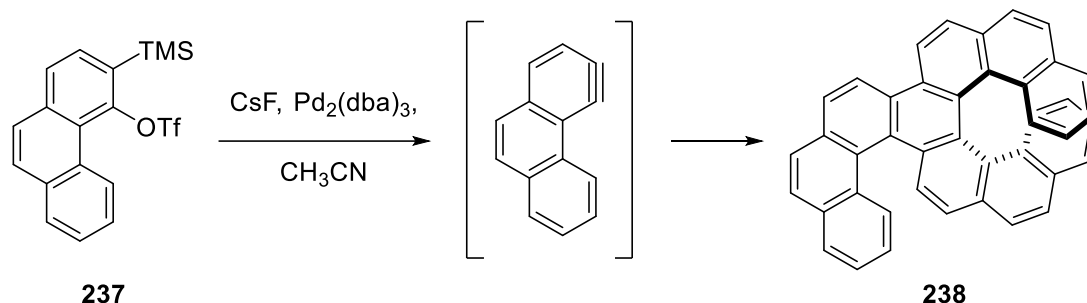
**Scheme 71:** a) Photocyclization methods for the synthesis of carbo[13]helicene  
b) Photocyclization methods for the synthesis of carbo[7]helicene.

In 1990, Katz<sup>[158,159]</sup> developed a new strategy to prepare [5]helicene derivatives using the Diels Alder reaction on quinones. Indeed, the functionalized helicene derivative **236a-c** could be prepared by refluxing *p*-benzoquinone and trichloroacetic acid in toluene with 2,3-dialkoxy-1,4-diethenylbenzenes **235a-c** up to 24% yield (Scheme 72).



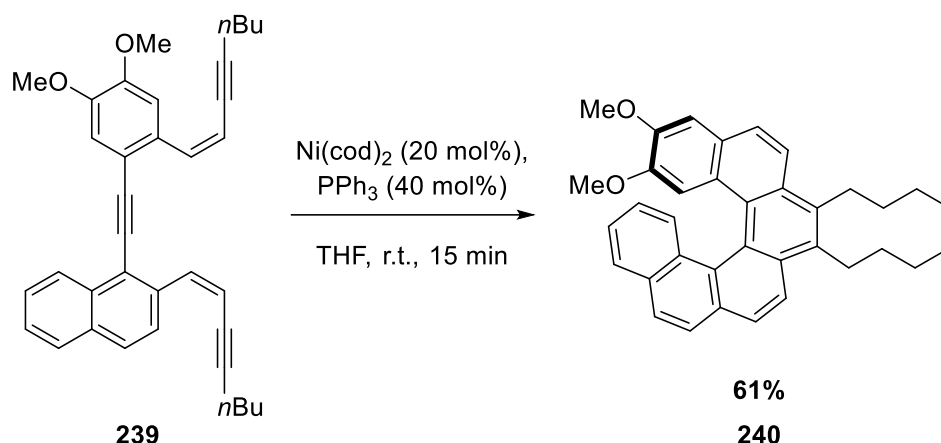
**Scheme 72:** Synthesis of carbo[5]helicene derivatives *via* Diels Alder reaction.

In 1998, Pérez and Guitián *et al.* reported a new method employing arynes *via* palladium catalyzed intermolecular [2+2+2] cyclotrimerization (Scheme 73) which revealed itself efficient for the synthesis  $D_3$  symmetric chiral scaffold. They notably synthesized molecules containing [4]helicene, [5]helicene and even [7]helicene moieties.<sup>[160,161]</sup>



**Scheme 73:** [2+2+2] cyclotrimerization for the synthesis of helicenes derivatives.

In 2002, Starý and Stará *et al.* published a method to synthesize carbo[5], [6] and [7]helicene derivatives *via* intramolecular [2+2+2] cyclotrimerization starting from triynes catalyzed by Ni or Co (Scheme 74).<sup>[162]</sup>



**Scheme 74:** Synthesis of substituted carbo[6]helicene reported by Starý and Stará *et al.*

## ii. Heterohelicenes synthesis

### a) Photocyclizations

Similarly to the synthesis of carbohelicenes, photoinduced synthetic pathway based on stilbene-type precursors (Figure 21) is a strategy commonly used for the preparation of heterohelicenes. However, it has been showed that the heteroatom affect the reactions.<sup>[163]</sup> For instance, the nitrogen atom in type B precursors can induce the ring closure to occur at the carbon sit of the pyridine ring (Scheme 75a) or

become involved in the photocyclization to yield a quaternary ammonium cation in the helicene scaffold **244a-b** (Scheme 75b).

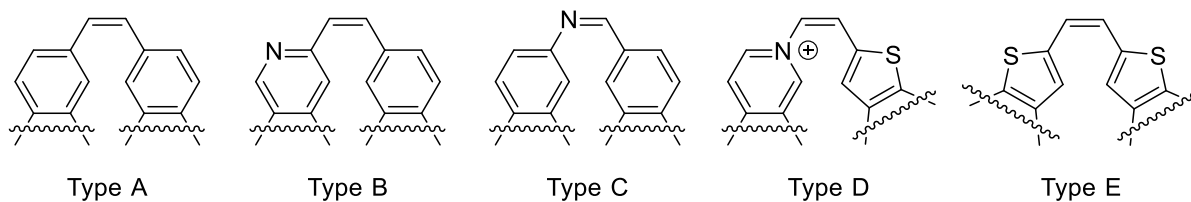
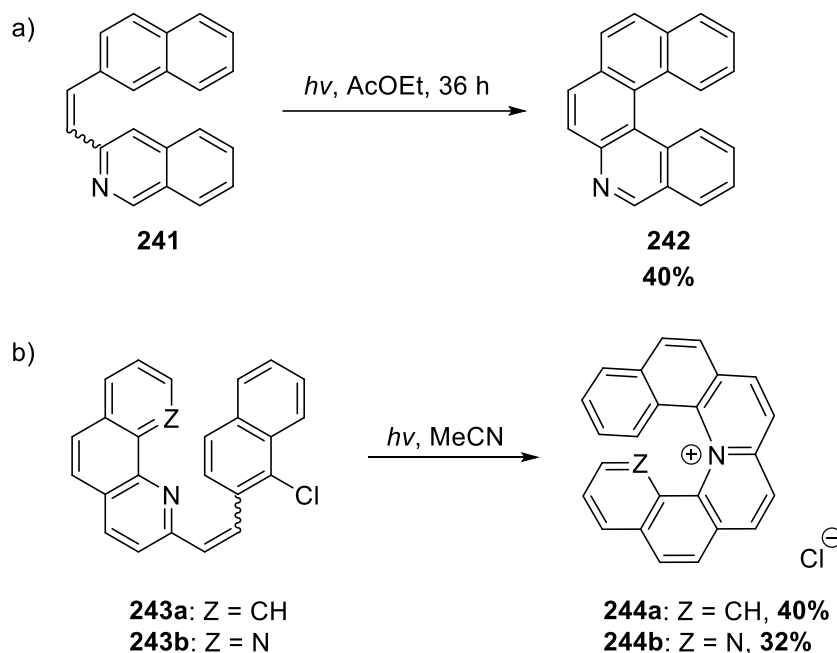
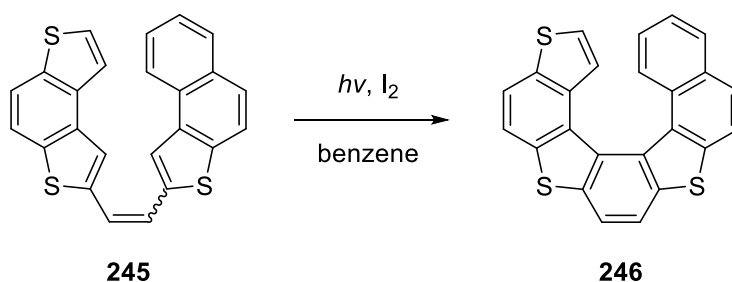


**Figure 21:** Different stilbene-type precursors for photocyclizations.



**Scheme 75:** Regioselectivities for the photocyclization of type B stilbene precursors.

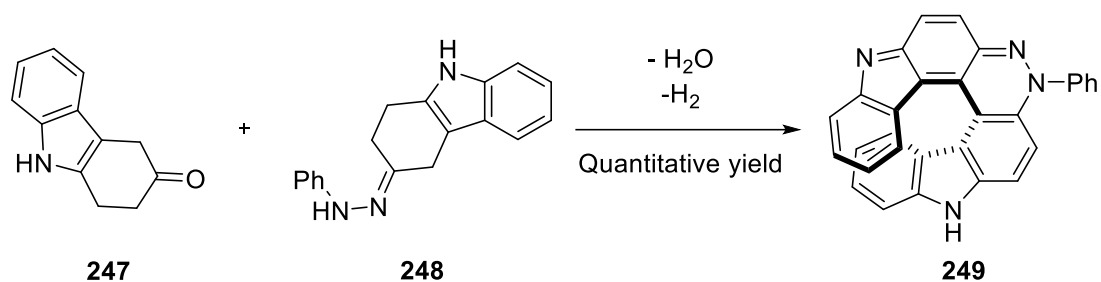
For type D and E, the low reactivity of sulfur atom only leads to the ring closure at the  $\beta$ -C of thiophenes (Scheme 76).



**Scheme 76:** Regioselectivity for the photocyclization of type E stilbene precursors.

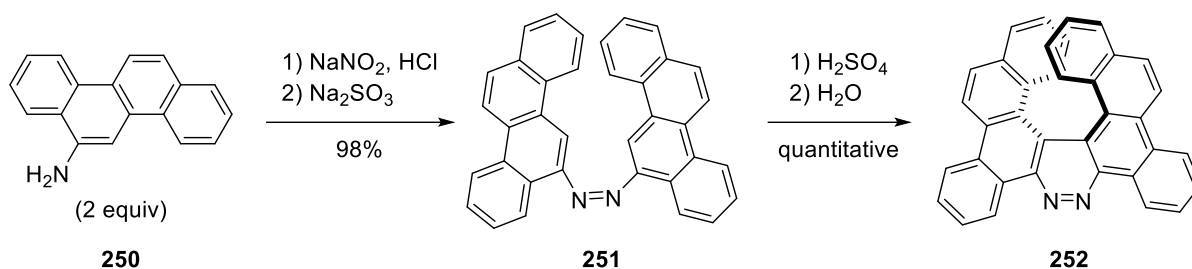
### b) Substitutions

In 1970, Vogel and Teuber reported a method for the synthesis of azahelicenes **249** proceeding *via* addition of hydrazines **248** on carbonyls **247** followed by a cyclization in quantitative yield (Scheme 77).<sup>[164]</sup>



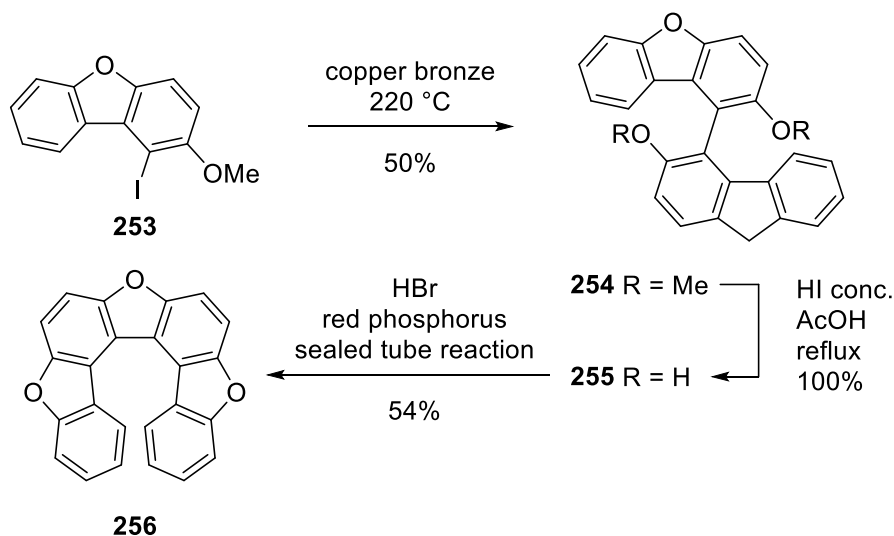
**Scheme 77:** Azahelicene synthesis *via* amines addition on ketones.

Subsequently, Schuster and Rau developed another two-step strategy for the synthesis of diazaheterohelicene **252** involving substitution of arenediazonium salt followed by cyclization under acidic conditions (Scheme 78).<sup>[165]</sup>



**Scheme 78:** Synthesis of diazaheterohelicene **252** reported by Schuster and Rau.

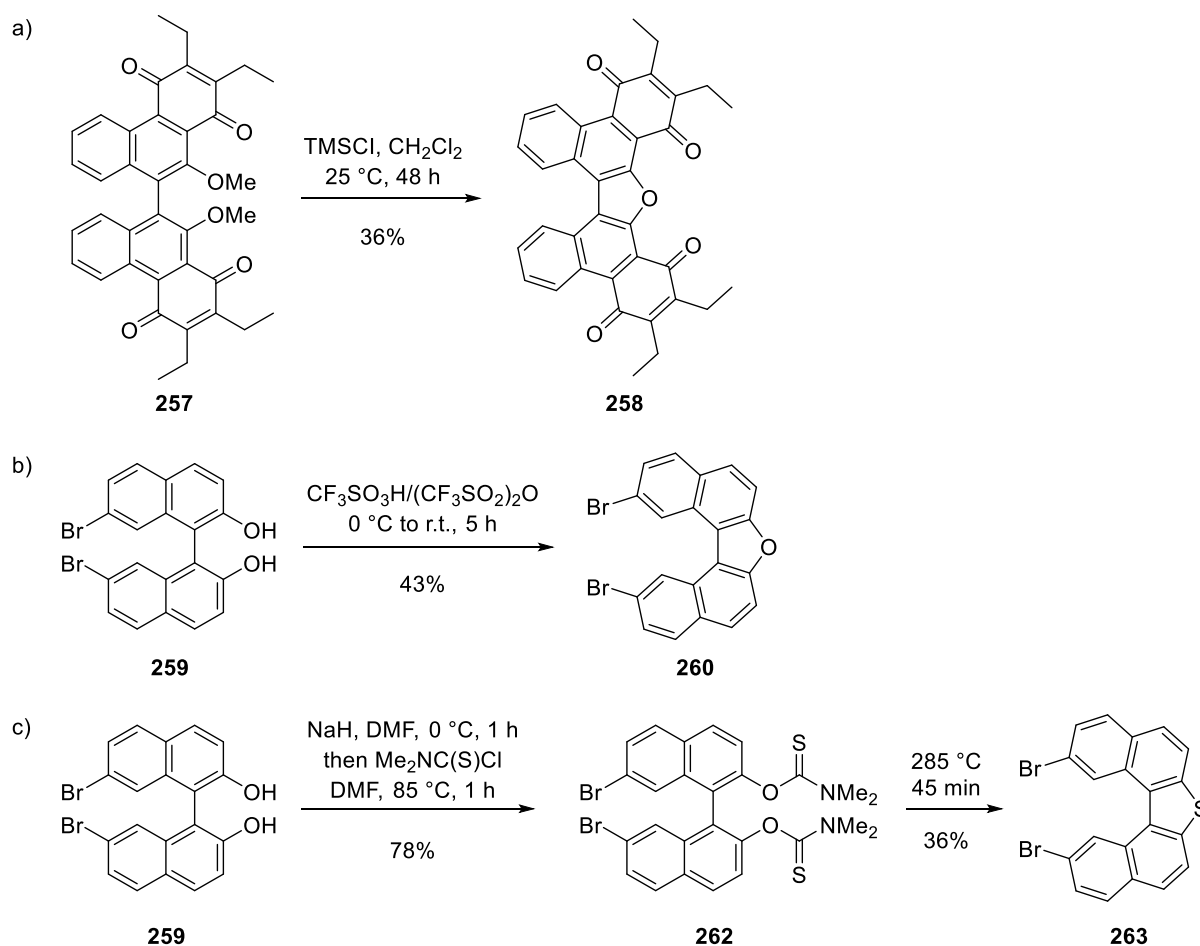
In 1973, Högberg reported the synthesis of diol **255** starting from dibenzofuran **253** performing Ullmann coupling followed by demethylation and acidic treatment. Subsequent heating in a sealed tube induced the ring closure to afford the oxahelicene **256** in 54% yield (Scheme 79).<sup>[166]</sup>



**Scheme 79:** Synthesis of oxahelicene **256** reported by Högberg.

More than 25 years later, Dötz and co-workers published another method for the preparation of the furan-based heterohelicenes **258**. Compound **257** was treated

with an excess of TMSI in DCM to cleave the ether, then an intramolecular nucleophilic substitution occurred to give the oxa[5]helicene derivative **258** in 36% yield (Scheme 80a).<sup>[167]</sup> Moreover, Dötz developed the synthesis of 7,7'-dibromo-oxa[5]helicene **260** *via* acid promoted ring closure in 43% yield (Scheme 80b). In this paper, he also reported the preparation of 7,7'-dibromo-thia[5]helicene **263** starting from 7,7'-dibromo-2,2'-dihydroxy-1,1'-binaphthyl **259** *via* a Newman-Kwart rearrangement (Scheme 80c).<sup>[168]</sup>

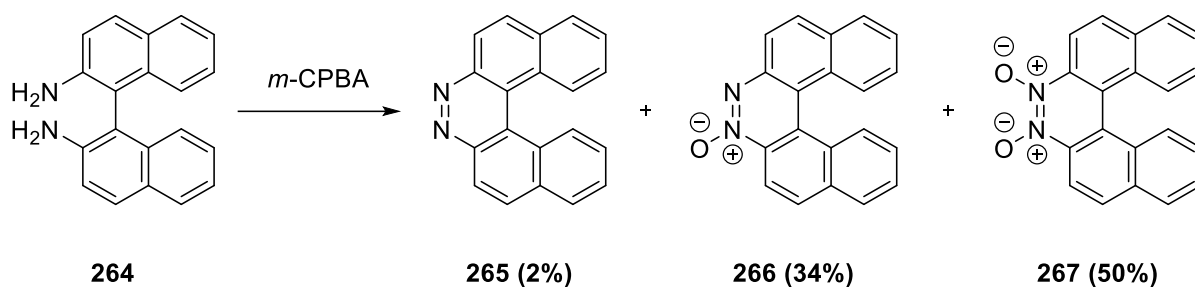


**Scheme 80:** a) Synthesis of furan-based helicene derivative

b) Synthesis of 7,7'-dibromo-oxa[5]helicene

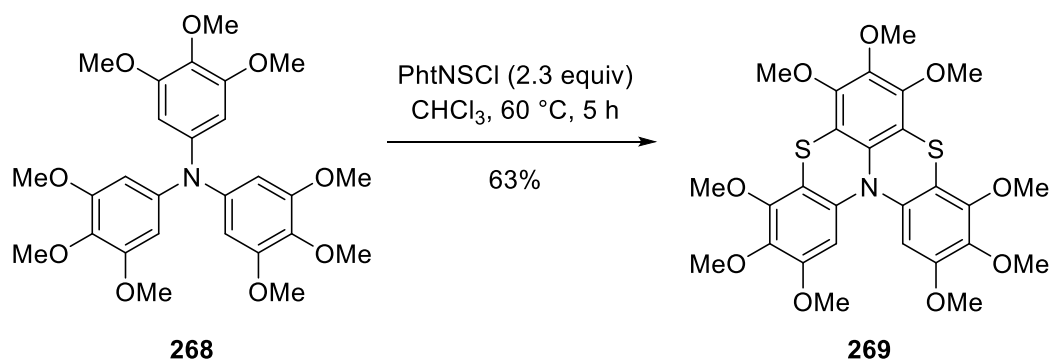
c) Synthesis of 7,7'-dibromo-thia[5]helicene.

More recently in 2008, Caronna *et al.* reported a strategy to synthesize 7,8-diaza[5]helicenes *via* oxidation of 2,2'-diamino-1,1'-binaphthyl **264** in the presence of *m*-CPBA.<sup>[169]</sup> The reaction yielded a mixture of diaza[5]helicene **265** as well as its N-oxide **266** and N,N'-dioxide **267** (Scheme 81) that can easily be reduced by LiAlH<sub>4</sub> to afford the diazahelicene in good yields.



**Scheme 81:** Synthesis of diazahelicene reported by Caronna *et al.*

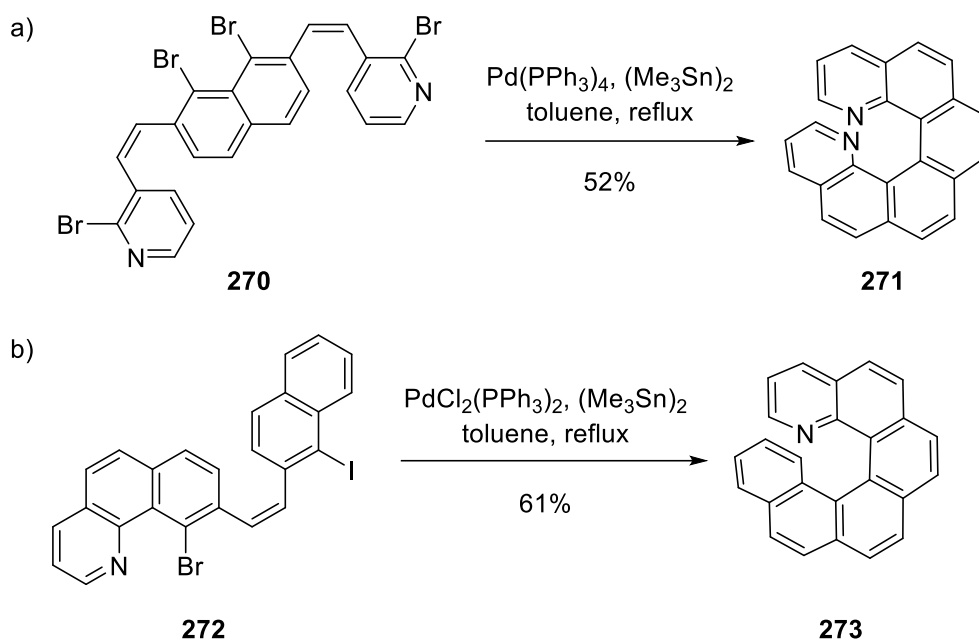
Menichetti *et al.* reported a practical method for the synthesis of thia-bridged triarylamine heterohelices.<sup>[170]</sup> A series of [4]- and [6]-heterohelices were synthesized in 46 to 72% yields employing Ph<sub>t</sub>N<sub>3</sub>Cl with or in the absence of a Lewis acid.<sup>[170,171]</sup> The preparation of **269** was facilitated by the trimethoxy-substituted benzene units and the possibility to protonate the N atom of the sulfonamide (Scheme 82). While synthesizing such helical cores with nine alkoxy groups is challenging *via* different methods, this strategy proved to be highly efficient (63% yield).



**Scheme 82:** Synthesis of thia-bridged triarylamine heterohelices.

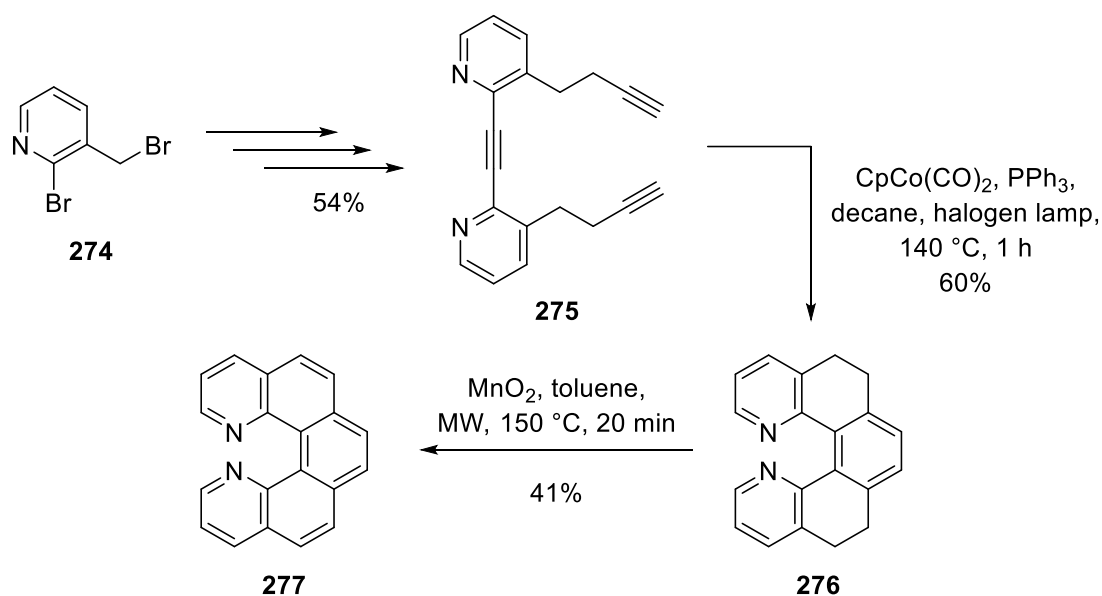
### c) Metal induced synthesis

Staab published a method for the preparation of 1,16-diaza[6]helicene **271** in 52% yield employing a Stille-Kelly coupling in presence of hexamethyl-distannane (Scheme 83a).<sup>[172]</sup> Takenaka *et al.* reported a similar synthetic pathway to afford 1-aza[6]helicene **273** in 61% yield (Scheme 83b).<sup>[173]</sup> The precursor can easily be prepared *via* highly Z-selective Wittig reaction of the halogen substituent. This is a useful method for the synthesis of a large variety of helicenes, as it only requires a simple modification of the precursors for the Wittig reaction.



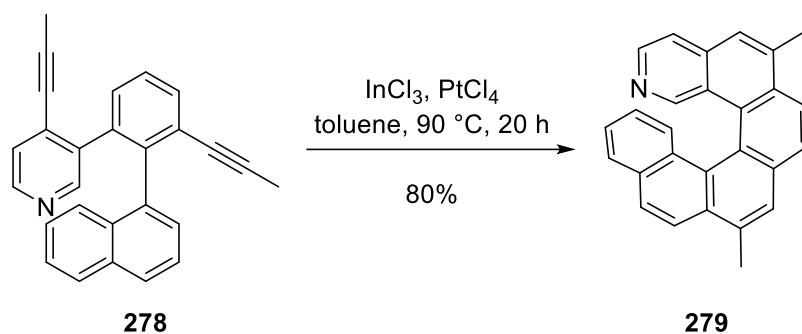
**Scheme 83:** a) Preparation of 1,16-diaza[6]helicene *via* Stille-Kelly coupling  
 b) Synthesis of 1-aza[6]helicene reported by Takenaka.

Furthermore, Starý, Stará and co-workers demonstrated that the cycloisomerization of triynes developed for the preparation of carbohelicenes<sup>[174]</sup> could also be extended to the synthesis of heterohelicenes (Scheme 84).<sup>[175]</sup> Starting from a bromopyridine derivative **274**, the precursor **275** was synthesized in 54% yield over 3 steps. Then a [2+2+2] cycloisomerization occurred in the presence of a Co<sup>I</sup> catalyst yielding the tetrahydrodiazahelicene **276**. Finally, an oxidation is performed employing MnO<sub>2</sub> under microwave irradiation to afford 1,14-diaza[5]helicene **277** in 41% yield overall. This strategy has also been used for the synthesis of 1- and 2-aza[6]helicene starting from the corresponding triynes in 47-53% yield.

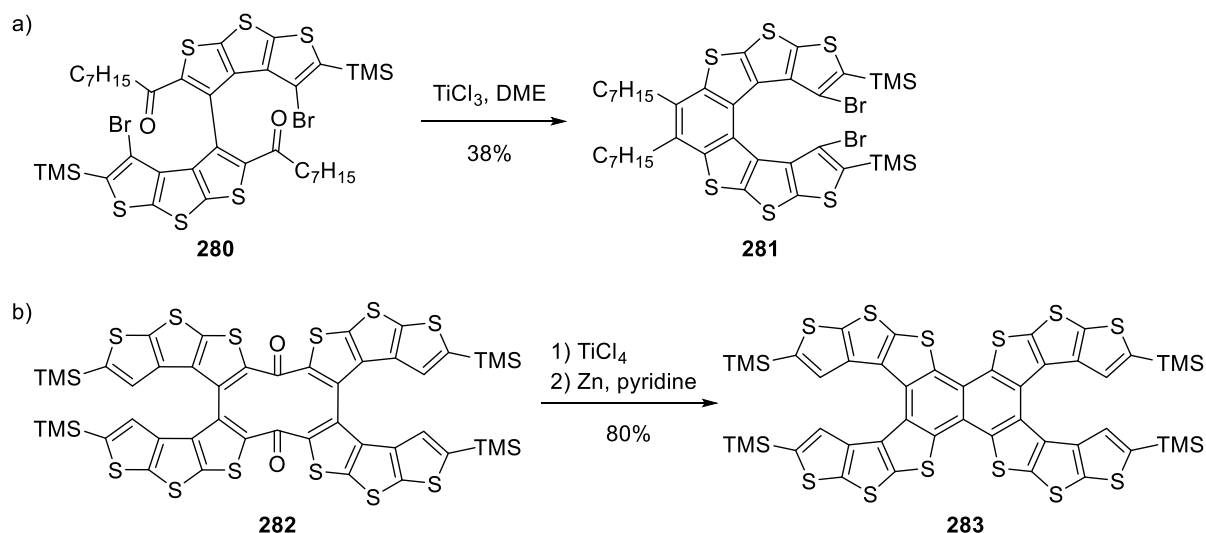


**Scheme 84:** Synthesis of diaza[5]helicene *via* [2+2+2] cycloisomerization.

Lately, Storch *et al.* performed a double cycloisomerization of nitrogen-containing biphenylnaphthalene **278** to prepare the aza[6]helicene **279** in 80% yield employing PtCl<sub>4</sub> and InCl<sub>3</sub> (Scheme 85).<sup>[176]</sup> In addition, Rajca *et al.* carried out McMurry coupling to synthesize the thiahelicene **281** in 38% yield (Scheme 86a). Analogously, Wang reported the preparation of the double thiahelicenes **283** in 80% yield from diketone **282** (Scheme 86b).<sup>[177]</sup>



**Scheme 85:** Synthesis of aza[6]helicene derivative *via* a double cycloisomerization.

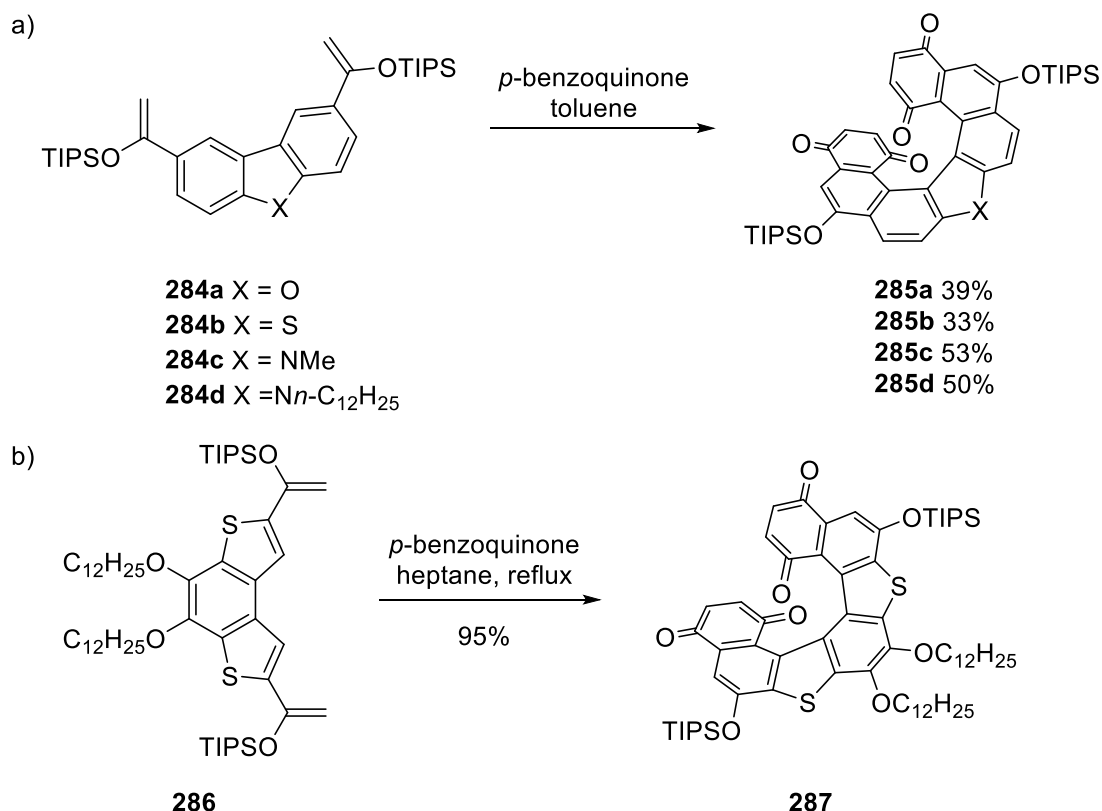


**Scheme 86:** a) Synthesis of thiahelicene derivative via McMurry coupling  
b) Synthesis of double thiahelicene reported by Wang.

#### d) Other cyclizations

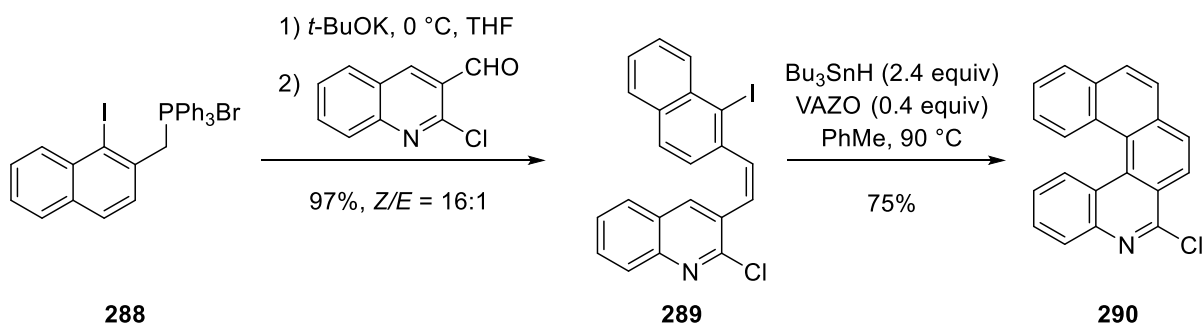
At the beginning of this century, Katz *et al.* developed the synthesis of heterohelicenes on a gram scale and in reasonable yields employing the Diels-Alder reaction between *p*-benzoquinone and dienes containing heteroaromatic rings (Scheme 87a and 87b).<sup>[178,179]</sup> Interestingly, they observed faster reaction rates than those in the synthesis of carbohelicenes, and the two *p*-benzoquinone moieties allow further functionalization of the helicenes and optical resolution.





**Scheme 87:** a) Synthesis of heterohelicenes *via* Diels-Alder reaction developed by Katz  
 b) Synthesis of thiahelicene derivative *via* Diels-Alder reaction.

Later, Harrowven and co-workers reported the synthesis of a series azahelicenes *via* homolytic aromatic substitution reactions of a stilbene-type precursor (Scheme 88).<sup>[180]</sup> The stereochemical course of the Wittig reaction relies on the cooperative *ortho* effects to afford a 16:1 mixture of *Z* and *E* isomers. Subsequent homolysis of the carbon-iodine bond was achieved to obtain the 5-azahelicene **290** in 75% yield.



**Scheme 88:** Synthesis of azahelicene *via* homolytic aromatic substitution.

### 3. Resolution

The first resolution of carbo[6]helicene was performed by Newman *et al.* by employing auxiliary TAPA (Figure 22) which formed diastereoisomers of different solubilities through the  $\pi$ - $\pi$  stacking between the helicene and TAPA.<sup>[147]</sup>

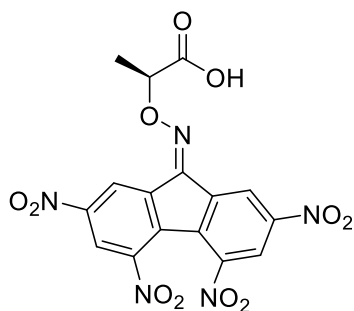


**Figure 22:** Structure of TAPA

The first resolution of helicene by chromatography was developed by Klemm and Reed in 1959.<sup>[181]</sup> In their work, they used silica gel impregnated with TAPA as stationary phase and manage to partially resolve carbo[5]helicene. Later, Mikeš and Gil-Av *et al.* started to use the high performance liquid chromatography for helicene resolution. Using TAPA or its homologues as the stationary phase, they successfully separated the two enantiomers from [5]- to [14]helicene.<sup>[182]</sup> This system also proved to be efficient for the resolution of some hetero-helicenes published by Wynberg *et al.*<sup>[183]</sup> Moreover, binaphthyl-2,2'-diyl hydrogen phosphate (BPA)<sup>[184]</sup> and riboflavin<sup>[185]</sup> were also found to be good candidates as coating reagent for helicene resolution by HPLC.<sup>[186]</sup>

#### 4. Properties

The helicoidal shape of helicenes is due to the twisting of the connections between the rings. As a consequence, C-C bond lengths depend on their position in the scaffold. Indeed, the C-C bond length in benzene is 1.393 Å against 1.430 Å for an internal C-C bond and 1.360 Å for an external C-C bond in helicenes. This particular shape makes helicenes chiral even if they do not have any asymmetric carbon or any other stereogenic center. According to the helicity rules defined by Cahn, Ingold and Prelog in 1966<sup>[187]</sup>, a left-handed helix is designated “minus” and denoted M while a right handed one is designated “plus” and denoted P. Moreover, a general trend has been observed: P-helicenes are dextrorotatory and M-helicenes are levorotatory. The interplanar angle of the two terminal cycles of the helicene is called dihedral angle (Figure 19c). Its value depends on the length of the helicene and its substituents. For carbohelicene this angle is 26.7° for the [4]-helicene and increased up to 58.5° with the [6]-helicene before decreasing if the helicene is further elongated ([11]-helicene displays a dihedral angle of 4° only).

Like several other cyclic aromatic compounds, helicenes are good  $\pi$ -donors and can form charge transfer complexes with numerous  $\pi$ -acceptors (Figure 23a)<sup>[188]</sup>. Helicenes tend to racemize, even at room temperature for some of them such as the [4]helicene which has an inversion barrier of 4 kJ.mol<sup>-1</sup> (Figure 23b). The racemization mechanism has been studied based on computational study on carbo[n]helicenes up to n=24. It has been reported to be a concerted process for carbo[n]helicenes up to n=7 while it follows a multi-step pathway with 2n-14 steps for n>7<sup>[189]</sup>. Moreover, computations showed that the changes in the energy barriers were due to steric hindrance and the number of  $\pi$ -interactions in the system. Indeed,

adding one *ortho*-fused ring on the [4]helicene will increase the energy barrier for the racemization up to 24.4 kcal.mol<sup>-1</sup>.

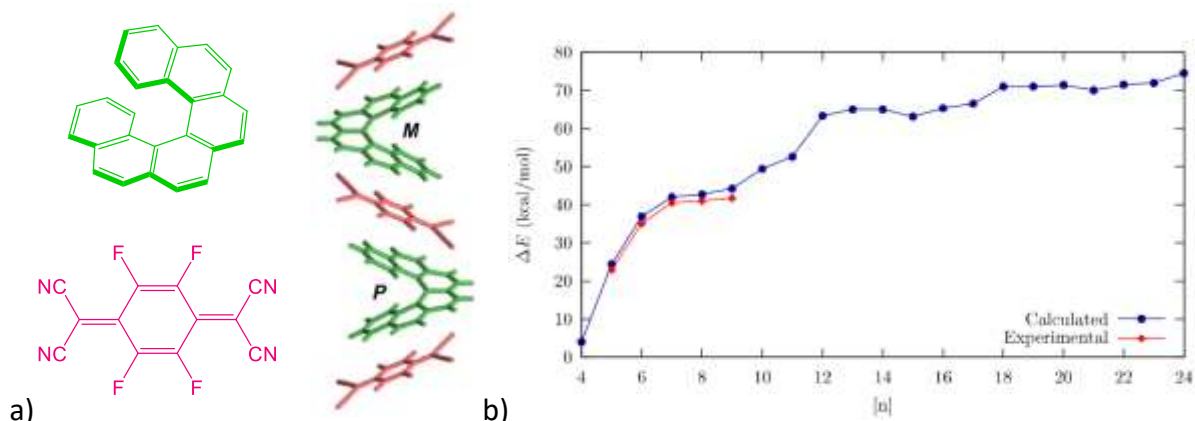
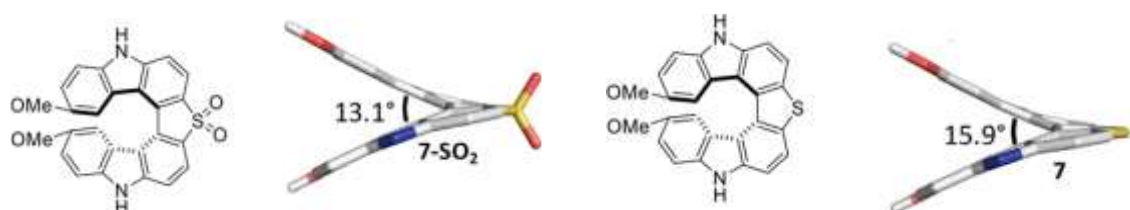


**Figure 23:** a) Example of charge transfer complex with carbo[6]helicene, b) Energy barriers for the racemization of carbo[n]helicenes (up to n=24).

Moreover, helicenes display another interesting property: they act like springs whose force constant could be modulated. Indeed, in 1997, Lipkowitz and al. showed that [12]- and [18]-helicenes follow Hooke's law as any other spring by carrying out quantum mechanical calculations to get their equilibrium structures and then constrain the terminal carbon atoms to distances greater than and less than their equilibrium positions.<sup>[190]</sup> Besides, they also studied the impact of adding or removing electrons to the structure on the spring stiffness. Recently, Pittelkow *et al.* also reported an example of heterohelicene whose oxidation have an impact on the value of his dihedral angle. Indeed, the hetero[7]helicene presented in Scheme 89 sees its dihedral angle decreasing when its sulfur atom is oxidized.<sup>[191]</sup>



**Scheme 89:** Impact of heteroatom oxidation on hetero[7]helicene geometry calculated using the B3LYP/6-31+G(d) method.

Their helical geometry and their extended  $\pi$ -system provide large optical activity to helicenes (see Table 9) as well as a strong response to circular dichroism but also interesting properties in the fields of conductivity, piezoelectricity, biological activity, self-assembly and catalytic activity.<sup>[192]</sup>

One of the most important properties of chiral molecules is that each enantiomer displays different interactions with polarized light. Compared to molecules having only one stereogenic center, helicenes are intrinsically chiral due to their structure. As a result, they have high optical rotations compared to commercial chiral compounds (Table 9).<sup>[193,194]</sup> We

note that specific optical rotation  $[\alpha]_D^{25}$  increase with the number of cycles in the helicene. Moreover, molar optical rotation  $[\phi]_D^{25}$  has been introduced to compare molecules with a large difference of molecular weight. It is defined by the following relation:

$$[\phi]_D^{25} = [\alpha]_D^{25} \cdot M_{mol} / 100 \text{ (with } M_{mol} = \text{molecular weight)}$$

**Table 9:** Selected specific rotation and molar rotation data for carbo[n]helicenes and other chiral molecules.<sup>[193,194]</sup>

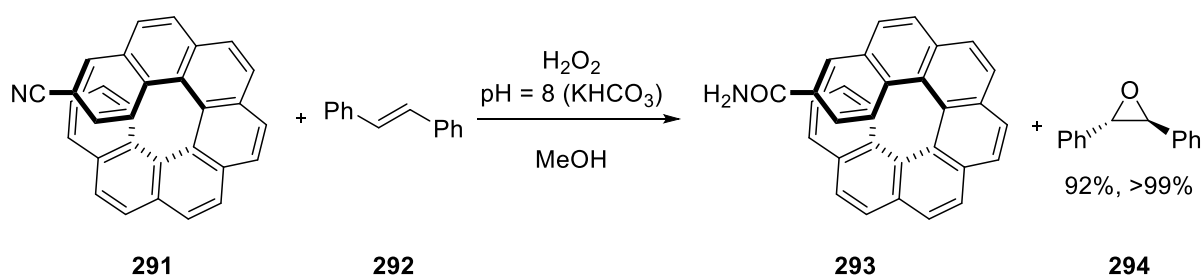
Compound	$[\alpha]_D^{25}$ ( $^{\circ}\cdot\text{cm}^{-3}\cdot\text{dm}^{-1}\cdot\text{g}^{-1}$ )	$[\phi]_D^{25}$ ( $^{\circ}\cdot\text{cm}^2\cdot\text{dmol}^{-1}$ )
<b>P-carbo[6]helicene</b>	+3640 (CHCl <sub>3</sub> ) <sup>a</sup>	+11900
<b>P-carbo[7]helicene</b>	+5900 (CHCl <sub>3</sub> , c=6x10 <sup>-2</sup> mol.L <sup>-1</sup> )	+22300
<b>P-carbo[8]helicene</b>	+7170 (CHCl <sub>3</sub> , c=4.3x10 <sup>-2</sup> mol.L <sup>-1</sup> )	+30600
<b>P-carbo[9]helicene</b>	+8100 (CHCl <sub>3</sub> , c=6.07x10 <sup>-2</sup> mol.L <sup>-1</sup> )	+38700
<b>(+)-menthol</b>	+50 (EtOH) <sup>a</sup>	+78
<b>(R)-(-)-1,1'-Binaphthyl-2,2'-diyl hydrogenphosphate</b>	+607 (MeOH) <sup>a</sup>	+2120

<sup>a</sup>The concentration is not mentioned in original publication.

## 5. Applications of helicenes

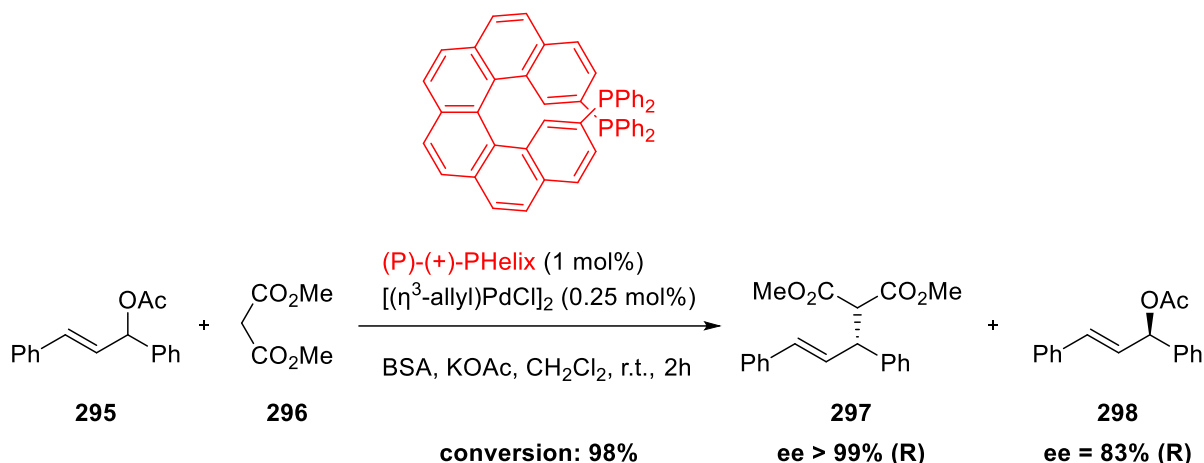
### i. Asymmetric synthesis

The first use of a helicene in the field of asymmetric synthesis has been reported by Martin *et al.* In this work, a functionalized [7]helicene was used as chiral auxiliary or chiral reagent in five reactions such as an epoxidation (Scheme 90) with high ee. Nevertheless, the helicene is used in stoichiometric quantity.<sup>[195]</sup>



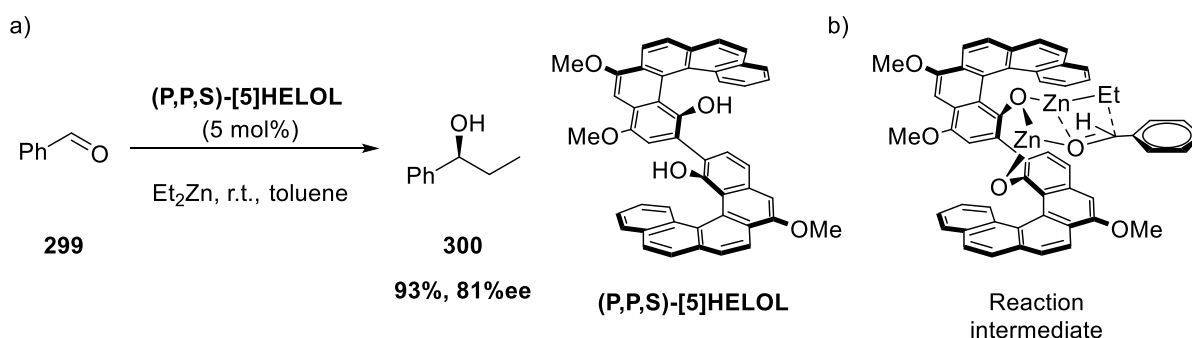
**Scheme 90:** Asymmetric epoxidation of stilbene

The first asymmetric synthesis using a helicene in catalytic amount has been developed by the group of Prof. Reetz. They reported the kinetic resolution *via* an allylic substitution catalyzed by palladium (Scheme 91). The PHelix behave has a monodentate ligand because of the large distance between the phosphorus atoms (6.481 Å). When the ratio palladium:PHelix is 1:4, enantiomeric enrichment reaches more than 99%. Moreover, using BSA and KOAc as additives to induce rapid racemization of the starting material **295** allow them to reach 81% yield.<sup>[196]</sup>



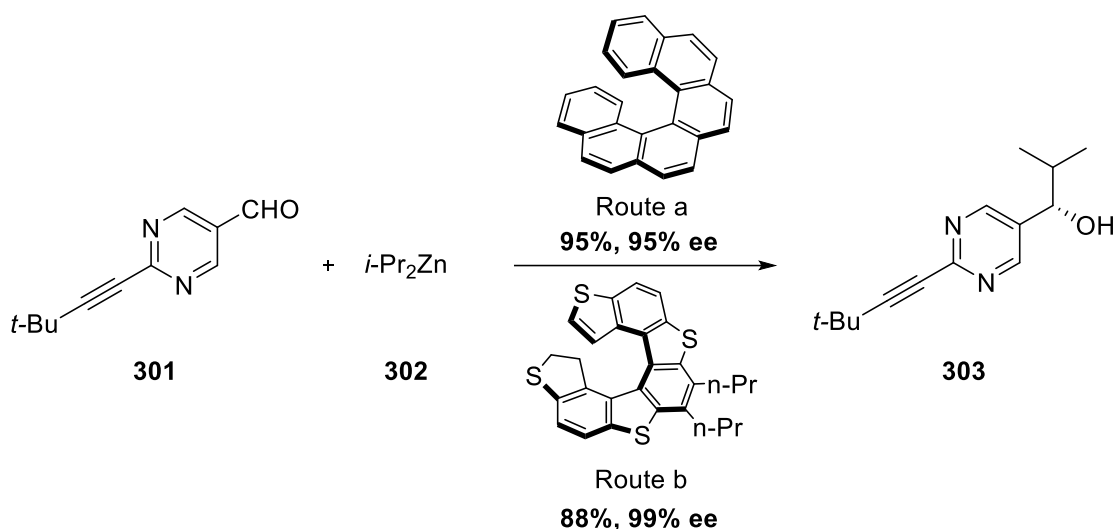
**Scheme 91:** Chiral resolution of 1,3-diphenylallylacetate by a helicene catalyst

In 2000, Katz and co-workers reported the catalytic asymmetric addition of diethylzinc to benzaldehyde using (P,P,S)-[5]HELOL which afforded (S)-product **300** in 81% ee (Scheme 92a). The suggested intermediate is presented in Scheme 92b. The benzaldehyde coordinates to the zinc in a way to reduce steric repulsions between its aromatic ring and the helicene leaving only its Si face accessible to the ethyl group.<sup>[197]</sup>



**Scheme 92:** a) Asymmetric addition of Et<sub>2</sub>Zn on benzaldehyde  
b) Reaction intermediate.

Soai *et al.* then showed that hexahelicene (route a) and a thia[7]helicene (route b) can induce chirality in the highly enantioselective synthesis of a pyrimidyl alkanol by adding *i*-Pr<sub>2</sub>Zn to a pyrimidyl aldehyde (Scheme 93).<sup>[198]</sup> Interestingly, moderate to good ee (56-83%) were still obtained while using low ee helicenes (0.13-2%). This phenomenon can be explained as follows: first hexahelicene or thia[7]helicene coordinates with the carbonyl moiety and the pyrimidine ring of the aldehyde **301** differentiating the *Re* and the *Si* face, then *i*Pr<sub>2</sub>Zn is added to aldehyde **301** generating a nonracemic zinc alkoxide of alkanol **303**, then zinc alkoxide of **303** act as an asymmetric autocatalyst to produce alkanol **303** in high *ee*.

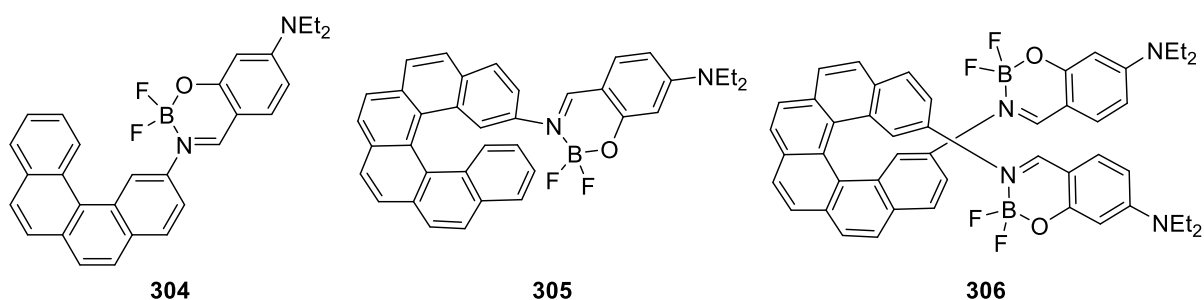


**Scheme 93:** Enantioselective synthesis of pyrimidyl alkanol

ii. *Electro-optical materials*

Helicenes exhibit rather strong circular polarized luminescence (CPL) activity but have rather low emission quantum yields. However, the possibility of synthesizing a large panel of helicene scaffolds by integrating heteroatoms and various substituents to the structure allows to tune the photophysical properties of these systems.

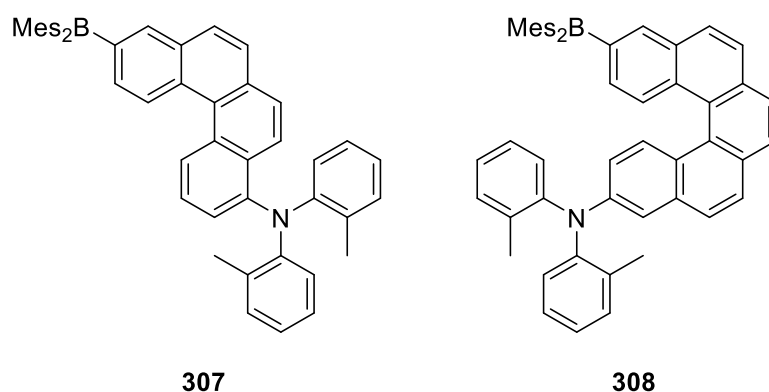
Indeed, Crassous *et al.* reported in 2021 the synthesis of boron based helicenes and the study of their chiroptical properties and circularly polarized fluorescence.<sup>[199]</sup> The target molecules are carbo[4]- and carbo[6]-helicenes bearing one or two boranyl units (Scheme 94). They showed that the helicenic part of the scaffold induces axial chirality along the C-N bond in the solid state which can be explained by the steric hindrance of the -BF<sub>2</sub> group and CH- $\pi$  interaction between the CH=N of the imine and the terminal ring of the helicene that “block” the system geometry.



**Scheme 94:** Helicenes-boranyl developed by Crassous *et al.*

In 2019, Todd B. Marder developed carbo[4]- and carbo[6]-helicenes bearing a -BMe<sub>2</sub> (electron acceptor) and a -N(*p*-tol)<sub>2</sub> (electron donor) moieties.<sup>[200]</sup> By combining such groups on the helicene scaffold, he created a molecule with a large dipole moment in the excited state and thus strong intramolecular charge transfer (Scheme 95). His studies unveiled that “push-pull” compounds have high emission quantum yields compared to unsubstituted

helicenes and that interactions decreasing molecular motion (such as  $\pi$ - $\pi$  stacking or hydrogen bonding) also lead to an improvement of quantum yields. It also showed that  $S_0$  to  $S_1$  transitions are HOMO to LUMO dominated internal charge transfer transitions. Moreover it has been observed that upon excitation with UV light, the dihedral angle of the hetero[5]helicene **308** decreased of  $7^\circ$ . Further computational calculations predicted that this spring behavior is even more exhibited with larger helix core ( $24^\circ$  for the corresponding hetero[7]helicene).

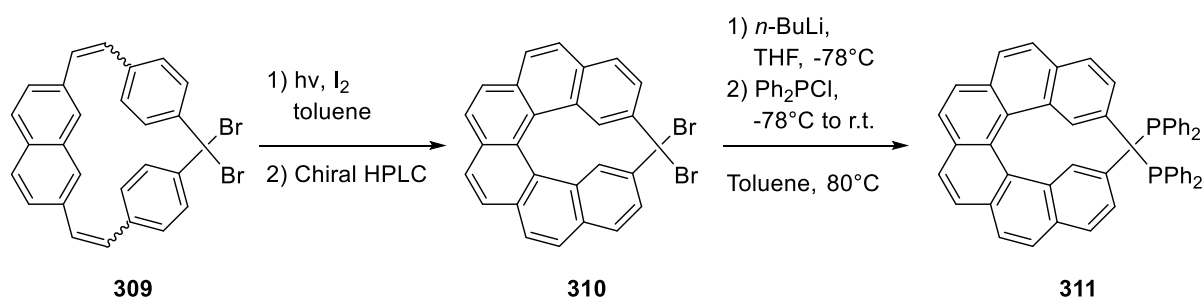


**Scheme 95:** Push-pull helicenes developed by Todd B. Marder

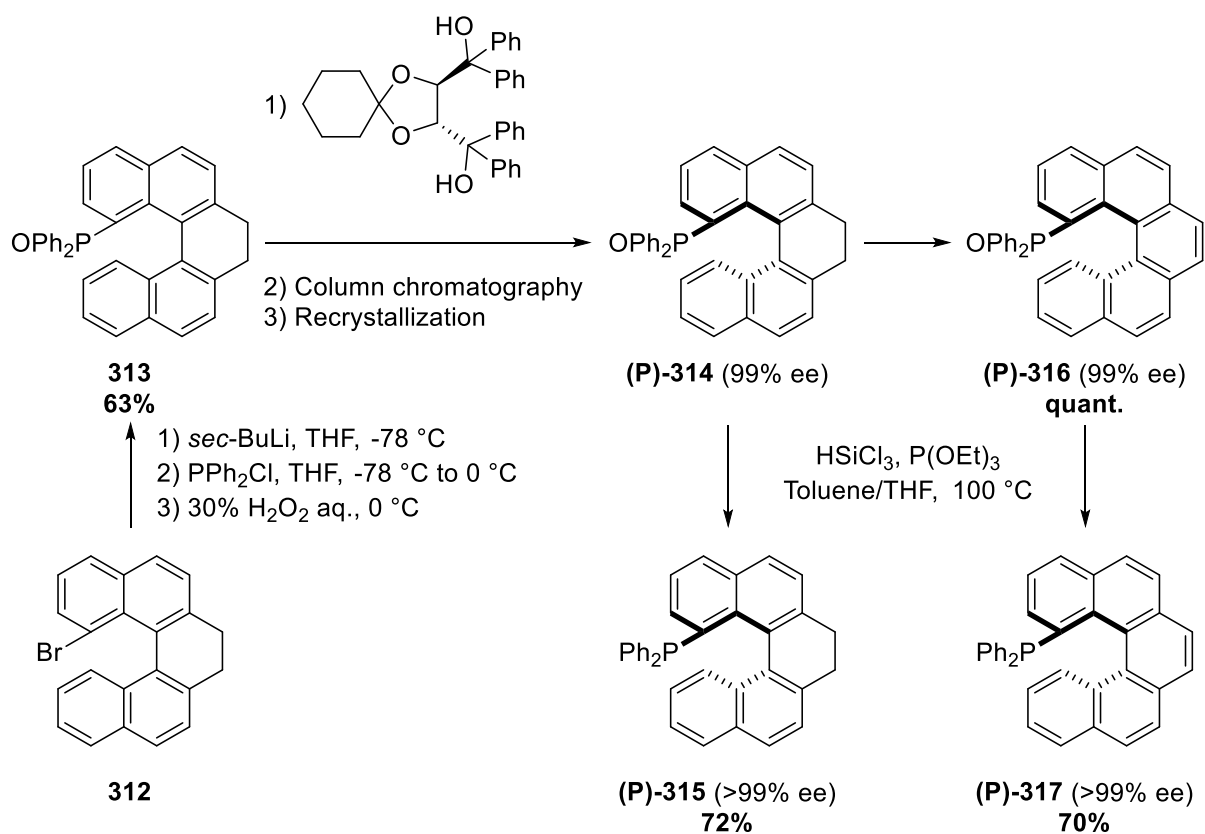
### iii. Helicenes grafted with phosphines

We saw previously that adding substituents on helicenes, such as in donor- $\pi$ -acceptor systems, enables to tune the properties of the molecule. In addition, grafting substituents with different steric hindrance allows to modulate the distance between the two terminal rings leading to the modification of the dihedral angle of the helicene. This class of compound is then a perfect candidate for the development of chiral ligands for enantioselective catalysis.

While Reetz *et al.* reported in 1997 the first synthesis of enantiopure 2,15-bis(diphenylphosphino)-hexahelicene named Heliphos or PHel (Scheme 96)<sup>[201]</sup>, the preparation of configurationally stable carbo[5]helicene phosphines has been performed only recently. Indeed, in 2016, Usui reported the synthesis of configurationally stable carbo[5]helicenes **315** and **317** (Scheme 97).<sup>[202]</sup>



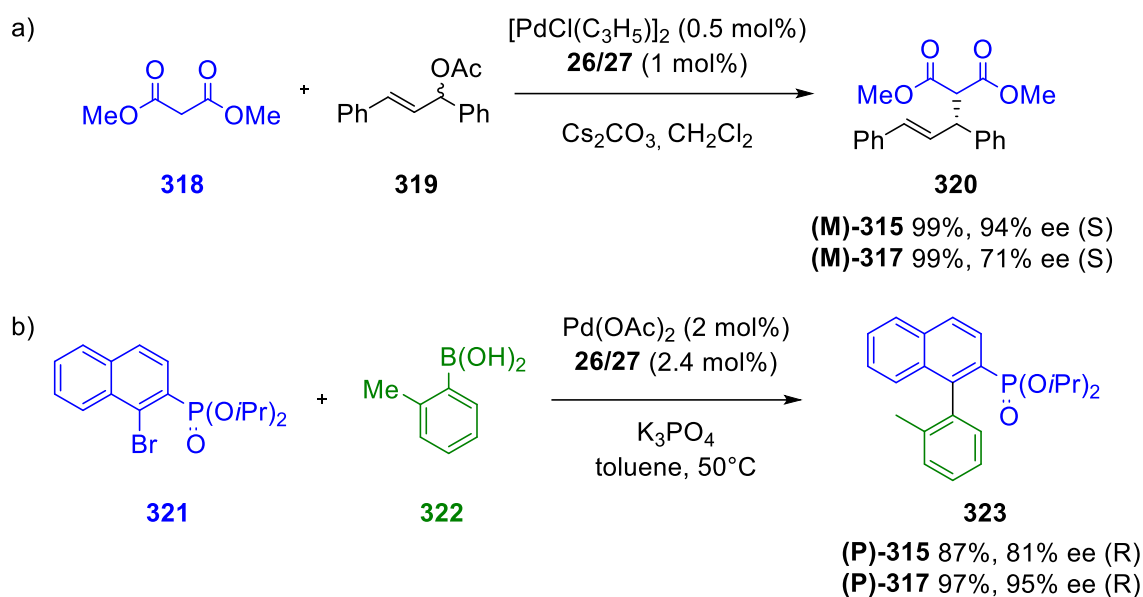
**Scheme 96:** Synthesis of enantiopure PHel.



**Scheme 97:** Preparation of configurationally stable carbo[5]helicenes **315** and **317**.

More interestingly, these helical phosphines showed a phosphine-metal-arene interaction in the complex with Pd(dba). As a matter of fact, Usui demonstrated that **315** is highly efficient in asymmetric allylic substitution (Scheme 98a) while **317** can be used as a highly enantioselective ligand in the asymmetric Suzuki-Miyaura coupling reaction to obtain chiral biaryl compounds (Scheme 98b).



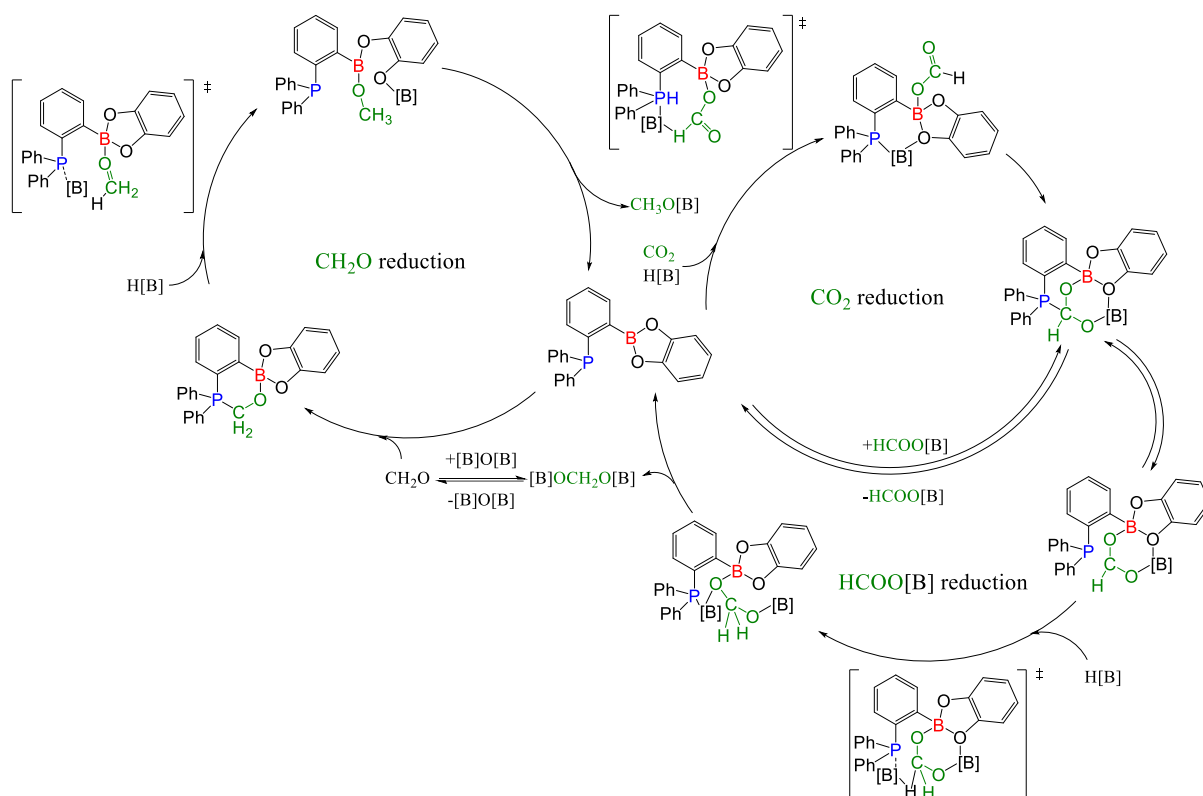


**Scheme 98:** a) Pd-catalyzed asymmetric allylic substitution reactions  
 b) Pd-catalyzed asymmetric Suzuki-Miyaura couplings

## 6. Objectives

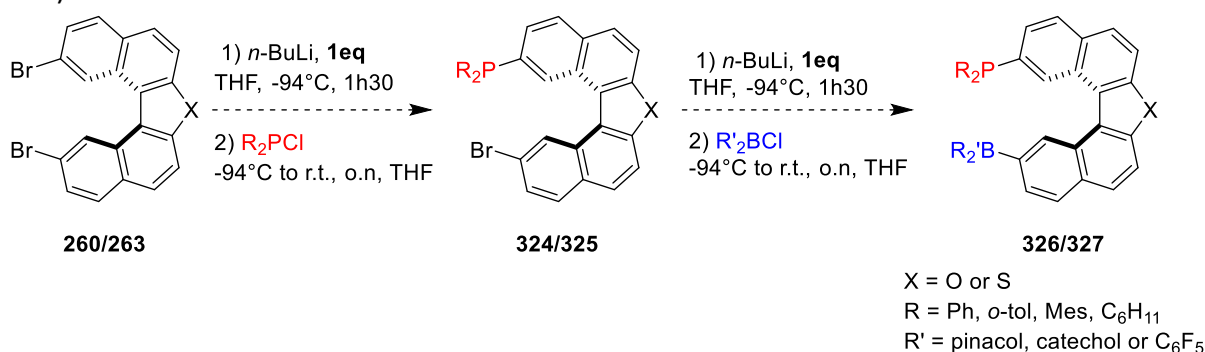
Intramolecular frustrated Lewis pair systems underwent a significant development in the last few years. Thanks to their steric hindrance, FLPs are able to activate small molecules such as  $\text{H}_2$ ,  $\text{SO}_2$ ,  $\text{CO}$ , or  $\text{CO}_2$ . Thus, they arouse a great interest in the field of catalysis as an alternative to classic metallic catalysis. Helicenes present an helicoidal structure and a  $\pi$ -extended system which provide unique properties. Therefore, these molecules found numerous applications in the field of catalysis or macrostructure development. Consequently, combining the properties of helicenes and frustrated Lewis pairs could set a milestone for the activation of small molecules and their use in asymmetric catalysis.

It is for example possible to catalytically reduce  $\text{CO}_2$  using frustrated Lewis pair combined to a reducing agent according to Fontaine.<sup>[203,204]</sup> In the article from 2014,<sup>[203]</sup> they reported several points to address while designing a FLP system for the catalytic reduction of  $\text{CO}_2$  in methanol via hydroboration. The catalyst should be an intramolecular FLP composed of a highly Lewis basic phosphine to bind  $\text{CO}_2$ , hinder hydride transfer and activate the reductant more efficiently. However, the use of a weak Lewis acid is recommended as it would release various hydroboration products more easily. Furthermore, the presence of oxygen atom as substituent for the boron is a great asset as their flexibility allows the formation of isomers and intermediates (Scheme 99).



**Scheme 99:** Mechanism for the reduction of CO<sub>2</sub> via a FLP system and a reducing agent.

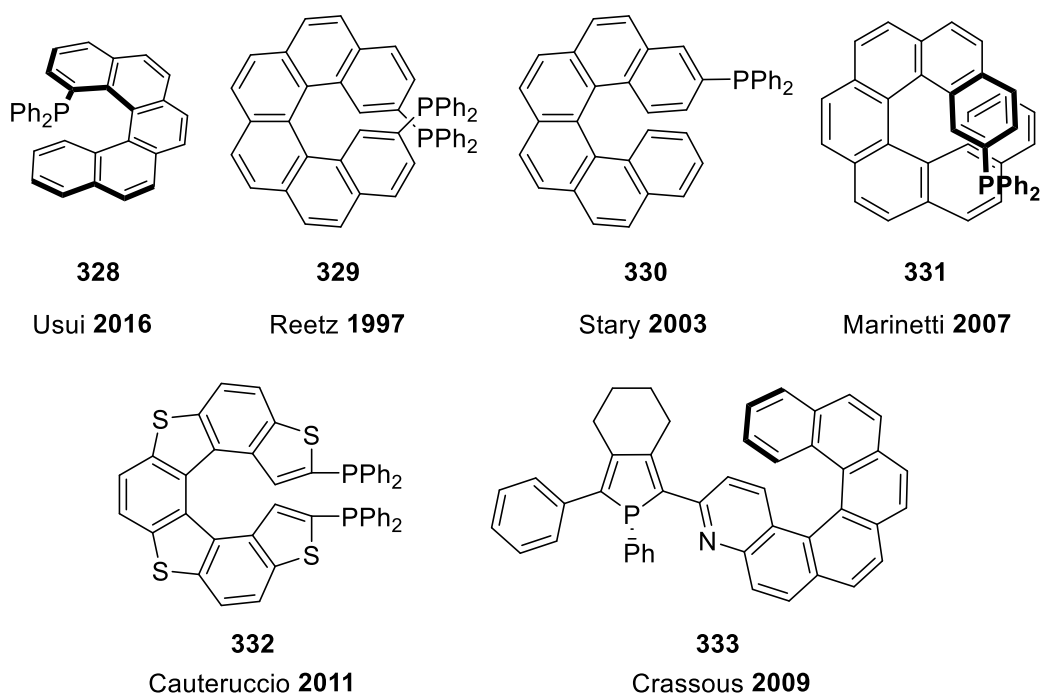
It would be then possible to study the effect of the helical linker on the reduction of CO<sub>2</sub> as its flexibility could be a valuable asset. Thus a future long term goal would be to develop catalysts based on the hetero[5]helicene scaffold in order to perform the catalytic hydrogenation of CO<sub>2</sub>. Starting from the readily synthesized dibromooxa[5]helicene or its derivative thia[5]helicene, it is possible to perform successive Br/Li exchange in order to craft the frustrated Lewis pair stepwise (Scheme 100).



**Scheme 100:** Synthesis of frustrated Lewis pair based on the hetero[5]helicene

## II. Synthesis of new hindered phosphines based on a heterohelicenes scaffold

To the best of our knowledge, only few helicenes bearing phosphorus atoms have been synthesized and even fewer ones have been studied in the field of asymmetric catalysis, none of them being heterohelicenes. Most of them are represented in Scheme 101. In 2000, Reetz *et al* reported the use of the already prepared enantioenriched 2,15-bis(diphenylphosphino)-hexahelicene as catalyst in enantioselective allylic substitutions between diphenylpropenyl acetate and dimethyl malonate. Usui then showed in 2016 that the diphenylphosphino-pentahelicene can be efficiently used in Suzuki-Miyaura coupling reaction and asymmetric allylic substitutions. Other systems have been developed but no investigation in asymmetric catalysis have been performed.

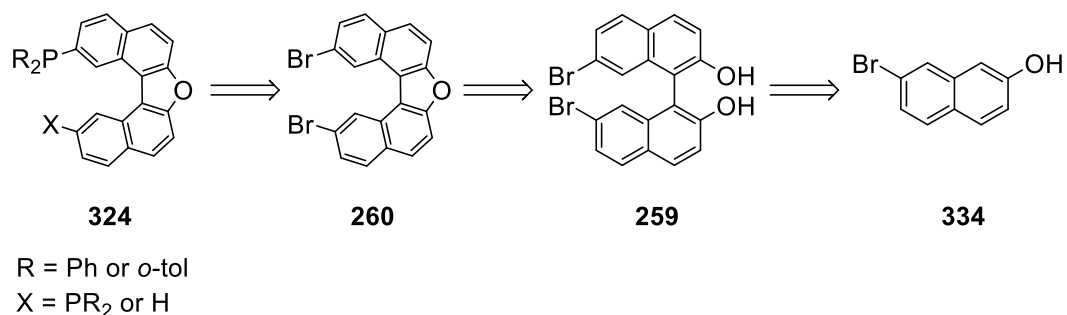


**Scheme 101:** Examples of phosphorylated helicenes in the literature.

Herein we report the synthesis of new mono- and diphosphines based on the oxa[5]helicene scaffold starting from 7-bromonapht-2-ol **334** (Scheme 102). This synthetic strategy allowed us to obtain new hetero[5]helicene phosphines in only three steps. Incorporating an oxygen atom in the structure of the classical carbopentahelicene induce a distortion of the structure that modify the dihedral angle of the helicene and thus the distance and orientation between the phosphines. This could open the way to new applications in asymmetric catalysis.

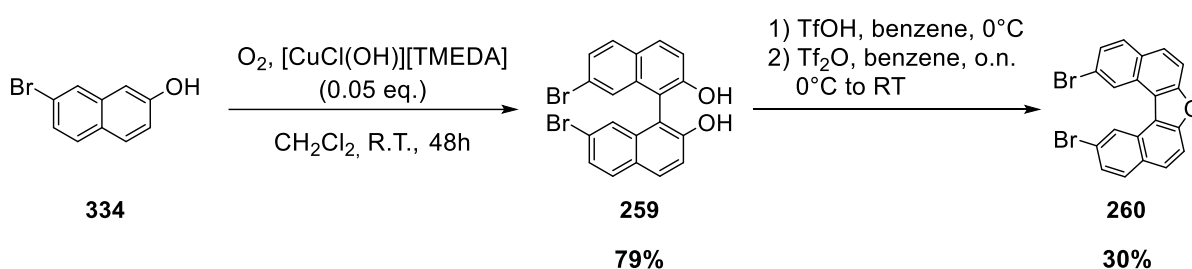
The first step is the oxidative coupling of bromonaphtol **334**. Then a cyclisation is performed starting from **259** to afford the 2,12-dibromooxa[5]helicene **260**. Eventually, a Br/Li exchange is carried out with *n*-BuLi solution in THF followed by quenching with the

appropriate chlorophosphine to obtain the targeted phosphines. The dibromooxa[5]helicene **260** has already been used to synthesize biscarbene complexes<sup>[205]</sup> via a Br/Li exchange which suggests that phosphines such as **324** could be easily obtained in the same way.

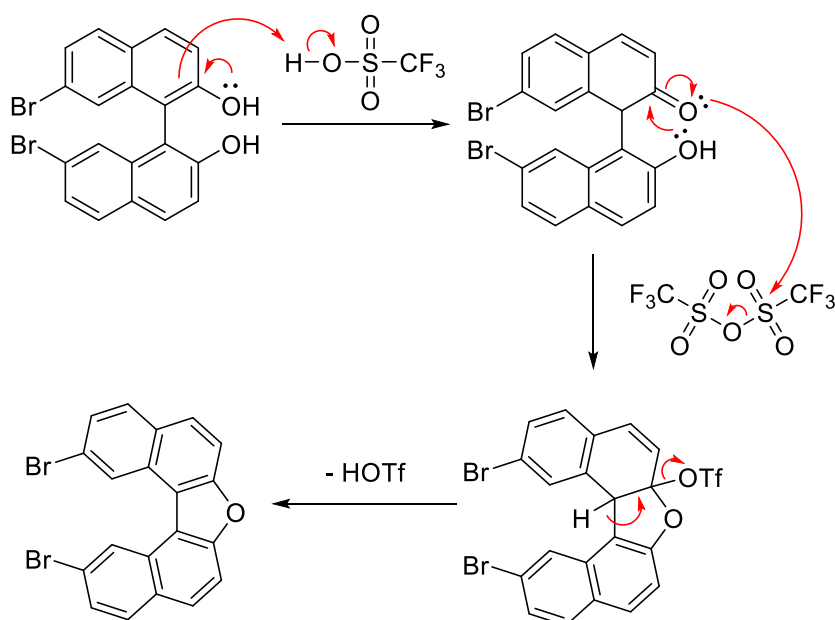
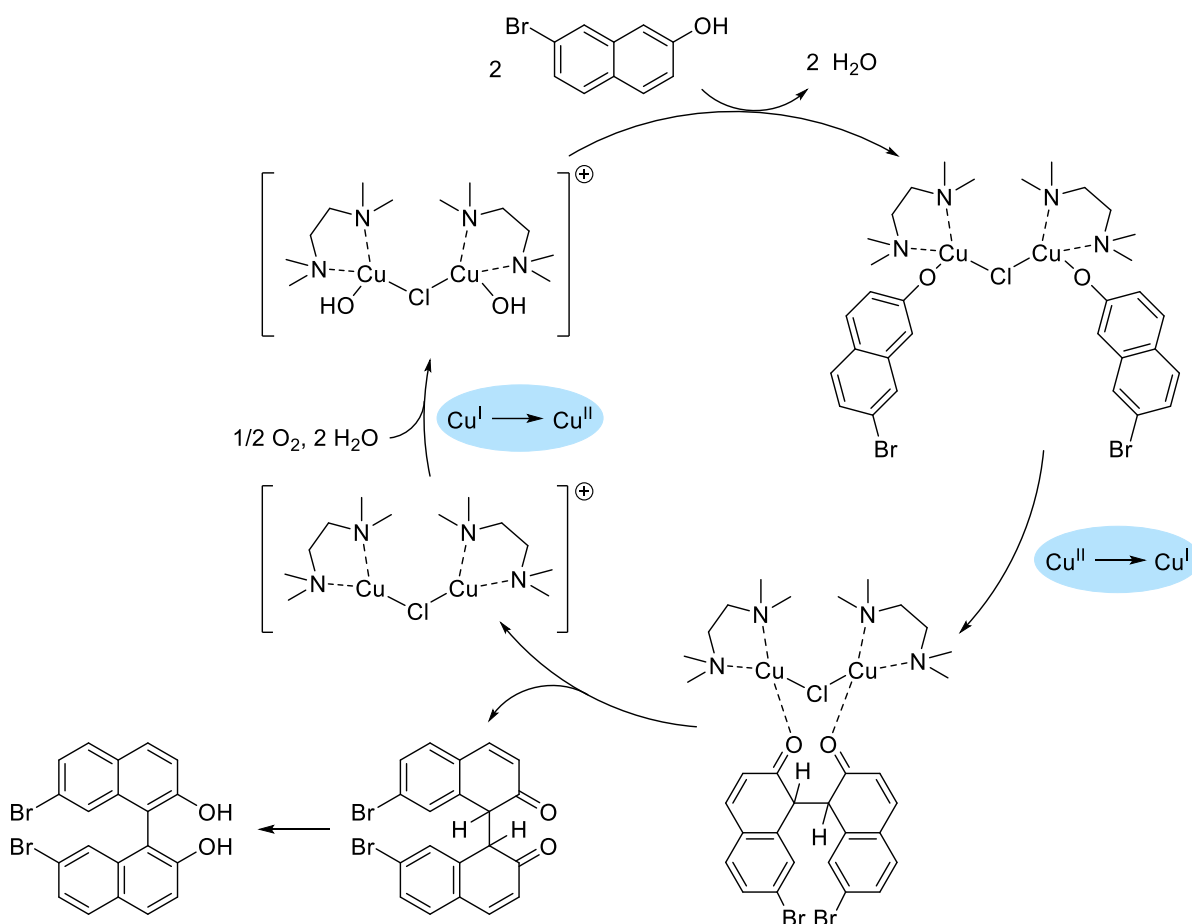


**Scheme 102:** Synthetic pathway to obtain mono- and diphosphines based on the oxa[5]helicene scaffold

We first focused on the synthesis of the 2,12-dibromooxa[5]helicene **260** which have already been reported in the literature<sup>[205]</sup> (Scheme 103). First, the oxidative coupling of 7,7'-dibromo[1,1'-binaphthalene]-2,2'-diol is performed. While Dötz *et al* reported it using an iron catalyst,<sup>[205]</sup> the procedure of Lustenberger<sup>[206]</sup> gave better yields. It involves the use of CuCl(OH)(TMEDA) catalyst and dioxygen from air to give the binol derivative **259** in 79% yield following the mechanism shown in Scheme 104. Then a cyclisation is performed using triflic acid in benzene to afford the 2,12-dibromooxa[5]helicene. During the treatment of this reaction, a water washing followed by extraction with DCM is performed. Benzene tends to produce a thick emulsion in which the product is trapped thus leading to a low yield of only 30% for this last step. The mechanism for this step is described in Scheme 105.

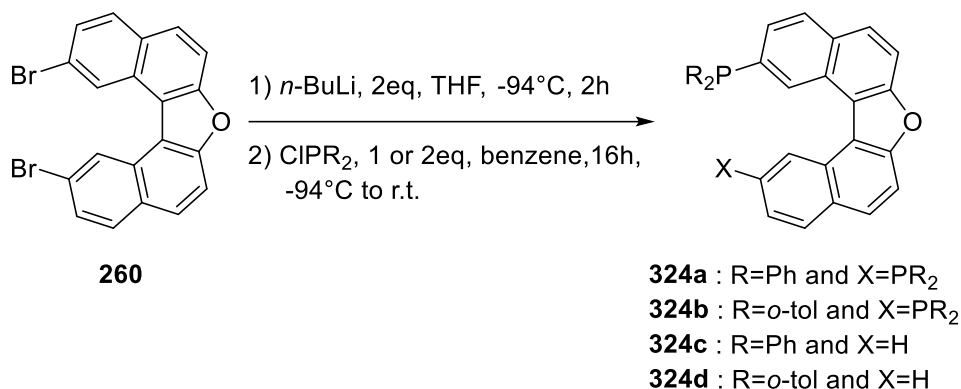


**Scheme 103:** Synthesis of 2,12-dibromooxa[5]helicene **260**.

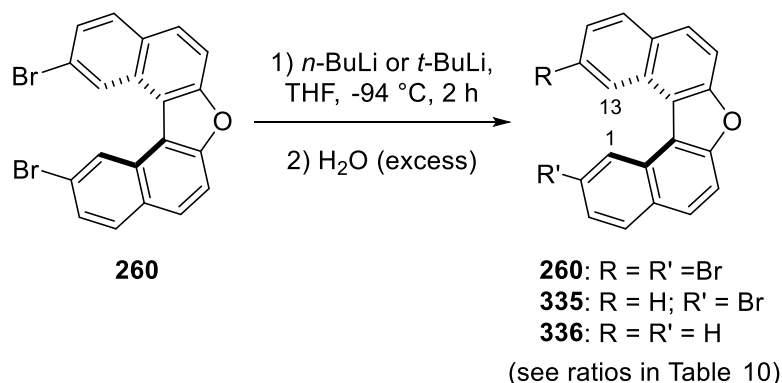


A Br/Li exchange is then carried out with *n*-BuLi solution in THF followed by quenching with the appropriate chlorophosphine to obtain the targeted molecules **324a** to **324d** (Scheme 106). However, yields could not have been determined. Indeed, the first

monosubstitution tests were performed *via* a metal/halogen exchange employing aryl and alkyl lithium compounds followed by hydrolysis to study the selectivity of this exchange (Scheme 107). These tests have been carried out using different equivalents of *n*-BuLi and *t*-BuLi in order to assess the optimal conditions for this reaction. Conversions have been determined by <sup>1</sup>H NMR analysis monitoring the signal of protons in position 1 and 13. These protons are highly deshielded ( $\delta$  between 9.0 and 9.5 ppm) as they are in the anisotropic cone of the aromatic ring facing them.

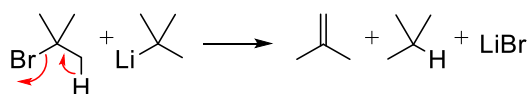


**Scheme 106:** Synthesis of new diphosphines based on oxa[5]helicene scaffold.



**Scheme 107:** Metal/halogen exchange reaction tests employing alkyl lithium compounds.

Using *n*-BuLi to perform only one metal/halogen exchange, the optimal conversion should be obtained with 1 equivalent of alkyl lithium reactant. However, the situation is different with *t*-BuLi because the *t*-BuBr generated after the metal/halogen exchange react with *t*-BuLi via elimination reaction to yield 2-methylpropene, isobutane and LiBr (Scheme 108). Thus, in theory, 2 equivalent *t*-BuLi are needed to perform one metal/halogen exchange and to obtain the monobrominated oxa[5]helicene **X**. The table 10 shows the results obtained employing 1 to 4 equivalents of alkyl lithium.



**Scheme 108:** Reaction of *t*-BuLi with *t*-BuBr during metal/halogen exchange.

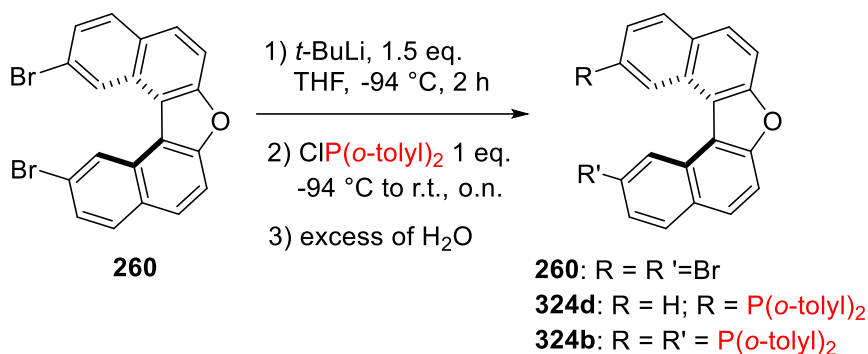
**Table 10:** Results for the metal/halogen exchange tests: Relative ratios (%) of compounds obtained for the reaction described in Scheme X.

Reactants		Relative ratios <sup>a</sup> (%)		
Alkyl lithium	Equivalent	<b>260</b>	<b>335</b>	<b>336</b>
<i>n</i> -BuLi	1	60	25	15
<i>t</i> -BuLi	2	25	40	35
<i>t</i> -BuLi	3	15	40	45
<i>t</i> -BuLi	4	4	1	95

<sup>a</sup>Ratios determined by <sup>1</sup>H NMR analysis

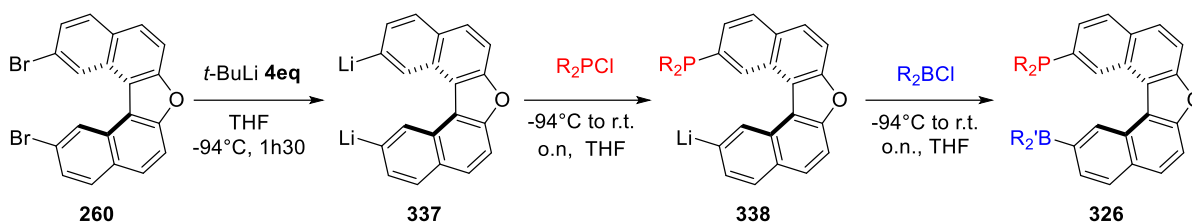
We observed that the reaction with 1 equivalent of *n*-BuLi led to poor conversions as 60% of the starting material is remaining. Thus, we decided to use *t*-BuLi. The results showed that only 40% of the monobrominated oxa[5]helicene **335** were formed with 2 equivalents while the compound **336** generated by a double metal/halogen exchange is produced in similar quantities. Moreover, employing more equivalents of *t*-BuLi led to higher ratios of double exchange.

Nevertheless, the functionalization of the oxa[5]helicene by the chlorodi(*o*-tolyl)phosphine (ClP(*o*-tolyl)<sub>2</sub>) has been tested according to the following procedure (Scheme 109) in order to afford the monophosphine **324d**. During this test, 1.5 equivalents of *t*-BuLi have been used to prevent the double exchange at most. One product has been isolated by precipitation in acetone and characterized by NMR and mass spectrometry. This isolated product was the diphosphine **324b**, demonstrating again a selectivity issue.



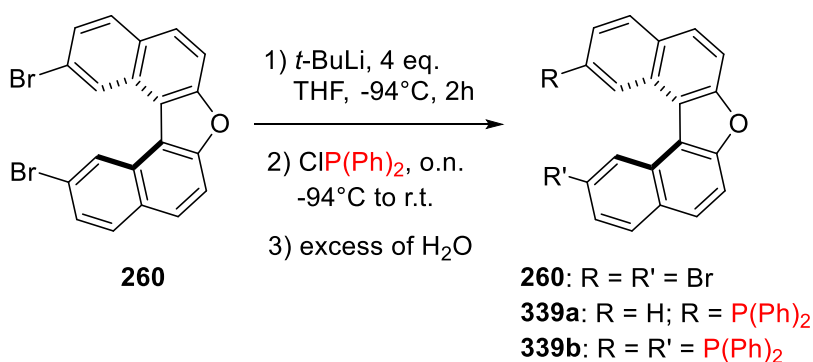
**Scheme 109:** Selective substitution test of chlorodi(*o*-tolyl)phosphine on oxa[5]helicene.

Another strategy has been considered to prevent this selectivity issue. It consists in performing the double metal/halogen exchange using 4 equivalents of *t*-BuLi followed by successive addition of chlorophosphine and fluoroborane (Scheme 110).



**Scheme 110:** Strategy for the synthesis of FLP systems based on oxa[5]helicene scaffold.

In order to study this method, we were first interested in the preparation of the compound **338** followed by a hydrolysis (Scheme 111). Unfortunately, a mix of oxa[5]helicene derivative **260** as the major product and diphosphine **339b** as the minor product were obtained.



**Scheme 111:** Selective substitution test of chlorodiphenylphosphine on oxa[5]helicene using 4 equivalents of *t*-BuLi.

After these unsuccessful tries, we noticed that the dibromooxa[5]helicene we were using as starting material was not pure causing the metal/halogen exchange to fail. Nevertheless, crystals of **339b** could be obtained by slow evaporation of a solution in EtOAc. Thus, we structurally characterized diphosphine **339b** in the solid state by X-ray diffraction analysis (see structure in Figure 24). Unfortunately, crystals couldn't be grown for the other phosphines.

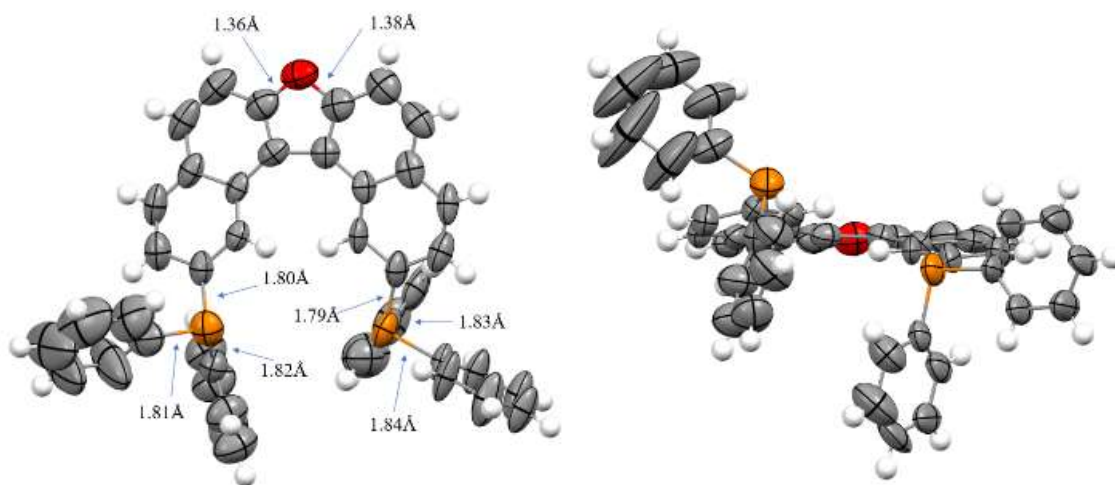


**Figure 24:** Crystal structure of **339b** seen from the top (left) and from the side (right).



We then compared this structure with the ones of analogous phosphines reported in the literature. First, we can compare the C-P and C-O bond lengths with those of triphenylphosphine<sup>[207]</sup> and dibenzofurane<sup>[208]</sup> (Figure 25).

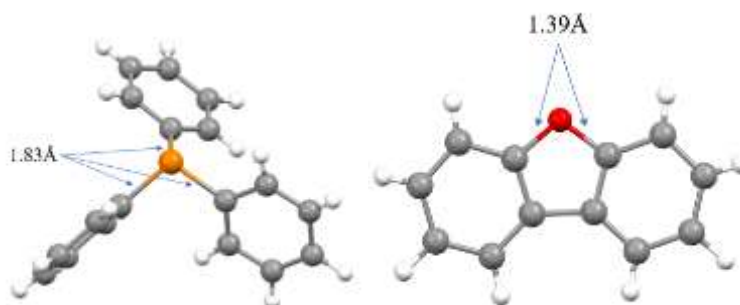


**Figure 25:** X-ray structure of triphenylphosphine (left) and dibenzofurane (right).

The C-P bond of triphenylphosphine measures 1.83 Å which is slightly longer than the C-P bonds in our molecule. It indicates that the phosphorus of **339b** is richer in electrons than that of triphenylphosphine. Moreover, the C-O bonds of the furane motif are slightly shorter in the oxa[5]helicene scaffold.

The structure of **339b** can also be compared to the one of the classical carbo[5]helicene analogous phosphine **340** already reported in the literature<sup>[209]</sup> showed in Figure 26.

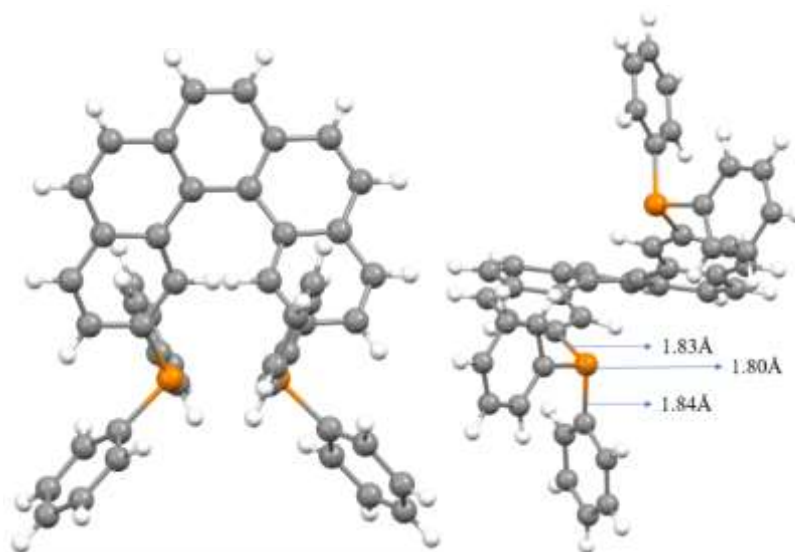


**Figure 26:** X-ray structure of carbo[5]helicene diphosphine **340** seen from top (left) and from the side (right)

The key structural parameters for this compound can be found in Table 11 along with those of the oxa[5]helicene diphosphines **339b** that we synthesized.

**Table 11:** Distances  $d_{pp}$  (Å) and dihedral angles ( $^{\circ}$ ) values for **339b** and carbo[5]helicene diphosphine **340** obtained after X-ray diffraction analysis.

Helicene type	Carbo[5]helicene <b>340</b>	Oxa[5]helicene <b>339b</b>
Dihedral angle ( $\alpha$ )	47.8 $^{\circ}$	24.5 $^{\circ}$
Distance between phosphines ( $d_{pp}$ )	5.02 Å	5.06 Å

We notice that the dihedral angle of **339b** is almost twice as small as the one of the carbo[5]helicene analog. It can be explained by the smaller internal angle of the furane motif compared to the benzene one. Moreover in the case of the oxa[5]helicene derivative, the phenyl substituents of a same phosphine lay on both sides of the helicene in order to interact with the phenyl substituents of the other phosphine which also explains the smaller angle. For the carbo[5]helicene derivative, the phenyl substituents of each phosphine lay on the same side of the helicene to reduce steric hindrance and no interaction is observed between them which tends to increase the interplanar angle of the terminal rings. Nevertheless, the higher dihedral angle of this helicene allows to direct phosphines toward each other more easily and thus to obtain a similar distance  $d_{pp}$  despite the difference of dihedral angles.

Remarkably, a supramolecular organization difference has been noticed between the two compounds in the solid state. Indeed, we observe a more compact layout for the oxa[5]helicene derivative **339b** due to its smaller dihedral angle and the arrangement of the phenyl groups. It organizes by pair of helicenes, one (M) and one (P), so that a  $\pi$ - $\pi$  stacking interaction occurs between the two. The supramolecular interaction of the carbo[5]helicene **340** is more spaced allowing the formation of an alternate network of (P) and (M) helicenes without any  $\pi$ -stacking between two molecules (Figure 27).

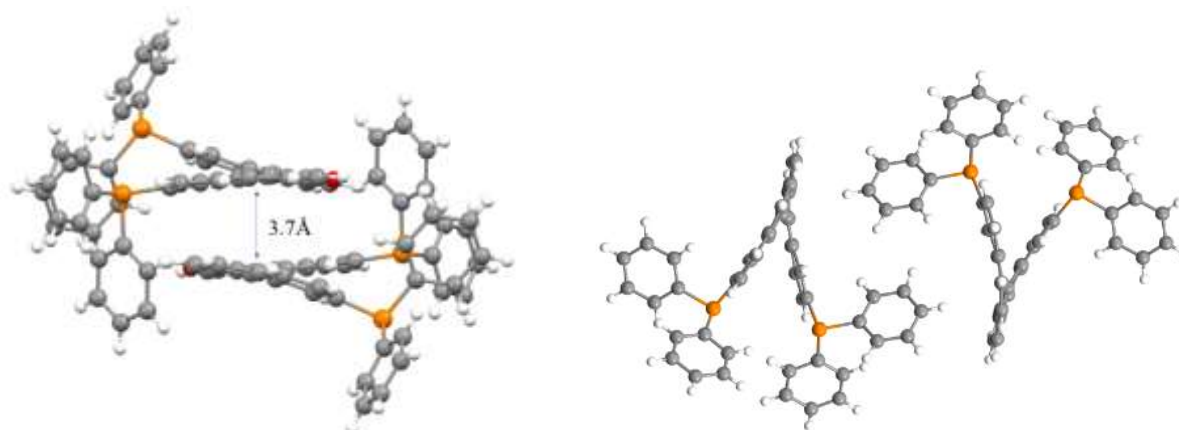


**Figure 27:** Supramolecular organization of the oxa[5]helicene (left) and the carbo[5]helicene derivatives (right).

In addition of these syntheses, we also focused on the theoretical design of frustrated Lewis pair systems based on hetero[5]helicene scaffold. We first selected an exchange-correlation energy functional in DFT to describe interactions between the Lewis acid and base of the FLPs, and to study the capture of CO<sub>2</sub> by a series of FLP systems. The exchange-correlation energy functional  $\omega$ B97X-D has been selected while the functional M06-2X has been found to be reliable.

DFT calculations performed by a master student, Thomas Bernard, that I supervised during his master thesis showed that the thia[5]helicene **327a** (with X=S, R=C<sub>6</sub>H<sub>11</sub> and R'=C<sub>6</sub>F<sub>5</sub>) would be the most favorable for the capture of CO<sub>2</sub> (Figure 28). These quantum calculations indicate that the distance between the phosphorus atom and the boron would be 4.38 Å in the compound **327a**. This distance has been shown to be appropriate for the catalytic hydrogenation of CO<sub>2</sub>.<sup>[67]</sup>

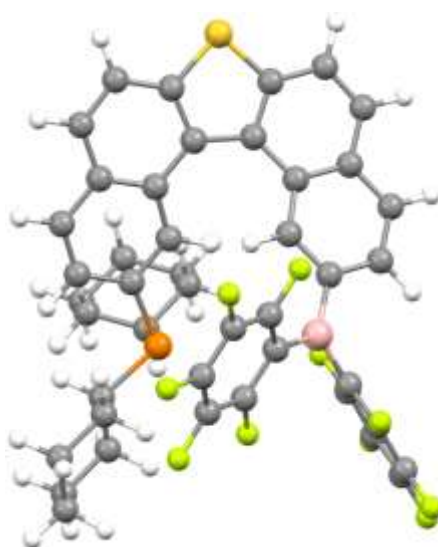


**Figure 28:** DFT structure of thia[5]helicene **341**.

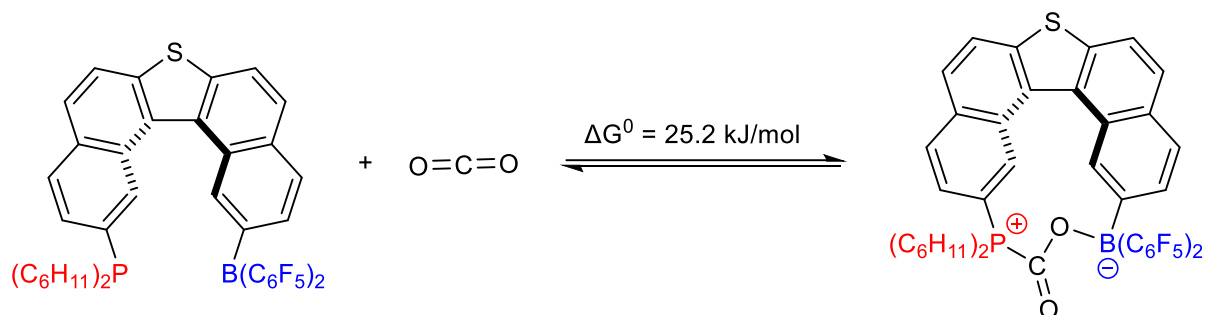
### III. Conclusion and perspectives

#### 1. Conclusions

Intramolecular FLP systems have been largely developed in the recent years. Due to their steric hindrance, FLPs are able to activate small molecules such as H<sub>2</sub>, SO<sub>2</sub>, CO or CO<sub>2</sub>, which spark the interest in the field of catalysis as potential alternative to transition metal catalysis. Helicenes display a helicoidal geometry and an extended  $\pi$ -system conferring unique properties. Combination of FLP and helicoidal linkers such as helicenes could thus be ideal for the catalytic reduction of CO<sub>2</sub>.

After the selection of a suitable exchange-correlation energy functional, we studied the capture of CO<sub>2</sub> by a series of FLP systems based on oxa[5]helicene and

thia[5]helicene scaffold. We discovered that  $-B(C_6F_5)_2$  is the most efficient Lewis acid for the activation  $CO_2$  because of its high Lewis acidity. Besides,  $-P(t-Bu)_2$  and  $-P(C_6H_{11})_2$  are the most favorable Lewis bases for the formation of the adduct with  $CO_2$  due to their high Lewis basicity and their low reorganization energy. Finally, the thia[5]helicene scaffold provided the most favorable results for the capture of  $CO_2$ . Thus, the most favorable equilibrium for the capture of  $CO_2$  is the following:



**Scheme 112:** Most favorable equilibrium for the capture of  $CO_2$  *via* a FLP based on thia[5]helicene.

In parallel to these calculations, we synthesized the precursor of the FLP systems (2,12-(dibromo)oxa[5]helicene) in two steps. The challenge of this part of the project was to selectively add the Lewis base then the Lewis acid. Several lithiation tests have been performed using organolithium reagents. However, selectivity and conversion issues have been encountered. Only weak conversion have been observed when *n*-BuLi was used while employing *t*-BuLi led to the double Br/Li exchange.

Even though FLPs based on hetero[5]helicene could not be synthesized, oxa[5]helicene diphosphines have been prepared and characterized (Figure 29).

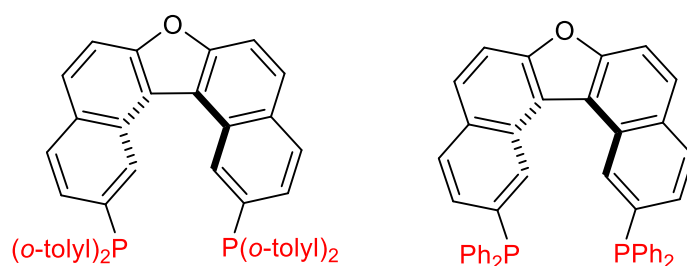
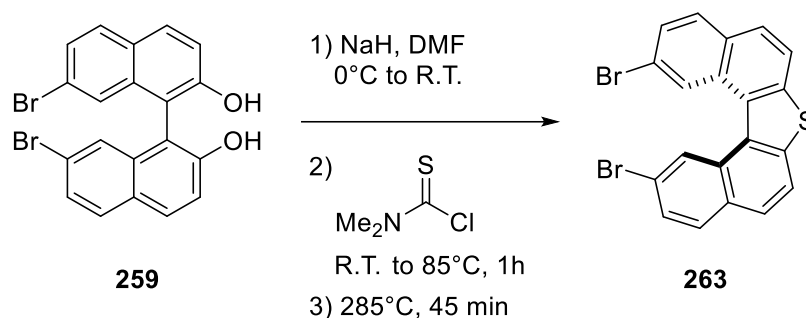


**Figure 29:** 2,12-bis(di(*o*-tolyl)phosphino)oxa[5]helicene and 2,12-bis(diphenylphosphino)oxa[5]helicene.

## 2. Perspectives

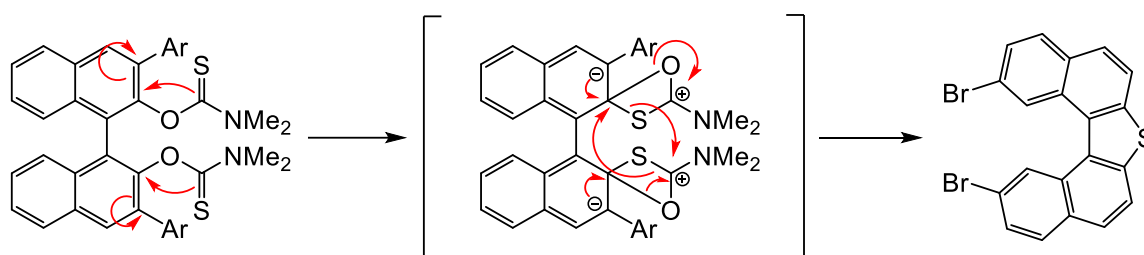
We demonstrated that we achieved the synthesis of new chiral phosphines based on the scaffold of the oxa[5]helicene which could have potential applications in asymmetric catalysis. Furthermore, DFT calculations have been conducted to study the impact of the size of the helicene (hetero[5]helicene or hetero[7]helicene) and of the heteroatom (oxygen or sulfur) on the interaction energy between the Lewis pairs and on the  $CO_2$  capture. These calculations revealed that thia[5]helicene gives the most

favorable results for the formation of FLP-CO<sub>2</sub> adduct. The development of another series of helicoidal catalyst is thus envisaged as the next step of the study. Indeed, it is also possible to synthesize the thia[5]helicene derivative **263** by adding one step to the synthetic pathway (Scheme 113).



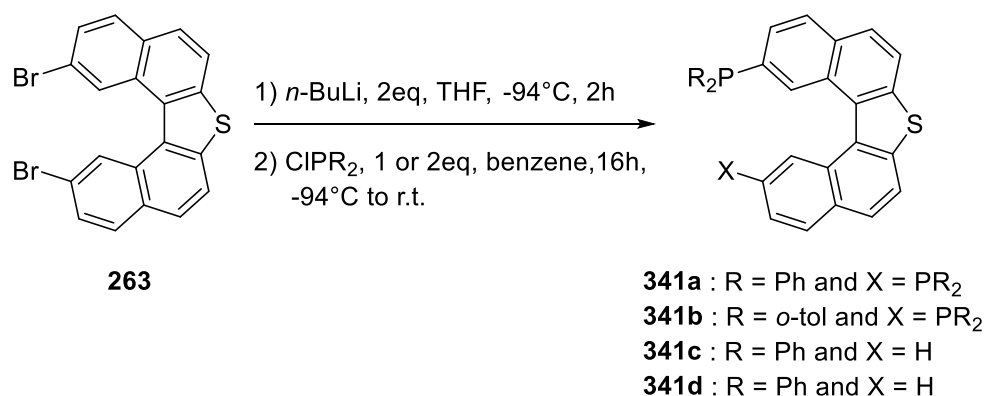
**Scheme 113:** Planned synthesis of the precursor of the thia[5]helicene phosphines.

The 7,7'-dibromo-1,1'-binaphthalene-2,2'-diol **259** is first deprotonated with NaH in DMF before adding the dimethylthiocarbamoyl chloride to get the compound **263**. Finally, this compound will undergo a Newman-Kwart rearrangement reaction<sup>[210]</sup> (Scheme 114).



**Scheme 114:** Mechanism for the parasite reaction of the Newman-Kwart rearrangement.

After obtention of precursor **263**, the synthetic pathway to get the phosphines would be identical as the one for the oxa[5]helicene via Br/Li exchange and addition of the appropriate chlorophosphine (Scheme 115). This new series of phosphine ligands would allow us to study the impact of structural and electronical modifications on the helix core in asymmetric catalysis. Besides, oxidizing the sulfur atom would push further the structural tuning possibilities of the catalyst.



**Scheme 115:** Synthesis of thia[5]helicene phosphines **341a-d** derivatives.

## References:

- [141] F. H. Allen, O. Kennard, D. G. Watson, L. Brammer, A. G. Orpen, R. Taylor, *J. Chem. Soc., Perkin Trans. 2*, **1987**, S1.
- [142] W. H. Laarhoven, W. J. C. Prinsen, *Top. Curr. Chem.*, **1984**, 125, 63.
- [143] K. P. Meurer, F. Vögtle, *Top. Curr. Chem.*, **1985**, 127, 1.
- [144] J. Meisenheimer, K. Witte, *Ber. Dtsch. Chem. Ges.*, **1903**, 36, 4153–4164.
- [145] R. Weitzenböck, H. Lieb, *Monatsh. Chem.* **1912**, 33, 549–565.
- [146] R. Weitzenböck, A. Klingler, *Monatsh. Chem.* **1918**, 39, 315–323.
- [147] a) M. S. Newman, W. B. Lutz, D. Lednicer, *J. Am. Chem. Soc.* **1955**, 77, 3420–3421. b) M. S. Newman, W. B. Lutz, *J. Am. Chem. Soc.* **1956**, 78, 2469–2473. c) M. S. Newman, D. Lednicer *J. Am. Chem. Soc.* **1956**, 78, 4765–4770.
- [148] M. Flammang-Barbieux, J. Nasielski, R. H. Martin, *Tetrahedron Lett.* **1967**, 8, 743–744.
- [149] R. H. Martin, M. Flammang-Barbieux, J. P. Cosyn, M. Gelbcke, *Tetrahedron Lett.* **1968**, 9, 3507–3510.
- [150] R. H. Martin, G. Morren, J. J. Schurter, *Tetrahedron Lett.* **1969**, 10, 3683–3688.
- [151] R. H. Martin, M. Baes, *Tetrahedron* **1975**, 31, 2135–2137.
- [152] K. Mori, T. Murase, M. Fujita, *Angew. Chem. Int. Ed.* **2015**, 54, 6847–6851.
- [153] H. Wynberg, *Accounts Chem. Res.* **1971**, 4, 65–73.
- [154] R. H. Martin, *Angew. Chem. Int. Ed. Eng.* **1974**, 13, 649–660.
- [155] a) W. Laarhoven, W. C. Prinsen, F. Vögtle, E. Weber, Eds.; Springer Berlin Heidelberg: 1984; Vol. 125, p 63–130., b) K. Meurer, F. Vögtle, Springer Berlin Heidelberg: 1985; Vol. 127, p 1–76., c) H. Osuga, H. Suzuki, *J. Syn. Org. Chem. Jpn.* **1994**, 52, 1020–1031., d) T. J. Katz, *Angew. Chem. Int. Ed.* **2000**, 39, 1921–1923., e) A. Urbano, *Angew. Chem. Int. Ed.* **2003**, 42, 3986–3989., f) Y. Shen, C. Chen, *Chem. Rev.* **2011**, 112, 1463–1535., g) M. Gingras, *Chem. Soc. Rev.* **2013**, 42, 1051–1095., h) M. Gingras, G. Felix, R. Peresutti, *Chem. Soc. Rev.* **2013**, 42, 1007–1050. i) M. Gingras, *Chem. Soc. Rev.* **2013**, 42, 968–1006. j) P. Aillard, A. Voituriez, A. Marinetti, *Dalton T.* **2014**, 43, 15263–15278. k) M. J. Narcis, N. Takenaka, *Eur. J. Org. Chem.* **2014**, 2014, 21–34. l) I. G. Stara, I. Stary, In *Aromatic Ring Assemblies, Polycyclic Aromatic Hydrocarbons, and Conjugated Polyenes*; J. S. Siegel, Y. Tobe, Eds.; Thieme: Stuttgart, 2010; Vol. 45b, p 885. m) N. J. Hoffmann, *Photochem. Photobiol.* **2014**, 19, 1–19.
- [156] N. Saleh, C. Shen, J. Crassous, *Chem. Sci.* **2014**, 5, 3680–3694.
- [157] J. Roose, S. Achermann, O. Dumele, F. Diederich, *Eur. J. Org. Chem.* **2013**, 2013, 3223–3231.
- [158] L. Liu, T. J. Katz, *Tetrahedron Lett.* **1990**, 31, 3983–3986.
- [159] T. J. Katz, L. Liu, N. D. Willmore, J. M. Fox, A. L. Rheingold, S. Shi, C. Nuckolls, B. H. Rickman, *J. Am. Chem. Soc.* **1997**, 119, 10054–10063.
- [160] D. Peña, A. Cobas, D. Pérez, E. Guitián, L. Castedo, *Org. Lett.* **2000**, 2, 1629–1632.
- [161] a) D. Peña, D. Pérez, E. Guitián, L. Castedo, *Org. Lett.* **1999**, 1, 1555–1557. b) D. Peña, A. Cobas, D. Pérez, E. Guitián, L. Castedo, *Org. Lett.* **2003**, 5, 1863–1866. c) J. Caeiro, D. Peña, A. Cobas, D. Pérez, E. Guitián, *Adv. Synth. Catal.* **2006**, 348, 2466–2474. d) C. Romero, D. Peña, D. Pérez, E. Guitián, *J. Org. Chem.* **2008**, 73, 7996–8000.

- [162] I. G. Stará, I. Starý, A. Kollárovič, F. Teplý, Š. Vyskočil, D. Šaman, *Tetrahedron Lett.* **1999**, 40, 1993–1996.
- [163] J. Roithová, D. Schröder, J. Mísek, I. G. Stará, I. Starý, *J. Mass Spectrom.* **2007**, 42, 1233.114
- [164] H. Teuber, L. Vogel, *Chem. Ber.* **1970**, 103, 3319.
- [165] H. Rau, O. Schuster, *Angew. Chem., Int. Ed. Engl.* **1976**, 15, 114.
- [166] H. E. Högberg, *Acta Chem. Scand.* **1973**, 27, 2591.
- [167] a) G. Stulen, G. J. Visser, *J. Chem. Soc. D: Chem. Commun.* **1969**, 965., b) J. C. Dewan, *Acta Crystallogr., Sect. B.* **1981**, 37, 1421.
- [168] J. F. Schneider, M. Nieger, K. Nattinen, K. H. Dötz, *Synthesis* **2005**, 1109.
- [169] T. Caronna, F. Fontana, A. Mele, I. N. Sora, W. Panzeri, L. Vigano, *Synthesis* **2008**, 413.
- [170] G. Lamanna, C. Faggi, F. Gasparrini, A. Ciogli, C. Villani, P. L. Stephens, F. L. Devlin, S. Menichetti, *Chem. Eur. J.* **2008**, 14, 5747.
- [171] a) G. Capozzi, F. Desio, S. Menichetti, C. Nativi, P. L. Pacini, *Synthesis* **1994**, 521. b) G. Lamanna, S. Menichetti, *Adv. Synth. Catal.* **2007**, 349, 2188.
- [172] H. A. Staab, M. Diehm, C. Krieger, *Tetrahedron Lett.* **1994**, 35, 8357.
- [173] N. Takenaka, R. S. Sarangthem, B. Captain, *Angew. Chem. Int. Ed.* **2008**, 47, 9708.
- [174] F. Teplý, I. G. Stará, I. Starý, A. Kollárovič, D. Saman, L. Rulísek, P. Fiedler, *J. Am. Chem. Soc.* **2002**, 124, 9175.114
- [175] J. Mísek, F. Teplý, I. G. Stará, M. Tichý, D. Saman, I. Cíсарová, P. Vojtísek, I. Starý, *Angew. Chem., Int. Ed.* **2008**, 47, 3188.114
- [176] J. Storch, J. Cermák, J. Karban, I. Cíсарová, J. Sýkora, *J. Org. Chem.* **2010**, 75, 3137.114
- [177] Z. H. Wang, J. W. Shi, J. E. Wang, C. L. Li, X. Y. Tian, Y. X. Cheng, H. Wang, *Org. Lett.* **2010**, 12, 456.
- [178] S. D. Dreher, D. J. Weix, T. J. Katz, *J. Org. Chem.* **1999**, 64, 3671.
- [179] K. E. S. Phillips, T. J. Katz, S. Jockusch, A. J. Lovinger, N. J. Turro, *J. Am. Chem. Soc.* **2001**, 123, 11899.
- [180] D. C. Harrowven, I. L. Guy, L. Nanson, *Angew. Chem. Int. Ed.* **2006**, 45, 2242.
- [181] L. H. Klemm, D. Reed, *J. Chromatogr. A* **1960**, 3, 364–368.
- [182] a) F. Mikeš, G. Boshart, E. Gil-Av, *J. Chromatogr. A* **1976**, 122, 205–221., b) F. Mikeš, G. Boshart, E. Gil-Av, *J. Chem. Soc. Chem. Commun.* **1976**, 99–100.
- [183] H. Numan, R. Helder, H. Wynberg, *Recl. Trav. Chim. Pays-Bas* **1976**, 95, 211–212.
- [184] a) F. Mikeš, G. Boshart, *J. Chromatogr. A* **1978**, 149, 455–464. b) F. Mikeš, G. Boshart, *J. Chem. Soc. Chem. Commun.* **1978**, 173–175.
- [185] Y. H. Kim, A. Tishbee, E. Gil-Av, *J. Am. Chem. Soc.* **1980**, 102, 5915–5917.
- [186] D. Kumano, S. Iwahana, H. Iida, C. Shen, J. Crassous, E. Yashima, *Chirality* **2015**, 27, 507–517.
- [187] R. S. Cahn, C. K. Ingold, V. Prelog, *Angew. Chem. Int. Ed.*, **1966**, 4, 385–415.
- [188] Y. Yoshida, Y. Nakamura, H. Kishida, H. Hayama, Y. Nakano, H. Yamochi, G. Saito, *CrystEngComm*, **2017**, 19, 3626–3632.
- [189] J. Barroso, J. L. Cabellos, S. Pan, F. Murillo, X. Zarate, M. A. Fernandez-Herrera, G. Merino, *Chem. Commun.*, **2018**, 54, 188–191.

- [190] M. Jalaie, S. Weatherhead, K. Lipkowitz, D. Robertson, *Electron. J. Theor. Chem.*, **1997**, *2*, 268.
- [191] B. Lousen, S. K. Pedersen, P. Bols, K. H. Hansen, M. R. Pedersen, O. Hammerich, S. Bondarchuk, B. Minaev, G. V. Baryshnikov, H. Agren, M. Pittelkow, *Chem. Eur. J.*, **2020**, *26*, 4935-4940.
- [192] N. Saleh, C. Shen, J. Crassous, *Chem. Sci.*, **2014**, *10*, 3680.
- [193] R. H. Martin, M. J. Marchant, *Tetrahedron* **1974**, *30*, 343–345.
- [194] M. S. Newman, R. S. Darlak, L. L. Tsai, *J. Am. Chem. Soc.* **1967**, *89*, 6191–6193.
- [195] B. B. Hassine, M. Gorsane, F. Geerts-Evrard, J. Pecher, R. H. Martin, D. Castelet, *Bull. Soc. Chim. Belg.*, **1986**, *95*, 547.
- [196] M. T. Reetz, S. J. Sostmann, *Organomet. Chem.*, **2000**, *603*, 105.
- [197] S. D. Dreher, T. J. Katz, K.-C. Lam, A. L. Rheingold, *J. Org. Chem.*, **2000**, *65*, 815-822.
- [198] I. Sato, R. Yamashima, K. Kadowaki, J. Yamamoto, T. Shibata, K. Soai, *Angew. Chem. Int. Ed.*, **2001**, *40*, 1096.
- [199] A. Macé, K. Hamrouni, E. S. Gauthier, M. Jean, N. Vanthuyne, L. Frédéric, G. Pieters, E. Caytan, T. Roisnel, F. Aloui, M. Srebro-Hooper, B. Carboni, F. Berrée, J. Crassous, *Chem. Eur. J.*, **2021**, *27*, 7959-7967.
- [200] X. Jia, J. Nitsch, L. Ji, Z. Wu, A. Friedrich, F. Kerner, M. Moos, C. Lambert, T. B. Marder, *Chem. Eur. J.*, **2019**, *25*, 10845-10857.
- [201] M. T. Reetz, E. W. Beuttenmüller, R. Goddard, *Tetrahedron Lett.*, **1997**, *38*, 3211-3214.
- [202] K. Yamamoto, T. Shimizu, K. Igawa, K. Tomooka, G. Hirai, H. Suemune, K. Usui, *Sci. Rep.*, **2016**, *6*, 36211.
- [203] M.- A. Courtemanche, M.- A. Légaré, L. Maron, F.- G. Fontaine, *J. Am. Chem. Soc.*, **2014**, *30*, 10708-10717.
- [204] F.- G. Fontaine, M.- A. Courtemanche, M.- A. Légaré, *Chem. Eur. J.*, **2014**, *20*, 2990 – 2996.
- [205] J. F. Schneider, M. Nieger, K. Nattinen, K. H. Dötz, *Synthesis*, **2005**, *7*, 1109-1124.
- [206] P. Lustenberger, F. Diederich, *Helvetica Chimica Acta*, **2000**, *11*, 2865–2883.
- [207] B. J. Dunne, A. G. Orpen, *Acta. Cryst.*, **1991**, *47*, 345-347.
- [208] O. Dideberg, L. Dupont, J. M. André, *Acta. Cryst.*, **1972**, *28*, 1002-1007.
- [209] A. Terfort, H. Görls, H. Brunner, *Synthesis*, **1997**, *1*, 79-86.
- [210] M. S. Newman, F. W. Hetzel, *Org. Synth.* **1971**, *51*, 139.



**Chapter IV:**  
**General conclusion**

This thesis presented the results of our research on the impact of unprecedented linkers and substituents of phosphine/borane catalysts in the field of FLP chemistry. These studies allowed us to design a series of new bulky phosphines and boranes as well as to investigate their properties towards activation of small molecules such as H<sub>2</sub> or CO<sub>2</sub> and unsaturated C-C bonds.

In the second chapter, we developed two synthetic strategies towards triptycene-derived bulky boranes, boronates and boron ate-complexes. Starting from borylated or brominated anthracenes and using a Br/Li exchange and [4+2] cycloaddition reaction with *in-situ* generated benzyne, we produced a series of triptycene boronates and borates with various boron substituents in positions 1 and 9. Single-crystal X-ray diffraction analysis and UV-Vis/fluorimetric measurements provided quantitative information on the effect of the triptycene scaffold on the photophysical and electronic properties of the obtained compounds. Next, the synthesis of sterically-hindered and electron-rich phosphines derived from triptycene is reported. Their coordination with transition metal (Rh) is investigated in solution and in the solid-state, which allowed the determination of their steric (cone angle, buried volume) and electronic parameters ( $\sigma$ -donating and  $\pi$ -accepting abilities). Quantum chemical calculations of their He<sub>8</sub>-ring steric parameter and of their proton and methyl cation affinities were performed to delineate their sizes and Lewis and Brønsted basicities. These studies showed that the steric hindrance of the 1-triptycenylyl substituent lies between the one of a phenyl substituent and the one of an ortho-tolyl. Unfortunately, the tris-triptycenylyl phosphine could not be prepared but the steric parameter seems to indicate that the steric hindrance of the phosphine reaches its maximum with two triptycenes as substituent. The association of the triptycenylyl-phosphines with tris(pentafluoro-phenyl)borane were quantified experimentally and computationally in the context of the development of new frustrated Lewis pairs. These structure-reactivity investigations allowed to identify new P/B FLPs which were employed for reacting with small molecules and for activating and splitting H<sub>2</sub>, illustrating their potential to be employed as new transition-metal free catalysts for hydrogenation reactions. In addition, we developed the synthesis of the precursor of new rigid intramolecular FLP systems based on the triptycene scaffold with large distances between the Lewis acid and the Lewis base. These structural features should reduce the energy barriers involved in the hydrogenation of CO<sub>2</sub> according to the recent work of Delarmelina.<sup>[67]</sup> Furthermore, the bulky phosphines synthesized in this work could find applications in the field of Ni catalyzed Suzuki couplings as their remote hindrance feature could have an impact on the activity of Ni catalysts.

In the third chapter, we reported the synthesis of new mono and diphosphines based on oxa[5]helicene scaffold starting from 7-bromonaphth-2-ol. This synthetic strategy allowed us to obtain the precursor of FLPs based on oxa[5]helicene scaffold in 2 steps as well as new oxa[5]helicene phosphines in one additional step. Incorporating an oxygen or sulfur atom in the structure of the classical carbopentahelicene induce a distortion of the structure that modify the dihedral angle of the helicene and thus the distance and orientation between the phosphines. This could set a milestone to new applications in asymmetric catalysis. In addition, we also carried out quantum calculations for the design of FLP systems based on the hetero[5]helicene structure able to perform the hydrogenation of CO<sub>2</sub>. These studies revealed

that the derivatives of the thia[5]helicene **327a** (Figure 28) is the most favorable for the capture of CO<sub>2</sub>. Thus, the synthesis of thia[5]helicene is also envisioned.

As perspectives to this project, several studies are envisioned. First, a synthetic method for the preparation of intramolecular FLP systems based on triptycene scaffold need to be developed. These FLPs will be then studied for the catalytic hydrogenation of a series of substrates such as ketones or CO<sub>2</sub>. Then the synthesis of a series of bulky phosphines is also envisaged such as the tristriptycenylyl phosphines **220** or the more sterically demanding 9-triptycenylyl phosphines **343** (Figure 30).

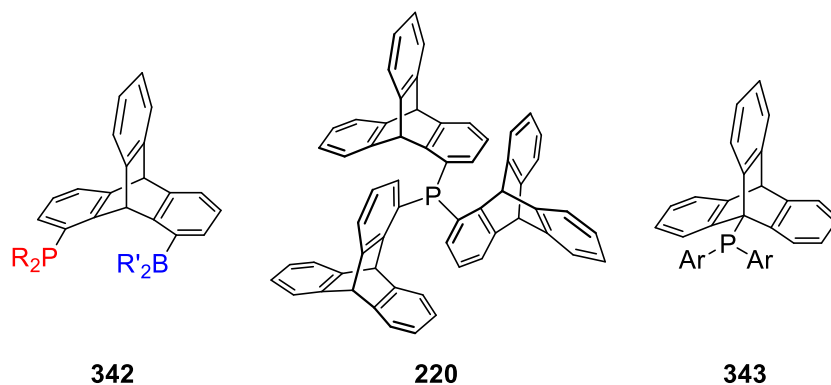


**Figure 30:** Structure of FLP based on triptycene scaffold **342**, tristriptycenylyl phosphine **220** and the 9-triptycenylyl phosphine **343**.

In addition, a synthetic method for the preparation of FLPs based on hetero[5]helicene scaffold also need to be developed (Figure 31). This second scaffold will allow to study the impact of the flexibility of the catalyst on its activity toward CO<sub>2</sub> hydrogenation. Furthermore, the determination of the steric and electronic parameters of the helicene phosphines still need to be done before investigating their reactivity with Lewis acid toward small molecules in the field of FLP.

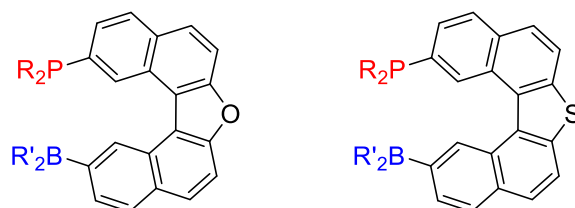


**Figure 31:** FLPs based on oxa[5]helicene and thia[5]helicene scaffold.

## **Appendix A: Experimental part**

# I. Methods for organic synthesis

## 1. Devices and materials

### i. <sup>1</sup>H-NMR Spectroscopy

Spectra were either recorded on a JEOL JNM EX-400 at 400 MHz or on JEOL JNM EX-500 at 500 MHz. All the samples were prepared in standard 5mm quartz tube at room temperature (between 18°C and 25°C) and without preliminary degassing., diluting the solvent in deuterated solvents. Spectra were resolved with MestreNova software. Chemical shifts ( $\delta$ ) are given in ppm referring to the partially deuterated nuclei of the used solvents (7.26 for CDCl<sub>3</sub>, 2.50 for DMSO-d<sub>6</sub>). All spectra are described in the first order. The coupling constants (J) are given in Hertz (Hz). The chemical shifts of signals featuring defined multiplicity were determine by the arithmetic mean of the signal lines. Therefore, the following abbreviations were used: s = singulet, d = doublet, t = triplet, q = quartet, m = multiplet and their combination.

### ii. <sup>13</sup>C-NMR Spectroscopy

Spectra were either recorded on a JEOL JNM EX-400 at 100.4 MHz or on JEOL JNM EX-500 at 125.7 MHz. All the samples were prepared in standard 5mm quartz tube at room temperature (between 18°C and 25°C) and without preliminary degassing., diluting the solvent in deuterated solvents. Spectra were resolved with MestreNova software. Chemical shifts ( $\delta$ ) are given in ppm referring to the partially deuterated nuclei of the used solvents (77.16 for CDCl<sub>3</sub>, 39.52 for DMSO-d<sub>6</sub>). All spectra are decoupled from hydrogen and the coupling constants (J) with <sup>31</sup>P or <sup>19</sup>F nucleus are given in Hertz (Hz).

### iii. <sup>31</sup>P-NMR Spectroscopy

Spectra were recorded on JEOL JNM EX-500 at 202 MHz. All the samples were prepared in standard 5mm quartz tube at room temperature (between 18°C and 25°C) and without preliminary degassing., diluting the solvent in deuterated solvents. Spectra were resolved with MestreNova software. Chemical shifts ( $\delta$ ) are given in ppm and are uncorrected. All spectra are decoupled from hydrogen and the coupling constants (J) are given in Hertz (Hz).

### iv. <sup>19</sup>F-NMR Spectroscopy

Spectra were either recorded on a JEOL JNM EX-400 at 376.5 MHz or on JEOL JNM EX-500 at 470.6 MHz. All the samples were prepared in standard 5mm quartz tube at

room temperature (between 18°C and 25°C) and without preliminary degassing, diluting the solvent in deuterated solvents. Spectra were resolved with MestreNova software. Chemical shifts ( $\delta$ ) are given in ppm and are uncorrected. All spectra are decoupled from hydrogen and the coupling constants (J) are given in Hertz (Hz).

**v. High Resolution Mass Spectrometry (HRMS)**

HRMS were performed on a Bruker MaXis Impact mass spectrometer Q-TOF by the MaSUN platform of University of Namur. The analytes were dissolved in a suitable solvent at the concentration of 1 mg.mL<sup>-1</sup> and diluted 500 times in a mixture of MeCN/H<sub>2</sub>O (50/50). The diluted solutions (200  $\mu$ L) were delivered to the ESI source by a Harvard syringe pump at flow rate of 180  $\mu$ L.min<sup>-1</sup>. ESI conditions were as follows: capillary voltage was set at 4.5 kV; dry nitrogen was used as nebulizing gas at 0.4 bar and as drying gas at 180°C. ESI-MS were recorded at 1 Hz in the range of 50-3000m/z. Calibration was performed with ESI-TOF tuning mix from Agilent. Data were processed using Bruker DataAnalysis 4.1 software. The masses found for [M+H]<sup>+</sup> were compared to the calculated values.

**vi. Crystal structures**

The crystal structures were determined from single-crystals X-ray diffraction data collected using an Oxford Diffraction Gemini Ultra R diffractometer. The data were integrated using the CrysAlisPro software.<sup>[1]</sup> The structures were solved by the dual-space algorithm implemented in SHELXT,<sup>[2]</sup> and refined by full-matrix least squares on  $|F|^2$  using SHELXL-2018/3,<sup>[3]</sup> the shelXL, <sup>[4]</sup> and Olex2 software.<sup>[5]</sup> Non-hydrogen atoms were refined anisotropically; and hydrogen atoms in most of the cases were located from the difference Fourier map but placed on calculated positions in riding mode with equivalent isotropic temperature factors fixed at 1.2 times U<sub>eq</sub> of the parent atoms (1.5 times U<sub>eq</sub> for methyl groups). Absolute configuration, in cases where applicable, were established by anomalous-dispersion effects in diffraction measurements on the crystal.

## **2. Chromatography**

**i. Thin Layer Chromatography (TLC)**

TLCs were performed with aluminium-baked 0.2mm thick Merck silica gel 60F<sub>254</sub> plates. The compounds were detected by fluorescence quenching detection at 254 nm.

**ii. Flash Chromatography**

Flash chromatography were performed of silica gel using Davisil® (particle size 60-200  $\mu$ m, 60 A) in usual conditions ( $\pm$  30 g of silica for 1 g of crude). Solvents were at least of technical grades. The indicated mixture ratios are given as volumic percentages.

### **3. Solvents and chemicals**

Reagents and chemicals were obtained from Fischer, Aldrich, Acros, ABCR, Fluorochem, TCI at ACS grade and were used without further purification. Reactions were performed using purified and dried solvent if necessary: toluene was refluxed over sodium. Tetrahydrofuran (THF), dichloromethane (DCM), tetrahydrofuran (THF), and diethyl ether (Et<sub>2</sub>O) were dried through a MBraun SPS System. Deionized water was used for reaction work-up.

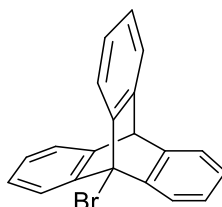
### **4. Quantum calculations**

Computations have been carried out using the Jaguar 8.5 pseudospectral program package. Density Functional Theory (DFT) was applied by the means of the M06-2X functional. The standard split valence polarized 6-31+G(d) basis set was used for all atoms. Electronic energies were obtained after corresponding fully analytical single point calculations, at the M06-2X/6-311+G(d,p) level of theory. Solvation energies were obtained by single point calculations using the PoissonBoltzmann polarisable continuum method as implemented in Jaguar, at the M06-2X/6-31+G(d) level, using the parameters appropriate for benzene. Zero point energy and thermal contributions to enthalpy were computed by performing frequency calculations at the M06-2X/6-31+G(d) level of theory. PA and MCA values are calculated (at the M06-2X/6-31+G(d)(benzene) level) as the difference in enthalpy at 298 K between the neutral and the protonated and methylated phosphine, respectively. The He8\_steric parameters were computed by optimizing the phosphines geometries at the BP86/6-31+G(d) level, their tertiary phosphorus atom constrained to lie at 2.28 Å above the centroid, and perpendicular to the plane, of a helium ring which is constituted by eight helium atoms with a 2.5 Å radius.

## II. Synthetic procedures and characterizations

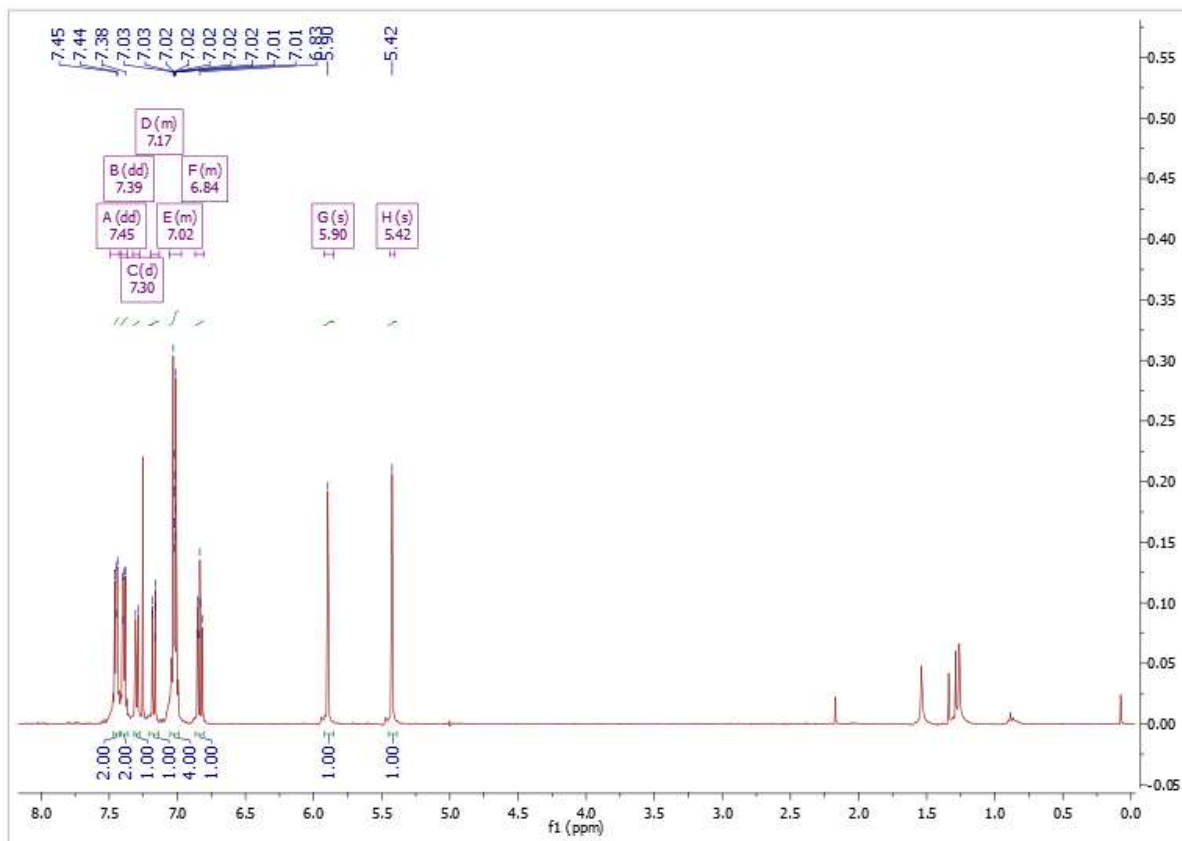
### 1. Preparation of the chapter two's molecules

#### 9-bromotriptycene 2.26:



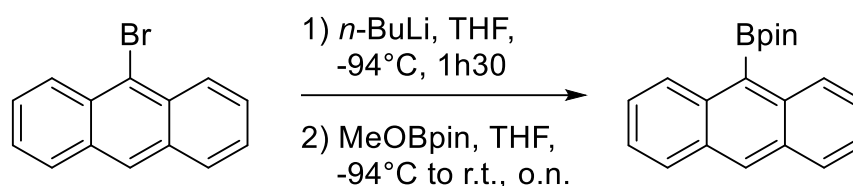
To a stirred solution of 9-bromoanthracene (5.00 g, 19.4 mmol, 1 eq) and isoamyl nitrite (12.0 mL, 93.8 mmol, 4.8 eq) in 100 mL of dichloroethane was added dropwise a solution of anthranilic acid (11.9 g, 86.9 mmol, 4.5 eq) in CH<sub>2</sub>Cl<sub>2</sub>/Acetone (1:1, 200 mL) at reflux. After the addition, the reflux was maintained 1h more and the reaction was then stirred overnight at room temperature. The day after, solvents were removed under reduced pressure and the crude product is purified by flash chromatography using cyclohexane to get the desired compound (4.45 g, 13.4 mmol, 69%).

<sup>1</sup>H NMR (400MHz, CDCl<sub>3</sub>): δ(ppm) = 7.45 (dd, 2H), 7.39 (dd, 2H), 7.30 (d, 1H), 7.17 (m, 1H), 6.84 (m, 4H), 5.90 (s, 1H), 5.42 (s, 1H).





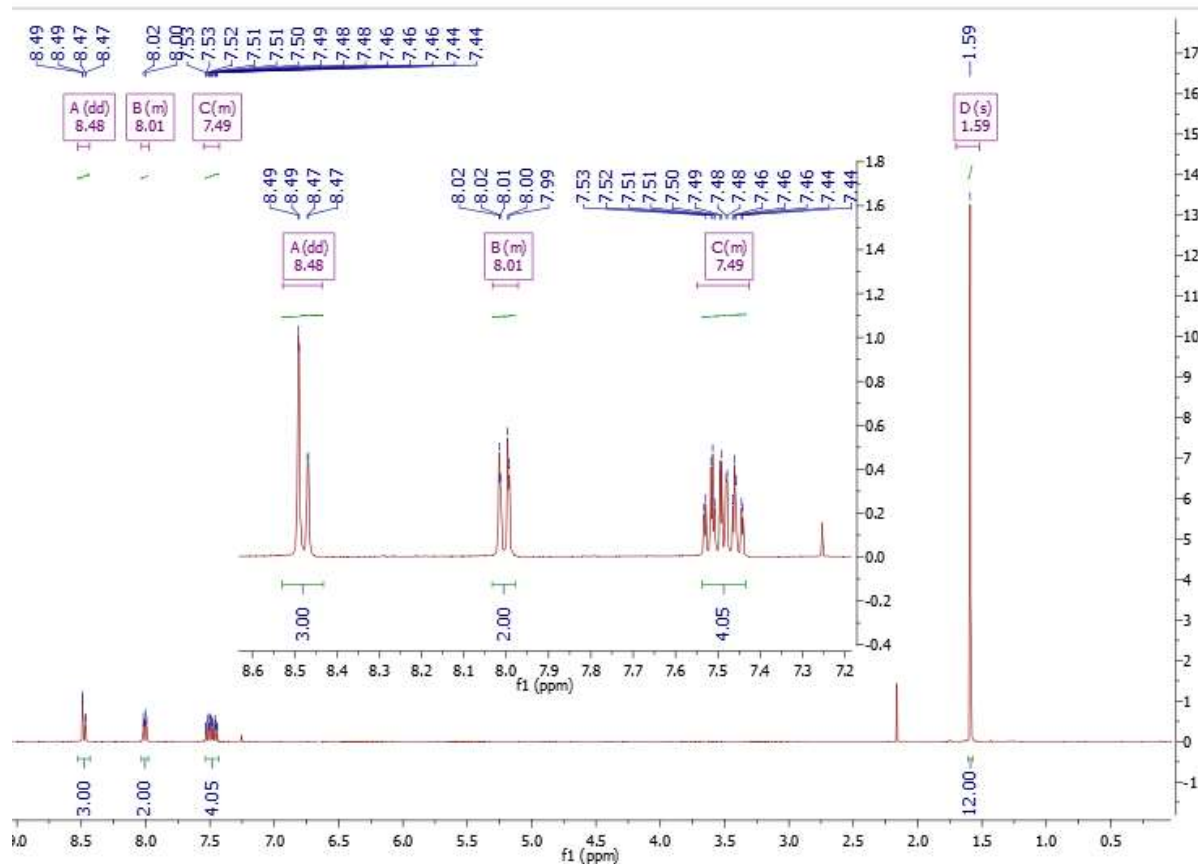
## 2-(anthracen-9-yl)-4,4,5,5-tetramethyl-1,3,2-dioxaborolane **2.27a**:

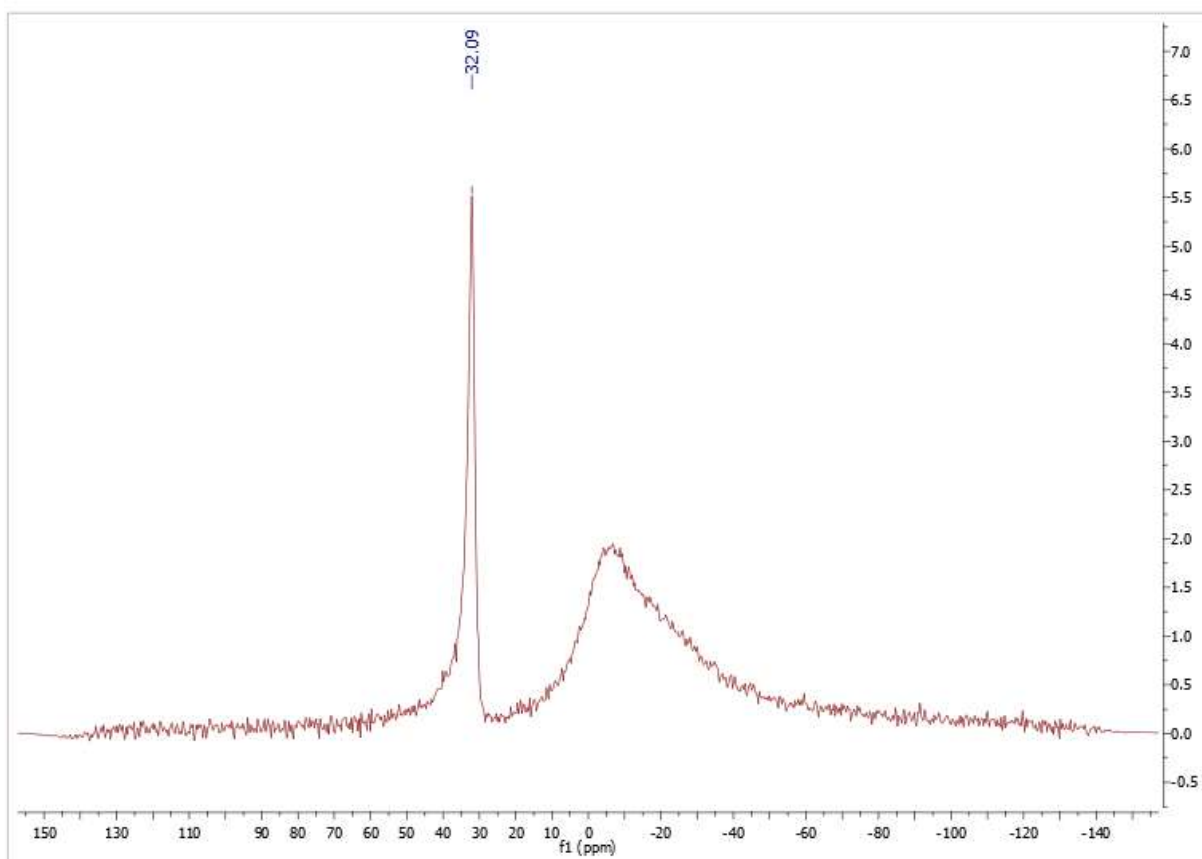


In a 100 mL Schlenk flask was added under inert atmosphere 9-bromoanthracene (2.50 g, 9.73 mmol, 1.0 eq) in suspension in THF (40 mL). The flask is cooled to -94°C with an acetone/N<sub>2</sub>(l) bath and *n*-BuLi (4.20 mL, 2.5 M in hexanes, 10.5 mmol, 1.1 eq) was added dropwise under vigorous stirring. The reaction mixture is then stirred for 1h30 at -94°C and 2-methoxy-4,4,5,5-tetramethyl-1,3,2-dioxaborolane (1.7 mL, 10.4 mmol, 1.1 eq) is added. 10 min after addition, the bath is removed and the reaction is allowed to reach room temperature and stirred overnight. After 16h at room temperature, the solvent is removed under vacuum and the crude product is dissolved in dichloromethane, filtered and dried over MgSO<sub>4</sub>. It is then filtered again and concentrated under reduced pressure. Purification by silica gel chromatography (cyclohexane:EtOAc, 98:2) afforded the compound **2.27** as a white powder (1.69 g, 5.55 mmol, 57%). Crystals suitable for X-ray analysis have been obtained by slow evaporation of a saturated solution of **2.27a** in chloroform.

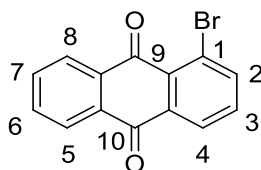
<sup>1</sup>H NMR (400MHz, CDCl<sub>3</sub>): δ(ppm) = 8.45 (dd, *J* = 13.3, 5.6 Hz, 3H), 8.02 – 7.97 (m, 2H), 7.53 – 7.41 (m, 4H), 1.58 (s, 12H).

<sup>11</sup>B NMR (128MHz, CDCl<sub>3</sub>): δ(ppm) = 32.33 (s).



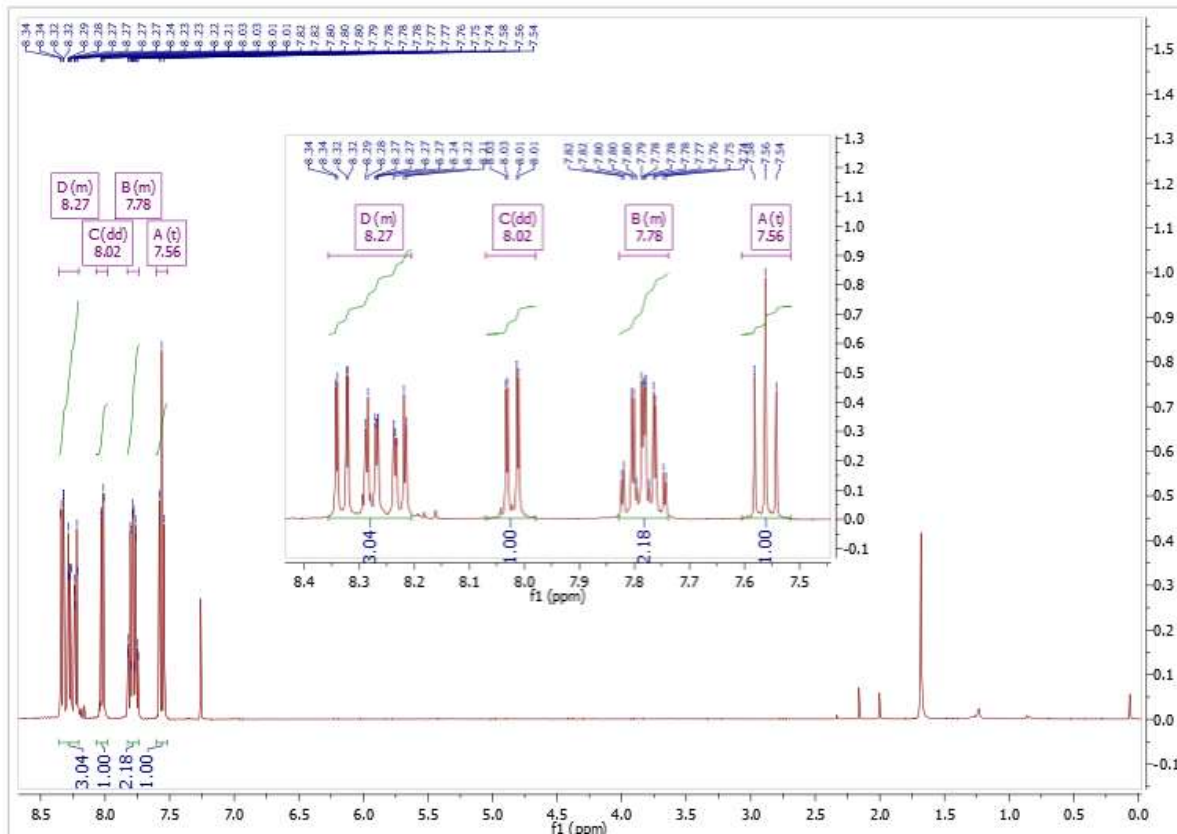


### 1-bromoanthracene-9,10-dione:

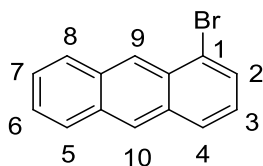


To a stirred solution of  $\text{CuBr}_2$  (12.6 g, 56.4 mmol, 1.25 eq) and  $t\text{-BuONO}$  (8.2 mL, 67.6 mmol, 1.5 eq) in acetonitrile (200 mL) is added 1-aminoanthracene-9,10-dione (10 g, 45.2 mmol, 1 eq) by portions at  $65^\circ\text{C}$ . The mixture is then stirred for 1h at  $65^\circ\text{C}$  and 3h at  $90^\circ\text{C}$ . After 3h, 200 mL of HCl 1M are added to the mixture at room temperature. The solid is then filtered and washed with a HCl 1M solution, distilled water and ethanol. The solid is then dried under vacuum, dissolved in DCM and pass on silica plug to afford the 1-bromoanthracene-9,10-dione 2 (12.392 g, 43.2 mmol, 96%).

$^1\text{H NMR}$  (400MHz,  $\text{CDCl}_3$ ):  $\delta$ (ppm) = 8.27 (m, 3H, H-2, H-3, H-4), 8.02 (dd, 1H, H-5), 7.78 (m, 2H, H-6, H-7), 7.56 (t, 1H, H-8).

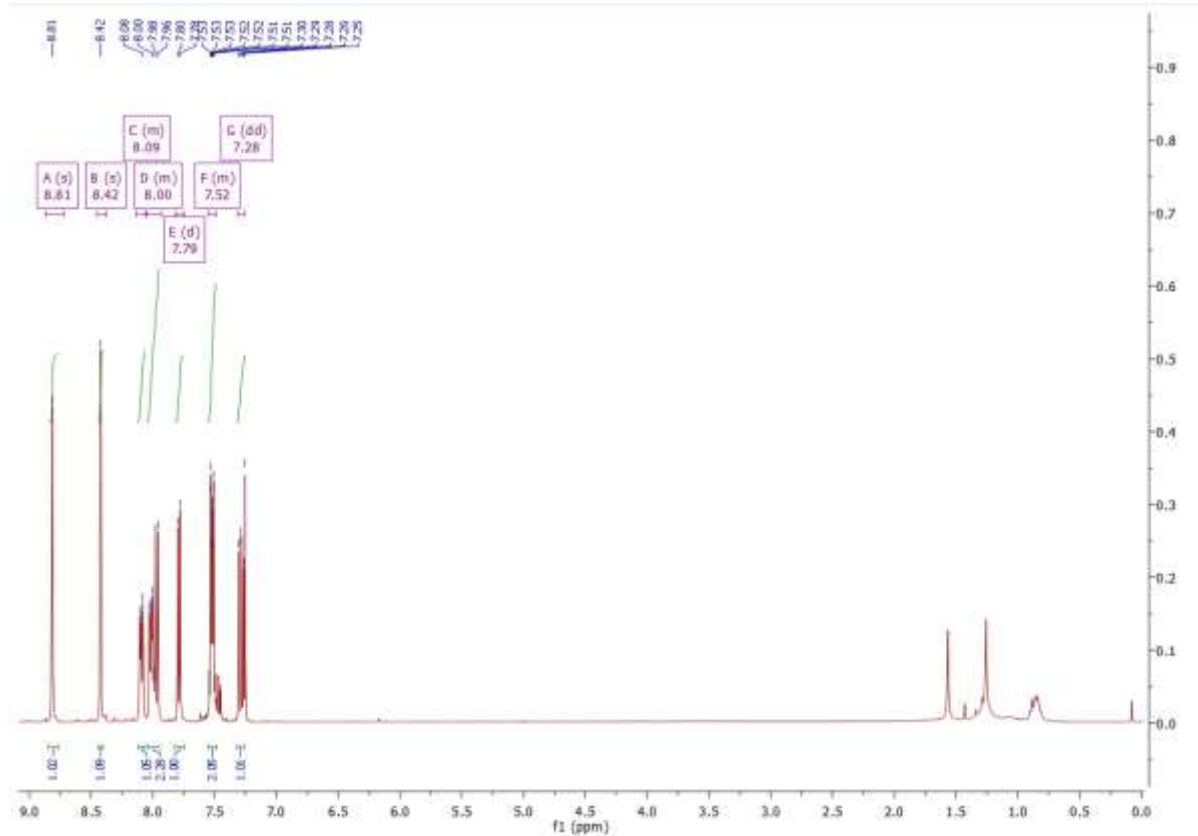


## 1-Bromoanthracene 2.29

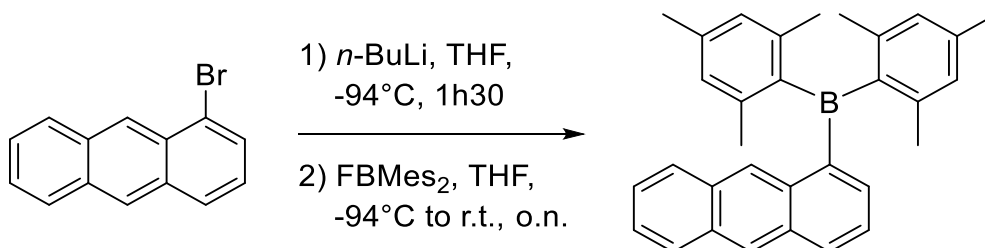


To a stirred suspension of 1-bromoanthracene-9,10-dione (12.39g, 43.2mmol, 1eq) in MeOH (500mL) is added NaBH<sub>4</sub> (13.07g, 345.6mmol, 8eq) at -78°C portionwise. The mixture is then stirred at room temperature for 3h. After, HCl conc. (40mL) is added at 0°C and the mixture is refluxed overnight. The day after, the yellow precipitate is filtrated and washed with water. This yellow solid is then put in suspension in diglyme and NaBH<sub>4</sub> (6.537g, 172.8mmol, 4eq) is added slowly at 0°C. The mixture is stirred for 3h at room temperature. After, MeOH (50mL) is added slowly and a new portion of NaBH<sub>4</sub> (2.451g, 64.8mmol, 1.5eq) is introduced in the flask. The orange solution is stirred overnight at room temperature. The day after, glacial acetic acid is added at 0°C until the mixture reach pH=3 and then HCl conc. is added until pH<2. The mixture is stirred for 3h and the yellow precipitate is collected, washed with water and dried under vacuum to get the desired compound (7.50g, 27.3mmol, 63%).

**<sup>1</sup>H NMR (400MHz, CDCl<sub>3</sub>):** δ(ppm) = 8.82 (s, 1H, H-9), 8.43 (s, 1H, H-10), 8.17-8.06 (m, 1H, H-2), 8.06-8.00 (m, 1H, H-3), 7.98 (dq, 1H, H-4), 7.79 (dd, J<sub>1</sub>=7.1Hz, J<sub>2</sub>=1.0Hz, 1H, H-5), 7.57-7.49 (m, 2H, H-6, H-7), 7.29 (dd, J<sub>1</sub>=8.5Hz, J<sub>2</sub>=7.2Hz, 1H, H-8).



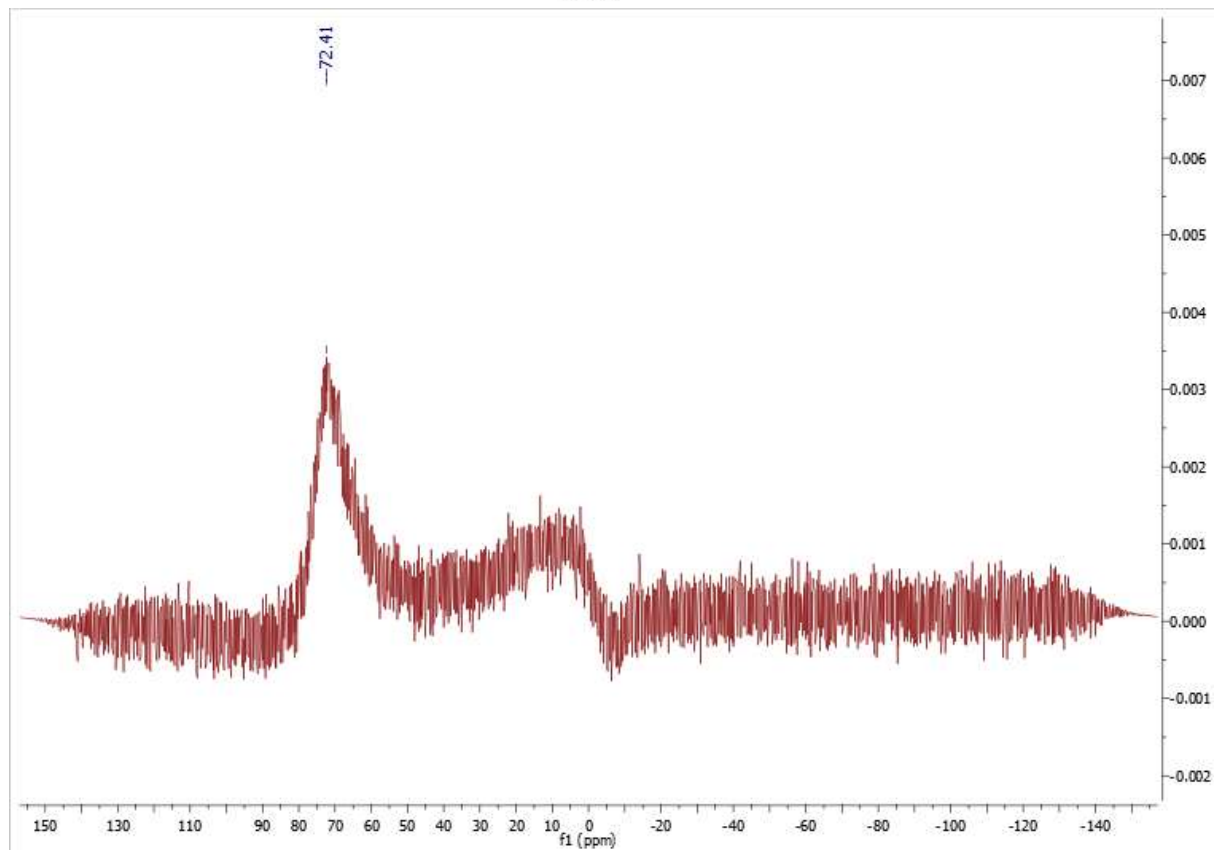
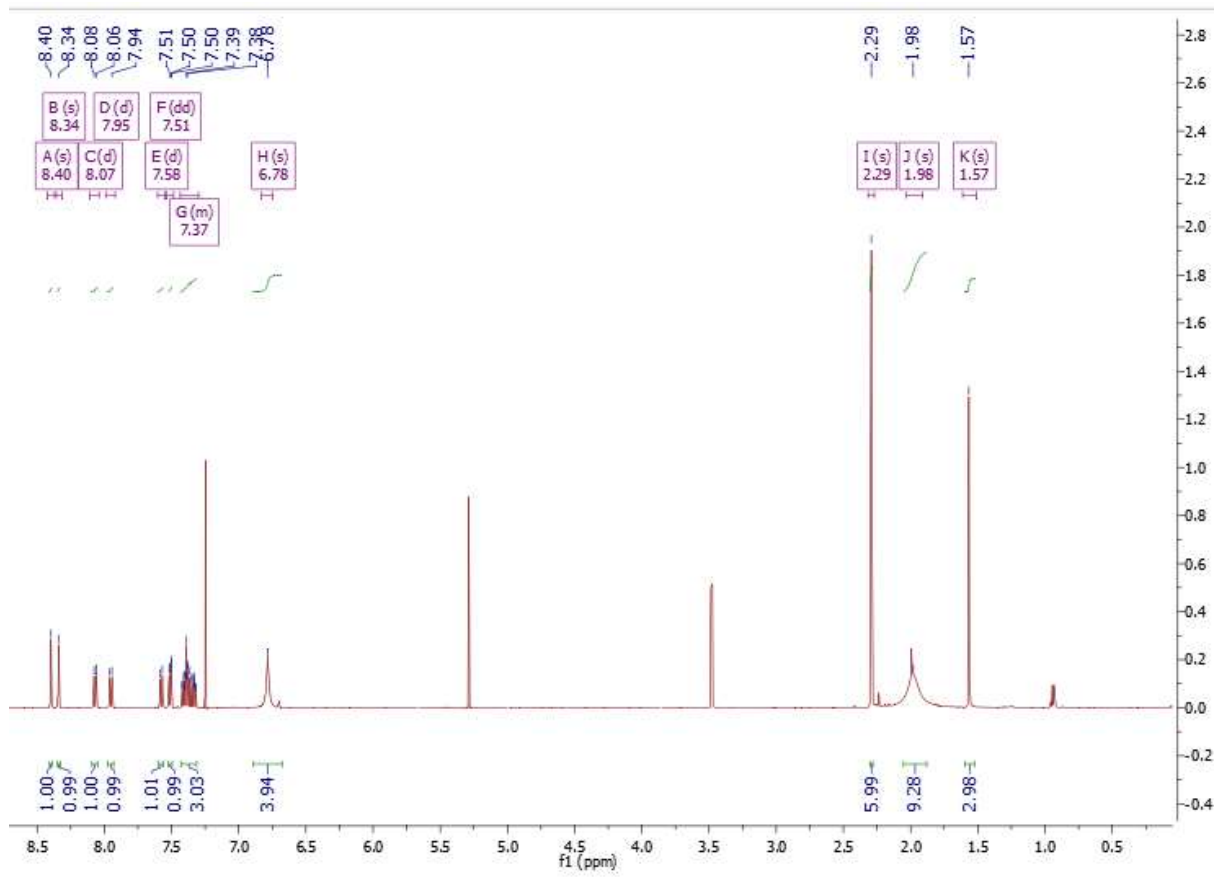
**(1-anthracenyl)dimesityl borane 2.31b:**



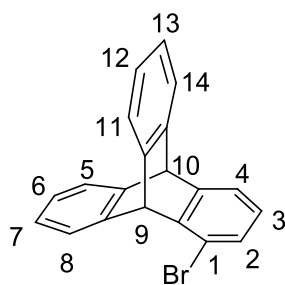
In a 100 mL Schlenk flask was added under inert atmosphere 1-bromoanthracene (2.67 g, 10.4 mmol, 1.0 eq) in suspension in THF (50 mL). The flask is cooled to -94°C with an acetone/N<sub>2</sub>(l) bath and *n*-BuLi (4.20 mL, 2.5 M in hexanes, 10.5 mmol, 1.1 eq) was added dropwise under vigorous stirring. The reaction mixture is then stirred for 90min at -94°C and fluorodimesitylborane (2.78 g, 10.4 mmol, 1.0 eq) is added as a solid under a strong flux of argon. 10 min after addition, the bath is removed and the reaction mixture is allowed to reach room temperature and stirred overnight. After 16h at room temperature, the solvent is removed under vacuum and the crude product is dissolved in dichloromethane, filtered and dried over MgSO<sub>4</sub>. It is then filtered again and concentrated under reduced pressure. Purification by silica gel chromatography (Cyclohexane/EtOAc, 95:5) afforded (1-anthracenyl)dimesityl borane **2.31b** as a white powder (3.76 g, 8.80 mmol, 85%).

<sup>1</sup>H NMR (400MHz, CDCl<sub>3</sub>): δ(ppm) = 8.40 (s, 1H), 8.34 (s, 1H), 8.07 (d, J=8.5 Hz, 1H), 7.95 (d, J=8.2 Hz, 1H), 7.58 (d, J=8.2 Hz, 1H), 7.51 (dd, J<sub>1</sub>=6.6 Hz, J<sub>2</sub>=1.2 Hz, 1H), 7.43-7.30 (m, 3H), 6.78 (s, 3H), 2.29 (s, 6H), 1.98 (broad s, 9H), 1.57 (s, 3H).

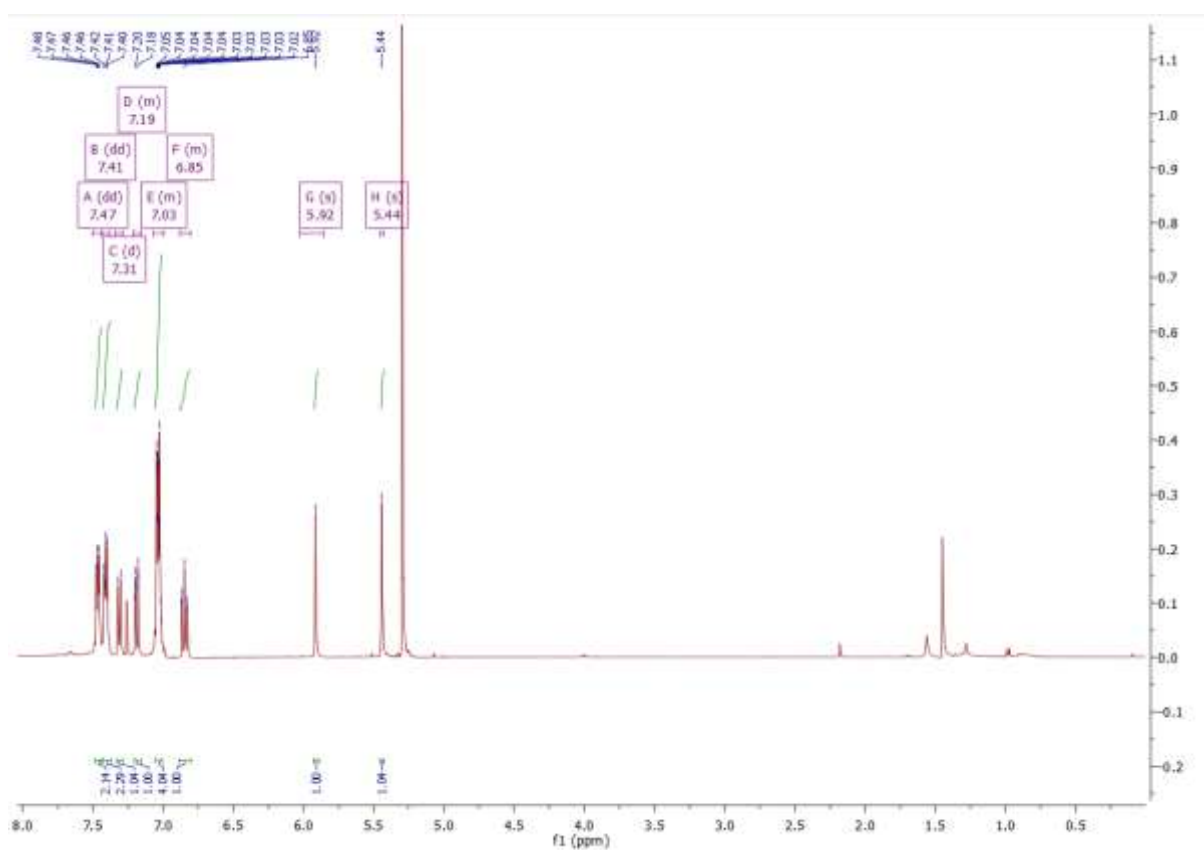
<sup>11</sup>B NMR (128MHz, CDCl<sub>3</sub>): δ(ppm) = 72.4



## 1-bromotriptycene 2.30

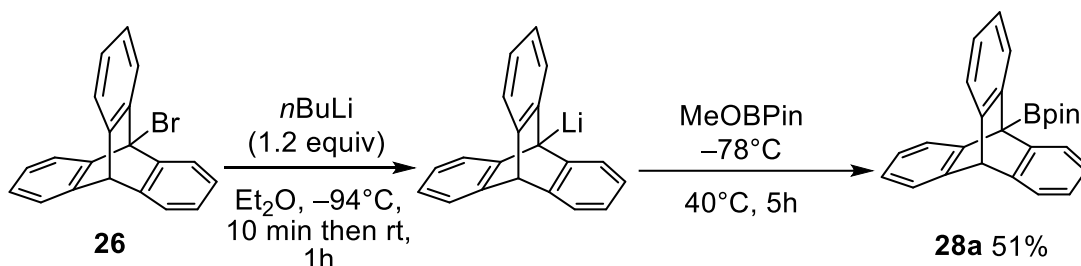


To a stirred solution of 1-bromoanthracene **14** (3.28 g, 12.8 mmol, 1 eq) and isoamyl nitrite (8.2 mL, 64 mmol, 5 eq) in 100 mL of dichloroethane was added dropwise a solution of anthranilic acid (8.76 g, 64 mmol, 5 eq) in diglyme (100 mL) at reflux. After the addition, the reflux was maintained 1h more and the reaction was then stirred overnight at room temperature. The day after, solvents were distilled and the crude product is purified by flash chromatography using cyclohexane to get the desired compound (2.30 g, 6.91 mmol, 54%)  $^1\text{H NMR}$  (400MHz,  $\text{CDCl}_3$ ):  $\delta$ (ppm) = 7.47-7.44 (m, 2H), 7.41-7.39 (m, 2H), 7.30 (d, 1H), 7.18 (dd, 1H), 7.04-7.02 (m, 4H), 6.84 (dd, 1H), 5.90 (s, 1H), 5.43 (s, 1H).



## 2-(tritypcen-9-yl)-4,4,5,5-tetramethyl-1,3,2-dioxaborolane **2.28a**:

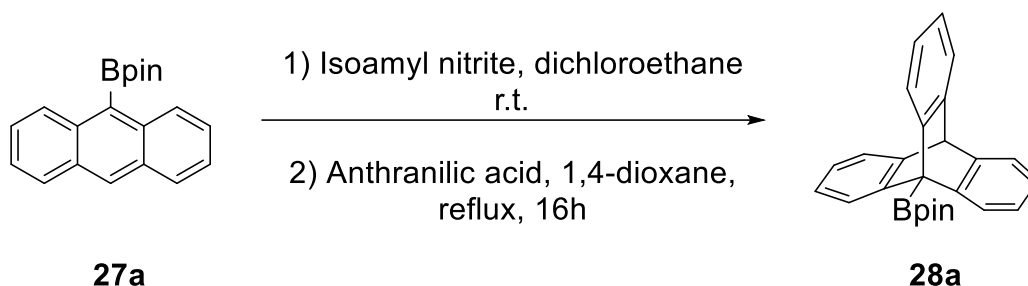
### Procedure A



In a 50 mL Schlenk flask was prepared 9-bromotriptycene **26** (200 mg, 0.602 mmol, 1.0 equiv) in suspension in dry  $\text{Et}_2\text{O}$  (15 mL). The flask is cooled to  $-94^\circ\text{C}$  thanks to an acetone/ $\text{N}_2(\text{l})$  bath and  $n\text{BuLi}$  (0.30 mL, 2.5 M in hexanes, 0.75 mmol, 1.2 equiv) was added dropwise under vigorous stirring. Just after the addition, the bath is removed to allow the reaction to warm up to r.t. during one hour. The reaction mixture is then cooled again to  $-94^\circ\text{C}$  and 2-methoxy-4,4,5,5-tetramethyl-1,3,2-dioxaborolane (0.15 mL, 0.89 mmol, 1.5 equiv) is added. The cooling bath is removed and the flask is equipped with a reflux condenser and the mixture is warmed to  $40^\circ\text{C}$  and stirred for 5h. The reaction is quenched with water (10 mL).

The combined organic layers are extracted with  $\text{EtOAc}$  (3x10 mL), dried over  $\text{MgSO}_4$ , filtered and concentrated under reduced pressure. The crude product is purified by flash chromatography using cyclohexane/ $\text{EtOAc}$  (9:1) as an eluant affording the pure product as a slightly brown powder (118 mg, 0.310 mmol, 51%). Crystals suitable for X-ray structure analysis have been obtained by slow evaporation of a saturated solution of **28a** in  $\text{EtOAc}$ .

### Procedure B



In a 500 mL two-necked flask equipped with a reflux condenser and a dropping funnel was added 2-(anthracen-9-yl)-4,4,5,5-tetramethyl-1,3,2-dioxaborolane **27a** (4.12 g, 13.5 mmol, 1.0 eq) as well as isoamyl nitrite (9.0 mL, 67.5 mmol, 5.0 eq) in dichloroethane (75 mL). In the dropping funnel was added anthranilic acid (9.30 g, 67.5 mmol, 5.0 eq) dissolved in dioxane (100 mL). The flask is warmed to  $90^\circ\text{C}$  and the dropping funnel contents were added dropwise under stirring during a period of 4h. The reaction mixture is then stirred overnight at  $90^\circ\text{C}$ . The solvents were removed under reduced pressure to give a dark brown oily residue. Silica gel chromatography (Cyclohexane/ $\text{EtOAc}$ , 95:5) afforded 2-(tritypcen-9-yl)-4,4,5,5-tetramethyl-1,3,2-dioxaborolane **28a** as a white powder (2.17 g, 5.7 mmol, 42%).

**TLC:**  $R_f$  = 0.29 (cyclohexane: $\text{EtOAc}$  = 95:5)

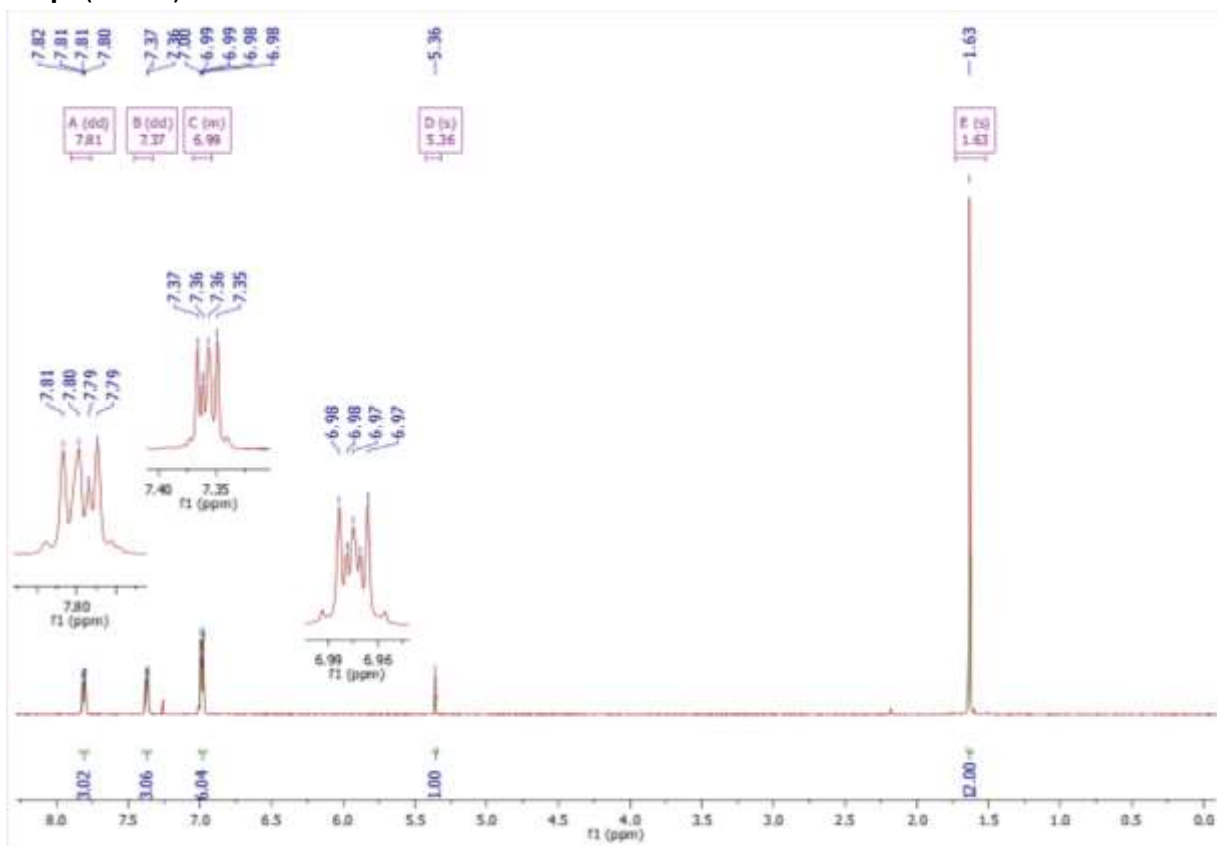
**$^1\text{H NMR}$  (400 MHz,  $\text{CDCl}_3$ ):**  $\delta$  (ppm) = 7.81 (dd,  $J$  = 5.6, 3.1 Hz, 3H), 7.37 (dd,  $J$  = 5.4, 3.2 Hz, 3H), 7.01-6.96 (m, 6H), 5.36 (s, 1H), 1.63 (s, 12H).

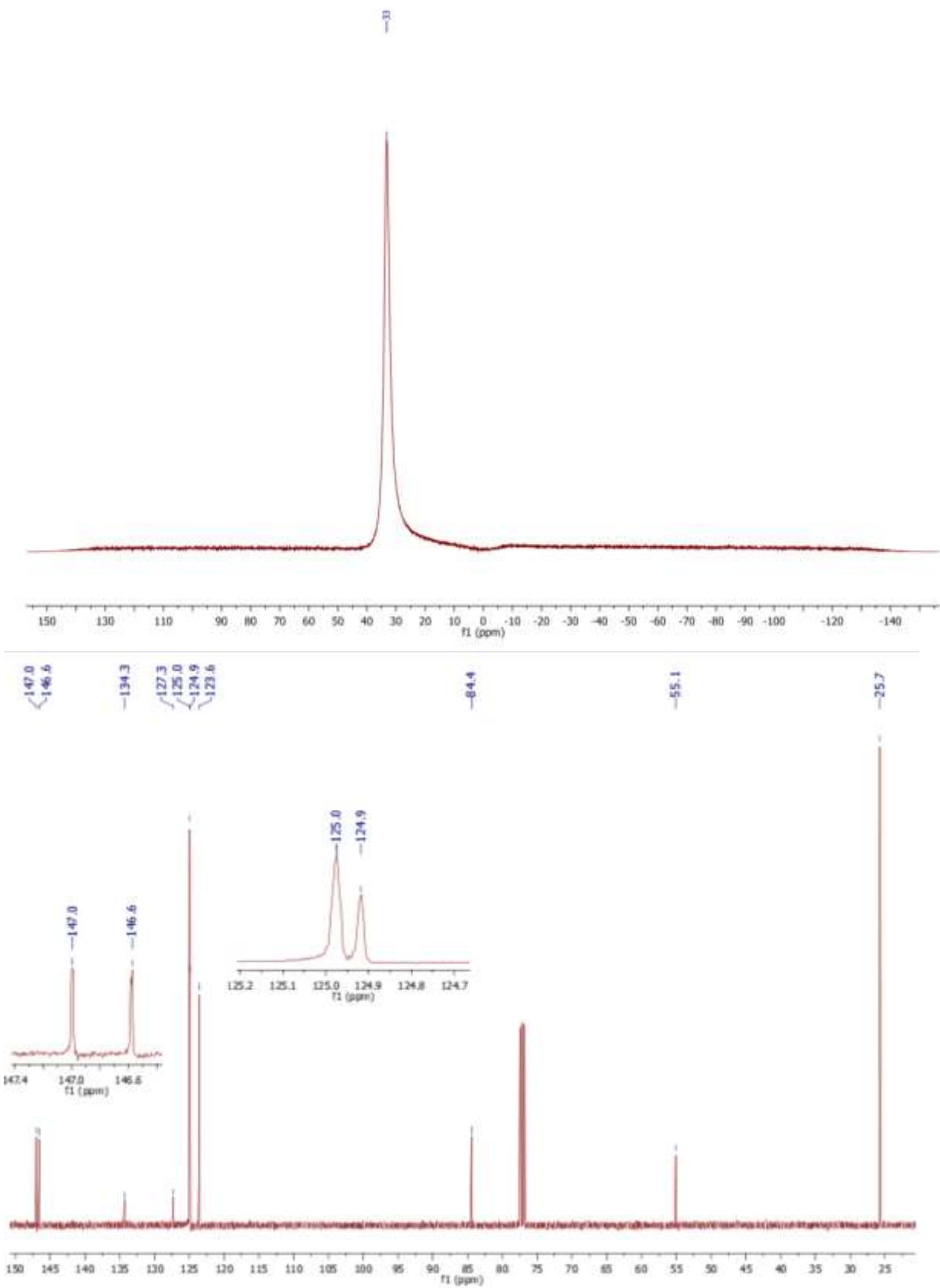


$^{13}\text{C}$  NMR (101 MHz,  $\text{CDCl}_3$ ):  $\delta$  (ppm) = 147.0, 146.6, 134.3, 127.3, 125.0, 124.9, 123.6, 84.4, 55.1, 25.7.

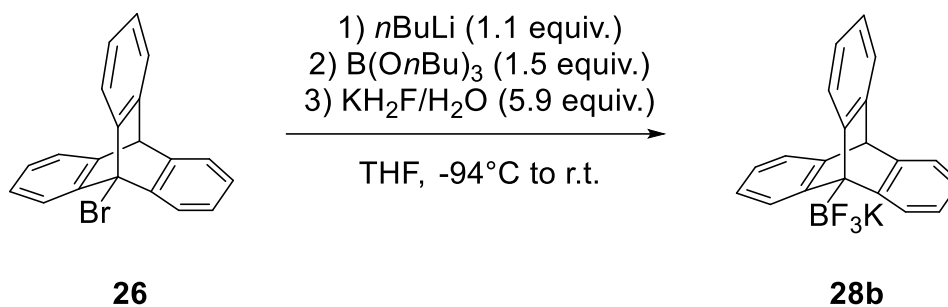
$^{11}\text{B}$  NMR (128 MHz,  $\text{CDCl}_3$ ):  $\delta$  (ppm) = 33

M. p. (EtOAc):  $>240^\circ\text{C}$





**Potassium 9-triptycyltrifluoroborate 2.28b:**



In a 500 mL Schlenk flask was added under inert atmosphere 9-bromotriptycene **26** (5.06 g, 15 mmol, 1.0 eq) in Et<sub>2</sub>O (250 mL). The flask was cooled to -94°C with an acetone/N<sub>2</sub>(l) bath and *n*-BuLi (6.6 mL, 2.5 M in hexanes, 17 mmol, 1.1 eq) was added dropwise under vigorous stirring. 10 min after addition, the bath was removed to allow the reaction mixture to warm up for a period of 1h. The reaction mixture was then cooled again to -94°C and tributyl borate (6.0 mL, 23 mmol, 1.5 eq) was added under stirring. Then, the reaction is warmed to 40°C and stirred overnight. After, the flask is cooled to 0°C with an ice bath and potassium hydrogenfluoride (7.03 g, 90 mmol, 5.9 eq) in water (50 mL) was added dropwise and the reaction is stirred for 1h at 0°C and then stirred at room temperature overnight. The solvents were then evaporated under reduced pressure and a filtration with hot acetone was performed. The filtrate was then evaporated until there is only few mL of acetone in the flask left and a precipitation was performed by adding Et<sub>2</sub>O. Then a filtration afforded pure potassium 9-triptycyltrifluoroborate **2.28a** as a white powder (2.13 g, 5.9 mmol, 39 %).

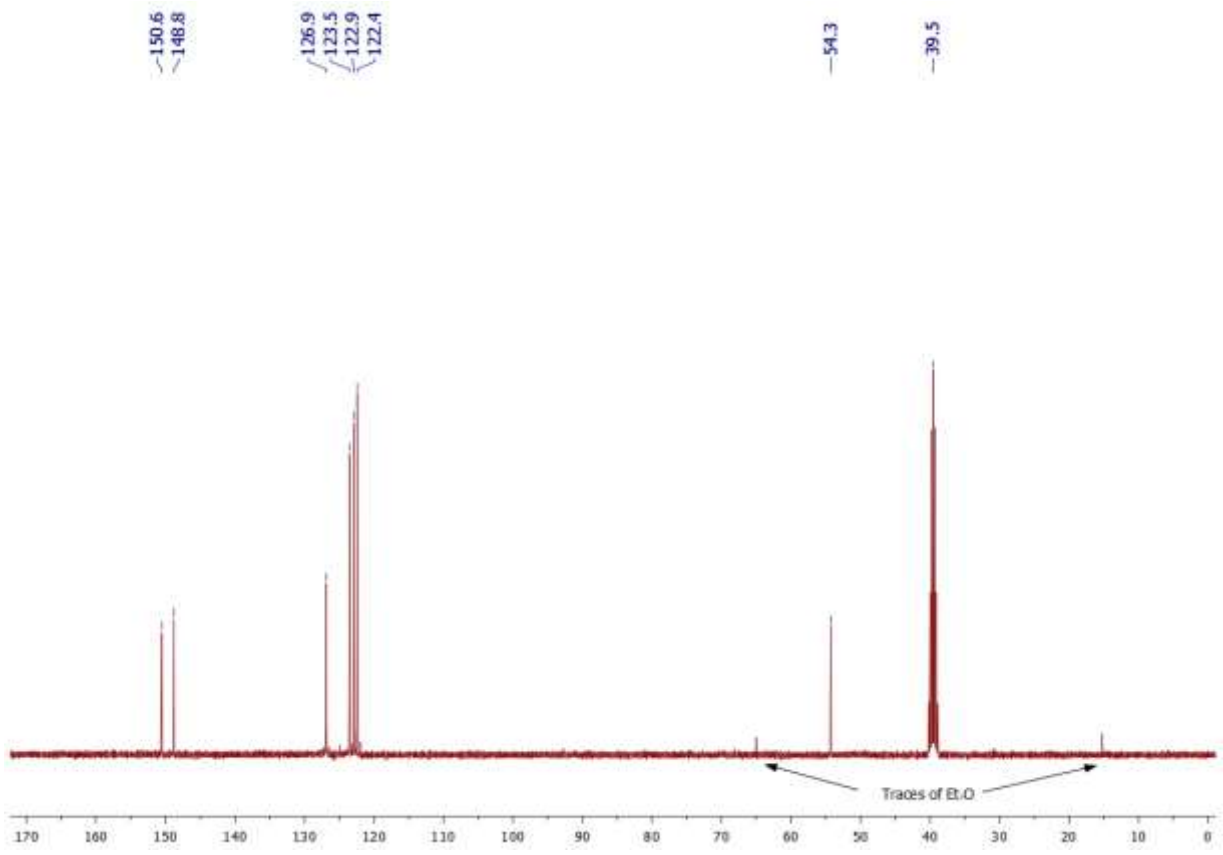
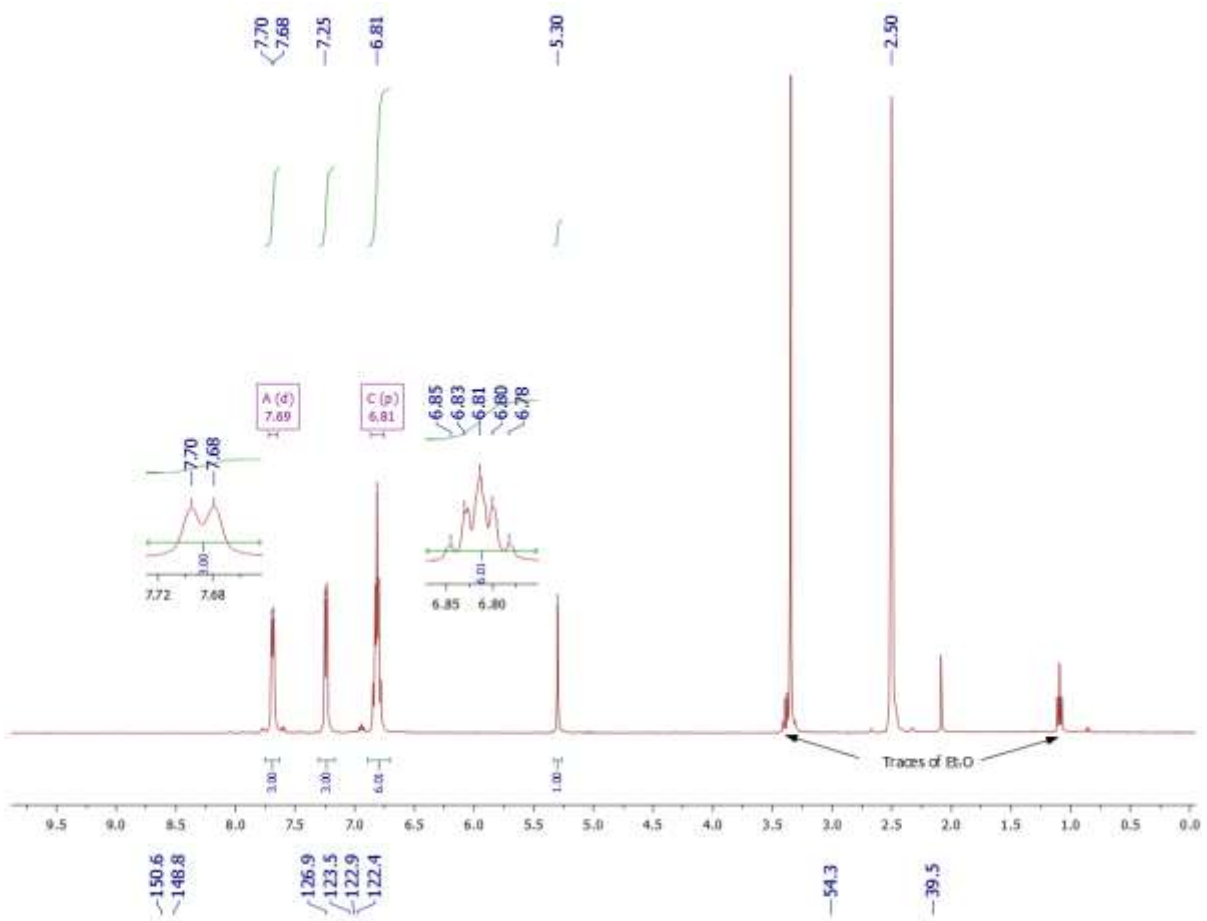
<sup>1</sup>H NMR (400 MHz, DMSO-*d*<sub>6</sub>): δ (ppm) = 7.69 (d, 3H, *J* = 6.5 Hz), 7.28-7.21 (m, 3H), 6.85-6.78 (m, 6H), 5.30 (s, 1H).

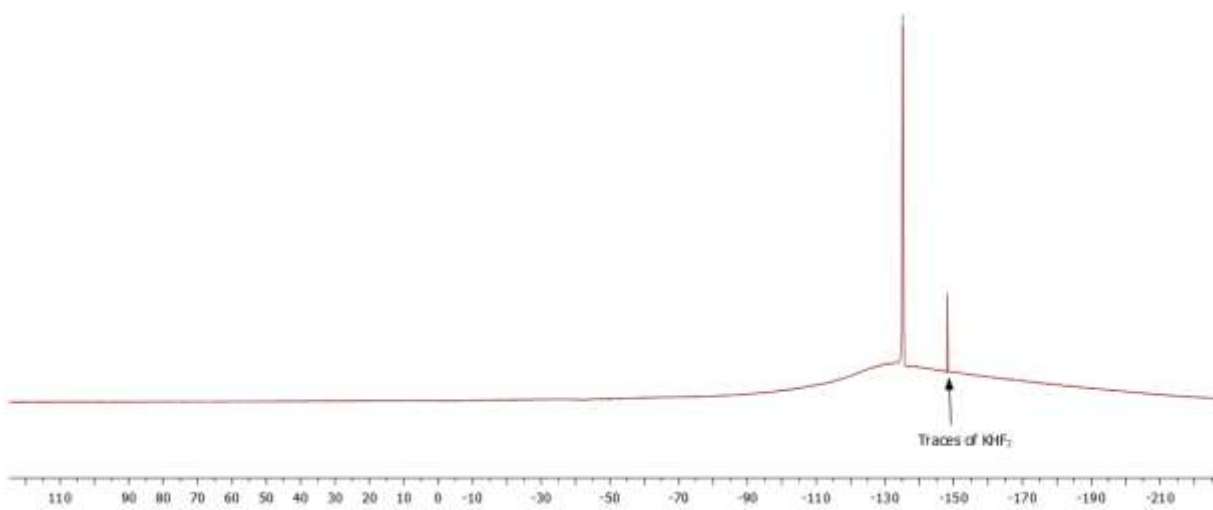
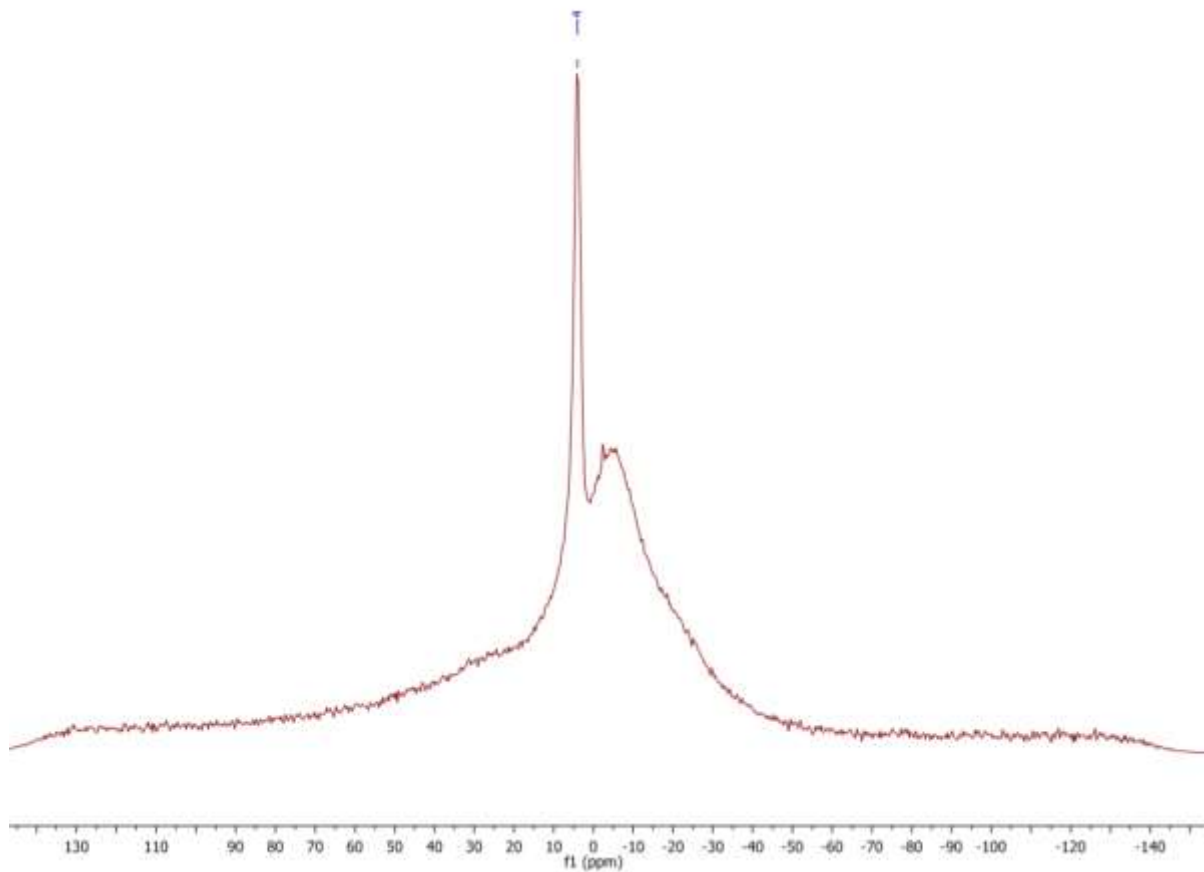
<sup>13</sup>C NMR (101 MHz, DMSO-*d*<sub>6</sub>): δ (ppm) = 150.6, 148.8, 126.9, 123.5, 122.9, 122.4, 54.3 (CH). The carbon directly attached to the boron atom on the triptycene core was not detected, likely due to quadrupolar relaxation

<sup>11</sup>B NMR (128 MHz, DMSO-*d*<sub>6</sub>): δ (ppm) = 4

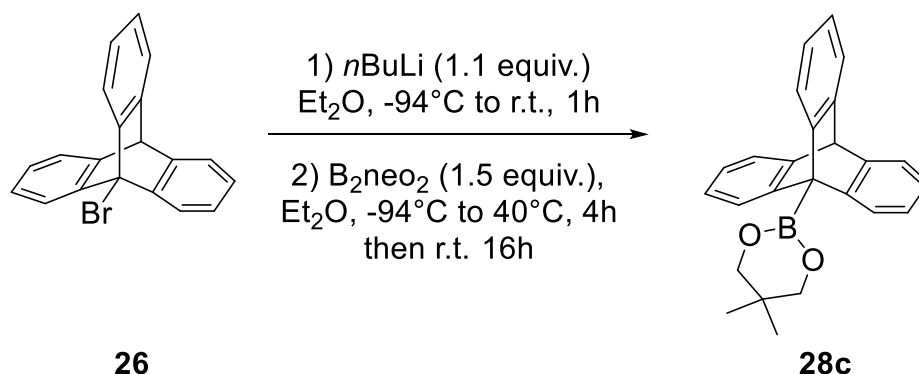
<sup>19</sup>F NMR (470 MHz, DMSO-*d*<sub>6</sub>): δ (ppm) = -135.2

M. p. (Et<sub>2</sub>O): >240°C





**(9-triptyceny)boronic acid neopentyl glycol ester 2.28c:**



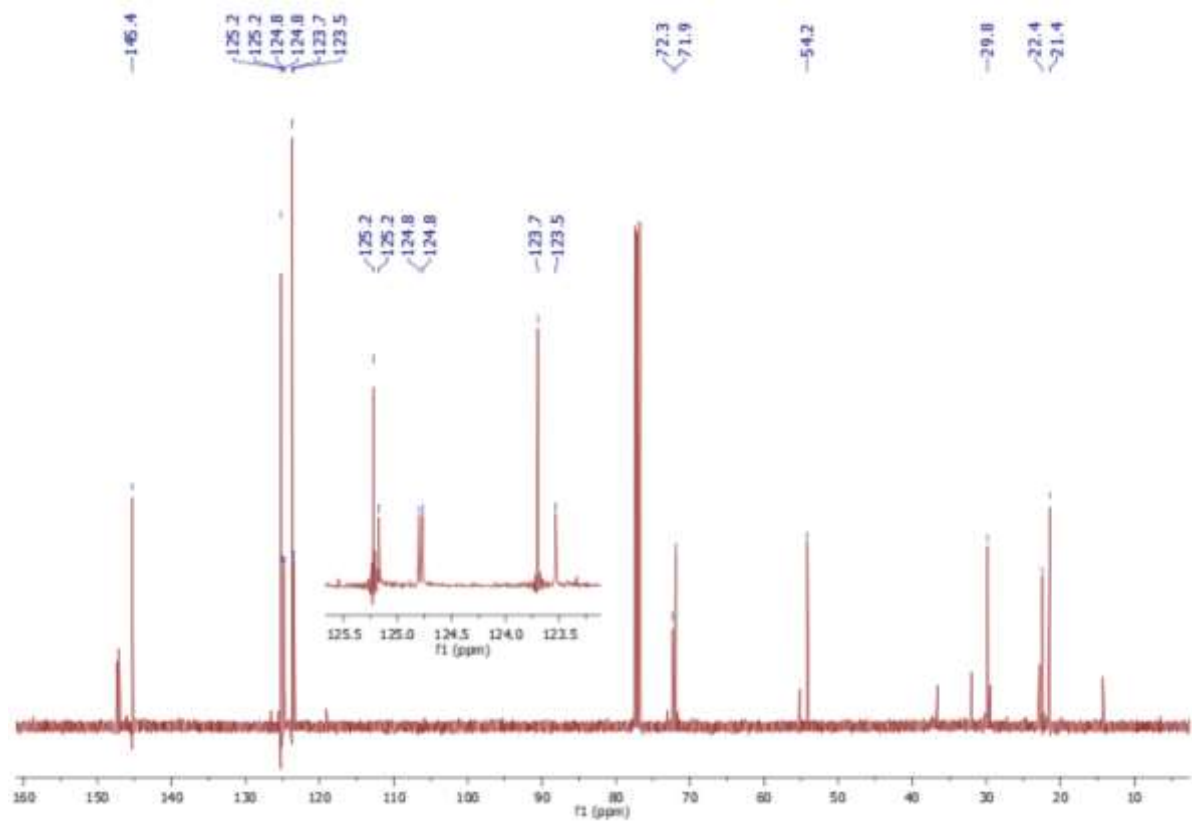
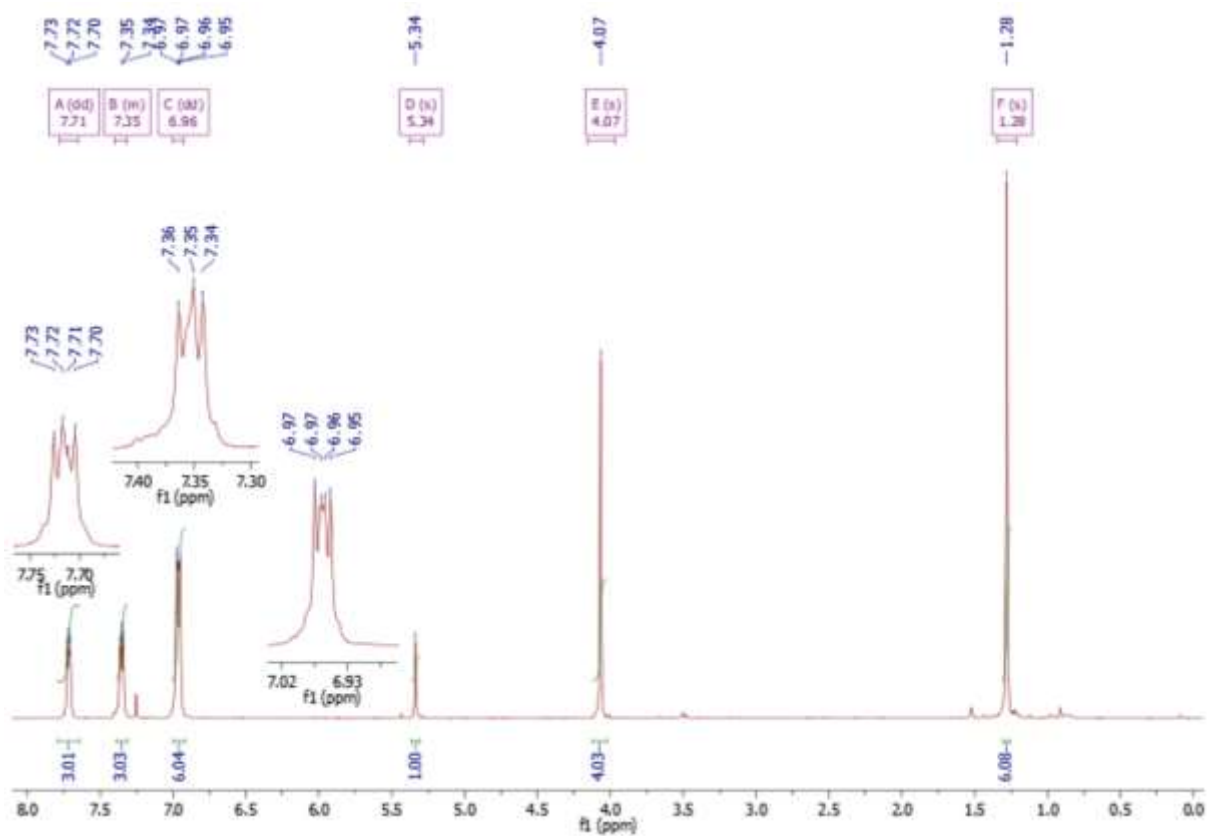
In a 50 mL Schlenk flask was added under inert atmosphere 9-bromotriptycene **26** (248 mg, 0.75 mmol, 1.0 equiv) in suspension in Et<sub>2</sub>O (15 mL). The flask is cooled to -94°C with an acetone/N<sub>2</sub>(l) bath and *n*-BuLi (0.35 mL, 2.5 M in hexanes, 0.88 mmol, 1.2 equiv) was added dropwise under vigorous stirring. 10 min after addition, the bath is removed to allow the reaction to warm up at room temperature and the reaction is stirred for an additional hour. The reaction mixture is then cooled again to -94°C and bis(neopentylglycolato)diboron (253 mg, 1.12 mmol, 1.5 equiv) is added. 10 min after addition, the bath is removed and the flask is equipped with a refrigerant after what the mixture is warmed to 40°C and stirred for 4h. The reaction is quenched with water (10 mL). The aqueous layer is extracted with Et<sub>2</sub>O (3x10 mL) and the combined organic layers are dried over MgSO<sub>4</sub>, filtered and concentrated under reduced pressure. The crude product is dissolved in CH<sub>2</sub>Cl<sub>2</sub> and precipitation by adding Et<sub>2</sub>O is performed affording the pure product after filtration as a white powder (63 mg, 0.17 mmol, 23%). The mother solution still contains a substantial amount of **2.28c** and the yield is largely underestimated. Crystals suitable for X-ray diffraction analysis have been obtained by slow evaporation of a saturated solution of **2.28c** in EtOAc.

**TLC:** *R<sub>f</sub>* = 0.24 (cyclohexane/EtOAc, 95/5)

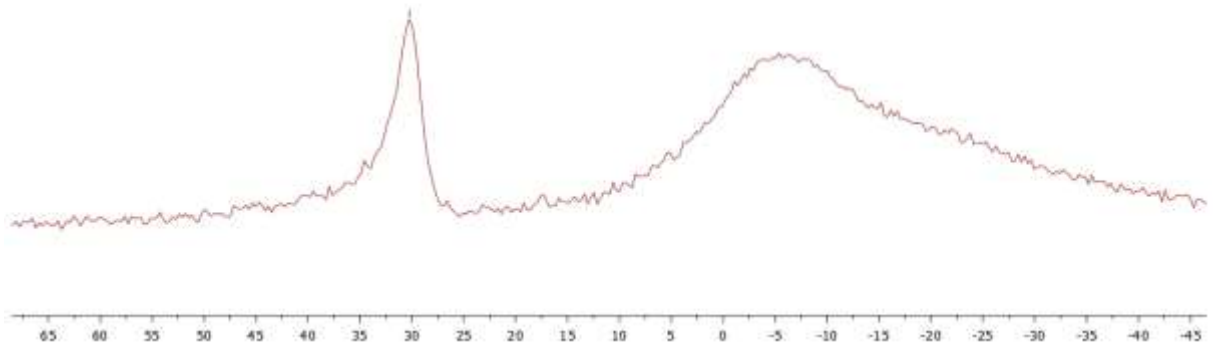
**<sup>1</sup>H NMR (400 MHz, CDCl<sub>3</sub>):** δ (ppm) = 7.72 (dd, *J* = 5.5, 3.1 Hz, 3H), 7.38-7.30 (m, 3H), 6.97 (dd, *J* = 5.3, 3.3 Hz, 6H), 5.34 (s, 1H), 4.07 (s, 4H), 1.29 (s, 6H).

**<sup>13</sup>C NMR (101 MHz, CDCl<sub>3</sub>):** δ (ppm) = 145.4, 125.2, 125.2, 124.8, 124.8, 123.7, 123.5, 72.3 (CH<sub>2</sub>), 71.9 (CH<sub>2</sub>), 54.2 (CH), 29.8 (Cq), 22.4 (CH<sub>3</sub>), 21.4 (CH<sub>3</sub>).

**<sup>11</sup>B NMR (128 MHz, CDCl<sub>3</sub>):** δ (ppm) = 30



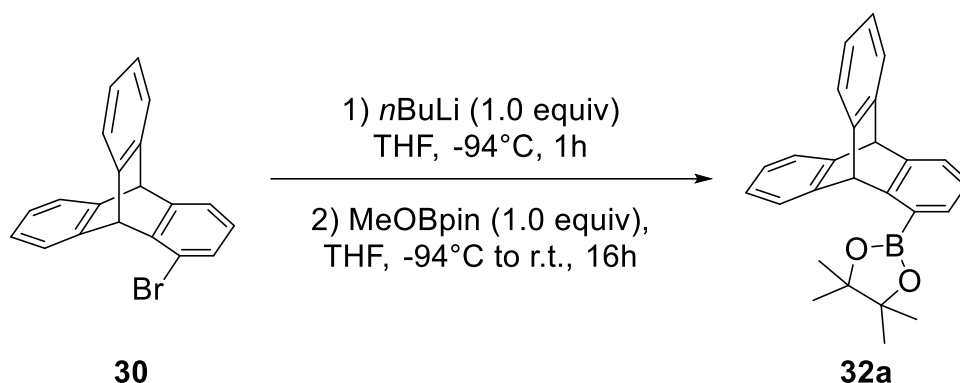
-30.2





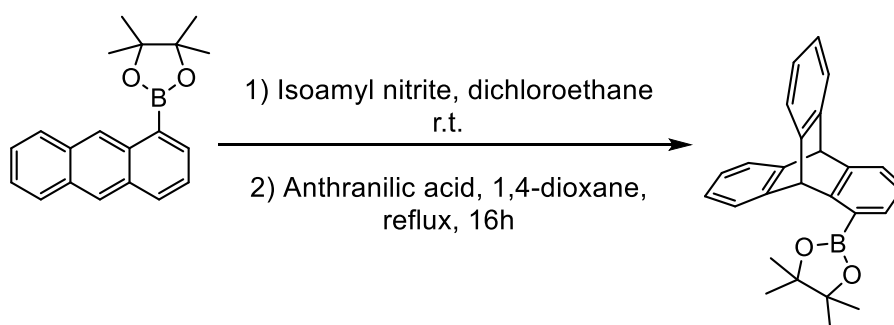
## 2-(tritypcen-1-yl)-4,4,5,5-tetramethyl-1,3,2-dioxaborolane **2.32a**:

### Procedure A



In a 100 mL Schlenk flask was added under inert atmosphere 1-bromotriptycene **2.30** (500 mg, 1.5 mmol, 1.0 eq) in suspension in THF (40 mL). The flask is cooled to -94°C with an acetone/N<sub>2</sub>(l) bath and *n*-BuLi (0.66 mL, 2.5 M in hexanes, 1.65 mmol, 1.1 eq) was added dropwise under vigorous stirring. The reaction mixture is then stirred for an additional hour at -94°C and 2-methoxy-4,4,5,5-tetramethyl-1,3,2-dioxaborolane (0.27 mL, 1.65 mmol, 1.1 eq) is added. 10 min after addition, the bath is removed and the reaction is allowed to reach room temperature and stirred overnight. After 16h at room temperature, the solvent is removed under vacuum and the crude product is dissolved in dichloromethane, filtered and dried over MgSO<sub>4</sub>. It is then filtered again and concentrated under reduced pressure. Purification by silica gel chromatography (cyclohexane/EtOAc, 95:5) afforded 2-(tritypcen-1-yl)-4,4,5,5-tetramethyl-1,3,2-dioxaborolane **2.32a** as a white powder (463 mg, 1.22 mmol, 81%). Crystals suitable for X-ray analysis have been obtained by slow evaporation of a saturated solution of **2.32a** in chloroform.

### Procedure B



To a stirred solution of 2-(anthracen-1-yl)-4,4,5,5-tetramethyl-1,3,2-dioxaborolane (2.993 g, 9.8 mmol, 1 equiv.) and isoamyl nitrite (6.6 mL, 49 mmol, 5 equiv.) in dichloroethane (75 mL) was added dropwise a solution of anthranilic acid (6.720 g, 49 mmol, 5eq) in 1,4-dioxane (100 mL) at 100°C. After the addition, the reaction was then refluxed overnight. After 16h, solvents were distilled and the crude product is then purified by silica gel chromatography

(Cyclohexane/EtOAc, 95:5) to obtain (9-triptycenyldimesityl borane **2.32a** as a white powder (1.987 g, 5.2 mmol, 53%).

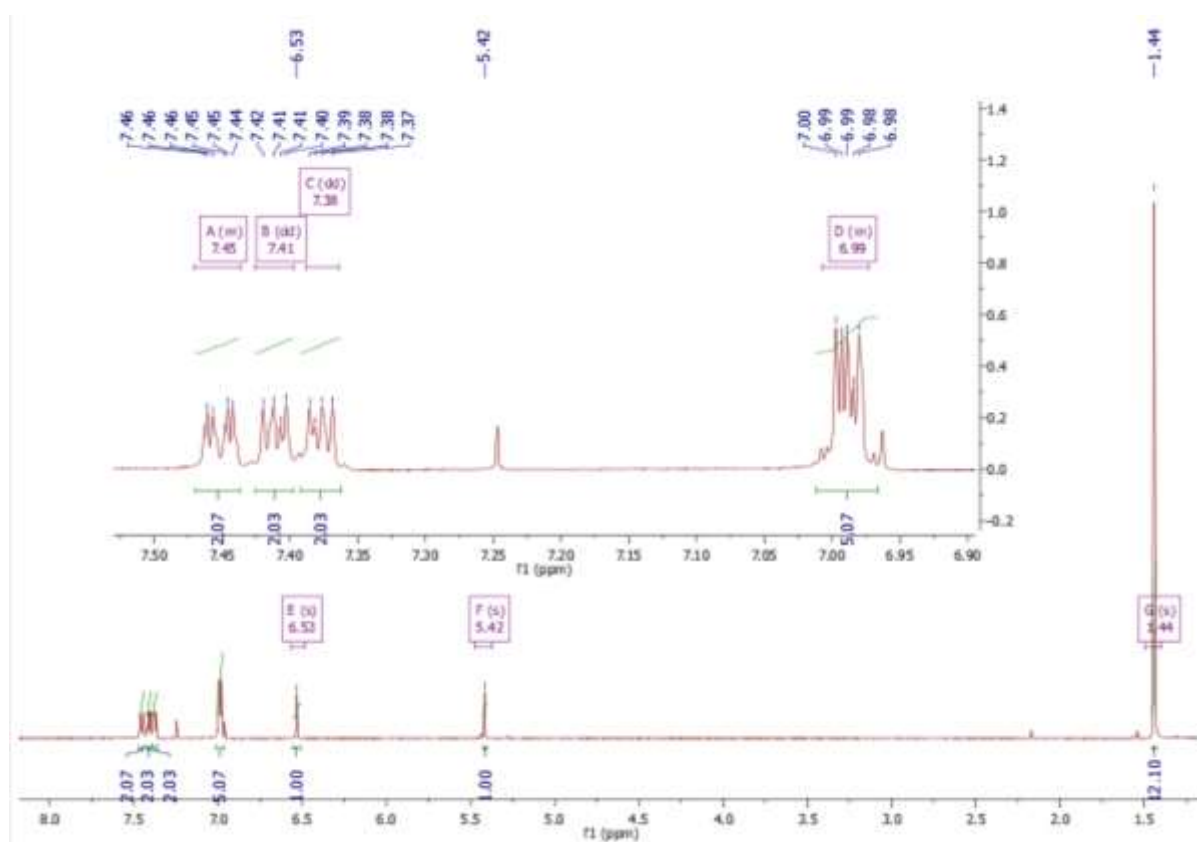
**TLC:** *R<sub>f</sub>* = 0.36 (cyclohexane/EtOAc, 95/5)

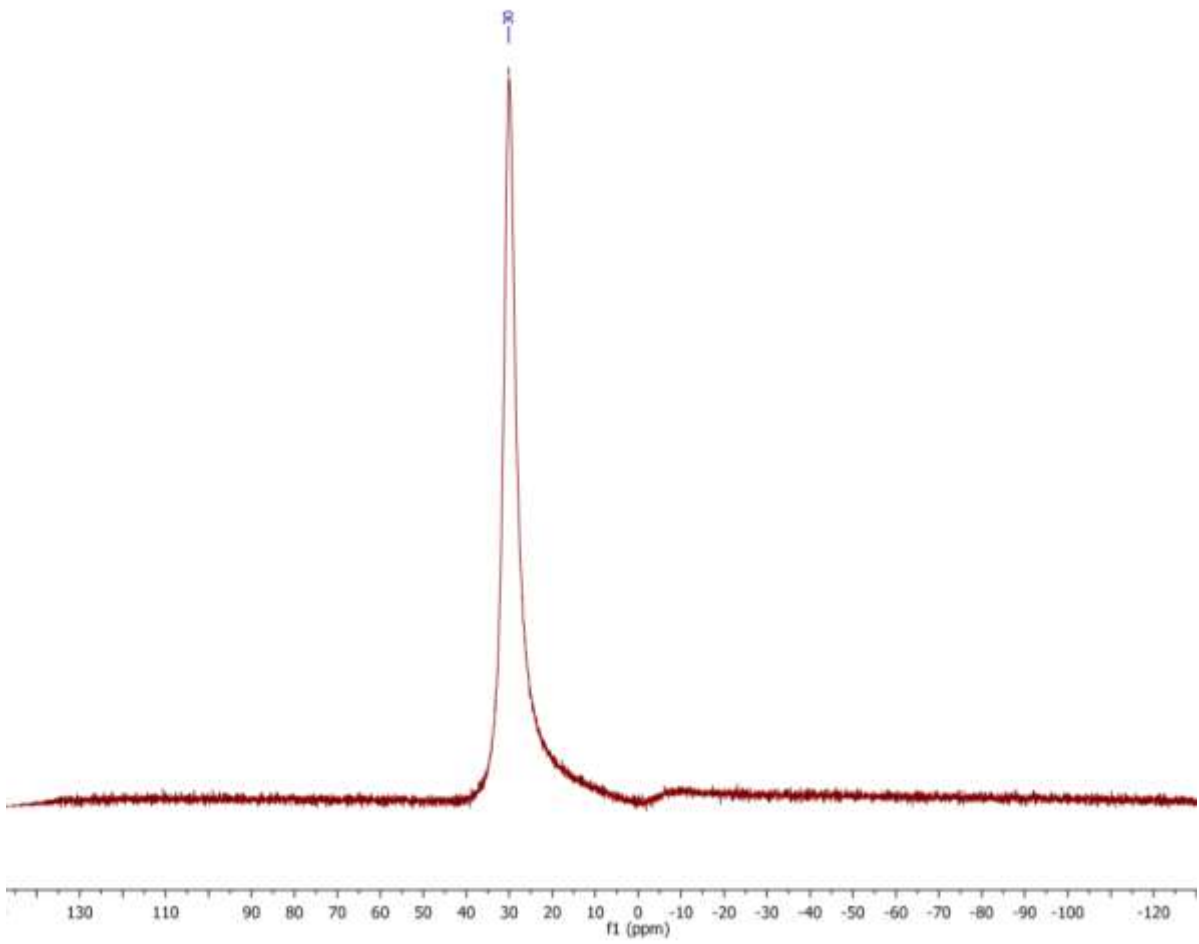
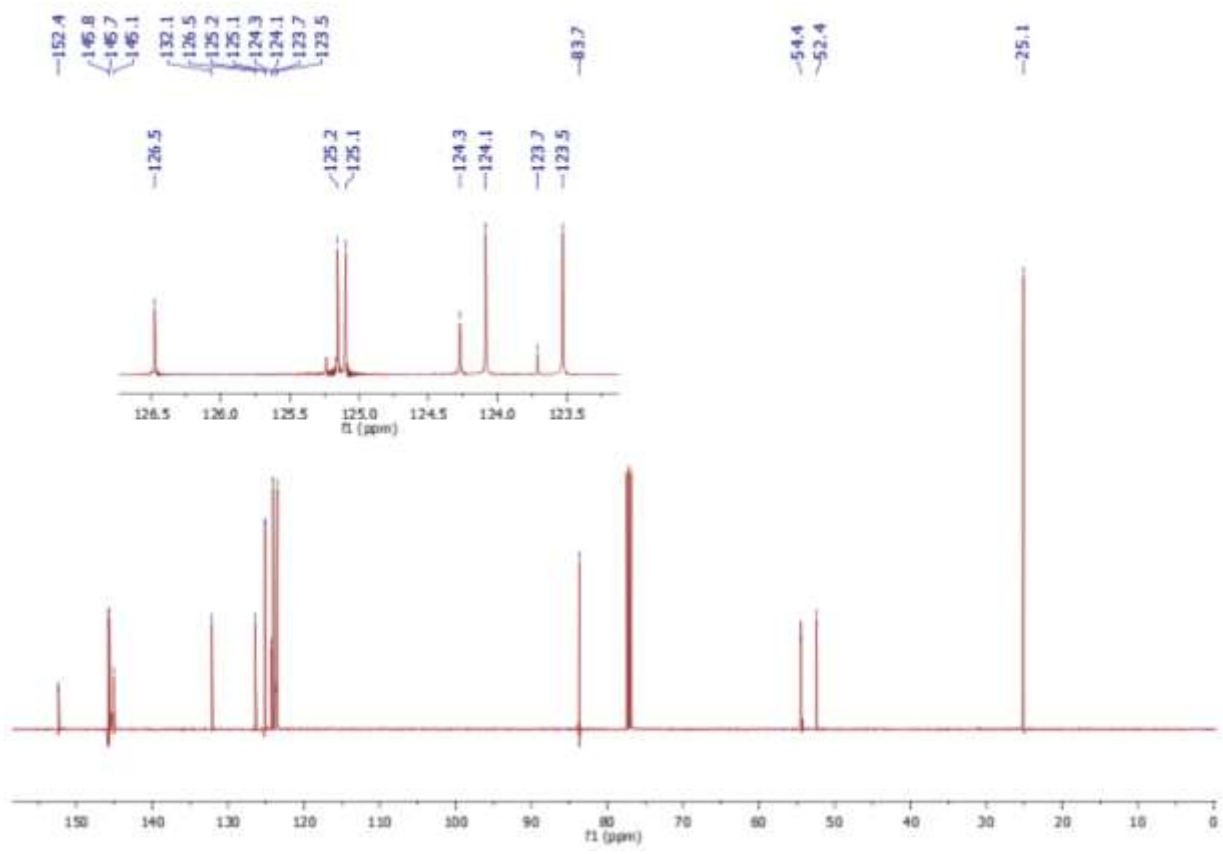
**<sup>1</sup>H NMR (500 MHz, CDCl<sub>3</sub>):** δ (ppm) = 7.47-7.44 (m, 2H), 7.41 (dd, 2H, *J* = 5.5, 3.0 Hz), 7.38 (dd, *J* = 5.5, 2.9 Hz, 2H), 7.01-6.97 (m, 5H), 6.53 (s, 1H), 5.42 (s, 1H), 1.44 (s, 12H).

**<sup>13</sup>C NMR (125 MHz, CDCl<sub>3</sub>):** δ (ppm) = 152.4, 145.8, 145.7, 145.1, 132.1, 126.5, 125.2, 125.1, 124.3, 124.1, 123.7, 123.5, 83.7, 54.4, 52.4, 25.1.

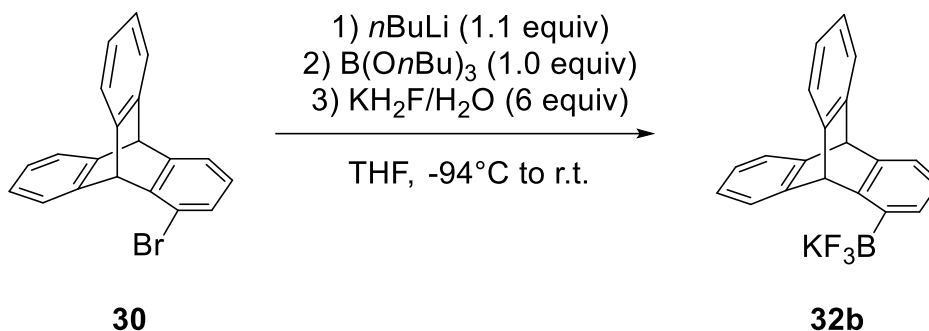
**<sup>11</sup>B NMR (160 MHz, CDCl<sub>3</sub>):** δ (ppm) = 30

**M. p.** (CHCl<sub>3</sub>): 201-203°C





### Potassium 1-triptycyltrifluoroborate **2.32b**:



A solution of *n*BuLi (2.5 M, 6.5 mmol, 2.6 ml, 1.1 equiv) was added dropwise to a solution of 1-bromotriptycene **2.30** (2.0 g, 6.0 mmol, 1.0 equiv.) in THF (20 mL) at -94°C. After stirring 1h30 at -94°C, B(*On*Bu)<sub>3</sub> (1.6 ml, 6.0 mmol, 1.0 equiv.) was added dropwise and the mixture was allowed to warm at room temperature. After stirring at room temperature for 4h, a solution of KHF<sub>2</sub> (2.8g, 36 mmol, 6 equiv.) in H<sub>2</sub>O (10 ml) was added and the reaction was stirred vigorously overnight. The mixture was evaporated to dryness then poured in ice cold water. The precipitate was filtrated and washed alternatively with ice cold water and ice-cold diethyl ether, affording pure potassium 1-triptycyltrifluoroborate **2.32b** (1.53 g, 4.1 mmol, 69%) as a white electrostatic powder.

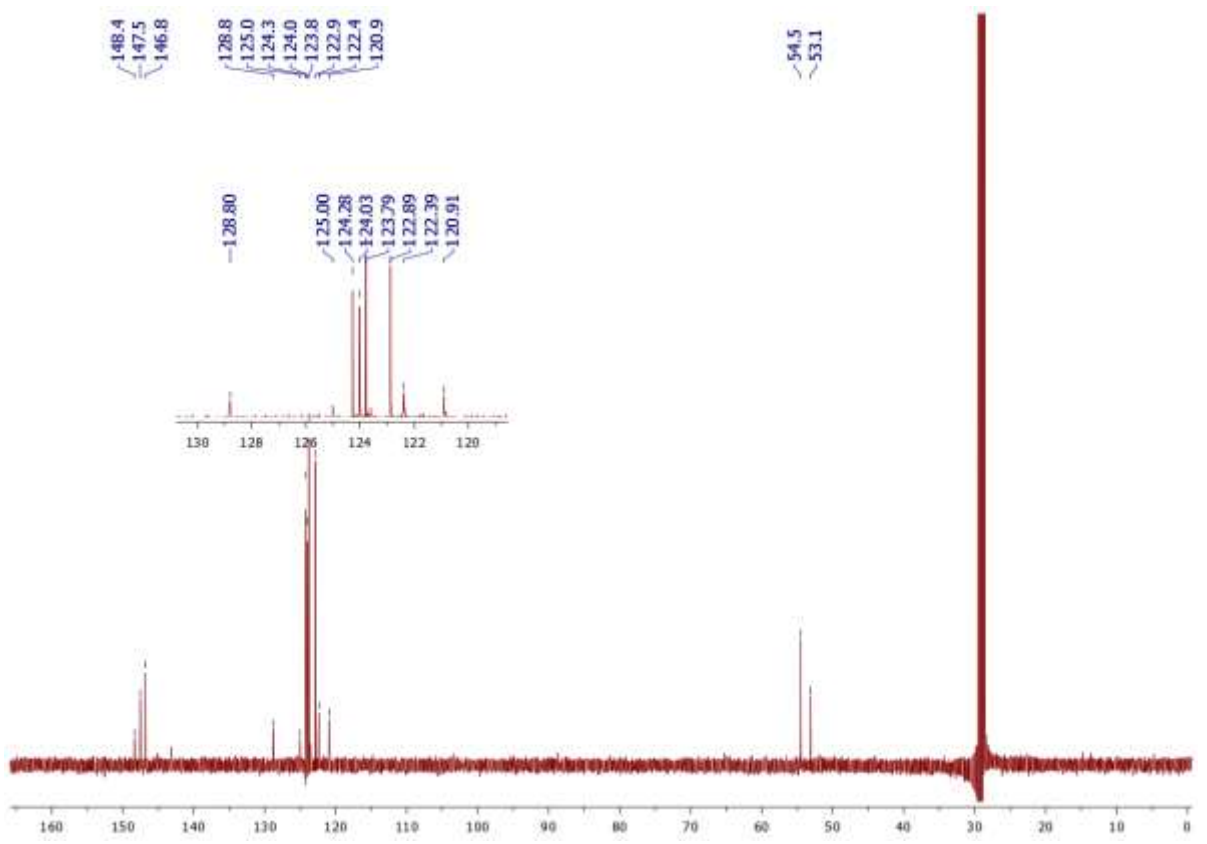
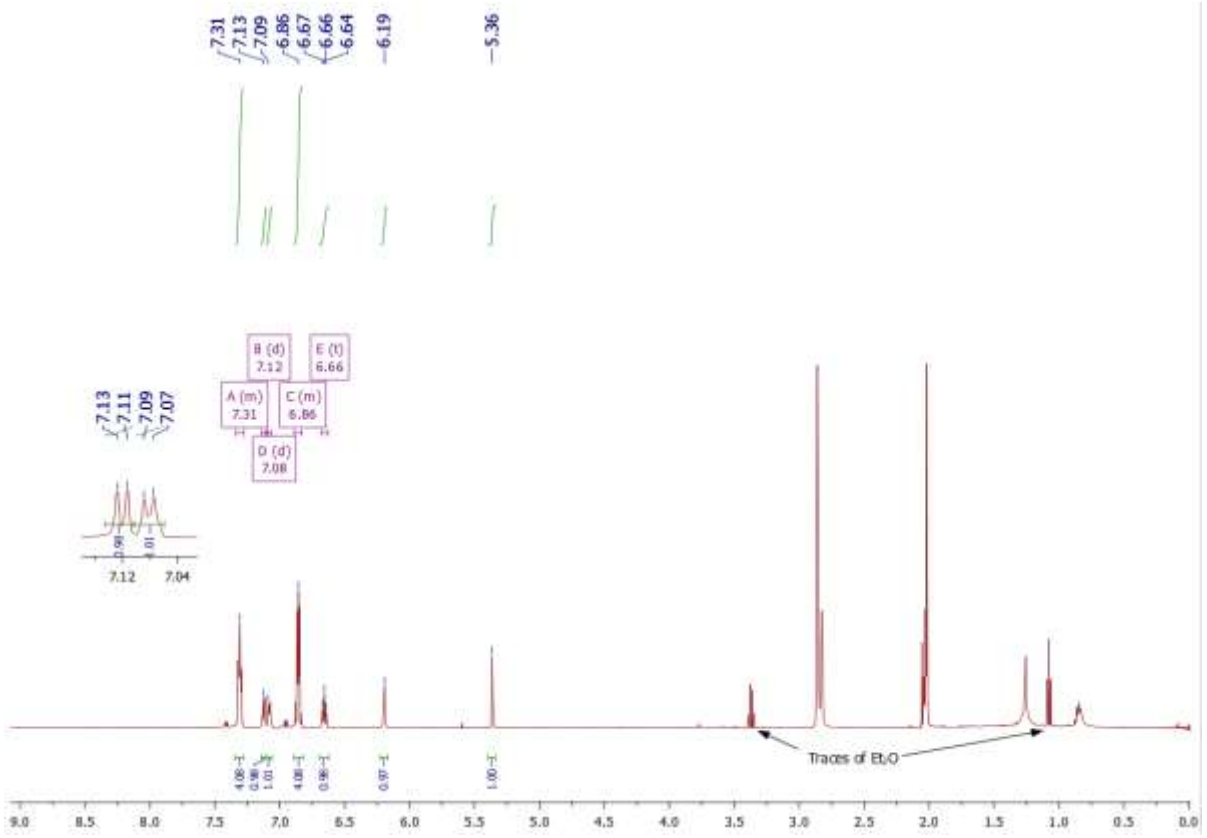
<sup>1</sup>H NMR (500 MHz, Acetone-*d*<sub>6</sub>): δ (ppm) = 7.34-7.28 (m, 4H), 7.12 (d, 1H, *J* = 7.1 Hz), 7.08 (d, *J* = 7.0 Hz, 1H), 6.88-6.82 (m, 4H), 6.66 (t, *J* = 7.2 Hz, 3H), 6.19 (s, 1H), 5.36 (s, 1H).

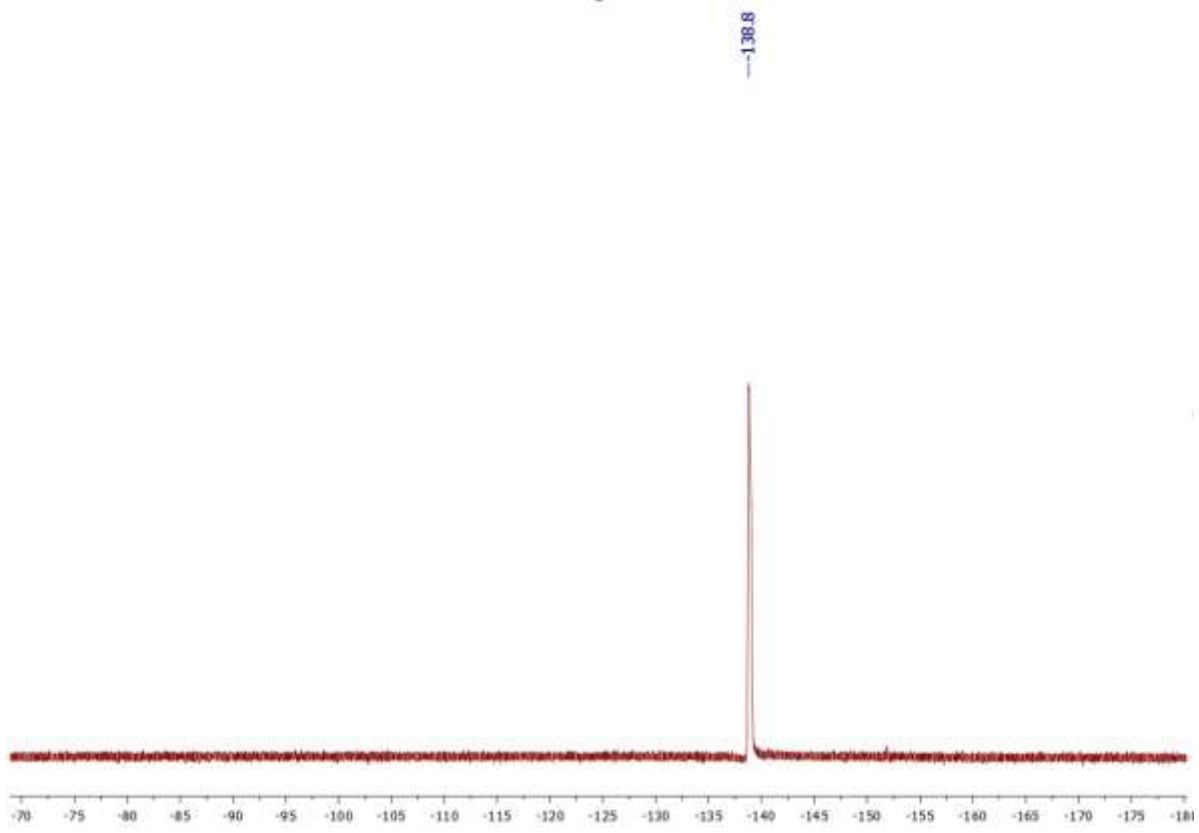
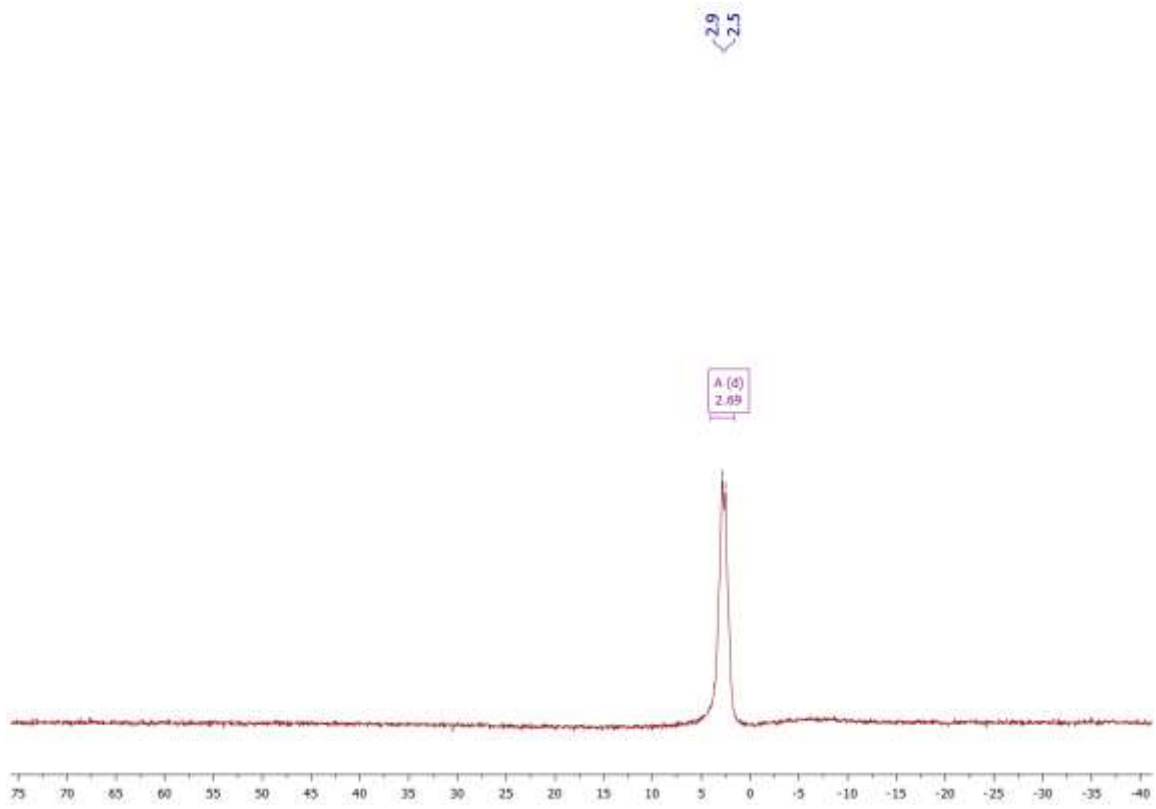
<sup>13</sup>C NMR (125 MHz, Acetone-*d*<sub>6</sub>): δ (ppm) = 148.4, 147.5, 146.8, 128.8, 125.0, 124.2, 124.0, 123.8, 122.9, 122.4, 120.9, 54.5 (Csp<sup>3</sup>H), 53.1 (Csp<sup>3</sup>H). The carbon directly attached to the boron atom on the triptycene core was not detected, likely due to quadrupolar relaxation.

<sup>11</sup>B NMR (160 MHz, Acetone-*d*<sub>6</sub>): δ (ppm) = 3 (d, *J* = 51.4 Hz)

<sup>19</sup>F NMR (470 MHz, Acetone-*d*<sub>6</sub>): δ (ppm) = -138.8

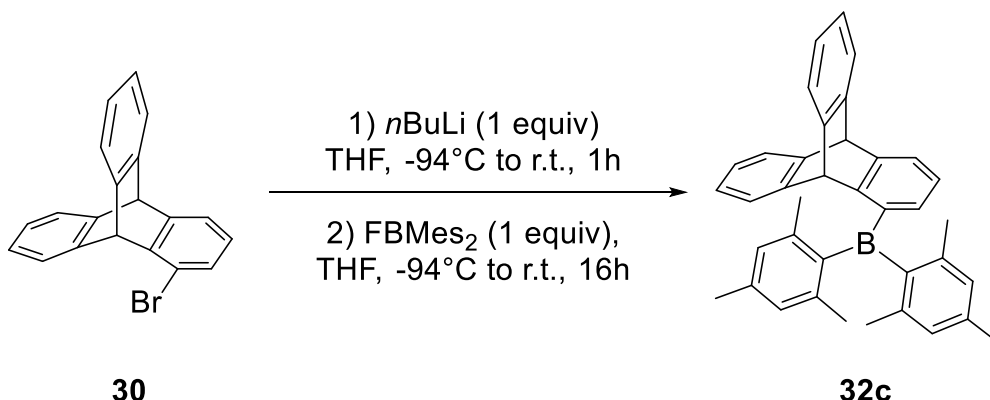
M. p. (acetone): >240°C





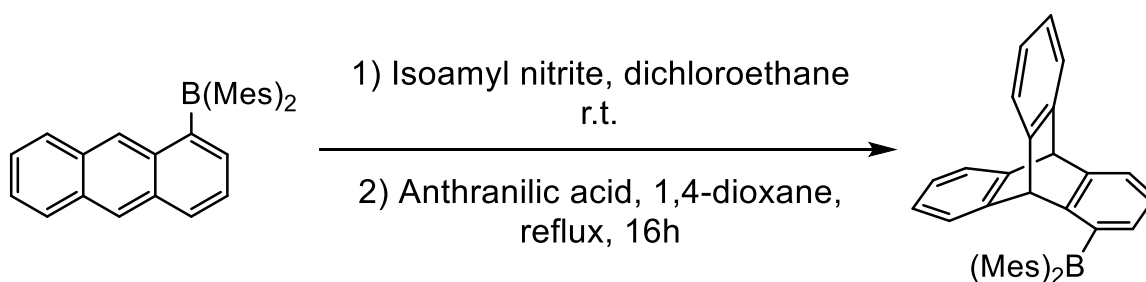
### (1-triptycenyldimesityl borane 2.32c:

#### Procedure A



In a 50 mL Schlenk flask was added under inert atmosphere 1-bromotriptycene **2.30** (436 mg, 1.3 mmol, 1.0 eq) in suspension in THF (15 mL). The flask is cooled to -94°C with an acetone/N<sub>2</sub>(l) bath and *n*-BuLi (0.52 mL, 2.5 M in hexanes, 1.3 mmol, 1.0 eq) was added dropwise under vigorous stirring. The reaction mixture is then stirred for an additional hour at -94°C and fluorodimesitylborane (349 mg, 1.3mmol, 1.0 eq) is added as a solid under a strong flux of argon. 10 min after addition, the bath is removed and the reaction mixture is allowed to reach room temperature and stirred overnight. After 16h at room temperature, the solvent is removed under vacuum and the crude product is dissolved in dichloromethane, filtered and dried over MgSO<sub>4</sub>. It is then filtered again and concentrated under reduced pressure. Purification by silica gel chromatography (Cyclohexane/EtOAc, 95:5) afforded (9-triptycenyldimesityl borane **2.32c** as a white powder (469 mg, 0.93 mmol, 71%). Crystals suitable for X-ray structure analysis have been obtained by slow evaporation of a saturated solution of **2.32c** in chloroform.

#### Procedure B



To a stirred solution of 1-dimesitylborane-anthracene (3.76 g, 8.80 mmol, 1 equiv.) and isoamyl nitrite (5.9 mL, 44 mmol, 5 equiv.) in dichloroethane (75 mL) was added dropwise a solution of anthranilic acid (6.03 g, 44 mmol, 5 equiv.) in 1,4-dioxane (100 mL) at 100°C. After the addition, the reaction was then stirred overnight at reflux. After 16h, solvents were distilled and the crude product is then purified by silica gel chromatography (cyclohexane/EtOAc, 95:5) to obtain (9-triptycenyldimesityl borane **2.32c** as a white powder (1.94 g, 3.87 mmol, 44%).

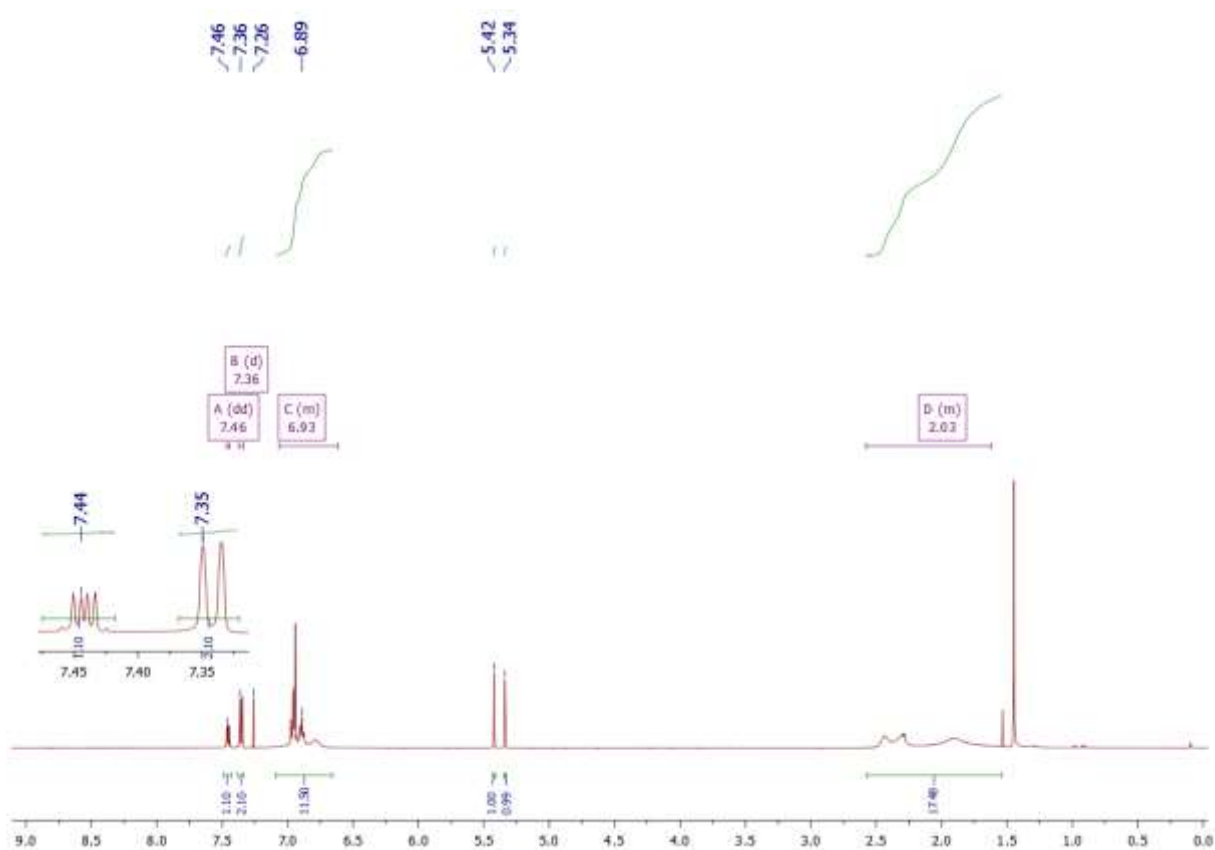
**TLC:** *R<sub>f</sub>* = 0.62 (cyclohexane/EtOAc, 95/5).

**<sup>1</sup>H NMR (500 MHz, CDCl<sub>3</sub>):** δ (ppm) = 7.46 (dd, 1H, *J* = 5.5, 3.1 Hz), 7.36 (d, 2H, *J* = 7.3 Hz), 7.10-6.70 (m, 12H), 5.42 (s, 1H), 5.34 (s, 1H), 2.50-1.50 (m, 18H).

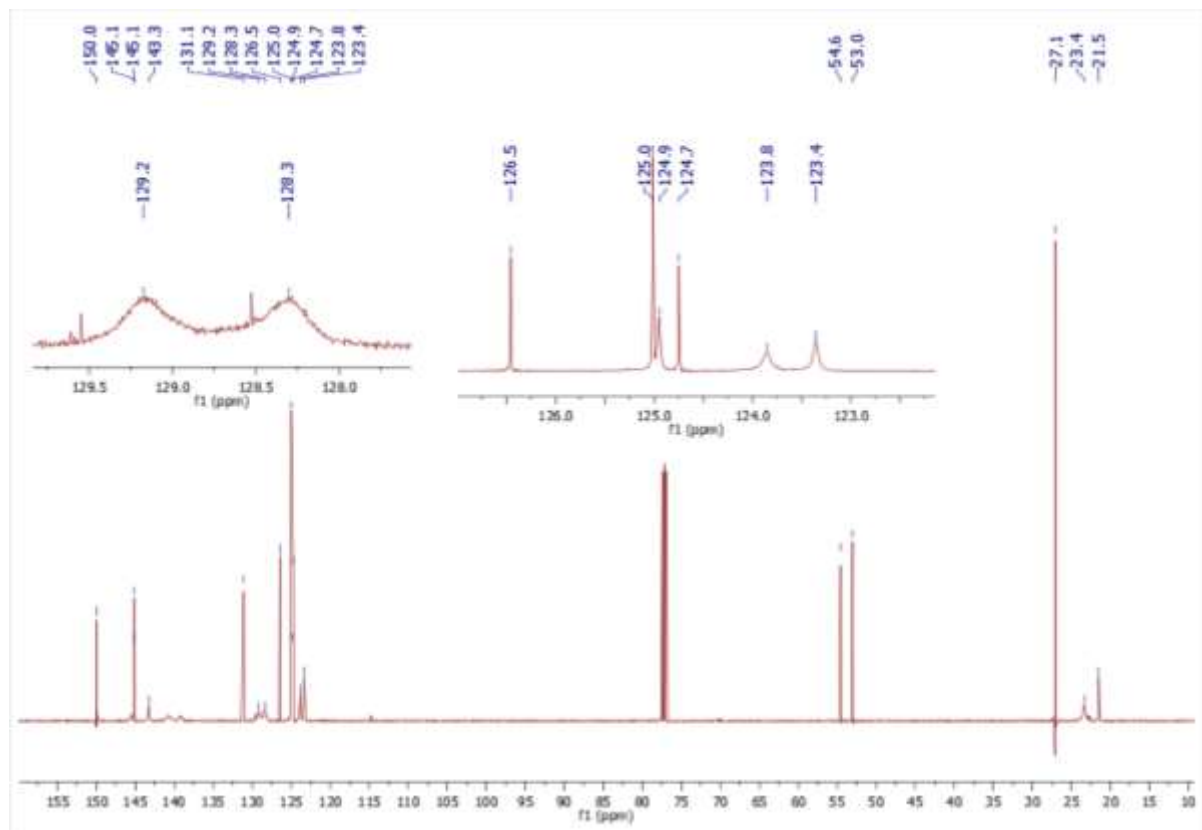
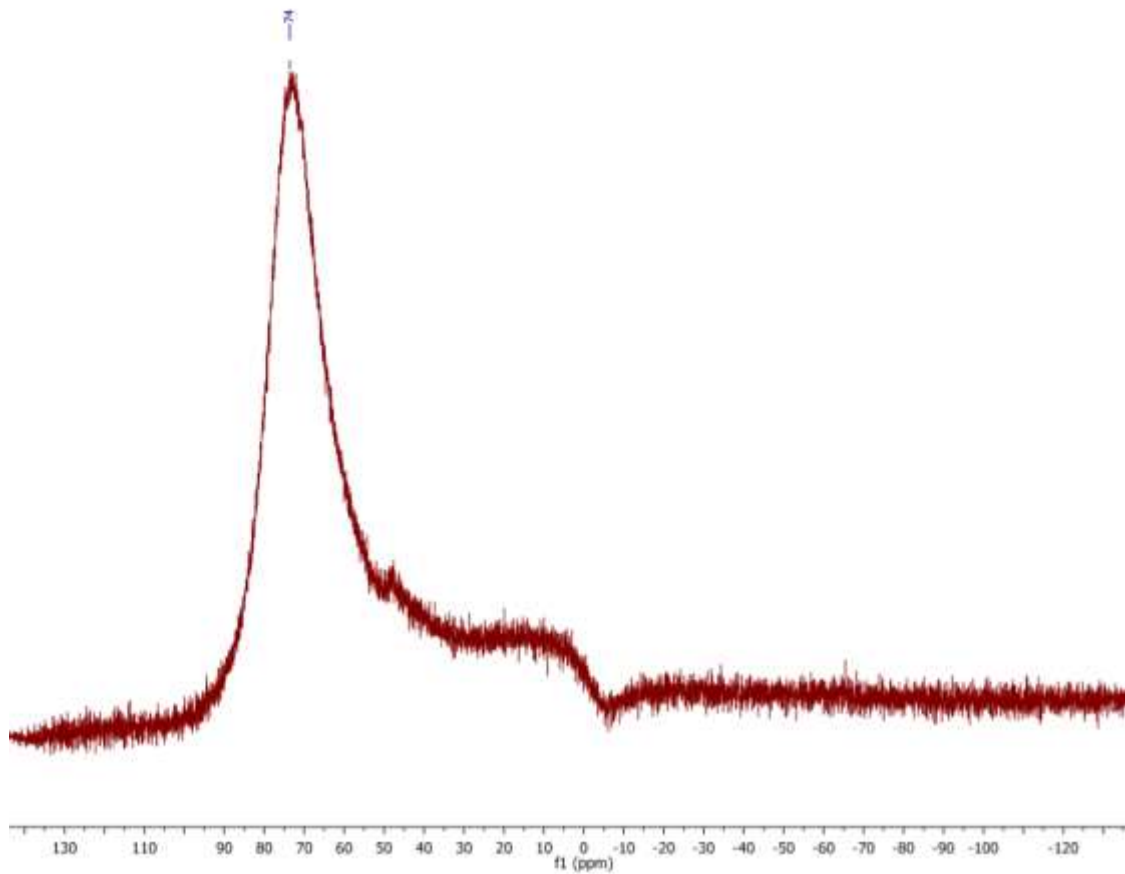
**<sup>13</sup>C NMR (125 MHz, CDCl<sub>3</sub>):** δ (ppm) = 150.0, 145.1, 145.1, 143.3, 131.1, 129.2 (br), 128.3 (br), 126.5, 125.0, 124.9, 124.7, 123.8, 123.4, 54.6, 53.0, 27.1, 23.4 (br), 21.5.

**<sup>11</sup>B NMR (160 MHz, CDCl<sub>3</sub>):** δ (ppm) = 74

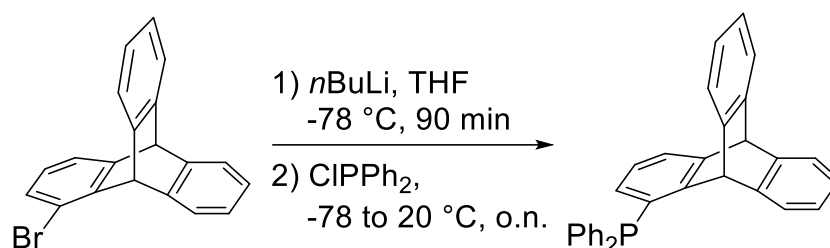
**M. p.** (EtOAc): 188-190°C







### 1-diphenylphosphinotriptycene **43a**:



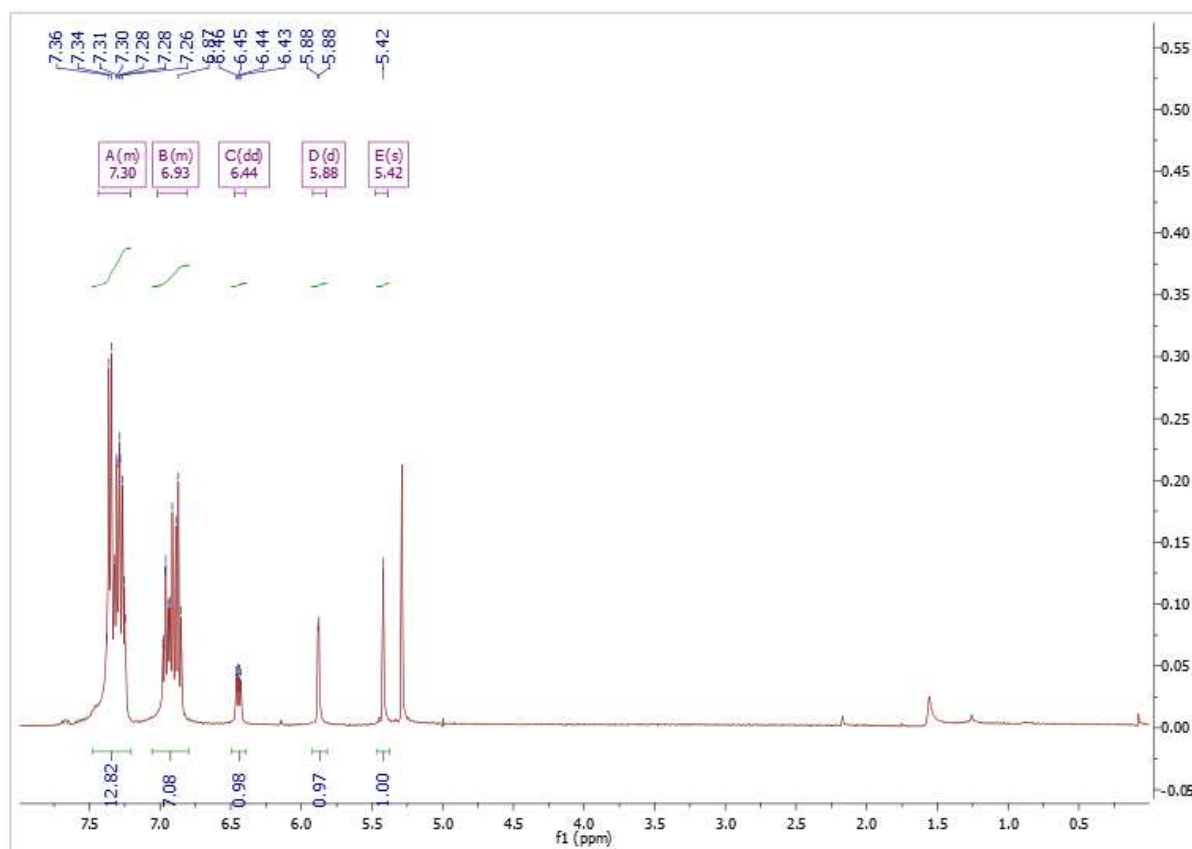
To a stirred solution of 1-bromotriptycene **2.30** (1.00g, 3.00mmol, 1.00eq) in THF (20mL) at -94°C was added dropwise *n*-BuLi (3.30 mmol, 1.10 eq, 2.50M, 1.32mL). After 2h at -94°C, diphenylchlorophosphine (662mg, 3.00mmol, 1.00eq) is added dropwise at -94°C and the reaction mixture is then stirred overnight at room temperature. The day after, 20mL of EtOAc are added and the mixture is washed 3 times with a saturated solution of NaHCO<sub>3</sub>. Organic layers are dried over anhydrous MgSO<sub>4</sub>, filtered and solvents are removed under vacuum. The crude product was then purified by flash chromatography using Hexane:EtOAc (1:0 to 9:1) to get the desired compound **2.43a** (904mg, 2.07 mmol, 69%).

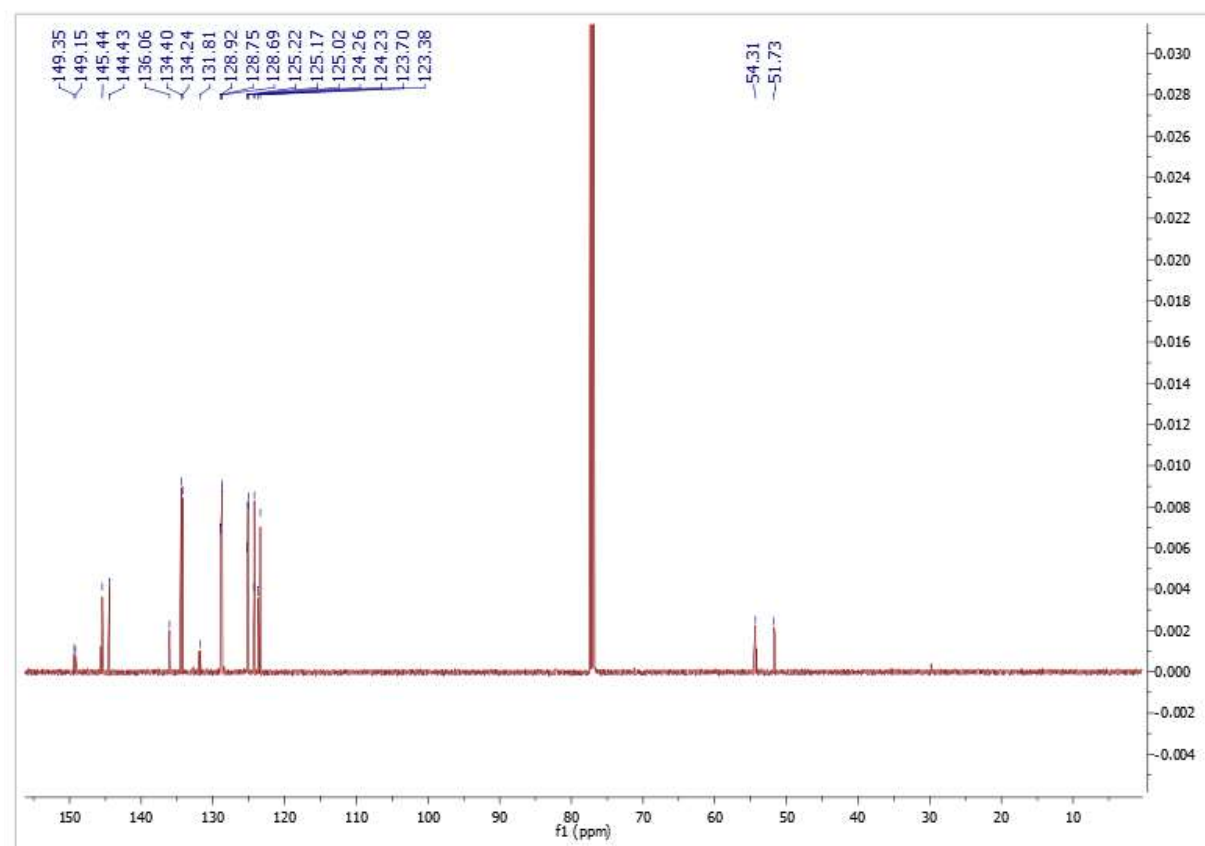
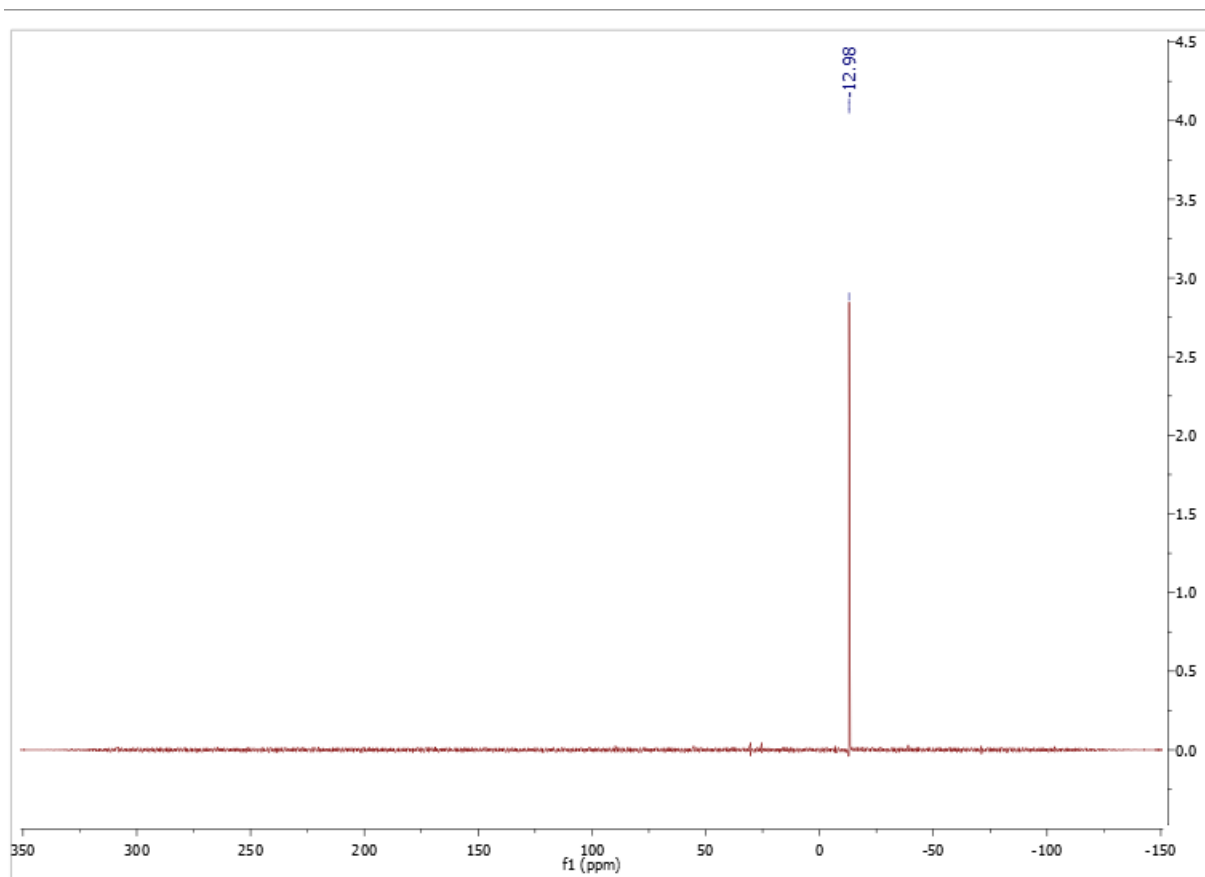
<sup>1</sup>H NMR (400MHz, CDCl<sub>3</sub>): δ(ppm) = 7.39-7.28 (m, 12H), 6.99-6.93 (m, 4H), 6.88 (t, 3H), 6.47 (q, 1H), 5.90 (d, 1H), 5.43 (s, 1H).

<sup>31</sup>P NMR (400MHz, CDCl<sub>3</sub>): δ(ppm) = -12.9ppm.

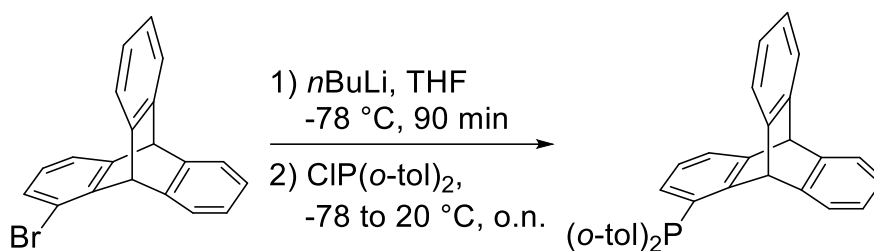
<sup>13</sup>C NMR (125 MHz, CDCl<sub>3</sub>): δ(ppm) = 149.4, 149.2, 145.4, 144.4, 136.1, 134.4, 134.2, 131.8, 128.9, 128.8, 128.7, 125.2, 125.0, 124.3, 124.2, 123.7, 123.4, 54.3, 51.7.

M.p. (CH<sub>2</sub>Cl<sub>2</sub>): >240°C





### 1-diorthotolylphosphinotriptycene **2.43b**:



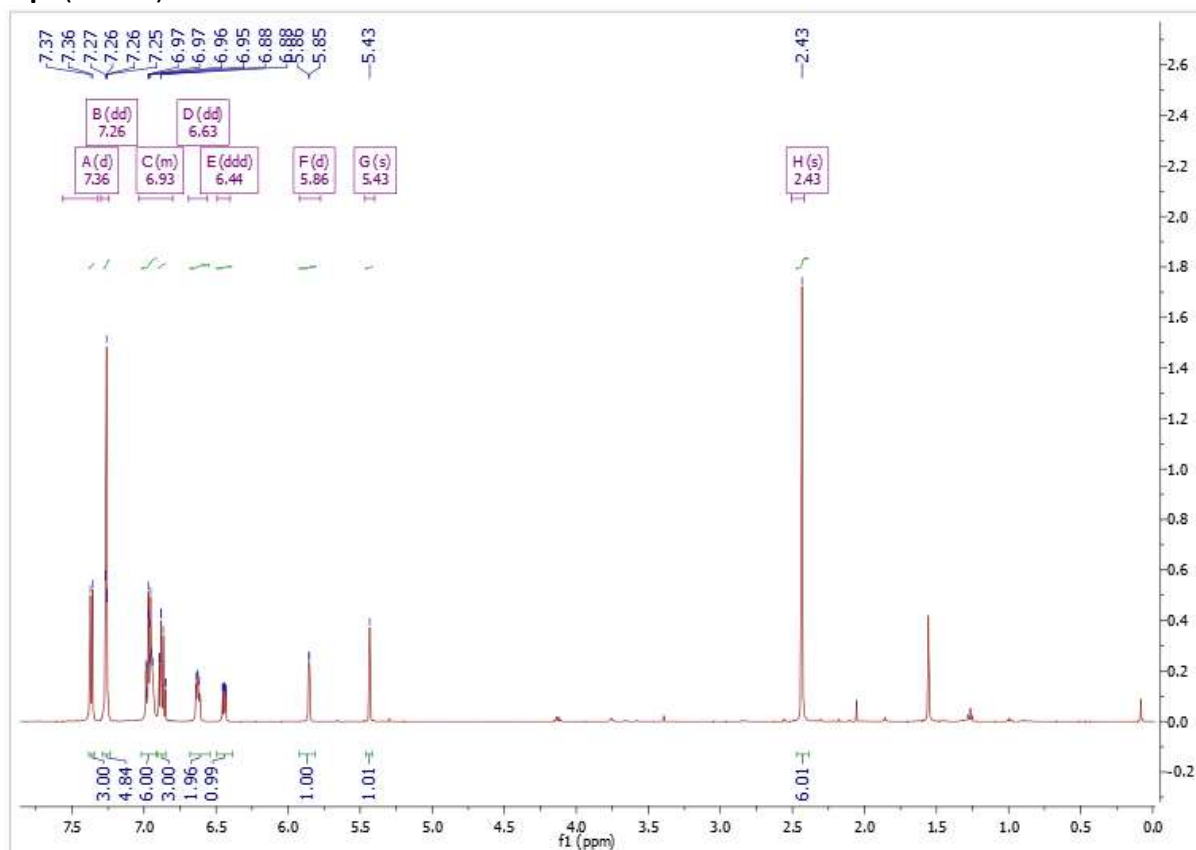
To a stirred solution of 1-bromotriptycene **2.30** (300mg, 0.09mmol, 1.00eq) in THF (10mL) at -94°C was added dropwise *n*-BuLi (0.99mmol, 1.1 eq, 2.5M, 0.4mL). After 2h at -94°C, diorthotolylchlorophosphine (0.90mmol, 1.00eq, 224mg) is added dropwise at -94°C and the reaction mixture is then stirred overnight at room temperature. The day after, 10mL of EtOAc are added and the mixture is washed 3 times with a saturated solution of NaHCO<sub>3</sub>. Organic layers are dried over anhydrous MgSO<sub>4</sub>, filtered and solvents are removed under vacuum. Washing the crude product with acetone afforded 1-diorthotolylphosphinotriptycene **2.43b** (281mg, 0.49mmol, 67%).

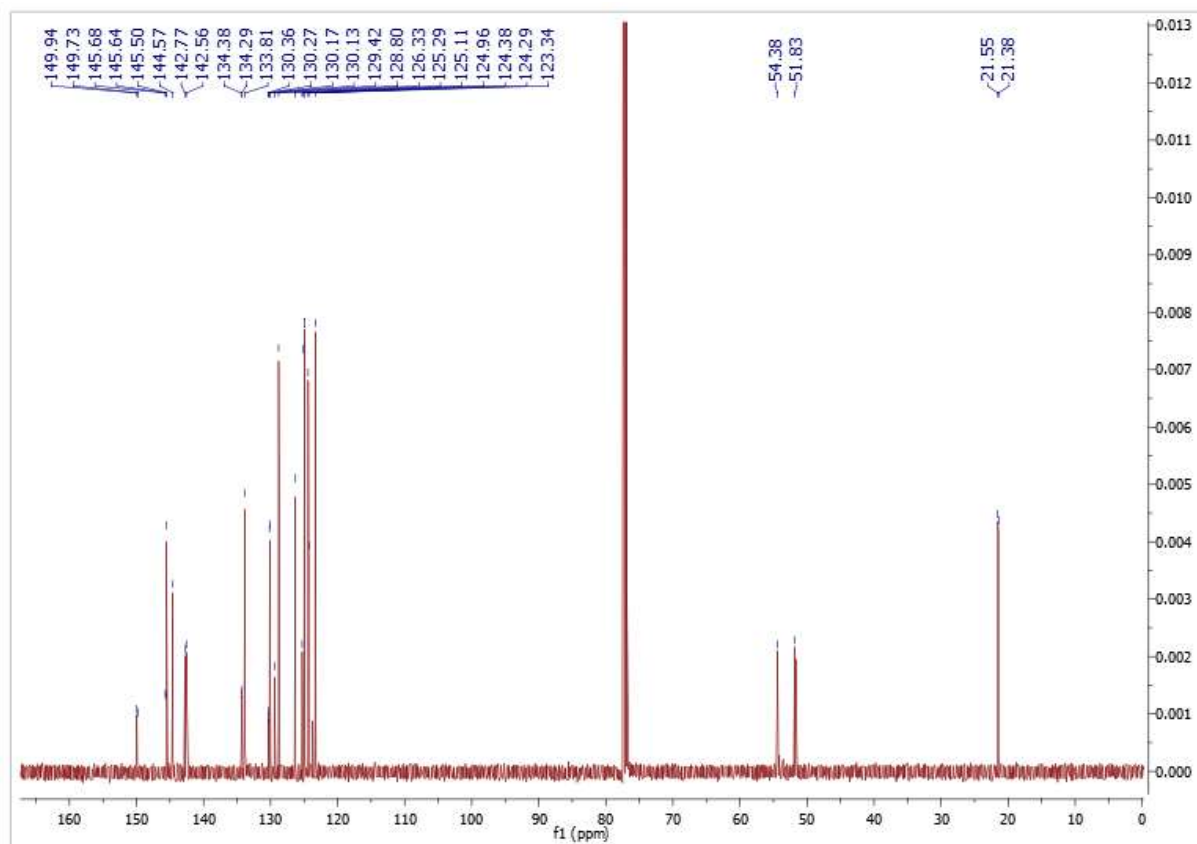
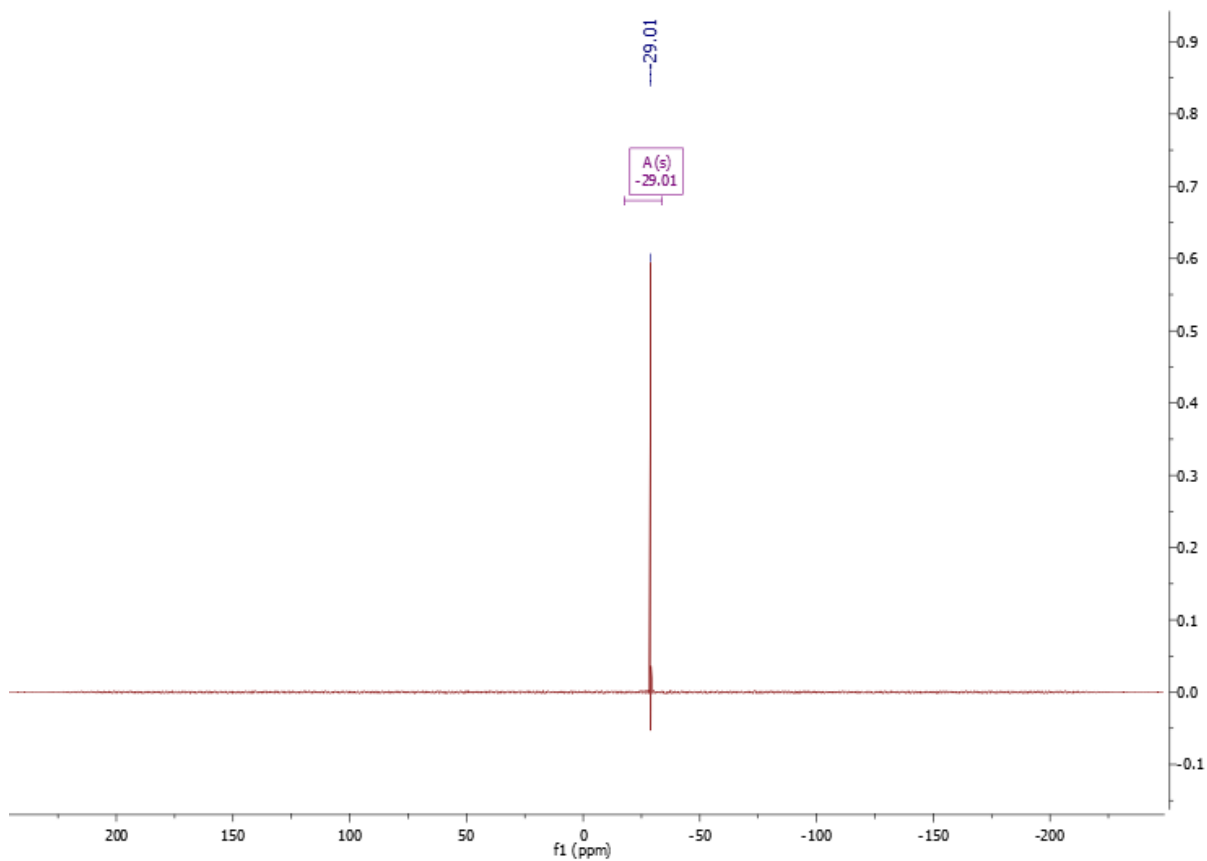
<sup>1</sup>H NMR (400MHz, CDCl<sub>3</sub>): δ(ppm) = 7.36 (d, 3H), 7.25 (t, 4H), 6.98-6.84 (m, 9H), 6.62 (q, 2H), 6.43 (qd, 1H), 5.85 (d, 1H), 5.43 (s, 1H), 2.42 (s, 6H).

<sup>31</sup>P NMR (400MHz, CDCl<sub>3</sub>): δ(ppm) = -29.0ppm.

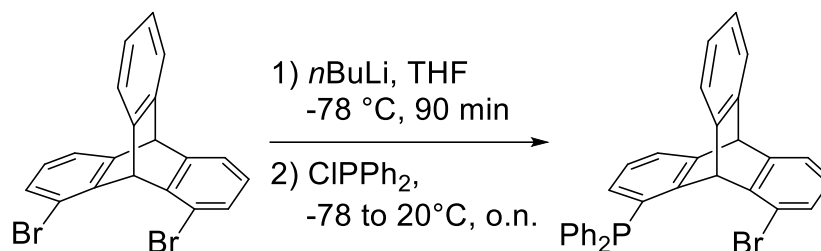
<sup>13</sup>C NMR (125 MHz, CDCl<sub>3</sub>): δ(ppm) = 150.0, 149.7, 145.7, 145.6, 145.5, 144.6, 142.8, 142.6, 134.4, 134.3, 133.8, 130.4, 130.3, 130.2, 130.1, 129.4, 128.8, 126.3, 125.3, 125.1, 125.0, 124.4, 124.3, 123.3, 54.4, 51.8, 21.6, 21.4.

M.p. (CH<sub>2</sub>Cl<sub>2</sub>): 285-287°C





### 1-bromo,8-diphenylphosphinotriptycene 43e:



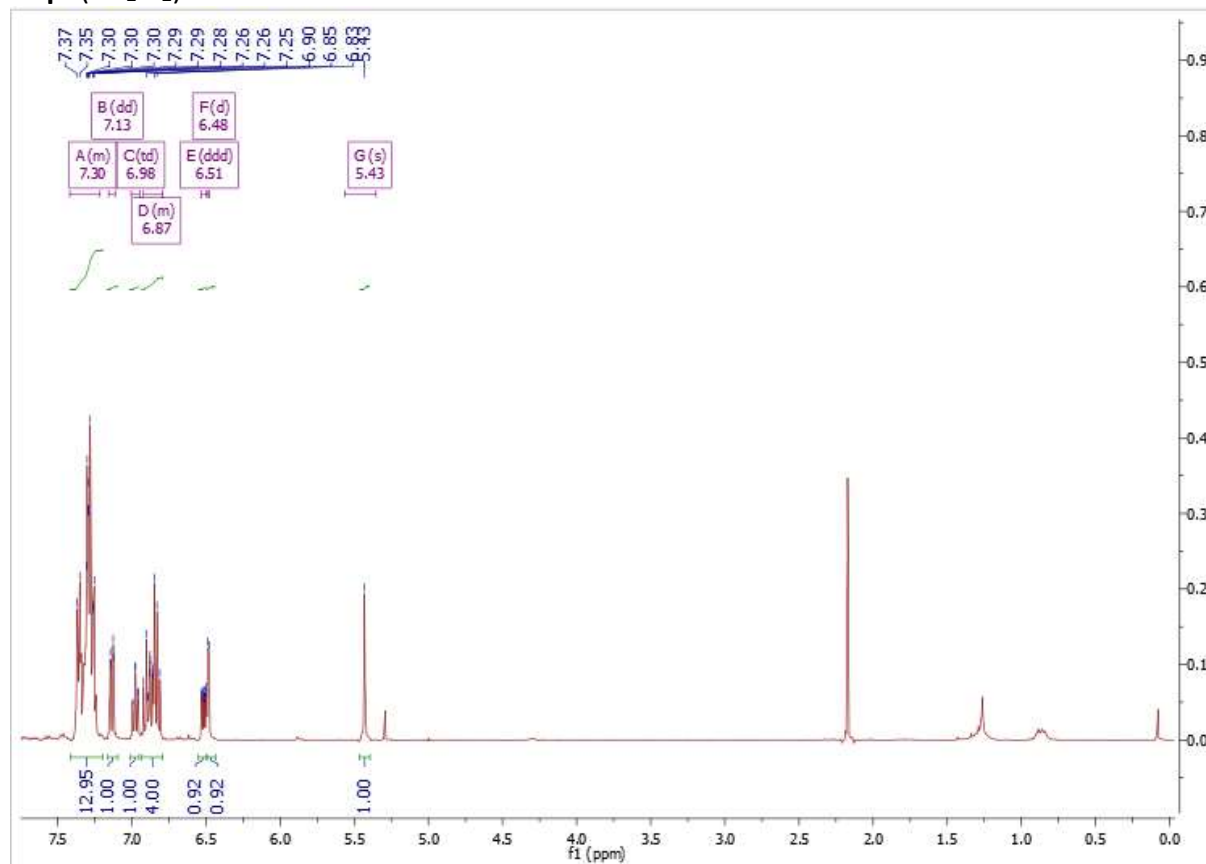
To a stirred solution of 1,8-dibromotriptycene (1.00g, 2.40mmol, 1.00eq) in THF (20mL) at -94°C was added dropwise *n*-BuLi (2.4 mmol, 1.00 eq, 2.50M, 0.97mL). After 2h at -94°C, diphenylchlorophosphine (536mg, 2.40mmol, 1.00eq) is added dropwise at -94°C and the reaction mixture is then stirred overnight at room temperature. The day after, 20mL of EtOAc are added and the mixture is washed 3 times with a saturated solution of NaHCO<sub>3</sub>. Organic layers are dried over anhydrous MgSO<sub>4</sub>, filtered and solvents are removed under vacuum. The crude product was then purified by flash chromatography using Hexane:EtOAc (1:0 to 9:1) to get the desired compound (801mg, 1.56 mmol, 65%).

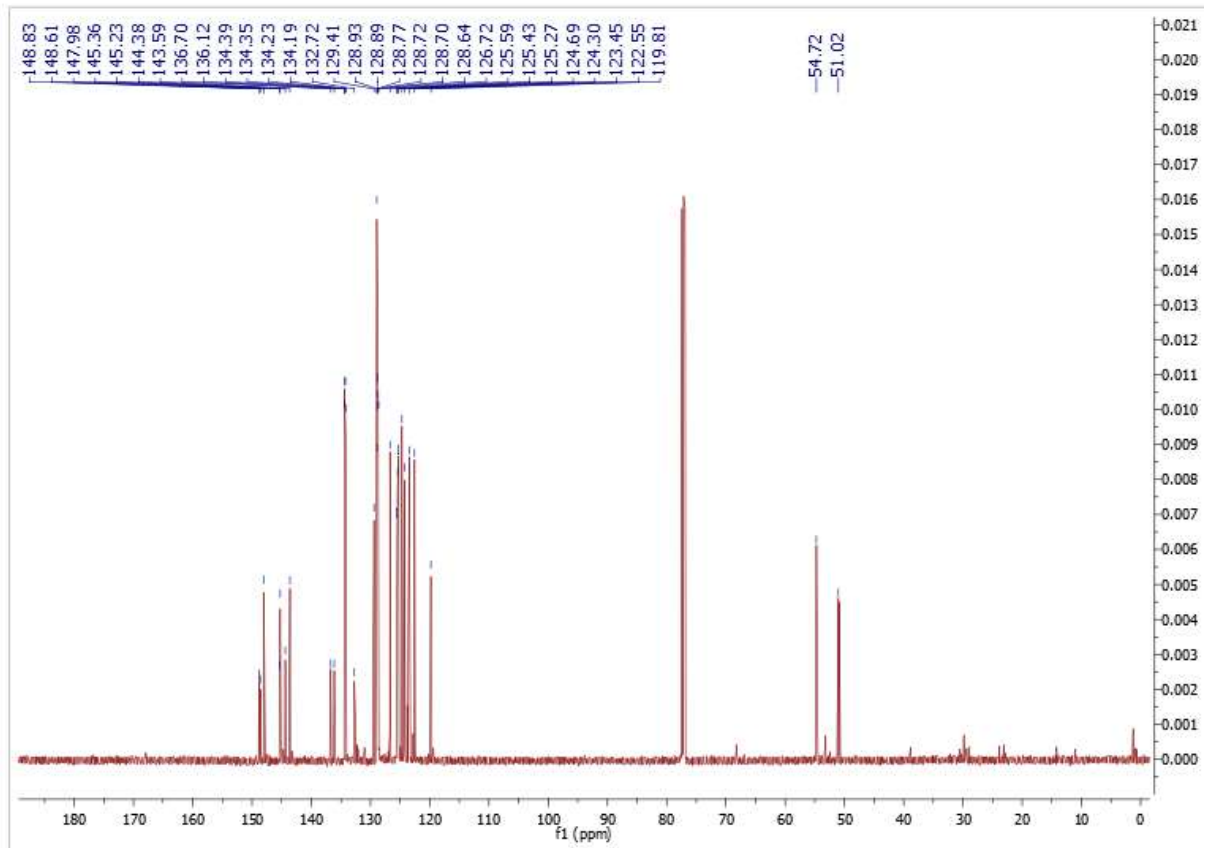
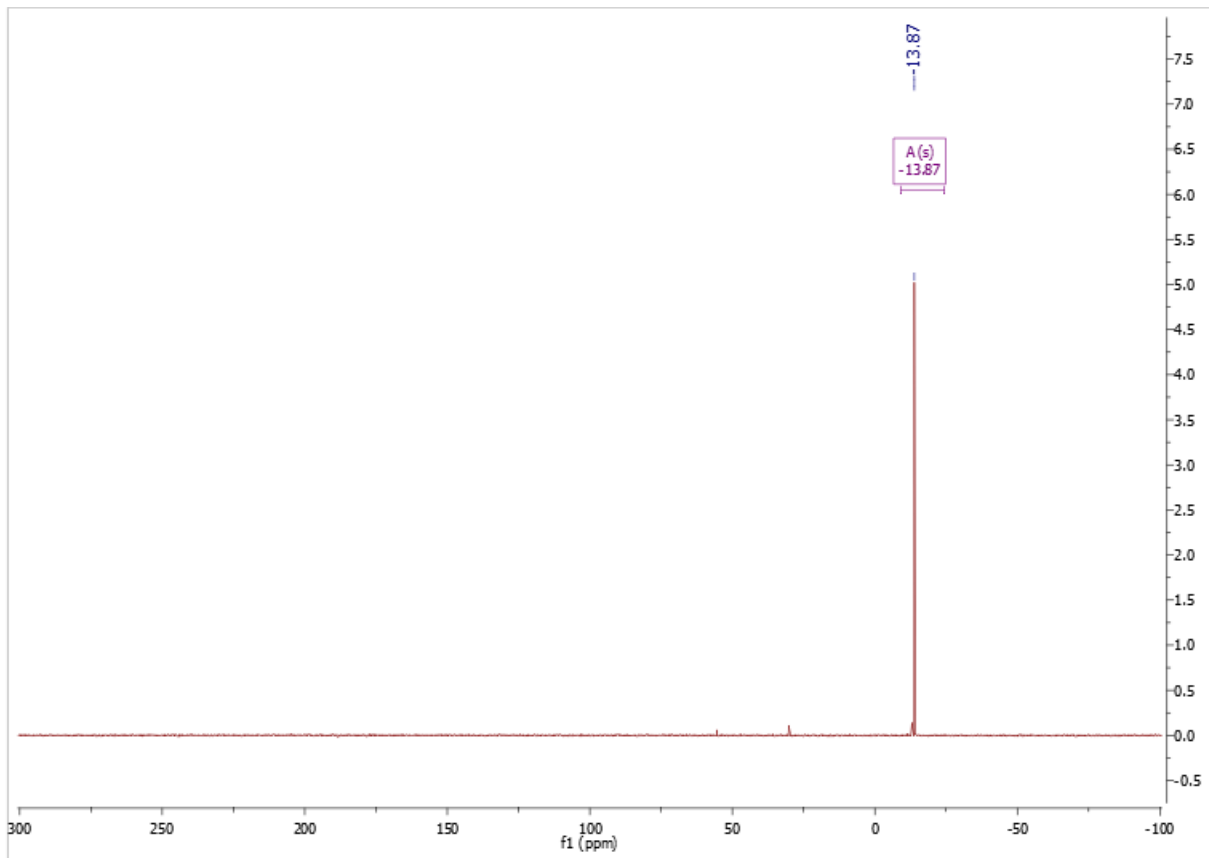
**<sup>1</sup>H NMR (400MHz, CDCl<sub>3</sub>):** δ(ppm) = 7.36-7.25 (m, 13H), 7.13 (dd, 1H), 6.97 (td, 1H), 6.92-6.80 (m, 4H), 6.51 (qd, 1H), 6.49 (d, 1H), 5.42 (s, 1H).

**<sup>31</sup>P NMR (400MHz, CDCl<sub>3</sub>):** δ(ppm) = -13.9ppm

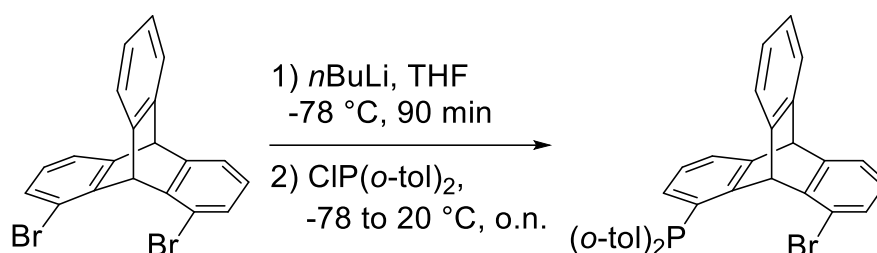
**<sup>13</sup>C NMR (125 MHz, CDCl<sub>3</sub>):** δ(ppm) = 148.8, 148.6, 148.0, 145.4, 145.2, 144.4143.6, 136.7, 136.1, 134.4, 134.4, 134.2, 134.2, 132.7, 129.4, 128.9, 128.9, 128.8, 128.7, 128.7, 128.6, 126.7, 125.6, 125.4, 125.3, 124.7, 124.3, 123.5, 122.6, 119.8, 54.7, 51.0.

**M.p.** (CH<sub>2</sub>Cl<sub>2</sub>): >240°C





### 1-bromo,8-diorthotolylphosphinotriptycene **43f**:



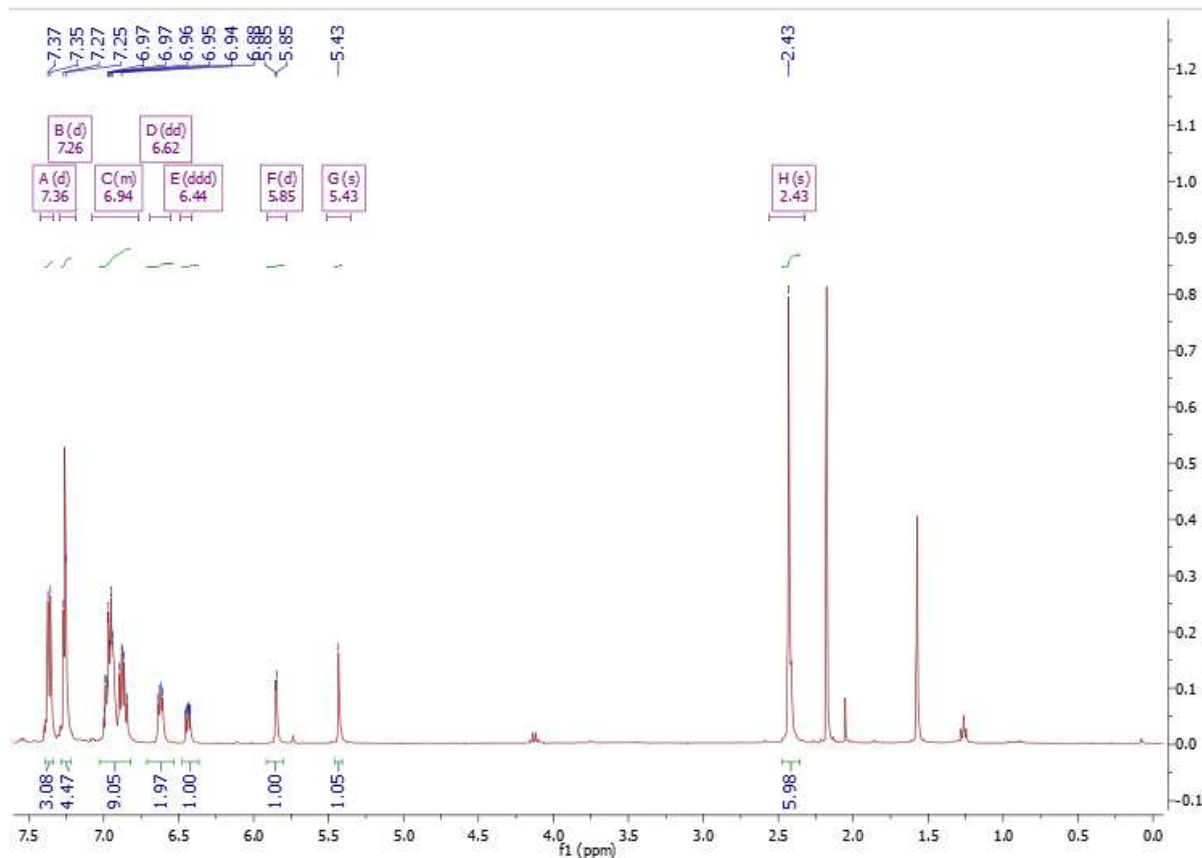
To a stirred solution of 1,8-dibromotriptycene (1.00g, 2.42mmol, 1.00eq) in THF (20mL) at -94°C was added dropwise *n*-BuLi (2.42 mmol, 1.00 eq, 2.50M, 0.96mL). After 2h at -94°C, a solution of diorthotolylchlorophosphine (662mg, 3.00mmol, 1.00eq) in THF (10mL) is added dropwise at -94°C and the reaction mixture is then stirred overnight at room temperature. The day after, 40mL of EtOAc are added and the mixture is washed 3 times with a saturated solution of NaHCO<sub>3</sub> (3x20mL). Organic layers are dried over anhydrous MgSO<sub>4</sub>, filtered and solvents are removed under vacuum. Washing the crude product with acetone afforded 1-bromo,8-diorthotolylphosphinotriptycene **2.43f** (779mg, 1.36mmol, 56%).

<sup>1</sup>H NMR (400MHz, CDCl<sub>3</sub>): δ(ppm) = 7.36 (d, 3H), 7.26 (d, 4H), 6.94 (m, 9H), 6.62 (dd, 2H), 6.44 (m, 1H), 5.85 (d, 1H), 5.43 (s, 1H), 2.43 (s, 6H).

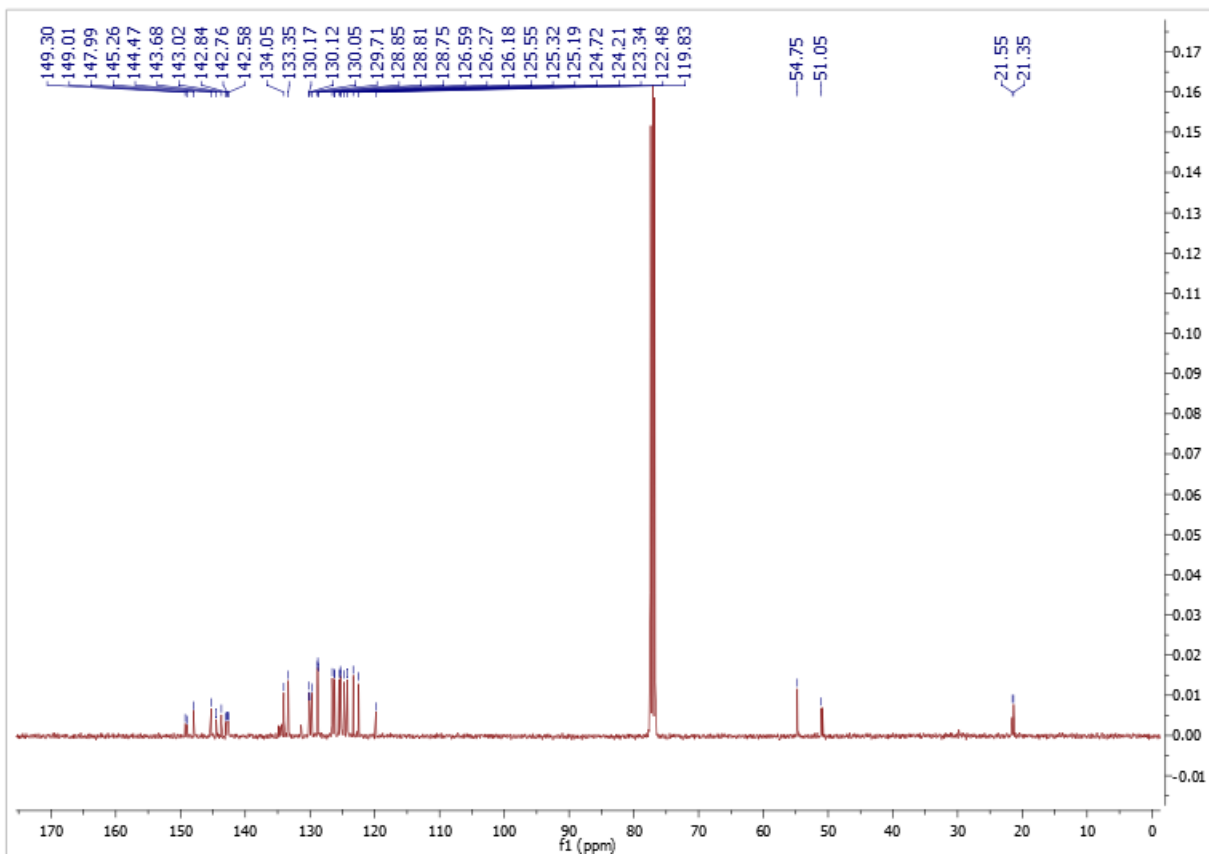
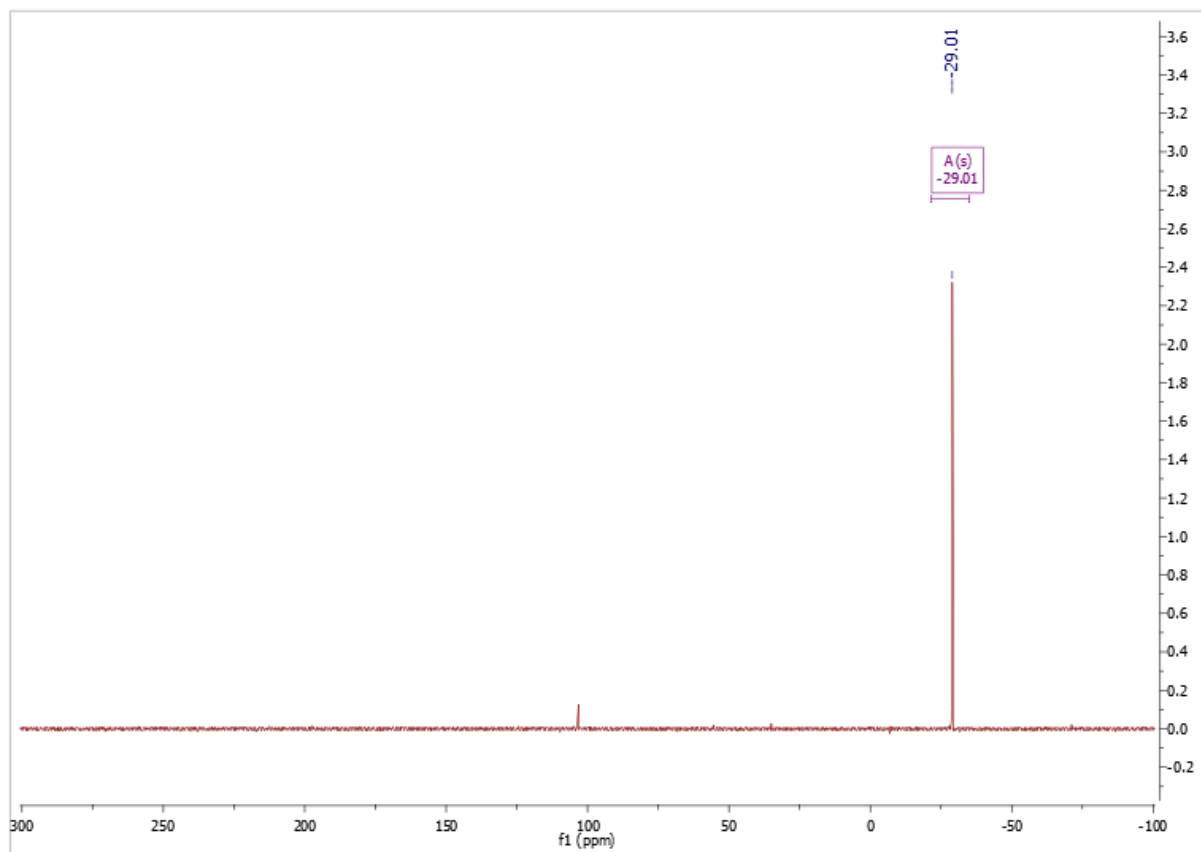
<sup>31</sup>P NMR (400MHz, CDCl<sub>3</sub>): δ(ppm) = -29.1ppm.

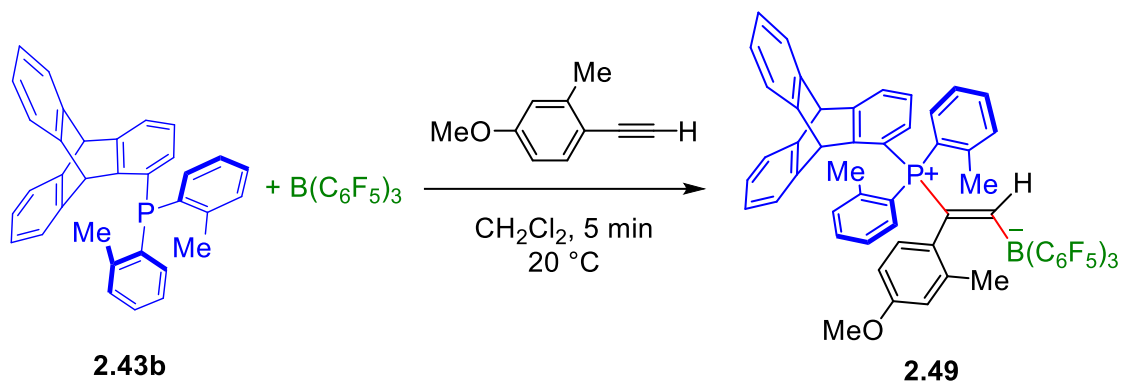
<sup>13</sup>C NMR (125 MHz, CDCl<sub>3</sub>): δ(ppm) = 149.3, 149.0, 148.0, 145.3, 144.5, 143.7, 143.0, 142.8, 142.8, 142.6, 134.1, 133.4, 130.2, 130.1, 130.0, 129.7, 128.9, 128.8, 128.8, 126.6, 126.3, 126.2, 125.6, 125.3, 125.2, 124.7, 124.2, 123.3, 122.5, 119.8, 54.8, 51.1, 21.6, 21.4.

M.p. (CH<sub>2</sub>Cl<sub>2</sub>): >240°C







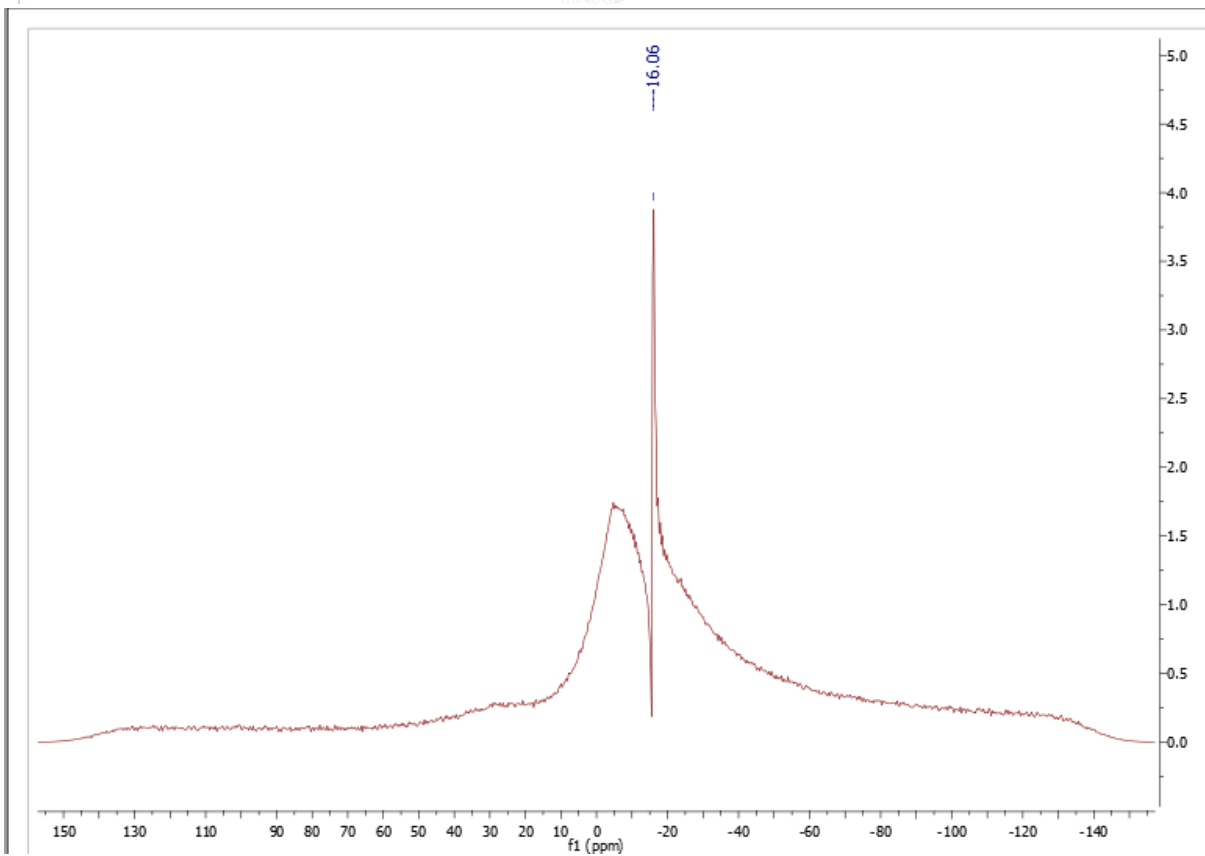
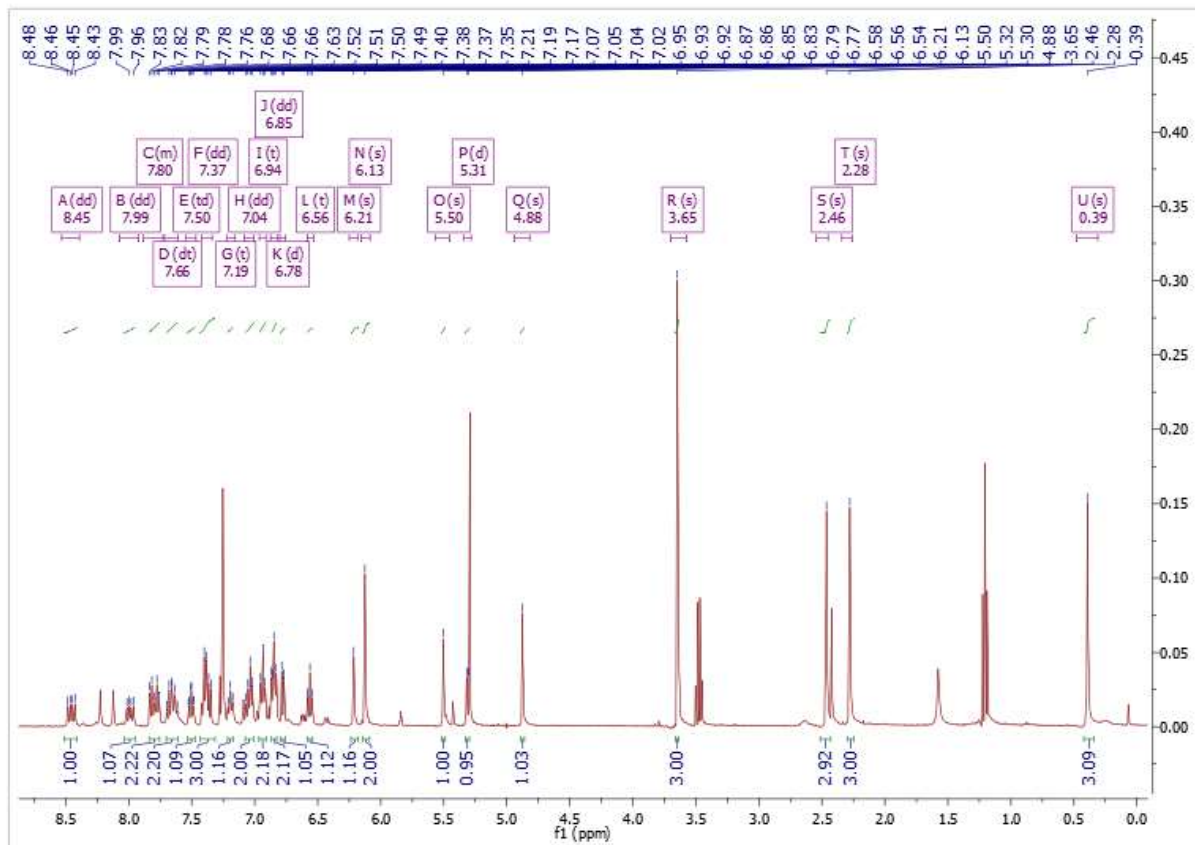
**Adduct 2.49:**

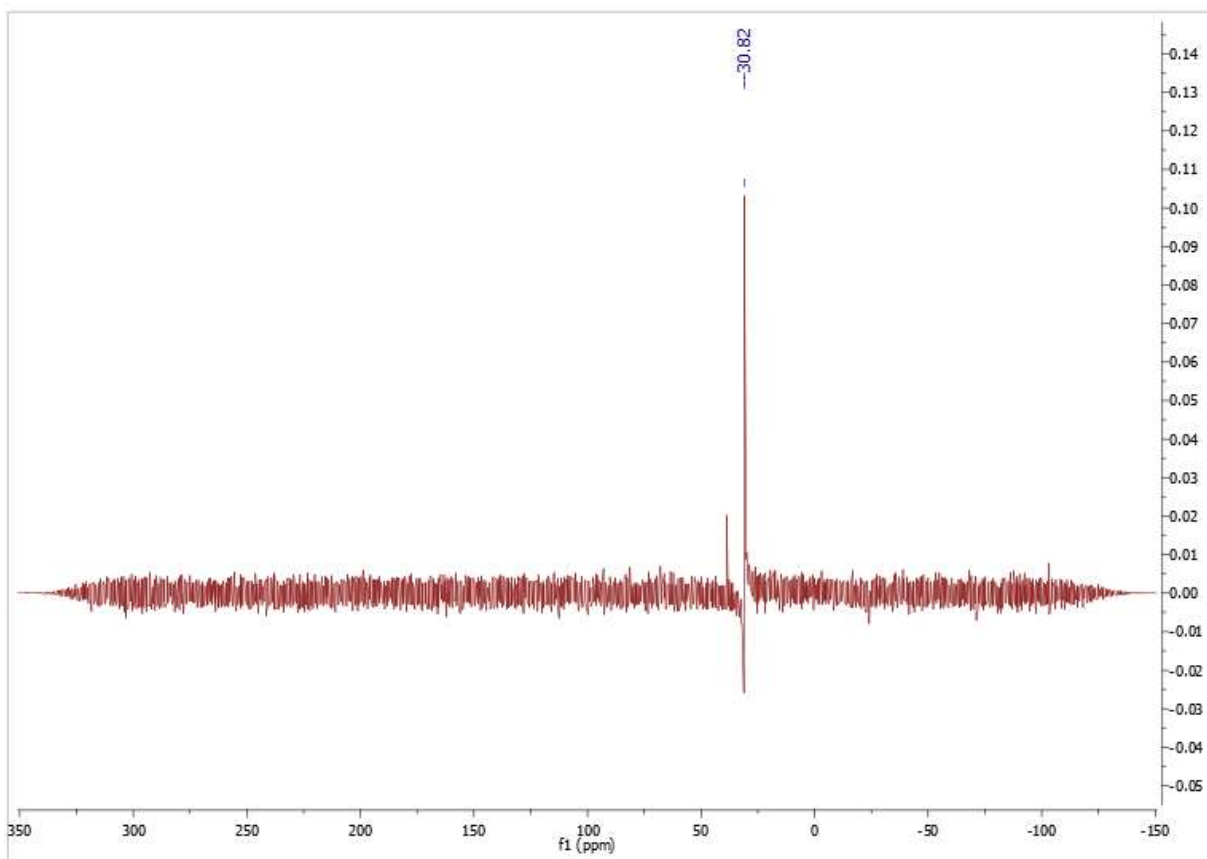
The reaction is carried in a glovebox. To a solution of 1-diorthotolylphosphinotriptycene (**5b**) (93.2mg, 0.200mmol, 1.00eq) in deuterated DCM (5mL) was added  $B(C_6F_5)_3$  (100mg, 0.2mmol, 1.00eq). In this mixture was then added 1-ethynyl-4-methoxy-2-methylbenzene (0.2mmol, 29.2mg, 1.00eq). The resulting mixture is then stirred for 1min and sent to NMR. The crystals of this adduct were obtained by evaporation of the  $CDCl_3$  of the NMR sample (174mg, 0.154mmol, 77%)

**$^1H$  NMR (400MHz,  $CDCl_3$ ):** 8.45 (dd,  $J_1 = 15.1$  Hz,  $J_2 = 8.0$  Hz, 1H), 7.99 (dd,  $J_1 = 13.6$  Hz,  $J_2 = 7.5$  Hz, 1H), 7.88 – 7.73 (m, 2H), 7.66 (dt,  $J_1 = 16.6$ ,  $J_2 = 7.6$  Hz, 2H), 7.50 (td,  $J_1 = 7.7$  Hz,  $J_2 = 2.1$  Hz, 1H), 7.37 (dd,  $J_1 = 13.9$  Hz,  $J_2 = 7.2$  Hz, 3H), 7.19 (t,  $J = 7.3$  Hz, 1H), 7.04 (dd,  $J_1 = 13.4$  Hz,  $J_2 = 6.4$  Hz, 2H), 6.94 (t,  $J = 7.1$  Hz, 2H), 6.85 (dd,  $J_1 = 9.5$ ,  $J_2 = 6.1$  Hz, 2H), 6.78 (d,  $J = 7.3$  Hz, 1H), 6.56 (t,  $J = 7.3$  Hz, 1H), 6.21 (s, 1H), 6.13 (s, 2H), 5.50 (s, 1H), 5.31 (d,  $J = 7.4$  Hz, 2H), 4.88 (s, 1H), 3.65 (s, 3H), 2.46 (s, 3H), 2.28 (s, 3H), 0.39 (s, 3H).

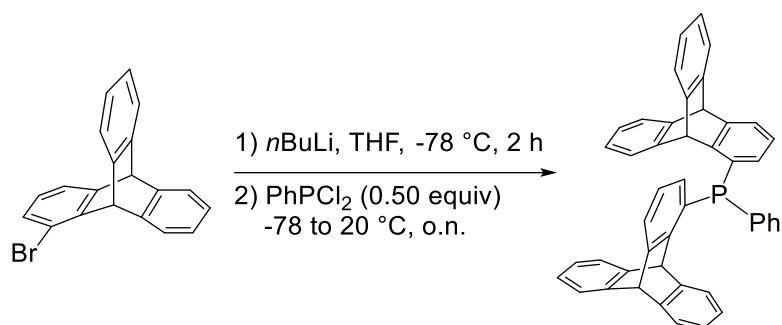
**$^{11}B$  NMR (400MHz,  $CDCl_3$ ):**  $\delta$ (ppm) = -16.1

**$^{31}P$  NMR (400MHz,  $CDCl_3$ ):**  $\delta$ (ppm) = 30.8





### 1-ditriptycenyphenylphosphine **44**:



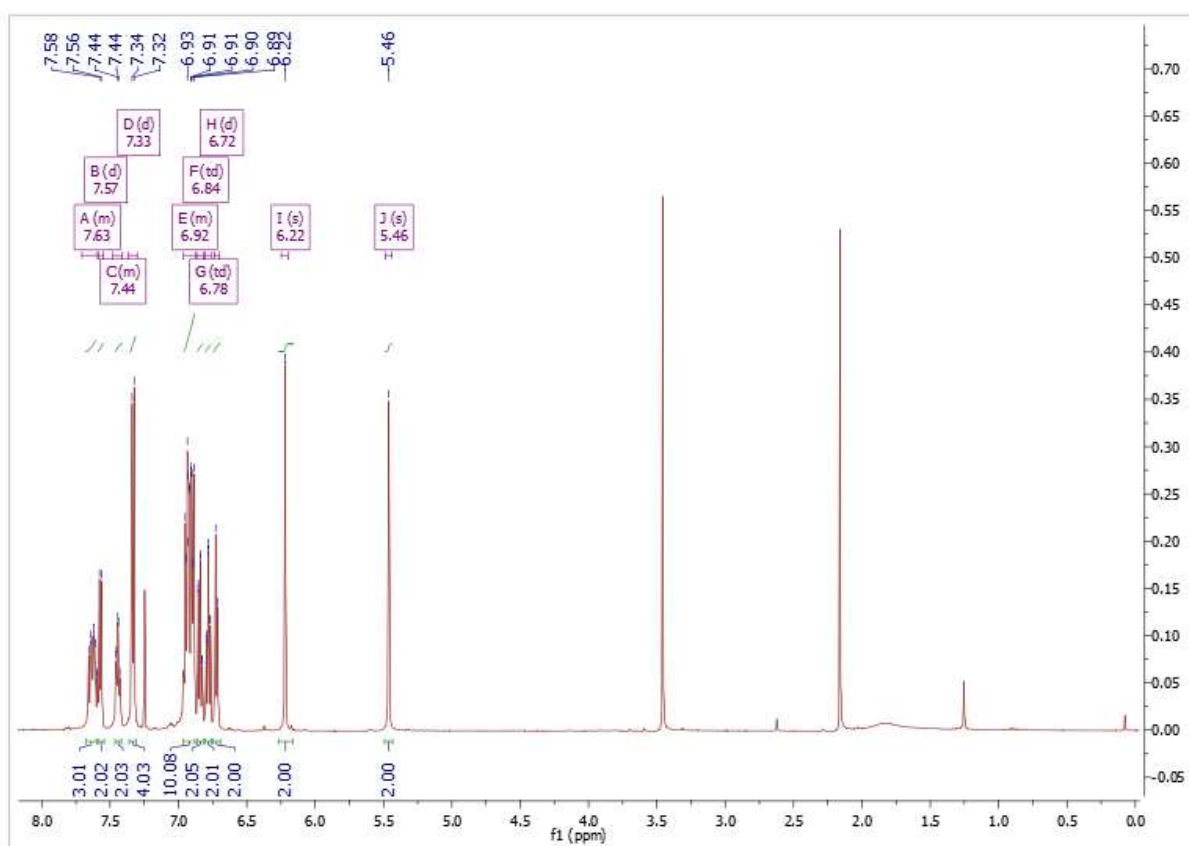
To a stirred solution of 1-bromotriptycene **2.30** (500mg, 1.50mmol, 2.00eq) in THF (20mL) at -94°C was added dropwise *n*-BuLi (1.50 mmol, 2.00 eq, 2.50M, 0.62mL) under argon atmosphere. After 2h at -94°C, dichlorophenylphosphine (0.1mL, 0.75mmol, 1.00eq) is added dropwise at -94°C and the reaction mixture is then stirred overnight at room temperature. The day after, solvent is removed under vacuum. The crude product was then diluted in chloroform and filtered under argon atmosphere (glovebox) to get the desired compound **2.43a** (278mg, 0.45 mmol, 30%).

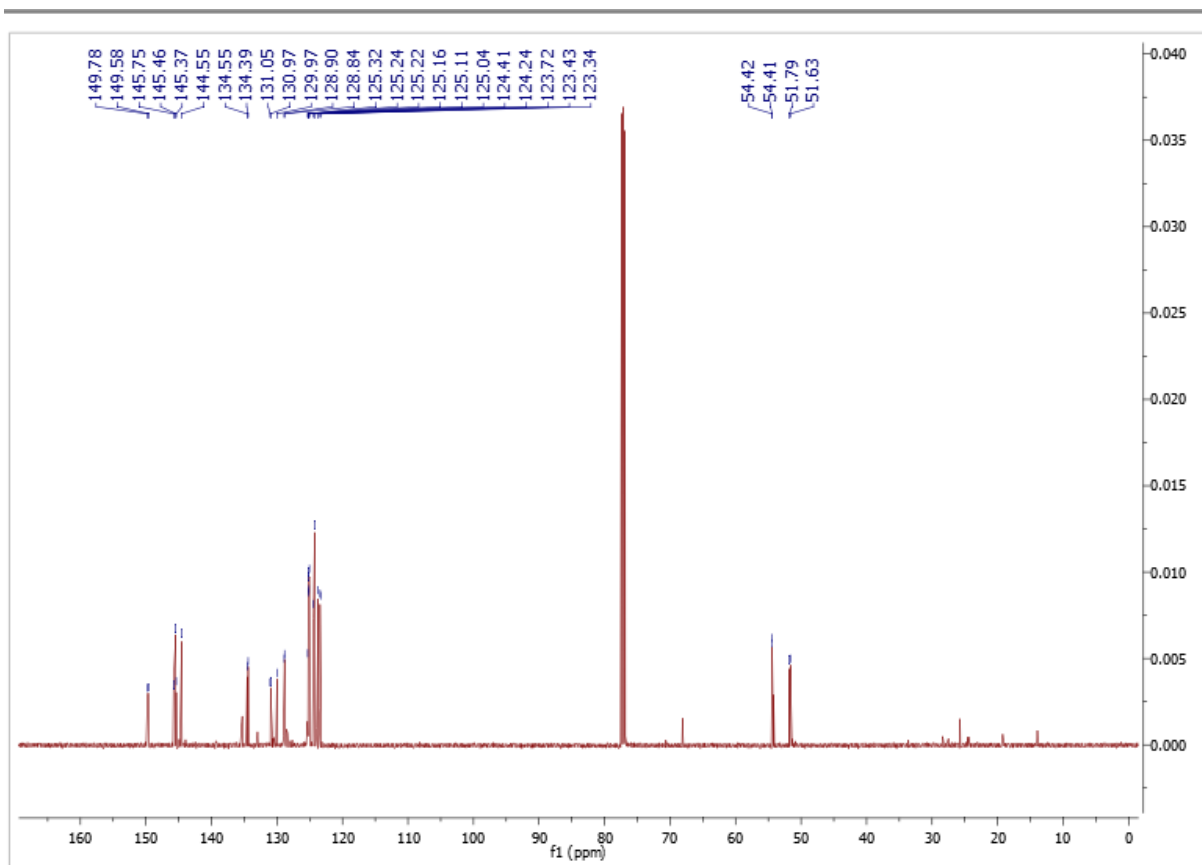
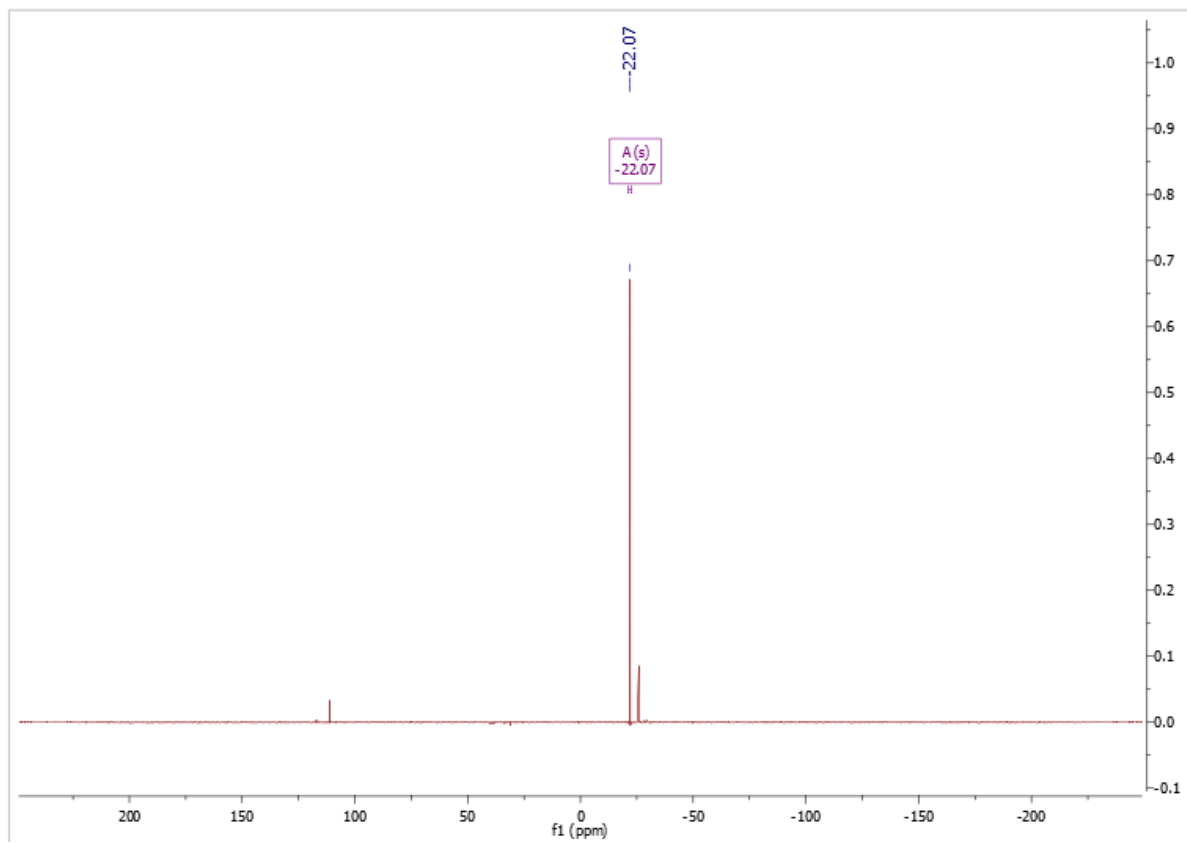
<sup>1</sup>H NMR (400MHz, CDCl<sub>3</sub>): δ(ppm) = 7.71 – 7.60 (m), 7.57 (d, *J* = 7.1 Hz), 7.48 – 7.41 (m), 7.33 (d, *J* = 7.2 Hz), 6.96 – 6.88 (m), 6.84 (td, *J*<sub>1</sub> = 7.4, *J*<sub>2</sub> = 0.8 Hz), 6.78 (td, *J*<sub>1</sub> = 7.4, *J*<sub>2</sub> = 0.8 Hz), 6.72 (d, *J* = 7.2 Hz), 6.22 (s), 5.46 (s).

<sup>31</sup>P NMR (400MHz, CDCl<sub>3</sub>): δ(ppm) = -22.1 ppm.

<sup>13</sup>C NMR (125 MHz, CDCl<sub>3</sub>): δ(ppm) = 149.8, 149.6, 145.8, 145.5, 145.4, 144.6, 134.6, 134.4, 131.1, 131.0, 130.0, 128.9, 128.8, 125.3, 125.2, 125.2, 125.2, 125.1, 125.0, 124.4, 124.2, 123.7, 123.4, 123.3, 54.4, 54.4, 51.8, 51.6.

M.p. (CH<sub>2</sub>Cl<sub>2</sub>): 311-313°C

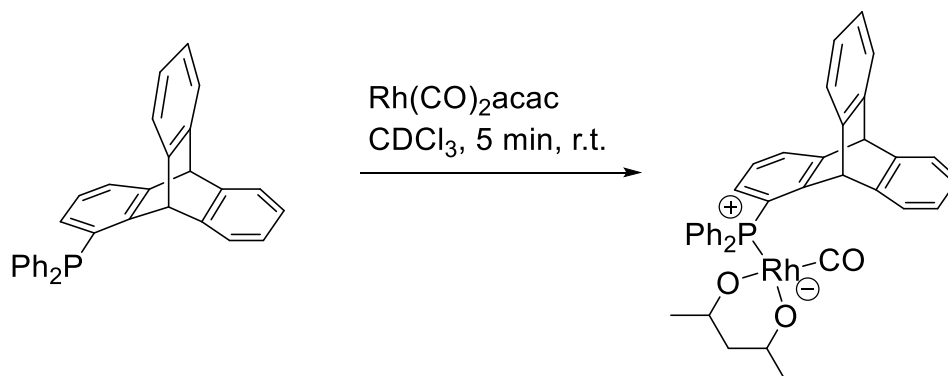




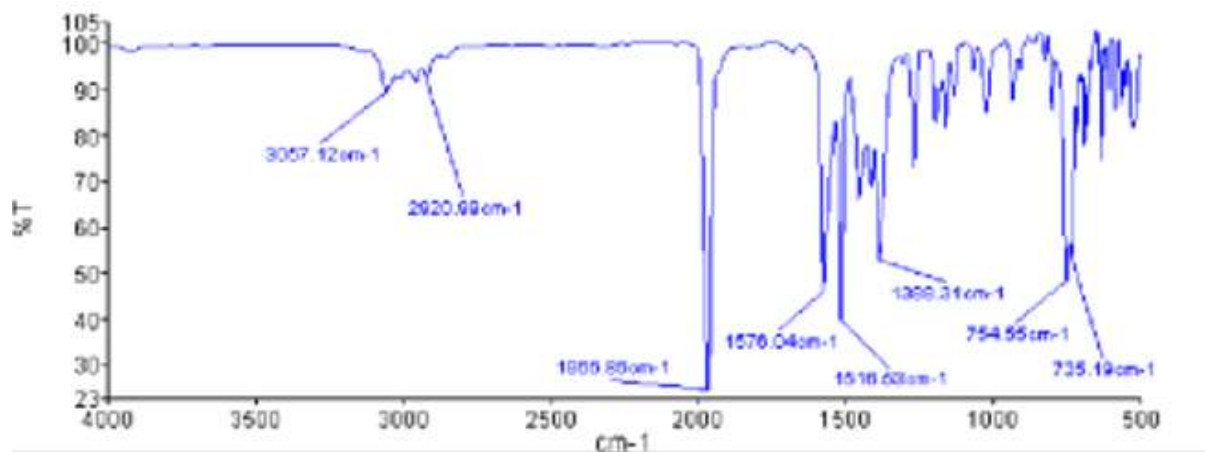
### Preparation of Rh complexes:

All the Rh complexes have been prepared under Argon atmosphere in a glovebox.

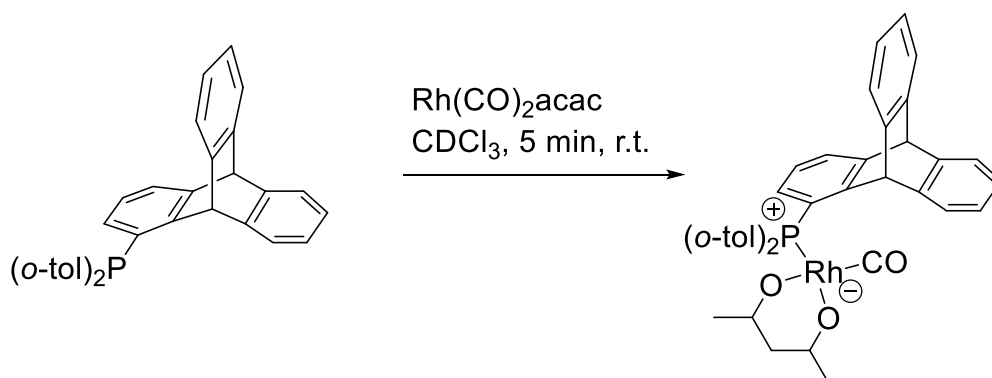
#### 2.43a Rhodium complex:



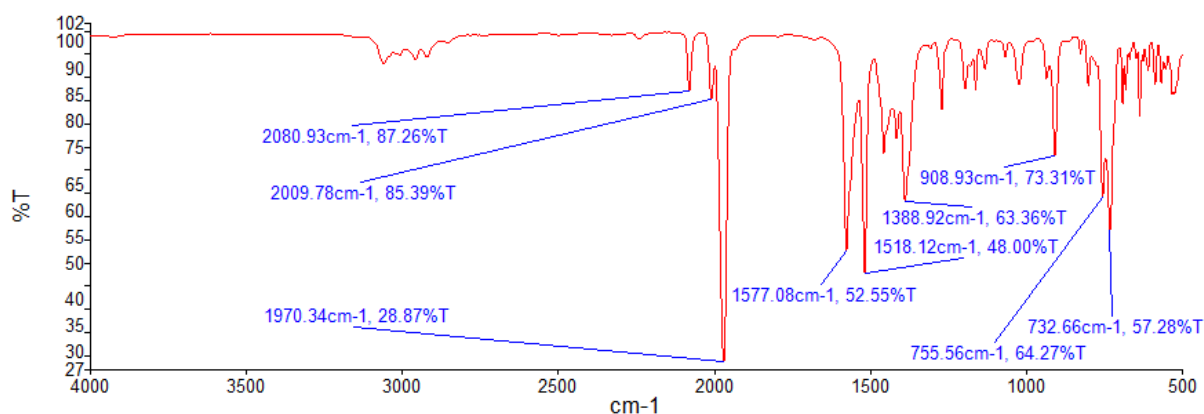
In a small vial, the phosphine **2.43a** (17 mg, 39  $\mu\text{mol}$ , 1 eq) is dissolved in  $\text{CDCl}_3$  (0.5 mL). Then a solution of  $\text{Rh}(\text{CO})_2\text{acac}$  (10 mg, 39  $\mu\text{mol}$ , 1 eq) in  $\text{CDCl}_3$  is added and the mixture is stirred for 5 min at room temperature. The complex is then analysed via X-ray diffraction and IR.



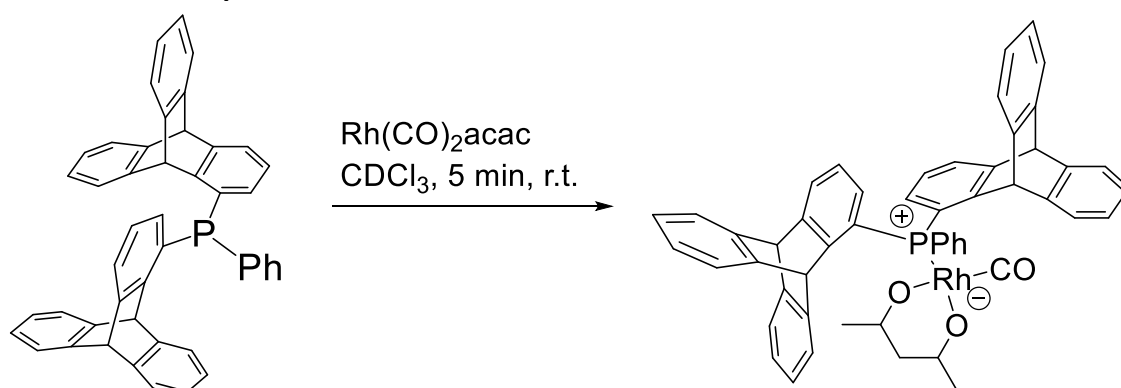
#### 2.43b Rhodium complex:



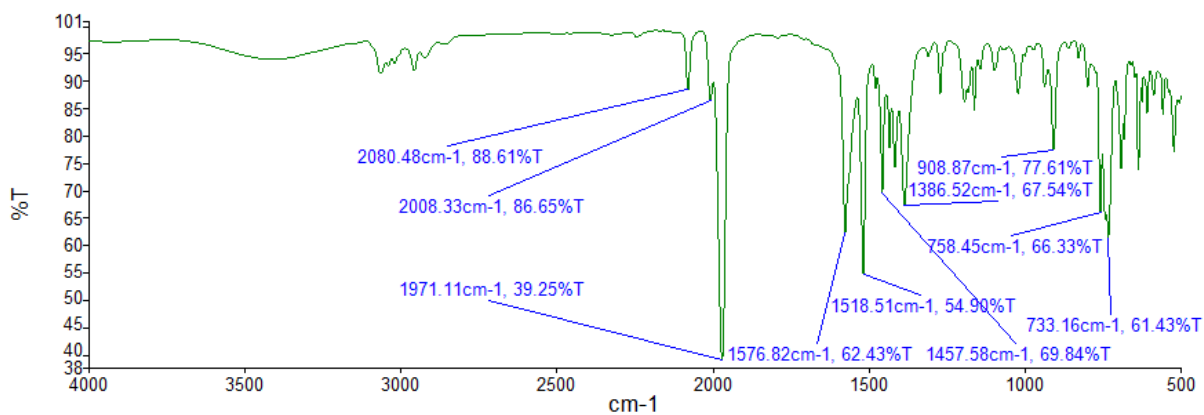
In a small vial, the phosphine **2.43b** (18 mg, 39  $\mu\text{mol}$ , 1 eq) is dissolved in  $\text{CDCl}_3$  (0.5 mL). Then a solution of  $\text{Rh}(\text{CO})_2\text{acac}$  (10 mg, 39  $\mu\text{mol}$ , 1 eq) in  $\text{CDCl}_3$  is added and the mixture is stirred for 5 min at room temperature. The complex is then analysed via X-ray diffraction and IR.



#### 2.44 Rhodium complex:



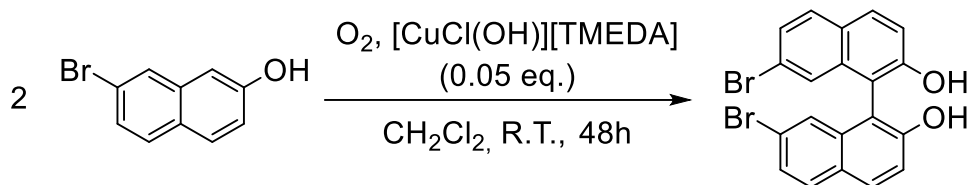
In a small vial, the phosphine **2.44** (24 mg, 39  $\mu\text{mol}$ , 1 eq) is dissolved in  $\text{CDCl}_3$  (0.5 mL). Then a solution of  $\text{Rh}(\text{CO})_2\text{acac}$  (10 mg, 39  $\mu\text{mol}$ , 1 eq) in  $\text{CDCl}_3$  is added and the mixture is stirred for 5 min at room temperature. The complex is then analysed via X-ray diffraction and IR.





## 2. Preparation of the chapter three's molecules

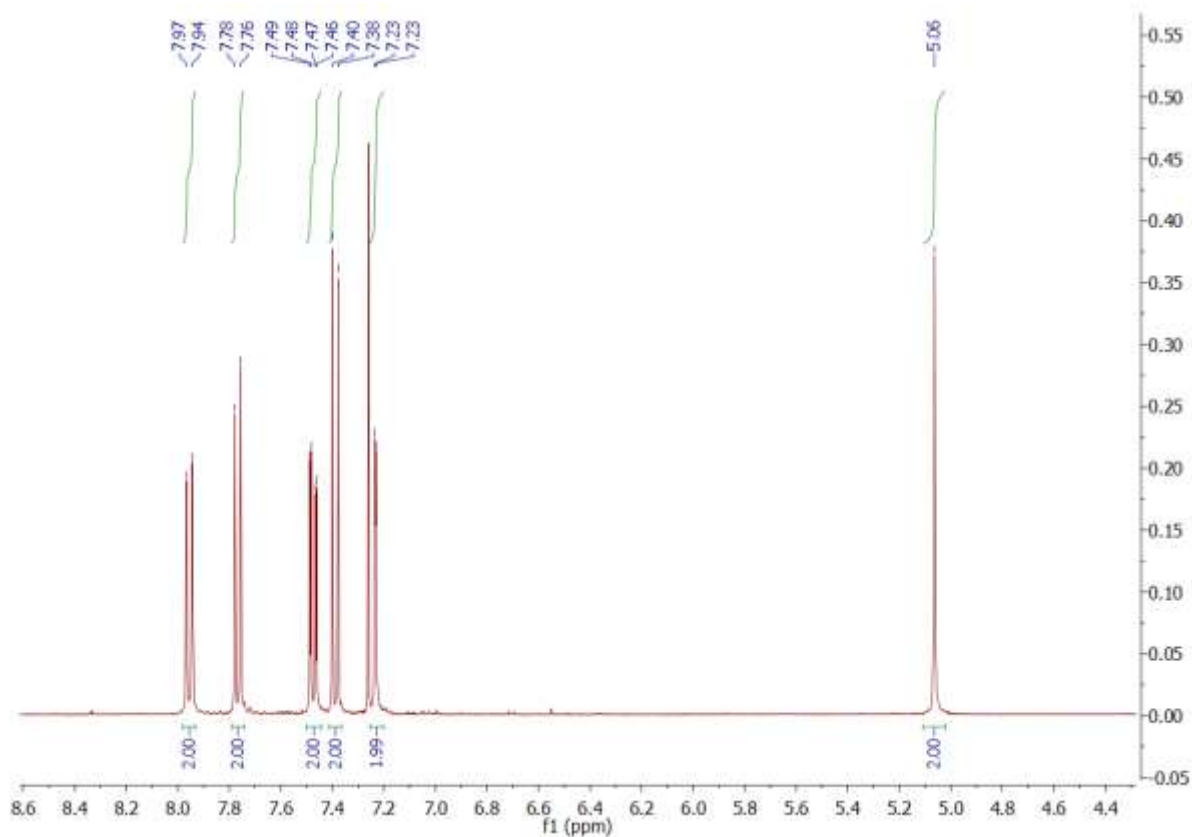
### (R,S)-7,7'-Dibromo-1,1'-binaphthalene-2,2'-diol **3.41**:



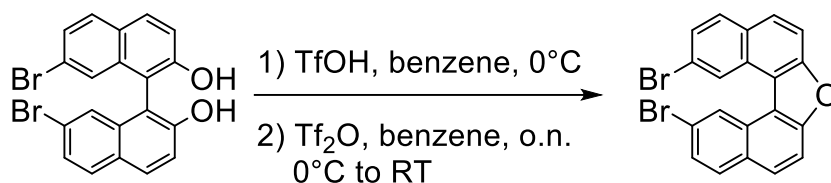
In a 1L open flask, 7-bromo-2-naphthol (10.0 g, 44.82 mmol, 1.00 eq) is added in 300 mL of  $CH_2Cl_2$ . After stirring for 5 min,  $[CuCl(OH)](TMEDA)$  (1.36 g, 2.92 mmol, 0.03 eq) is added. The mixture is then stirred vigorously for 48h. Afterwards, the solvent is removed under reduced pressure and the crude product is purified by flash chromatography using cyclohexane:EtOAc (1:0 to 3:1) to obtain pure (R,S)-7,7'-dibromo-1,1'-binaphthalene-2,2'-diol **3.41** (7.86g, 17.7mmol, 79%).

Rf = 0.30 (eluant = cyclohexane/EtOAc: 3/1)

$^1H$  NMR (400MHz,  $CDCl_3$ ):  $\delta$ (ppm) = 5.06 (s, 2H); 7.23 (d, J=1.91 Hz, 2H); 7.38-7.40 (d, J=8.94 Hz, 2H); 7.46-7.49 (dd, J=1.93, 8.65 Hz, 2H); 7.76-7.78 (d, J=8.65 Hz, 2H); 7.94-7.97 (d, J=8.87 Hz, 2H).



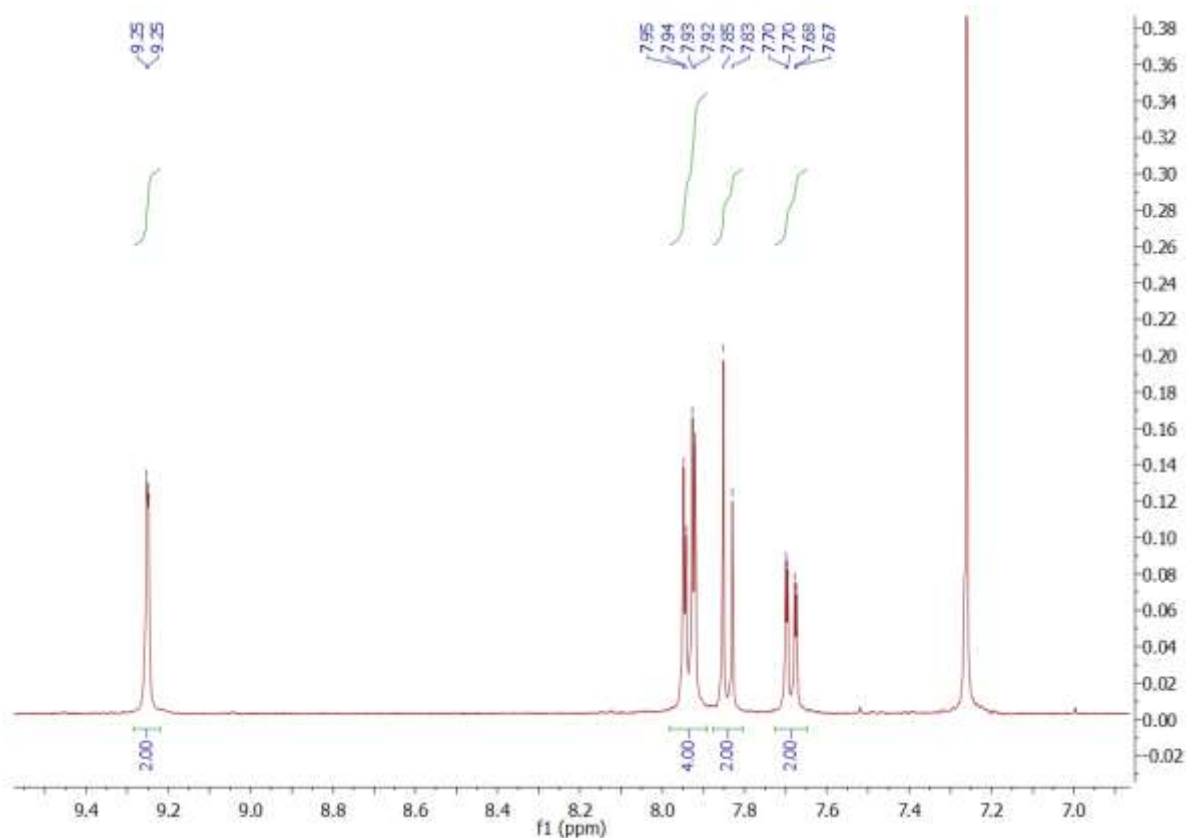
### 2,12-(dibromo)oxa[5]helicène 3.42:



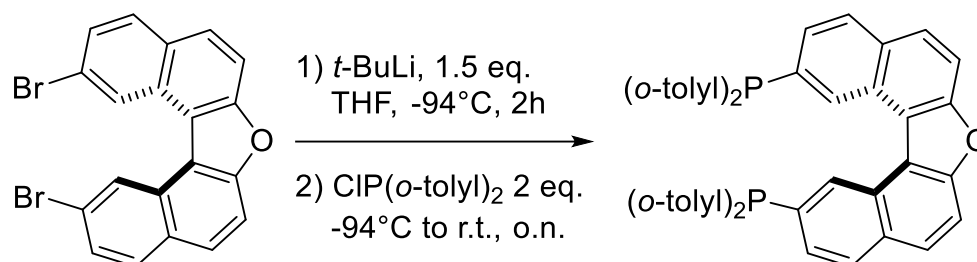
(*R,S*)-7,7'-dibromo-1,1'-binaphthalene-2,2'-diol (2.93g, 6.60mmol, 1.0 eq.) is dissolved in 60 mL of benzene under ambient atmosphere in a 250 mL round bottom flask. The mixture is then stirred at 0°C and TfOH (2.4 mL, 27 mmol, 4.1 eq) are added dropwise to the mixture. After, a solution of Tf<sub>2</sub>O (4.5 mL, 27 mmol, 4.1 eq) in benzene (20 mL) is slowly added at 0°C and the mixture is stirred overnight at room temperature. The day after, 100 mL of CH<sub>2</sub>Cl<sub>2</sub> are added and the mixture is washed with a saturated solution of NaHCO<sub>3</sub> (3x20 mL). The aqueous phases are then extracted with CH<sub>2</sub>Cl<sub>2</sub> (3x30 mL) and all the organic phases are combined, dried over MgSO<sub>4</sub> before the solvent is removed under reduced pressure. The crude product is purified by flash chromatography using cyclohexane:CH<sub>2</sub>Cl<sub>2</sub> (1:0 to 1:1) to obtain 2,12-(dibromo)oxa[5]helicène **3.42** (843 mg, 1.98 mmol, 30%).

R<sub>f</sub> = 0.81 (eluant : cyclohexane/CH<sub>2</sub>Cl<sub>2</sub> : 1/1)

<sup>1</sup>H NMR (400MHz, CDCl<sub>3</sub>): δ(ppm) 7.67-7.70 (dd, J=1.76, 8.68 Hz, 2H) ; 7.83-7.85 (d, J=8.87 Hz, 2H) ; 7.92-7.94 (d, J=8.87 Hz, 4H) ; 7.93-7.95 (d, J=8.67 Hz, 2H) ; 9.25 (d, J=1.56 Hz, 2H).



**2,12-bis(di(*o*-tolyl)phosphino)oxa[5]helicene 3.43b:**



Compound **3.43b** has been synthesized following a procedure that was initially optimized for the synthesis of 2-bromo-12-(*o*-tolyl)phosphino)oxa[5]helicene:

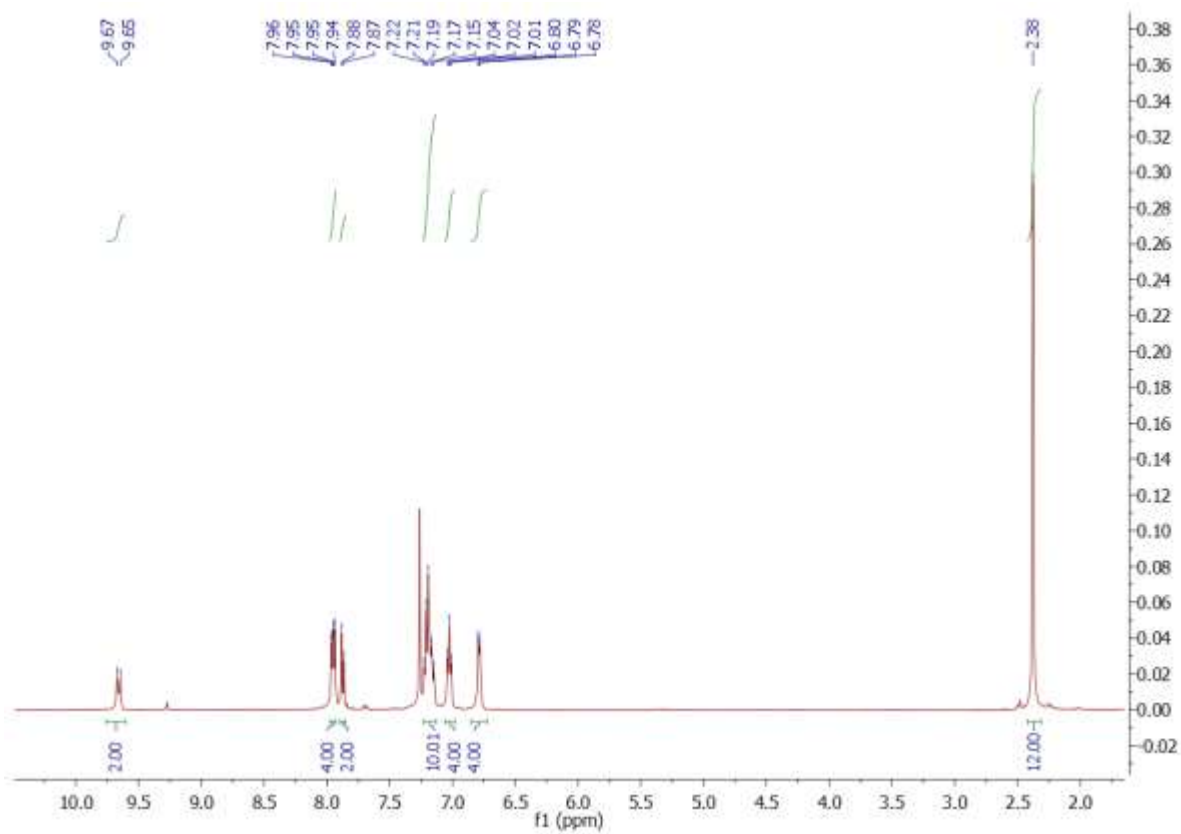
Under argon atmosphere, a *t*-BuLi solution in pentane (0.46 mL, 0.88 mL, 1.5 eq) is added dropwise at -94 °C to a solution of (R,S)-7,7'-dibromo-1,1'-binaphthalene-2,2'-diol (250 mg, 0.59 mmol, 1.00 eq) in THF (20 mL). The mixture is then stirred for 2h at -94 °C and a solution of chlorodi(*o*-tolyl)phosphine (146 mg, 0.59 mmol, 1.00 eq) in THF (5 mL) is added dropwise. The mixture is then stirred overnight at room temperature. The day after, 50 mL of EtOAc are added to the mixture and the solution is washed with a saturated solution of NH<sub>4</sub>Cl (3x20 mL). The organic layer is dried over MgSO<sub>4</sub> and the solvent are removed under reduced pressure.

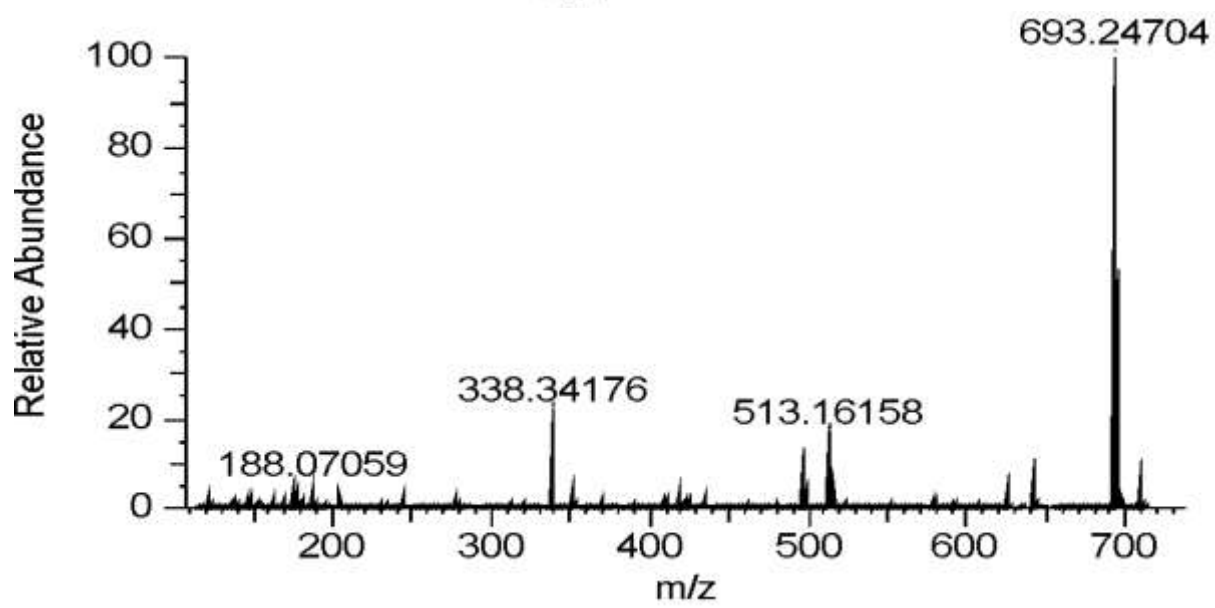
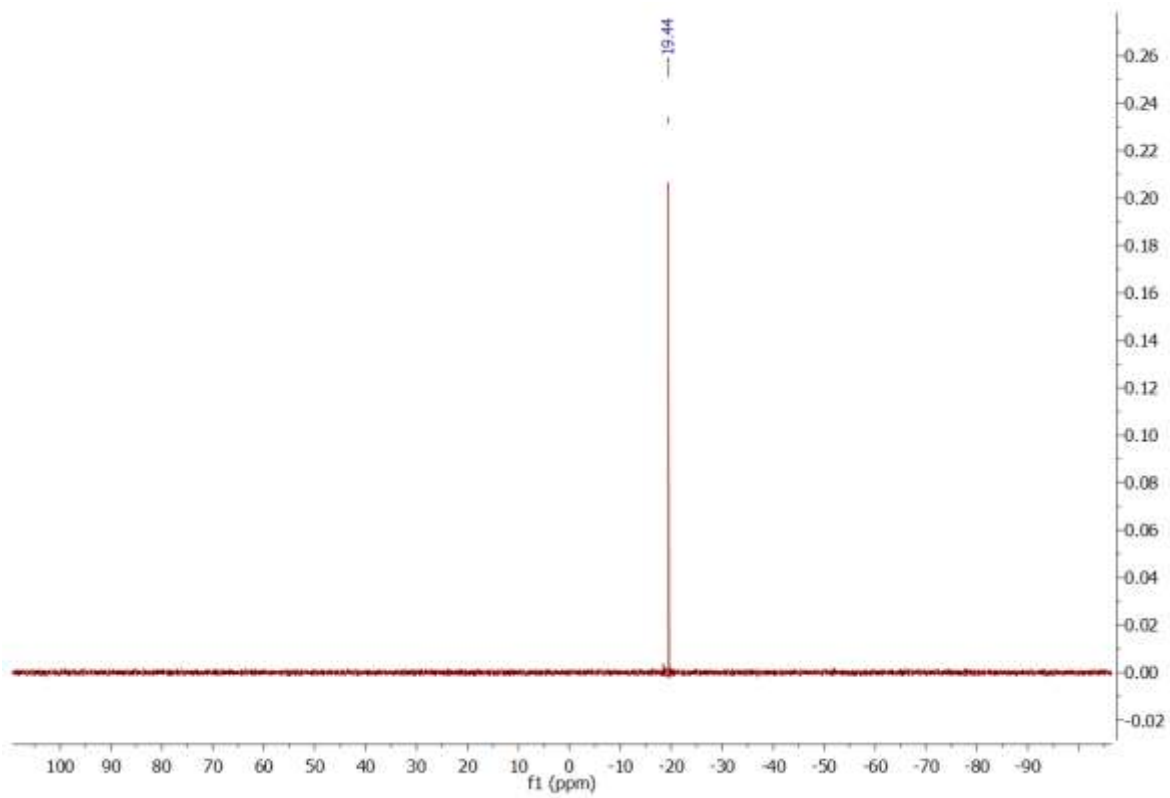
The crude product is purified by precipitation in acetone to give pure 2,12-bis(di(*o*-tolyl)phosphino)oxa[5]helicene **3.43b** as a white powder.

<sup>1</sup>H RMN (500 MHz, CDCl<sub>3</sub>): δ = 2.39 (*s*, 12H) ; 6.78-6.80 (*m*, 4H) ; 7.01-7.04 (*t*, J=7.02 Hz, 4H) ; 7.15-7.22 (*m*, 10H) ; 7.87-7.88 (*d*, J=8.82 Hz, 2H) ; 7.94-7.95 (*d*, J=8.64 Hz, 2H) ; 7.95 (*d*, J=8.2 Hz, 2H), 9.65-9.67 (*d*, J=12.11 Hz, 2H)

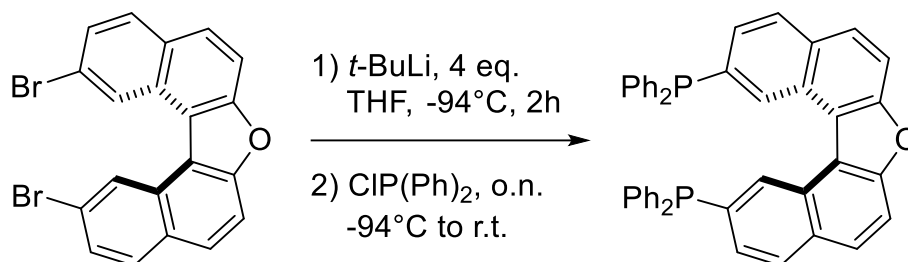
<sup>31</sup>P RMN (162 MHz, CDCl<sub>3</sub>): δ = -19.4

HRMS (ESI+): [M+H]<sup>+</sup> = 693.247





**2,12-bis(diphénylphosphino)oxa[5]hélécène 3.43a:**



Compound **3.43a** has been synthesized following a procedure that wasn't initially optimized for this compound:

Under argon atmosphere, a *t*-BuLi solution in pentane (2.5 mL, 4.74 mmol, 4.00 eq) is added dropwise at -94 °C to a solution of (R,S)-7,7'-dibromo-1,1'-binaphthalene-2,2'-diol (500 mg, 1.17 mmol, 1.00 eq) in THF (50 mL). The mixture is then stirred for 2h at -94 °C and a solution of chlorodiphenylphosphine (0.22 mL, 1.17 mmol, 1.00 eq) in THF (5 mL) is added dropwise. The mixture is then stirred overnight at room temperature. The day after, 100 mL of EtOAc are added to the mixture and the solution is washed with a saturated solution of NH<sub>4</sub>Cl (3x30 mL). The organic layer is dried over MgSO<sub>4</sub> and the solvent are removed under reduced pressure.

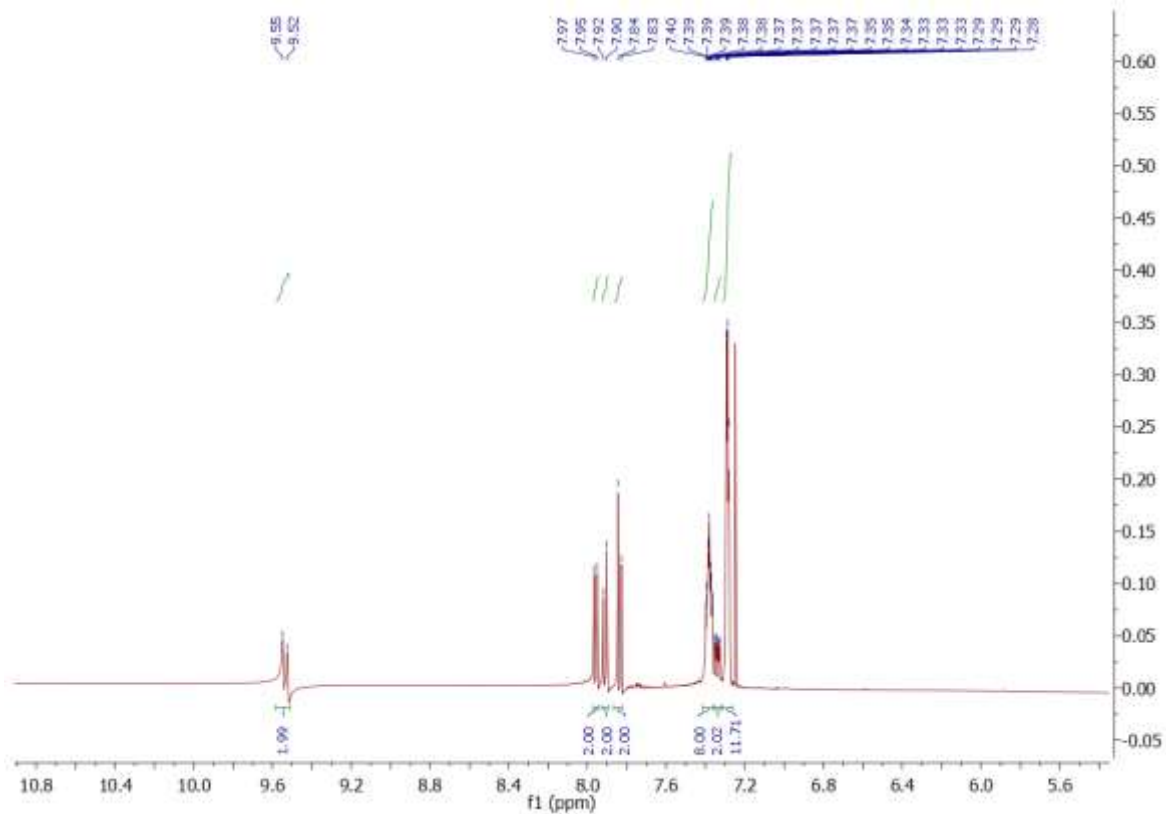
The crude product is purified by flash chromatography using hexane/CH<sub>2</sub>Cl<sub>2</sub> (1:0 to 4:1) to obtain 2,12-bis(diphénylphosphino)oxa[5]hélécène **3.43a** as a white powder.

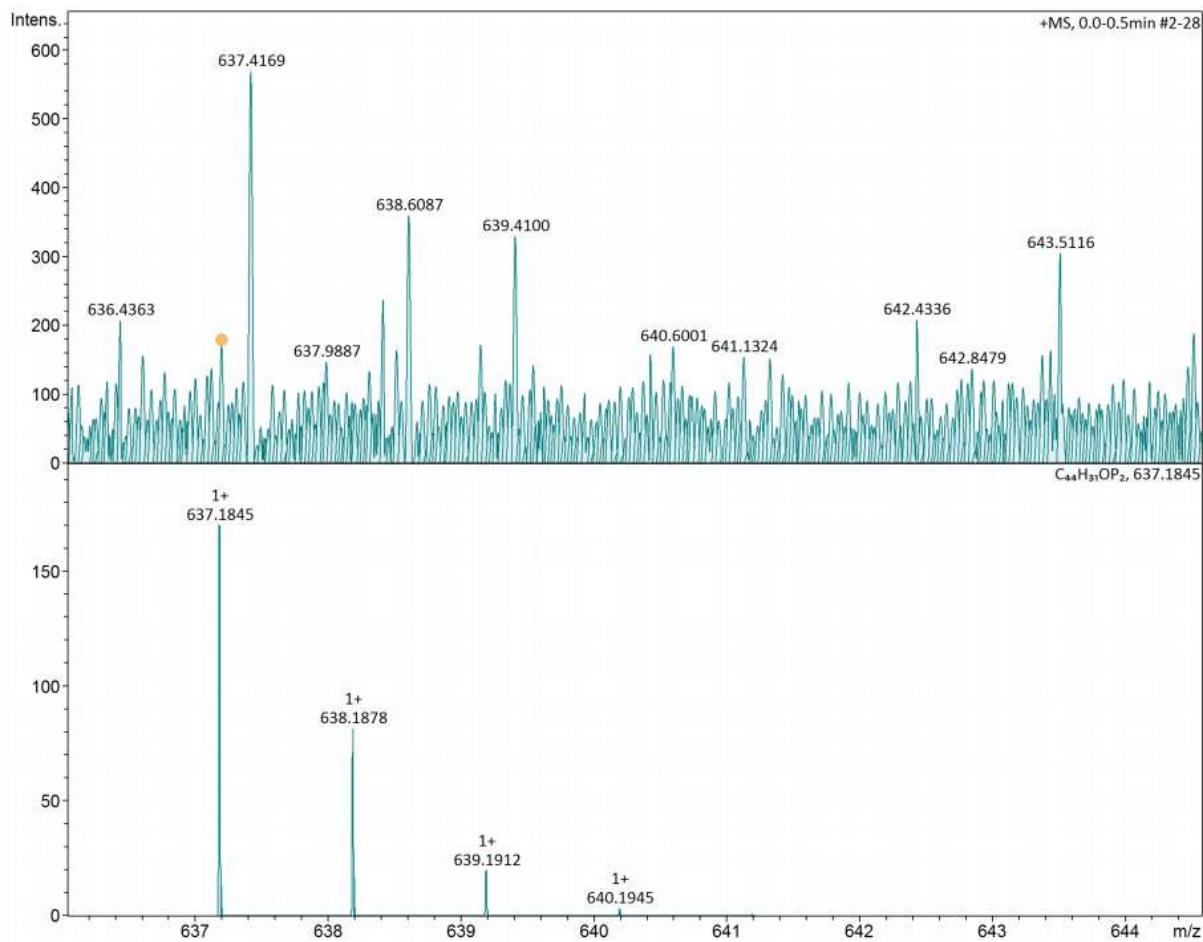
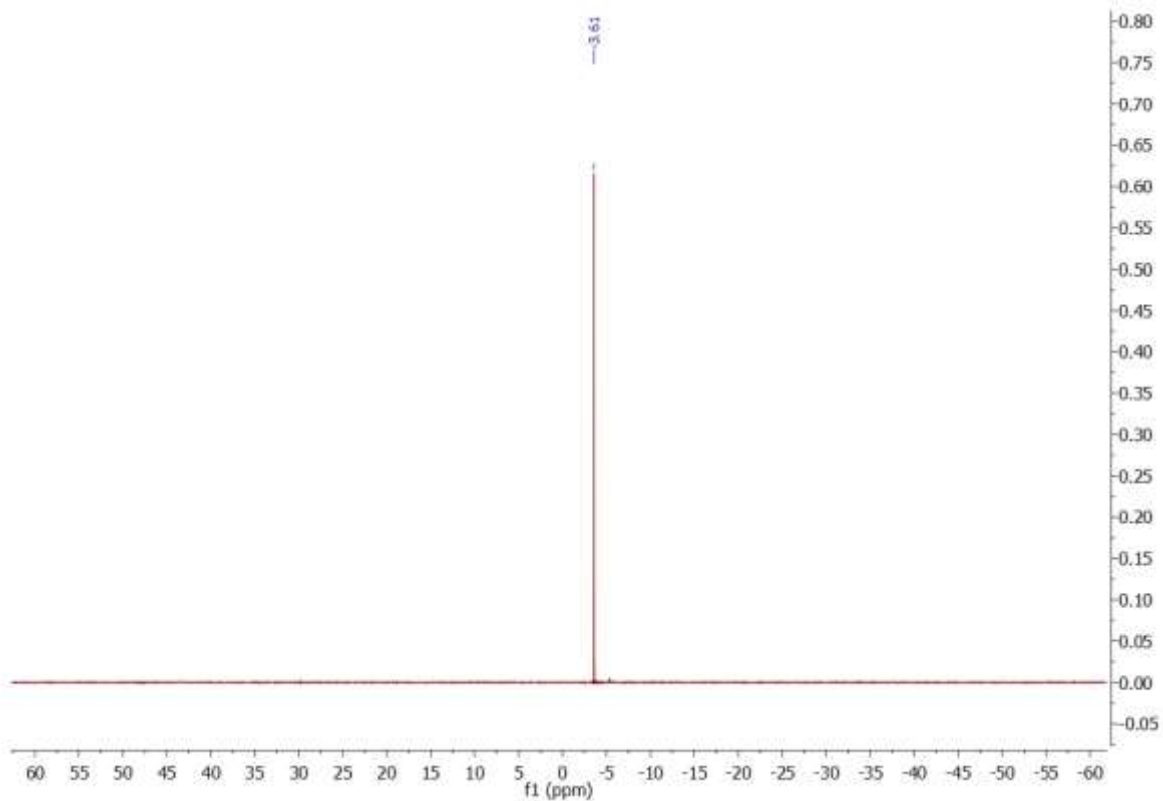
**R<sub>f</sub>** = 0.19 (eluant : hexane/CH<sub>2</sub>Cl<sub>2</sub> : 4:1)

**<sup>1</sup>H RMN (500 MHz, CDCl<sub>3</sub>):** δ = 7.28-7.29 (m, 12H), 7.33-7.35 (m, 2H) 7.37-7.40 (m, 8H) ; 7.83-7.84 (d, J=8.81 Hz, 2H) ; 7.90-7.92 (d, J=8.88 Hz, 2H) ; 7.95-7.97 (d, J=8.33 Hz, 2H), 9.52-9.55 (d, J=11.73 Hz, 2H)

**<sup>31</sup>P RMN (162 MHz, CDCl<sub>3</sub>):** δ = -3.6

**HRMS (ESI+):** [M+H]<sup>+</sup> = 637.184







### III. Crystal structures

**Table 1. Experimental details**

	<b>2.28a</b>	<b>2.28d</b>	<b>2.32a</b>
Chemical formula	C <sub>26</sub> H <sub>25</sub> BO <sub>2</sub>	C <sub>25</sub> H <sub>23</sub> BO <sub>2</sub>	C <sub>26</sub> H <sub>25</sub> BO <sub>2</sub>
$M_r$	380.27	366.24	380.27
Crystal system, space group	Orthorhombic, <i>Pbca</i>	Monoclinic, <i>P2<sub>1</sub>/c</i>	Orthorhombic, <i>Pna2<sub>1</sub></i>
Temperature (K)	295		
$a, b, c$ (Å)	16.5002 (3), 12.02774 (17), 21.0103 (3)	8.3625 (1), 20.1714 (2), 12.3275 (1)	16.8832 (2), 8.96605 (11), 14.09311 (18)
$\alpha, \beta, \gamma$ (°)	90, 90, 90	90, 107.360 (1), 90	90, 90, 90
$V$ (Å <sup>3</sup> )	4169.71 (11)	1984.72 (4)	2133.36 (5)
$Z$	8	4	4
Radiation type	Cu $K\alpha$		
$\mu$ (mm <sup>-1</sup> )	0.58	0.59	0.56
Crystal size (mm)	0.51 × 0.37 × 0.22	0.33 × 0.19 × 0.13	0.19 × 0.17 × 0.11
Diffractometer	Oxford Diffraction Xcalibur, Ruby, Gemini ultra		
Absorption correction	Analytical		
$T_{\min}, T_{\max}$	0.835, 0.914	0.885, 0.945	0.935, 0.962
No. of measured, independent and observed [ $I > 2\sigma(I)$ ] reflections	14427, 3674, 3283	9774, 3500, 3186	6717, 3021, 2934
$R_{\text{int}}$	0.026	0.017	0.023
$(\sin \theta/\lambda)_{\text{max}}$ (Å <sup>-1</sup> )	0.597	0.597	0.598
$R[F^2 > 2\sigma(F^2)], wR(F^2), S$	0.042, 0.119, 1.03	0.050, 0.135, 1.06	0.030, 0.084, 1.03
No. of reflections	3674	3500	3021
No. of parameters	339	322	266
No. of restraints	308	34	1
H-atom treatment	H-atom parameters constrained		
$\Delta\rho_{\text{max}}, \Delta\rho_{\text{min}}$ (e Å <sup>-3</sup> )	0.26, -0.15	0.40, -0.23	0.13, -0.11
Absolute structure	–	–	Flack $x$ determined using 988 quotients [( $I^+$ )-( $I^-$ )]/[( $I^+$ )+( $I^-$ )] (Parsons, Flack and Wagner, Acta Cryst. B69 (2013) 249).
Absolute structure parameter	–	–	-0.02 (11)
CCDC deposition number	2051342	2051343	2051344

	<b>2.32c</b>	<b>2.32b</b>	<b>2.27a</b>
Chemical formula	C <sub>25</sub> H <sub>23</sub> BO <sub>2</sub>	2(C <sub>38</sub> H <sub>35</sub> B)·C <sub>4</sub> H <sub>10</sub> O	C <sub>20</sub> H <sub>21</sub> BO <sub>2</sub>
<i>M<sub>r</sub></i>	366.24	1079.06	304.18
Crystal system, space group	Monoclinic, <i>P</i> 2 <sub>1</sub> / <i>n</i>	Monoclinic, <i>P</i> 2 <sub>1</sub>	Monoclinic, <i>P</i> 2 <sub>1</sub>
Temperature (K)	295		100
<i>a</i> , <i>b</i> , <i>c</i> (Å)	9.4005 (2), 8.2807 (2), 26.3582 (8)	8.26518 (15), 32.7662 (7), 11.8032 (2)	10.6573 (3), 11.1974 (2), 15.0320 (4)
$\alpha$ , $\beta$ , $\gamma$ (°)	90, 97.316 (3), 90	90, 91.3028 (18), 90	90, 109.917 (3), 90
<i>V</i> (Å <sup>3</sup> )	2035.08 (10)	3195.70 (11)	1686.53 (8)
<i>Z</i>	4	2	4
Radiation type	Cu <i>K</i> $\alpha$		Mo <i>K</i> $\alpha$
$\mu$ (mm <sup>-1</sup> )	0.57	0.48	0.08
Crystal size (mm)	0.44 × 0.24 × 0.03	0.69 × 0.15 × 0.06	0.49 × 0.20 × 0.06
Diffractometer	Oxford Diffraction Xcalibur, Ruby, Gemini Ultra		
Absorption correction	Gaussian		Analytical
<i>T</i> <sub>min</sub> , <i>T</i> <sub>max</sub>	0.855, 0.981	0.763, 0.973	0.984, 0.996
No. of measured, independent and observed [ <i>I</i> > 2 $\sigma$ ( <i>I</i> )] reflections	5715, 5715, 3865	18146, 18146, 13813	11673, 8571, 7379
<i>R</i> <sub>int</sub>	0.041	?	0.022
(sin $\theta$ / $\lambda$ ) <sub>max</sub> (Å <sup>-1</sup> )	0.598	0.598	0.761
<i>R</i> [ <i>F</i> <sup>2</sup> > 2 $\sigma$ ( <i>F</i> <sup>2</sup> )], <i>wR</i> ( <i>F</i> <sup>2</sup> ), <i>S</i>	0.044, 0.136, 0.97	0.048, 0.116, 1.08	0.047, 0.115, 1.03
No. of reflections	5715	18146	8571
No. of parameters	323	765	478
No. of restraints	269	48	1
H-atom treatment	H-atom parameters constrained		H atoms treated by a mixture of independent and constrained refinement
$\Delta$ <sub>max</sub> , $\Delta$ <sub>min</sub> (e Å <sup>-3</sup> )	0.14, -0.16	0.33, -0.19	0.27, -0.22
Absolute structure	–	n/a	n/a
Absolute structure parameter	–	n/a	n/a
CCDC deposition number	2051345	2051346	2051347

	<b>2.43a</b>	<b>2.43b</b>	<b>2.43e</b>
Chemical formula	2(C <sub>32</sub> H <sub>23</sub> P)·C <sub>4</sub> H <sub>8</sub> O <sub>2</sub>	C <sub>34</sub> H <sub>27</sub> P	C <sub>32</sub> H <sub>22</sub> BrP
<i>M</i> <sub>r</sub>	965.05	466.52	517.37
Crystal system, space group	Triclinic, <i>P</i> <sup>-</sup> 1	Monoclinic, <i>Ia</i>	Monoclinic, <i>P2</i> <sub>1</sub> / <i>c</i>
Temperature (K)	295	295	295
<i>a</i> , <i>b</i> , <i>c</i> (Å)	10.7786 (11), 10.8021 (8), 23.5917 (18)	18.2881 (3), 8.43492 (11), 17.4051 (3)	15.17129 (15), 9.32397 (8), 18.56068 (16)
$\alpha$ , $\beta$ , $\gamma$ (°)	103.124 (7), 101.071 (8), 93.684 (7)	90, 110.821 (2), 90	90, 109.6059 (10), 90
<i>V</i> (Å <sup>3</sup> )	2608.5 (4)	2509.55 (8)	2473.31 (4)
<i>Z</i>	2	4	4
Radiation type	Cu <i>K</i> $\alpha$	Mo <i>K</i> $\alpha$	Cu <i>K</i> $\alpha$
$\mu$ (mm <sup>-1</sup> )	1.11	0.13	3.00
Crystal size (mm)	0.28 × 0.24 × 0.03	0.41 × 0.38 × 0.18	0.58 × 0.31 × 0.24
Diffractometer	Oxford Diffraction Xcalibur Gemini Ultra R		
Absorption correction	Gaussian	Analytical	Gaussian
<i>T</i> <sub>min</sub> , <i>T</i> <sub>max</sub>	0.830, 0.963	0.956, 0.978	0.416, 0.729
No. of measured, independent and observed [ <i>I</i> > 2 $\sigma$ ( <i>I</i> )] reflections	4260, 4260, 3502	18752, 8305, 7618	34035, 4403, 4159
<i>R</i> <sub>int</sub>	0.030	0.014	0.023
$\theta$ <sub>max</sub> (°)	40.3	32.7	67.1
( $\sin \theta/\lambda$ ) <sub>max</sub> (Å <sup>-1</sup> )	0.420	0.760	0.597
<i>R</i> [ <i>F</i> <sup>2</sup> > 2 $\sigma$ ( <i>F</i> <sup>2</sup> )], <i>wR</i> ( <i>F</i> <sup>2</sup> ), <i>S</i>	0.079, 0.259, 1.16	0.038, 0.108, 1.05	0.041, 0.113, 1.05
No. of reflections	4260	8305	4403
No. of parameters	652	319	317
No. of restraints	33	2	1
H-atom treatment	H-atom parameters constrained		
$\Delta\rho$ <sub>max</sub> , $\Delta\rho$ <sub>min</sub> (e·Å <sup>-3</sup> )	0.40, -0.36	0.26, -0.14	0.43, -0.64
Absolute structure	–	Refined as an inversion twin.	–
Absolute structure parameter	–	0.28 (7)	–

	<b>2.43e</b>	oxide tritypcenyl- phosphine <b>2.44</b>	of Rh(acac)CO( <b>2.43a</b> )
Chemical formula	C <sub>32</sub> H <sub>22</sub> BrP	0.76(C <sub>46</sub> H <sub>31</sub> P)·0.24(C <sub>4</sub> H <sub>31</sub> OP)	C <sub>38</sub> H <sub>30</sub> O <sub>3</sub> PRh
<i>M</i> <sub>r</sub>	517.37	618.57	668.50
Crystal system, space group	Monoclinic, <i>P</i> 2 <sub>1</sub> / <i>c</i>	Triclinic, <i>P</i> <sup>-</sup> 1	Triclinic, <i>P</i> <sup>-</sup> 1
Temperature (K)	100	100	295
<i>a</i> , <i>b</i> , <i>c</i> (Å)	14.9902 (3), 9.26951 (13), 18.4132 (3)	8.5214 (6), 11.0664 (7), 18.1858 (11)	10.84421 (18), 15.5989 (3), 18.2430 (3)
$\alpha$ , $\beta$ , $\gamma$ (°)	90, 109.7869 (19), 90	74.875 (5), 77.433 (5), 72.594 (6)	95.1226 (14), 90.4535 (14), 99.7839 (14)
<i>V</i> (Å <sup>3</sup> )	2407.48 (7)	1561.50 (18)	3028.07 (9)
<i>Z</i>	4	2	4
Radiation type	Mo <i>K</i> $\alpha$	Cu <i>K</i> $\alpha$	Cu <i>K</i> $\alpha$
$\mu$ (mm <sup>-1</sup> )	1.79	1.04	5.35
Crystal size (mm)	0.38 × 0.32 × 0.13	0.19 × 0.14 × 0.04	0.44 × 0.22 × 0.12
Diffractometer	Oxford Diffraction Xcalibur Gemini Ultra R		
Absorption correction	Analytical		
<i>T</i> <sub>min</sub> , <i>T</i> <sub>max</sub>	0.618, 0.811	0.862, 0.966	0.295, 0.610
No. of measured, independent and observed [ <i>I</i> > 2 $\sigma$ ( <i>I</i> )] reflections	29216, 7354, 6287	13386, 5349, 4558	31044, 10704, 10072
<i>R</i> <sub>int</sub>	0.027	0.036	0.030
$\theta$ <sub>max</sub> (°)	30.5	67.1	67.1
(sin $\theta$ / $\lambda$ ) <sub>max</sub> (Å <sup>-1</sup> )	0.714	0.598	0.597
<i>R</i> [ <i>F</i> <sup>2</sup> > 2 $\sigma$ ( <i>F</i> <sup>2</sup> )], <i>wR</i> ( <i>F</i> <sup>2</sup> ), <i>S</i>	0.036, 0.093, 1.04	0.048, 0.125, 1.02	0.025, 0.064, 1.04
No. of reflections	7354	5349	10704
No. of parameters	317	435	1554
No. of restraints	1	0	1020
H-atom treatment	H-atom parameters constrained		
$\Delta\rho$ <sub>max</sub> , $\Delta\rho$ <sub>min</sub> (e·Å <sup>-3</sup> )	0.56, -0.59	0.41, -0.42	0.23, -0.48

	Rh(acac)CO( <b>2.44</b> )	<b>2.43f</b>	<b>2.48</b>	<b>2.49</b>
Chemical formula	C <sub>52</sub> H <sub>38</sub> O <sub>3</sub> PRh·CH <sub>2</sub> Cl <sub>2</sub>	C <sub>34</sub> H <sub>26</sub> BrP	C <sub>34</sub> H <sub>27</sub> BrP <sup>+</sup> ·BF <sub>4</sub> <sup>-</sup>	C <sub>62</sub> H <sub>37</sub> BF <sub>15</sub> OP·0.177(C <sub>4</sub> H <sub>10</sub> O)·0.647(CH <sub>2</sub> Cl <sub>2</sub> )
<i>M<sub>r</sub></i>	929.63	545.43	633.24	1192.72
Crystal system, space group	Triclinic, <i>P</i> <sup>-</sup> 1	Triclinic, <i>P</i> <sup>-</sup> 1	Monoclinic, <i>P</i> 2 <sub>1</sub> / <i>n</i>	Triclinic, <i>P</i> <sup>-</sup> 1
Temperature (K)	295	100	295	100
<i>a</i> , <i>b</i> , <i>c</i> (Å)	10.7708 (4), 13.4235 (7), 16.5371 (8)	8.2351 (3), 10.7029 (5), 15.4060 (7)	15.12485 (14), 11.88558 (11), 16.96686 (13)	12.5223 (2), 14.9480 (4), 15.1679 (5)
$\alpha$ , $\beta$ , $\gamma$ (°)	75.903 (4), 73.923 (4), 72.549 (4)	72.692 (4), 87.281 (3), 76.917 (4)	90, 105.8220 (9), 90	72.901 (3), 76.444 (2), 87.812 (2)
<i>V</i> (Å <sup>3</sup> )	2157.85 (18)	1262.45 (10)	2934.53 (5)	2636.65 (13)
<i>Z</i>	2	2	4	2
Radiation type	Mo <i>K</i> $\alpha$	Cu <i>K</i> $\alpha$		
$\mu$ (mm <sup>-1</sup> )	0.60	2.97	2.83	1.94
Crystal size (mm)	0.58 × 0.28 × 0.11	0.11 × 0.03 × 0.02	0.44 × 0.33 × 0.14	0.32 × 0.22 × 0.09
Diffractometer	Oxford Diffraction Xcalibur Gemini Ultra R			
Absorption correction	Gaussian	Analytical		
<i>T</i> <sub>min</sub> , <i>T</i> <sub>max</sub>	0.516, 1.000	0.769, 0.936	0.439, 0.736	0.688, 0.861
No. of measured, independent and observed [ <i>I</i> > 2 $\sigma$ ( <i>I</i> )] reflections	29944, 29944, 20092	11231, 4465, 3833	16760, 5157, 4732	26431, 9304, 8169
<i>R</i> <sub>int</sub>	0.025	0.036	0.021	0.029
$\theta$ <sub>max</sub> (°)	32.8	67.0	67.1	67.1
(sin $\theta$ / $\lambda$ ) <sub>max</sub> (Å <sup>-1</sup> )	0.762	0.597	0.597	0.597
<i>R</i> [ <i>F</i> <sup>2</sup> > 2 $\sigma$ ( <i>F</i> <sup>2</sup> )], <i>wR</i> ( <i>F</i> <sup>2</sup> ), <i>S</i>	0.049, 0.130, 0.95	0.036, 0.093, 1.04	0.045, 0.134, 1.03	0.038, 0.100, 1.04
No. of reflections	29944	4465	5157	9304
No. of parameters	544	337	376	799
No. of restraints	0	1	0	58
H-atom treatment	H-atom parameters constrained		H atoms treated by a mixture of independent and constrained refinement	H-atom parameters constrained
$\Delta\rho$ <sub>max</sub> , $\Delta\rho$ <sub>min</sub> (e·Å <sup>-3</sup> )	1.04, -0.79	0.46, -0.41	0.36, -0.89	0.41, -0.33

## References :

- [1] Rigaku Oxford Diffraction. CrysAlisPro Software system. Rigaku Corporation, Wroclaw, Poland, **2020**.
- [2] G. M. Sheldrick, *Acta Crystallogr. Sect. A Found. Adv.* **2015**, *71*, 3.
- [3] G. M. Sheldrick, *Acta Crystallogr. Sect. C Struct. Chem.* **2015**, *71*, 3.
- [4] C. B. Hübschle, G. M. Sheldrick, B. Dittrich, *J. Appl. Crystallogr.* **2011**, *44*, 1281.
- [5] O. V. Dolomanov, L. J. Bourhis, R. J. Gildea, J. A. K. Howard, Puschmann, H. J. *Appl. Crystallogr.* **2009**, *42*, 339.

## **Appendix B: List of conferences**

1. Participated, 16<sup>th</sup> Belgian Organic Synthesis Symposium, 8-13 Jul 2018, Université Libre de Bruxelles, Belgium.
2. Poster presentation, Annual NISM meeting, 21 Sep 2018, University of Namur, Belgium.
3. Poster presentation, MOCS Symposium, 6-7 Dec 2018, Blankerberge, Belgium.
4. Oral communication, Annual CHIM meeting, 23 May 2019, University of Namur, Belgium.
5. Participated, Symposium – Tribute to István Markó, Université Catholique de Louvain, Belgium.
6. Poster presentation, Annual NISM meeting, 20 Sep 2019, University of Namur, Belgium.
7. Poster presentation, JCO Symposium, 29-31 Oct 2019, Ecole Polytechnique, Palaiseau, France.
8. Poster presentation, Journée Rencontres des Jeunes Chimistes, 6 Mar 2020, University of Namur, Belgium.
9. Poster presentation, GIDW Virtual Symposium, 9 Jul 2020.
10. Poster presentation, RSCPosterLive 2021, 2 Mar 2021, (Virtual).
11. Poster presentation, Virtual MOCS Symposium, 2-3 Dec 2021.



## **Appendix C: List of publications**

**Accepted article:**

[1] **M. Gama**, X. Antognini Silva, T. -H. Doan, A. Osi, A. Chardon, N. Tumanov, J. Wouters, G. Berionni, Triptycene boronates, boranes, and boron ate-complexes: toward sterically hindered triarylboranes and trifluoroborates, *Eur. J. Org. Chem.*, **2021**, *9*, 1440-1445.

**Article not submitted yet:**

[2] **M. Gama**, L. Hu, N. Tumanov, R. Robiette, G. Berionni, Sterically Hindered Phosphines Derived from Triptycene: Reactivity and Applications in Frustrated Lewis Pairs Chemistry.